

The relation between variable active galactic
nuclei, their immediate environments, and the
conditions for star formation

INAUGURAL-DISSERTATION

zur

Erlangung des Doktorgrades
der Mathematisch-Naturwissenschaftlichen Fakultät
der Universität zu Köln



vorgelegt von

Yasir Ezzuldeen Rashed

aus Bagdad, Irak

Köln 2015

Berichtersteller:

Prof. Dr. Andreas Eckart

Prof. Dr. Anton Zensus

Tag der letzten mündlichen Prüfung: 26 Oktober 2015

To Allah "Almighty"

To my father's soul, my mother, my brothers (Ammar & Musaab), and my
beloved wife Inas.

Zusammenfassung

Die Kerne der meisten aktiven Galaxien (AGN) - wenn nicht sogar alle - beherbergen in ihren Zentren ein super-massives Schwarzes Loch (SMBH). Dieses SMBH entwickelt sich zusammen mit dem Bulge (der zentralen Verdickung einer Spiralgalaxie oder das Innere einer Elliptischen Galaxie). Die Korrelation zwischen dem SMBH und den Entwicklungsprozessen der Gastgalaxie ist bisher jedoch noch nicht vollständig verstanden. Das liegt unter anderem daran, dass bisher in vielen Fällen Beobachtungen eindeutiger Hinweise auf eine solche Entwicklung fehlen. In dieser Arbeit trage ich einige Teile des grossen Puzzels zur Entwicklung und der Physik aktiver Galaxien bei.

Diese Arbeit ist in drei Hauptabschnitte unterteilt:

Erstes Projekt: In diesem Projekt behandle ich eine Doppel-Keulen Radiogalaxie ('Double-lobe') die ideal dazu geeignet ist, die Wechselwirkungen der einzelnen Komponenten der Radiostruktur mit dem intergalaktischen Medium (IGM) und dem Interstellaren Medium (ISM) der Gastgalaxie zu untersuchen. Die Quelle SDSS J080800.99+483807.7 ist von uns zufällig bei der Analyse von 18 cm Beobachtungsdaten des MERLIN Radiointerferometers als Doppel-Keulen Radiogalaxie entdeckt worden.

Da es sich um eine schwache optische Quelle handelt waren Basisinformationen, wie linearer Durchmesser, Masse des zentralen Schwarzen Lochs, Rotverschiebung und Quellstruktur bisher unbekannt oder unvollständig. Weiterhin gabe es keine optischen Spektren in zugänglichen Archiven. Ziel dieser Arbeit war es die grundlegenden physikalischen Eigenschaften der Quelle SDSS J080800.99+483807.7 zu ermitteln und die Möglichkeit einer Wechselwirkung zwischen Radio-Jets (Düsenstrahlen aus dem Kern der Galaxie) und dem ISM der Gastgalaxie zu untersuchen.

In diesem Projekt habe ich radiointerferometrische und optische Spektroskopiedaten benutzt. Die optischen Daten wurden mit dem Multi-Objekt Doppel-Spektrographen (MODS) am Large Binocular Telescope (LBT) gewonnen. Die Radiodaten, bei einer Wellenlänge von 18 cm, stammen von dem Radiointerferometer MERLIN. Die Rotverschiebung der Galaxie beträgt $z = 0.2805 \pm 0.0003$, und ergibt für den Durchmesser der beobachteten Radiostruktur etwa 26.3 kpc. Zusätzlich zu dem Infrarot- und Kontinuumsspektrum weisen die optischen Emissionslinien auf eine hohe Sternentstehungsaktivität hin. Die Masse des zentralen Schwarzen Lochs kann als $\log(M_{\text{BH}}/M_{\odot}) \approx 6.9$ abgeschätzt werden. Schliesslich ergibt sich aus den optischen Bildern des

Sloan Digital Sky Survey's sowie aus dem von mir ermittelten optischen Spektrum, dass die Quelle SDSS J080800.99+483807.7 eine Elliptische Galaxie ist.

Zweites Projekt: In diesem Projekt habe ich auf Abbildungen basierende photometrische sowie spektroskopische Daten von 18 Galaxien mit AGN von 2 bis 3 Beobachtungsepochen verglichen. Die Beobachtungen überdecken typischer Weise einen Zeitraum von 5 bis 10 Jahren. Hier wurden die Beobachtungsdaten wieder am LBT genommen oder entstammen dem SDSS bzw. der Literatur. Für 4 von 8 Quellen mit neuen LBT Beobachtungsdaten habe ich Anzeichen von Linien- oder Kontinuumsvariabilität festgestellt, die auf eine Zunahme der ionisierenden Strahlung aus den Kernen dieser Quellen hinweist. Diese Objekte zeigen Flußveränderngen in den Wasserstoff- Rekombinationslinien und den verbotenen Linienüberängen unter anderem des Sauerstoffs. Für die verbleibenden 4 Quellen find ich, dass im Rahmen der Kalibrationsunsicherheiten die Linien- und Kontinuumsvariabilitäten klein sind. In einer, duch Hinzunahme von Quellen aus der Literatur erweiteren Stichprobe, find ich, dass die Seyfert 2/NLS1 Quellen im Vergleich zu BLS1 und QSO Quellen generell einen kleineren Variabilitätsgrad in Kontinuums- ($\Delta L_{cont.}$) und in Linienleuchtkraft (ΔL_{line}) aufweisen.

Ich zeige, dass hauptsächlich die zwischen den Stichproben unterschiedliche Masse des zentralen Schwarzen Lochs für der unterschiedlichen Variabilitätsgrad in Kontinuum und Linie verantwortlich ist. Zusätzlich finde ich, dass für eine, ansonsten konstante Akkretionsrate, die totale Linienvariabilität (dominiert durch die Beträge der schmalen Linien) die Kontinuumsvariabilität mit einer Abhängigkeit $\Delta L_{line} \propto (\Delta L_{cont.})^{\frac{3}{2}}$ widerspiegelt ('reverberation'). Da sich diese Abhängigkeit sehr deutlich in der Emission der schmalen Linien ausdrückt, impliziert dies, dass der die Linienleuchtkraft dominierende Teil der 'narrow line region' (NLR) sehr kompakt sein muß und eine Größe von mindestens 10 Lichtjahren aufweist. Ein Vergleich zu Literaturdaten zeigt, dass dieser Schluß das Variabilitätsverhalten von insgesamt 61 AGN erklärt, die von breiter oder schmaller Linienemission dominiert werden.

Drittes Projekt: In diesem Kapitel behandle ich die Variabilität von Quasaren mit breiten Absorptionslinienträgen ('Broad Absorption Lines Quasars' oder BAL QSO). Der Untersuchung liegen für zwei Beobachtungsepochen mit 5-10 Jahren Abstand spektrophotometrische Daten (in den optische Bändern u, g, r, i, und z) sowie optische Spektren vom Large Binocular Telescope (LBT), vom MMT (Multiple Mirror Telescope) und aus dem SDDS vor. Für drei Quellen habe ich neue LBT-Daten reduziert. Hierbei handelt es sich um die beiden leuchtstarken HiBAL-Quellen SDSS J012412.45-010049.9 und SDSS J093403.96+315331.3 sowie

um die LoBAL-Quelle SDSS J072831.64+402616.0 mit niedriger Leuchtkraft. Da mir unterschiedliche Steigungen in den Spektren der Quellen auffielen, habe ich die Stichproben aus dem SDSS auf je 50 zufällig ausgewählte HiBAL, LoBAL und intermediäre (in ihren BAL-Eigenschaften zwischen HiBAL und LoBAL) Quellen erweitert. Ich kann zeigen, dass die gemittelte wellenlängenabhängige Variabilität der Quellgruppen deutliche Unterschiede aufweist. Dies ist vermutlich einerseits auf den Unterschied in der mittleren Rotverschiebung der Quellen und andererseits auf deren unterschiedliche Leuchtkraft zurückzuführen. Ich vermute, dass sich dieses unterschiedliche Verhalten auch in der Linienvariabilität widerspiegelt. Dies ist Ziel einer laufenden Untersuchung.

Zusammenfassung: Ich habe eine kurze Zusammenfassung mit Ausblick an das Ende meiner Arbeit gestellt. Weitaus detailliertere Unter-Zusammenfassungen sind an den Enden der einzelnen Kapitel zu finden. Zusammenfassend konnte ich zeigen, dass das supermassive Schwarze Loch als zentraler Kern des AGN weitreichenden Einfluß auf seine Umgebung hat. Durch Rückflußphänomene in Double - lobe Radiogalaxien can die Sternentstehung in der Gastgalaxie über viele Kiloparsek hinweg beeinflusst werden. Für die Kernregion selbs, konnte ich zeigen, dass nicht nur die BLR ('broad line region') sondern auch der mehr compacte Teil der NLR ('narrow line region') die Variabilität des Kerns widerspiegelt ('reverberation') Diese aussagekräftigen Ergebnisse konnte ich nur durch Beobachtungen bei mehreren Wellenlängen und unter Benutzung von mehreren Instrumenten und Beobachtungseinrichtungen erzielen.

Abstract

Most of the active galactic nuclei (AGN) in active galaxies - if not all of them - host a super-massive black hole (SMBH) at their center. This SMBH is co-evolving with the nuclear bulge of the host. However, the correlation between the SMBH and the evolutionary processes is not yet fully understood. This is due to the fact that strong observational evidences that may help to understand the processes are still missing in many cases. In this work I try to add some pieces to the large puzzle of the evolution and physics of active galaxies.

This work has been divided into three main projects:

First project: In this project, I deal with a Double-lobe radio galaxy that is ideally suited to investigate the interaction of the individual components of the radio structure with the intergalactic medium (IGM) and the interstellar medium (ISM) of the host galaxy. SDSS J080800.99+483807.7 has been serendipitously discovered in MERLIN 18 cm observations to be a double-lobed radio galaxy. Because it is an optically faint source, basic information like linear size, mass of the central black hole, redshift, and structure has been incomplete or even missing until now. Additionally, there were no spectra for this object available in any databases. The aim of this project is to derive the main physical properties of SDSS J080800.99+483807.7 and study the possible interaction between the radio jets and the interstellar medium of the host galaxy. In this project I used data from optical spectroscopy and radio interferometry. The optical data were obtained by the Multi-Object Double Spectrograph (MODS) at the Large Binocular Telescope (LBT), and the radio data were observed by MERLIN at a wavelength of 18 cm. The redshift of the galaxy calculated to be $z = 0.2805 \pm 0.0003$, resulting in a linear size of the observed radio structure of ~ 26.3 kpc. The emission lines of the optical spectrum in addition to the infrared and radio continuum emission suggest that this source has high activity of star-formation. Furthermore, the central black

hole mass estimated be $\log(M_{\text{BH}}/M_{\odot}) \approx 6.9$. Finally, the optical images from Sloan Digital Sky Survey as well as the optical spectrum of this source suggest that SDSS J080800.99+483807.7 is associated with an elliptical host galaxy.

Second project: In this project, I compare image-based photometry as well as optical spectroscopy data for 18 galaxies hosting an AGN over 2 to 3 epochs which span time intervals of typically 5 to 10 years. The data in this chapter has been taken by LBT and SDSS and from the literature. For 4 out of 8 objects with new LBT observations I noticed that there are indications of line or continuum variations that may be elucidated as a result of an increased ionizing radiation field originating at the nuclei of these objects. I find variations in the hydrogen recombination lines as well as in the forbidden oxygen lines of these objects. For the rest of the four sources I find that within the calibration uncertainties the line and continuum variability of the sources are very small. Enlarging the sample by adding additional data from the literature I find that the Seyfert 2/NLS1 sources if compared to BLS1 and QSO sources, show in general a smaller degree of variability in the continuum $\Delta L_{\text{cont.}}$ and line luminosity ΔL_{line} . I present that it is mainly the difference in black hole mass between the samples that is responsible for the different degrees of continuum variability. In addition I find that for an otherwise constant accretion rate the total line variability (dominated by the narrow line contributions) reverberates the continuum variability with a dependency $\Delta L_{\text{line}} \propto (\Delta L_{\text{cont.}})^{\frac{3}{2}}$. Since this dependency is prominently expressed in the narrow line emission it implies that the luminosity dominating part of the narrow line region must be very compact with a size of the order of at least 10 light years. A comparison to literature data exhibits that these conclusions clarify the variability characteristics of a total of 61 broad and narrow line sources.

Third project: In this part of the thesis I investigate the variability of Broad Absorption Lines Quasars (BAL QSO). My research is based on spectrophotometric data in the optical u, g, r, i, and z bands as well as optical spectra. The data cover two epochs over typically 5-10 years and have been taken with the Large Binocular Telescope (LBT), the MMT (Multiple Mirror Telescope) and from the SDSS. For three sources I reduced newly taken LBT. The sources include the two luminous HiBAL objects SDSS J012412.45-010049.9 and SDSS J093403.96+315331.3 as

well as the low luminosity LoBAL source SDSS J072831.64+402616.0. Since I noticed that the sources show different spectral slopes I extended the samples using the SDSS to contain 50 randomly selected objects for each of the subgroups: HiBal, LoBal, and intermediate class objects. I show that the wavelength averaged variability properties of these sources exhibit clear differences. Most likely this is on the one hand due to the different average redshifts of these source classes and on the other hand this may be due to the different average luminosities. I suspect that these different properties will also be reflected in the line variability. This is a subject in my ongoing investigation.

Summary: I attached a brief summary and an outlook at the end of the thesis. More detailed sub-summaries can be found at the ends of the individual chapters. In summary I could show that the SMBH as the very nucleus of the AGN has far-reaching influences on its surroundings. Through back-flow phenomena in double-lobe radio galaxies the star formation in the host galaxy can be influenced over scales of many kiloparsecs. In the nuclear region itself, I could show that not only the broad line region (BLR) but also the more compact part of the narrow line region (NLR) reverberates the variability of the nucleus. This achievement was only possible through a multi wavelength approach using data from several instruments and observing facilities.

Contents

List of Figures	xi
List of Tables	xvii
1 Introduction	1
1.1 Galaxies	2
1.2 Active galaxies	3
1.2.1 Seyfert Galaxies	9
1.2.2 Quasars	10
1.2.3 Radio galaxies	12
1.2.3.1 Fanaroff-Riley type I (FR-I)	14
1.2.3.2 Fanaroff-Riley type II (FR-II)	15
1.2.4 Blazars, OVV's, and BL Lac objects	16
1.3 Broad absorption line quasars (BALQSO)	17
1.3.1 HiBAL	17
1.3.2 LoBAL	18
1.3.3 FeLoBAL	18
1.4 LINERs	18
1.5 variability	19
1.6 Diagnostic Diagrams	20
2 Instrumentation and Data Reduction	23
2.1 Radio and Optical instruments	23
2.1.1 MERLIN Radio telescopes	23
2.1.2 The Large Binocular Telescope and Multi-Object Double Spectrograph	24
2.2 Data reduction and calibration	26

CONTENTS

2.2.1	Data Reduction	26
2.2.2	Wavelength calibration	27
2.2.3	Flux calibration	27
2.3	Public Survey	28
2.3.1	The Sloan Digital Sky Survey	29
2.3.2	The Wide-field Infrared Survey Explorer	29
3	High-resolution observations of SDSS J080800.99+483807.7 in the optical and radio domains	35
3.1	Introduction	35
3.2	Radio observation of J0808	36
3.3	Optical and infrared observations of J0808	37
3.4	Results	39
3.4.1	Emission-lines measurements	39
3.4.2	The linear size of J0808	42
3.4.3	The radio loudness of J0808	44
3.4.4	The central black hole of J0808	49
3.4.5	Star formation in the host galaxy of J0808	53
3.5	Discussion and Conclusions	54
4	Line and Continuum Variability in Active Galaxies	57
4.1	Introduction	57
4.2	How the source samples were selected	59
4.3	Optical observations LBT and SDSS	60
4.3.1	Measurements of the magnitude	63
4.4	Analysis	67
4.4.1	Stellar continuum subtraction	67
4.4.2	Fe II subtraction	71
4.4.3	Fitting the Emission-lines	71
4.5	Results	71
4.5.1	SDSS J093801.63+135317.0	74
4.5.2	SDSS J120300.19+162443.8	76
4.5.3	SDSS J115816.72+132624.1	77
4.5.4	SDSS J091146.06+403501.0	79

4.5.5	SDSS J080248.18+551328.9	81
4.5.6	2MASX J035409.48+024930.7	84
4.5.7	GALEXASC J015328.23+260938.5	86
4.5.8	SDSS J034740.18+010514.0	86
4.6	Discussion	88
4.6.1	How to probe the degree of variability	91
4.6.1.1	Robustness of the separation	92
4.6.2	Accretion dominated variability	94
4.6.3	NLR response to the nuclear continuum variability	96
4.7	Conclusions	99
5	Variability in a Broad Absorption Lines Quasars (BAL QSO)	105
5.1	Introduction	105
5.2	The LBT, SDSS, and MMT observations	106
5.3	Results	107
5.3.1	SDSS J012412-010049	107
5.3.2	SDSS J093403+315331	112
5.3.3	FBQS J072831.64+402616.0	112
5.4	Discussion and Conclusions	115
6	Summary and Outlook	119
	References	123

CONTENTS

List of Figures

1.1	galaxies: (a) Galaxy cluster Abell 1689, observed by Hubble’s Advanced Camera for Surveys. (b) SDSS color images of isolated spiral galaxy NGC 4662, take from isolated galaxies Catalog Karachentseva (1973)	2
1.2	Hubble scheme. This image organized by Dr. John Kormendy, Department of Astronomy, University of Texas at Austin.	4
1.3	Several typical spectra of active galaxies and normal galaxy. Plot credit: Brooks/Cole Thomson learning.	5
1.4	Active galaxies scheme. The layout of the scheme was designed by me.	6
1.5	Structure of active galaxies Beckmann and Shrader (2012)	7
1.6	Optical spectra for the two types Seyferts: (Top) shows a spectrum for Seyfert 1 with broad and narrow emission lines, (Bottom) shows a spectrum for Seyfert 2 with just narrow emission lines.	11
1.7	A typical QSO spectrum.	12
1.8	X-shape radio galaxies (3C403 and 3C223.1) observed by NRAO VLA, presented by Dennett-Thorpe et al. (2002)	14
1.9	FR-I radio galaxies, where the left one is (3C 296) taken by VLA 20cm Leahy and Perley (1991) , and the right one is Radio map of FR-I (M84) obtained by VLA at 4.9 GHz Laing and Bridle (1987)	15
1.10	FR-II radio galaxies, where the left one (3C 219) taken by VLA at 1.4 GHz Clarke et al. (1992) , and the right one is Radio map of FR-II (3C 175) obtained by VLA at 4.9 GHz Bridle et al. (1994)	16
1.11	BALQSOs spectra for different types.	18
1.12	An optical spectrum for the LINER galaxy NGC 7213.	19

LIST OF FIGURES

1.13	Long time scale spectroscopic variability of BLS1 PKS 2349-14. These spectra have been taken between 1990 till 2004. From 1990 – 1994 observed by Calar Alto Observatory, The 2004 spectrum stems from a monitoring program with the Hobby-Eberly Telescope (Kollatschny <i>et al.</i> , 2006a).	20
1.14	PBT diagrams.	22
2.1	Merlin array. Image credit: http://www.merlin.ac.uk/	25
2.2	LBT telescope.	26
2.3	Data reduction steps.	31
2.4	The standard stars Feige67 and G191B2B.	32
2.5	SDSS telescope.	33
2.6	The SDSS website.	33
2.7	WISE space telescope.	34
3.1	18 cm MERLIN image of SDSS J080800.99+483807.7. The J2000 coordinates of the central source are $\alpha = 08:08:00.99$ and $\delta = +48:38:07.73$. <i>Top:</i> original image at a noise level of about $1.1e-4$ Jy/beam. <i>Bottom:</i> 10 pixel smoothed image at a noise level of about $4.5e-4$ Jy/beam. The contour levels are each at -3, -2, 1, 2, 4, 5.5, 8, 12, 14 times the noise level.	38
3.3	Optical spectrum of J0808. The blue and red spectra represent the data from the respective channel. A gap between the two channels that has been excluded because of high noise and a region that shows telluric features are marked. . . .	40
3.4	Diagnostic diagrams $[N II]/H\alpha$ vs. $[O III]/H\beta$, $[S II]/H\alpha$ vs. $[O III]/H\beta$ and $[O I]/H\alpha$ vs. $[O III]/H\beta$ for the radio emitters taken from Vitale <i>et al.</i> (2012). The contours show galaxy densities in steps of 80 galaxies per each additional contour. The position of the source analyzed here is shown as a red dot.	43
3.5	Linear size versus redshift. J0808 is show by the red hexagon, the plus signs represent the position of the 3CRR sources, the square signs represent the 7CRS objects (Wang <i>et al.</i> , 2011).	44
3.6	Flux density values at different positions for each lobe (Northeast & Southwest) compared with other FR II sources (Treichel <i>et al.</i> , 2001).	45
3.7	Radio loudness scheme (Blundell, 2003).	48

3.8	Flux density and uncertainty versus frequency of J0808 from different surveys (Becker <i>et al.</i> , 1991; Condon <i>et al.</i> , 1998; Douglas <i>et al.</i> , 1996; Gregory and Condon, 1991).	49
3.9	Radio loudness (R) versus Eddington ratio η . J0808 is represented by a red hexagon, BLRGs are marked by the blue circles, radio loud quasars by the Black circles, Seyfert galaxies and LINERs by the crosses, FR I radio galaxies by the green triangles, and PG quasars by the yellow stars (Sikora <i>et al.</i> , 2007).	51
3.10	Radio loudness versus black hole mass. See caption of Fig. 3.9.	52
4.1	Left: For all sources I present the distribution of the intensity drops of the fainter exposures with respect to the brightest once. The data is shown in bin widths of 0.05 (fat dots) and for comparison half the value obtained with a bin width of 0.10 (black line). Right: Intensity drop due to the combination of variable seeing and slit offset. Case α indicates the level (dotted line) to which the spectra can be calibrated if for individual sources the fainter exposures are corrected to the level of the brightest once. For case β I assume that the brightest exposures all are subjected to the mean drop (fat black line) indicated by the statistics of the faintest with respect to the brightest exposures. The arrow and the dashed lines indicate the standard deviation from the mean.	62
4.2	The plot shows <i>from left to right</i> an SDSS image of the galaxies J1203, J0938, and J0347, a stars/point sources from the same SDSS frame for each object (coordinates are listed in Tab. 4.4) and the residuum that is left after subtracting the scaled star from the galaxy. The same plots for the other galaxies can be found in the next figure (4.3).	64
4.3	The same as Fig. 4.2 but for the other galaxies J1158, J0802, and J0911.	65
4.4	Results from the [Fe II] emission-subtraction. In the first plot, I present the spectrum of J034740.18+010514.0 together with a fit of the [Fe II] emission (yellow). In the second plot, shows the spectrum after subtraction of the [Fe II] emission.	72
4.5	The plot shows the fit of the H β and [OIII] emission line complex with multiple Gauss functions for J0347.	73

LIST OF FIGURES

4.6	The plot shows the optical spectrum of J0938 as observed by SDSS and LBT-MODS. The second row shows zooms into the spectrum in different regions. The third row shows the differences between SDSS and LBT spectrum in these regions, while the fourth row shows the ratios of these spectra.	75
4.7	The optical spectrum of J1203 and the result of calculating the difference and ratio of spectra from different epochs.	78
4.8	The same as Fig. 4.6 but for J1158.	80
4.9	The optical spectrum of J0911 and the result of calculating the difference and ratio of spectra from different epochs.	82
4.10	The optical spectrum of J0802 and the result of calculating the difference and ratio of spectra from different epochs.	83
4.11	The optical spectrum of J0354 and the result of calculating the difference and ratio of spectra from different epochs.	85
4.12	The optical spectrum of J0153 and the result of calculating the difference and ratio of spectra from different epochs.	87
4.13	The optical spectrum of J0347 and the result of calculating the difference and ratio of spectra from different epochs.	89
4.14	The variability percentage in the continuum. The data for the NLS1 sources ESO 012-G21, NGC 1365, and MKN 1044 are taken from Giannuzzo and Stirpe (1996) . The data for the BLS1 sources NGC 7603 and PKS 2349-14 are based on spectra from Kollatschny et al. (2000) and Kollatschny et al. (2006a) , respectively.	90
4.15	The variability percentage in the emission lines. The line measurements of ESO 012-G21, NGC 1365, and MKN 1044 are taken from Giannuzzo and Stirpe (1996)	90
4.16	Three epoch SDSS spectra for J014412 and J022205. These spectra allow us to derive variability estimates of $\Delta_{cont.}=0.18$ and $\Delta_{line.}=0.45$ for J014412 and $\Delta_{cont.}=0.27$ and $\Delta_{line.}=0.26$ for J022205. These values lie well above the low calibration uncertainties for the SDSS data (section 4.3).	98

4.17 The continuum variability plotted against the line variability. The solid and dashed black lines represent the relation $\Delta L_{line} = \epsilon(\Delta L_{cont.})^{\frac{3}{2}}$ (see text). The filled colored dots are QSO variability data ($H\beta$ and continuum) from (Kollatschny *et al.*, 2006b), (Peterson *et al.*, 2004), and (Kaspi *et al.*, 2000). The Black crosses represent the median values and their uncertainties as I derived them for my sample ($H\beta$ and other lines plus continuum) and as they are shown in Figs. 4.14 & 4.15. 100

5.1 The plot shows *from left to right* an SDSS image of the galaxies J0124, J0934, and J0728, a star as a point sources reference from the same SDSS frame for each object (coordinates are listed in Tab. 5.3) and the residuum that is left after subtracting the scaled star from the galaxy. 111

5.2 The optical spectrum of J0124 and the result of calculating the difference and ratio of spectra from different epochs. 113

5.3 The optical spectrum of J0934 and the result of calculating the difference and ratio of spectra from different epochs. 114

5.4 The optical spectrum of J0728 and the result of calculating the difference and ratio of spectra from different epochs. 116

5.5 Median variability percentage for continuum of the BAL quasars. 117

5.6 histogram for the redshift distribution of BALQSs of my samples.. . . . 117

LIST OF FIGURES

List of Tables

3.1	Photometric measurements of J0808 in the SDSS and WISE photometric systems.	39
3.2	Observed emission lines: wavelengths, redshifts, flux densities, and line widths	46
3.3	Radio flux density at different frequencies.	47
3.4	The rest radio flux densities and luminosities for source components of the J0808 radio counterpart at 18 cm.	52
4.1	Coordinates, redshifts, classification and observing parameters for all sources. .	66
4.2	Comparison of seeing conditions for the sources for which I analyzed the spectra.	67
4.3	The observed continuum flux density variability between LBT and SDSS/OHP of J0938, J1203, J1158, J0911, J0802, and J0347 from the photometry and spectroscopy aspect. ^(a) For J0347 first epoch spectroscopy obtained by OHP. . .	68
4.4	Comparison of the apparent sizes of the sources and reference stars in the field .	69
4.5	Continuum fits.	70
4.6	Median and median deviations for the variability in the continuum & emission lines.	88
4.7	The T-test statistic for the variability in the continuum & emission lines.	88
4.8	The variability percentage in continuum at rest wavelength 5100Å and H β , for AGNs taken from reverberation mapping (light curve).	92
4.9	The line fitting results for J0938, J1203, 1158, J0911, J0802, J0354, J0153, and J0347.	102
4.9	Continued.	103
4.10	Broad and narrow emission lines variability.	104
5.1	Coordinates, redshifts, classification and observing parameters for all sources. .	108

LIST OF TABLES

- 5.2 The continuum flux density variability between LBT and SDSS of J0124, J0934,
and J0728 from the photometry and spectroscopy aspect. 109
- 5.3 Comparison of apparent sizes of target galaxies and stars. 110

1

Introduction

Astronomy and Astrophysics are the sciences of celestial objects and phenomena that may happen outside the atmosphere of Earth. It includes planets and their moons, asteroids, comets, nebulae, stars, and galaxies including cosmology. Astronomy was established in ancient times and is now continued using astrophysical methods. In astrophysics we try to investigate and understand the physical processes that take place in outer space.

In this present work I will study a type of the celestial objects called galaxies. This is known to be a very broad topic, therefore, and to be more precise, I will focus on special type of galaxy named active galaxies. These are galaxies that host an active galactic nucleus (AGN) in their center. This type of sources is still not fully understood and many aspects of it still remain mysterious, e.g. dynamic, evolution, morphology ... etc.

The way to study these galaxies is through the electromagnetic emission that come from these objects. These emission is investigated across the entire electromagnetic spectrum searching for information such as luminosity, mass, gas density, temperature, chemical composition, morphology etc., to understand how these objects evolved. Many things have been discovered about the galaxies in the last decades due to the great development of telescopes. Therefore, many thanks to the creativity spawned by the modern sensitive monitoring instruments, which help us to observe deep in the sky and explore it. Nevertheless, galaxy formation, evolution, and other properties still require to be examined and fully understood. Collecting the data, testing, analyzing, and clarifying it, will help us to write new chapters of the story of galaxies. According to the most recent observations of the universe, the number of galaxies is exceedingly high. This number was estimated to be 1.7×10^{11} (Gott *et al.*, 2005), and each galaxy contains a huge number of stars, up to 10^{12} (Sparke and Gallagher, 2007). In general, a galaxy

1. INTRODUCTION

hosts a supermassive black hole (SMBH) in its center. When studied in detail, these galaxies appear to have a unique set of features. The best way to determine this set of features is to split these objects into sub-classes in which the physical properties are similar. In the following I will give a short list of possible subclasses:

1.1 Galaxies

Galaxies mainly consist of stars, interstellar matter, gas, dust, and dark matter. These objects can be found in groups (clusters) from few galaxies up to thousands, see Fig.1.1(a), connected to each other by gravitation, or they can be isolated like NGC 4662 in Fig.1.1(b). These circumstances establish the so-called environment which is scientifically confirmed to have an effect on a galaxy's morphology, mass, color, and other properties (e.g., Dressler, 1980; Whitmore *et al.*, 1993). Hubble and Humason (1931) were the first scientists who noted the effect of the environment on the morphology of the galaxies. In general, the most common interaction between galaxies known as fly-by leads to a disturbance or an exchange of gas and dust between the two objects or even to mergers.

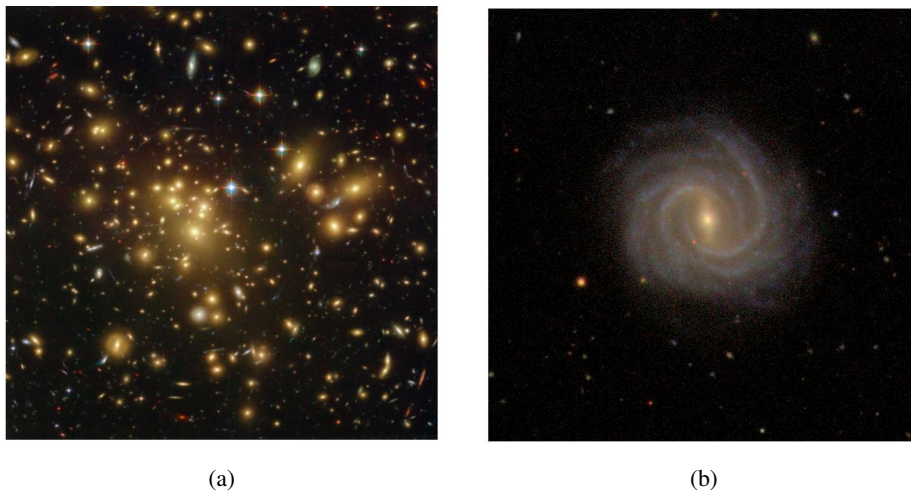


Figure 1.1: galaxies: (a) Galaxy cluster Abell 1689, observed by Hubble's Advanced Camera for Surveys. (b) SDSS color images of isolated spiral galaxy NGC 4662, take from isolated galaxies Catalog Karachentseva (1973).

Galaxies are studied and classified based on different physical properties such as visual appearance, size, age of the stellar population in the host, nuclear activity, mass, and color

...etc. In the thirties of the last century Hubble proposed a classification for the galaxies (Hubble, 1926a,b, 1927, 1936), depending on their appearance (see Fig. 1.2). Scientists still use this classification today. Hubbles scheme splits galaxies into into three main groups or types: ellipticals¹, spirals², and the last type of the classification is intermediate between the ellipticals and the spirals and is named lenticular. Furthermore, there is one more type of galaxies characterized by a non-regular shape named irregular galaxy.

The first two types of the classification splits into subtypes depending on the visual appearance as following (see Fig. 1.2): Ellipticals galaxies are divided into 7 subtypes (0 – 7), depending on the degree of ellipticity (e), where e is interpreted as the ratio between major (a) and minor (b) axis $e = 1 - \frac{b}{a}$. As for spiral galaxies the sub-classification is based on bar that extends from the central bulge (B) or the absence of a bar. For spiral galaxies the letters “a” through “d” refer to how tight the arms are around the bulge. “S0” referring to lenticular galaxies. “Irr” referring to irregular galaxy. The masses of these galaxies are³: 10^9 to $10^{12} M_{\odot}$ for spirals, 10^7 to $10^{13} M_{\odot}$ for ellipticals, while the masses of irregular galaxies are 10^8 to 10^{10} . Since the Hubble classification for galaxies is completely depending on visual appearance (morphology), consequently, this classification may miss an important features about the galaxies like the rate of the star formation in the starburst objects, as well as the activity in the centers of active galaxies.

1.2 Active galaxies

Active galaxies are galaxies that feature specific properties which are not exhibited in typical (normal) galaxies, like high luminosity, non-thermal emission (spectra), radiation in most wavelength bands (radio, microwaves, infrared, optical, ultra-violet, X-ray and gamma ray), high variability, and radio jets in most cases. These objects are hosting a very compact region at the center named Active Galactic Nucleus (AGN), where the most energetic activity is forced. It is usually believed that the active galactic nuclei host a supermassive black holes (SMBH) located at the center. This SMBH connecting the active galaxies to the non-stellar phenomena.

¹Elliptical galaxies refer to early-type galaxies (Baldry, 2008).

²Spiral galaxies refer to late-type galaxies (Baldry, 2008).

³The masses of the normal galaxies are taken from this site: <http://csep10.phys.utk.edu/astr162/lect/index.html>.

1. INTRODUCTION

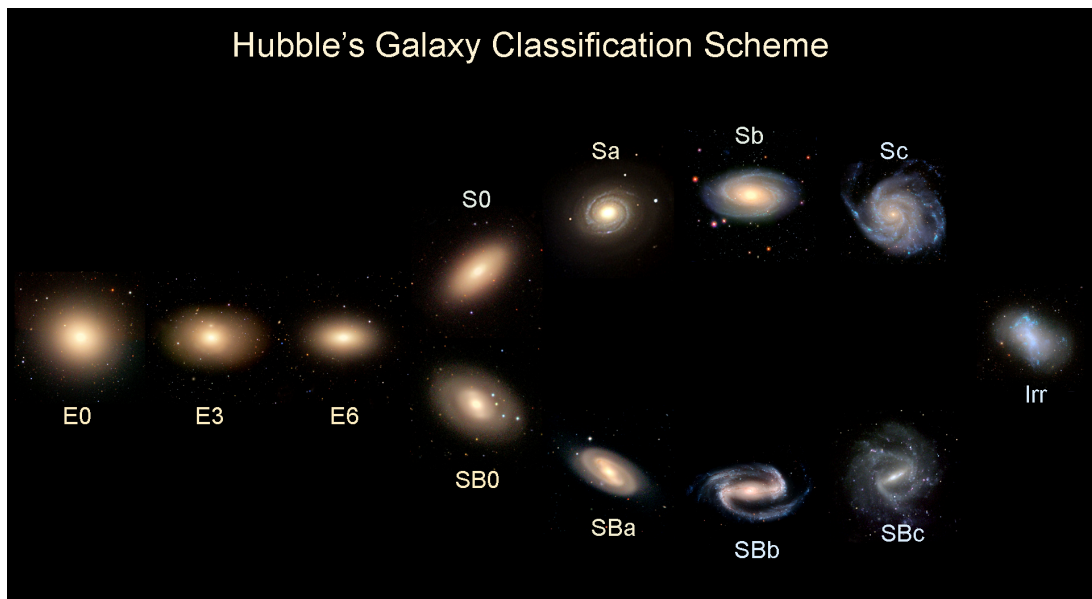


Figure 1.2: Hubble scheme. This image organized by Dr. John Kormendy, Department of Astronomy, University of Texas at Austin.

As I mention early in this section this kind of sources is characterized by a high luminosity, where the typical luminosity of active galaxies between $(10^{11}L_{\odot}$ to $10^{15}L_{\odot})$ ¹, while the luminosity of normal galaxies are $< 10^{11}L_{\odot}$, with respect that in general quasars are more luminous than Seyferts as shown in figure 1.3. Additionally, active galaxies exhibit strong (emission and absorption) lines in their spectra like forbidden lines (e.g. $[O\ II]$) and permitted lines (e.g. H_{β}). It is believed that the strong emission lines and the high luminosity are not caused by the stellar population of the host. It has been suggested that the strong emissions are caused by the accretion disk that is orbiting around the SMBH. The temperature in the disk can be characterized by a very high temperature that may reach levels of $\geq 10^5\text{K}$ because of frictional processes and non-thermal influences. The large distant of this sources from us adds more difficulties to spatially resolving and fully understanding them.

The spectral variability is one of the properties that features active galaxies. This variability can be shown in different wavelength bands (e.g. optical band as I will show in chapter four). Generally, active galaxies are divided into four main types as shown in figure 1.4.

- Seyfert galaxies.

¹The luminosity of the sun L_{\odot} is $3.846 \times 10^{32}\text{erg s}^{-1}$

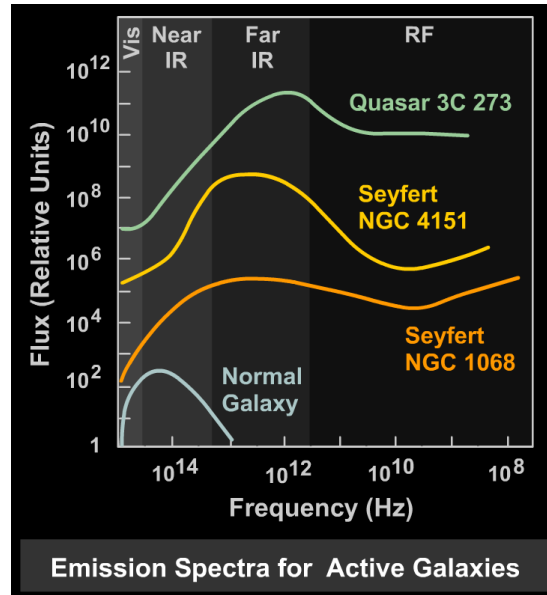


Figure 1.3: Several typical spectra of active galaxies and normal galaxy. Plot credit: Brooks/Cole Thomson learning.

- Quasars.
- Radio galaxies.
- Blazars.

It is believed that some of these types of active galaxies are intrinsically similar and their appearance is mainly due to the inclination of the galaxies with respect to the line of sight. For instance, Seyfert 1 and Seyfert 2 are believed to be the same type of galaxies (Choudhuri, 2010; Rodriguez-Pascual *et al.*, 1993), although the differences in properties, as shown in figure 1.5. Usually, active galactic nuclei consist of six main regions:

- Broad-Line Region (BLR)
- Narrow-Line Region (NLR)
- Dusty torus
- Jet (in most cases)
- Accretion Disc

1. INTRODUCTION

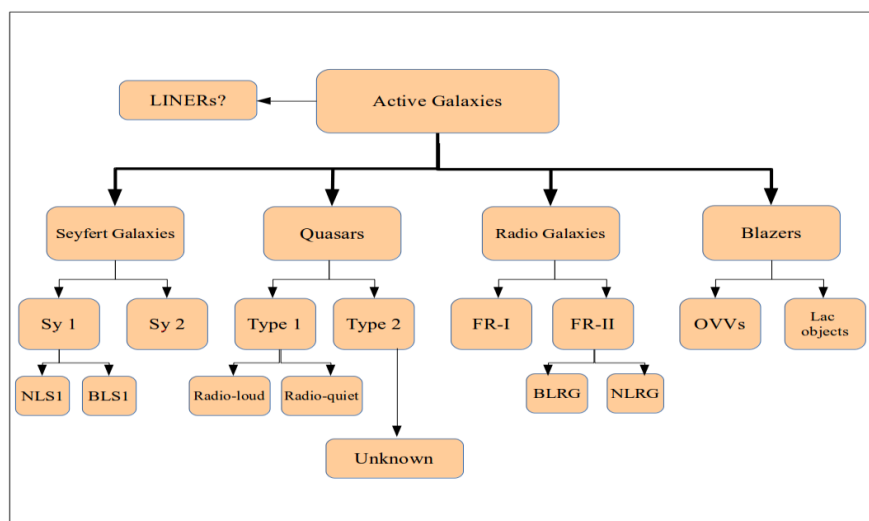


Figure 1.4: Active galaxies scheme. The layout of the scheme was designed by me.

- Super-massive Black Hole

Broad-Line Region (BLR): the BLR is the region that emits highly Doppler broadened lines. The broadening of these lines are due to the proximity of this region to the central massive black hole of the host as shown in figure 1.5. Furthermore, because of the radiation of the photo-ionizing continuum that comes from the AGN, the flux of these emission lines are variable and strongly correlated with the changes in the continuum intensity (e.g., [Peterson et al., 1984](#); [Rosenblatt et al., 1992](#); [Wanders and Peterson, 1996](#)). The variability of the recombination lines also suggest that the BLR is composed of optically dense clouds which are ionized by the nuclear radiation. The responding time of the BLR to the continuum variation is fast, implying that the mean distance of BLR clouds to the nucleus is determined to be approximately between light-days to light-weeks. The temperature in BLR can be estimated from the permitted lines to be $T \sim 35000$ K (e.g., [Osterbrock, 1991](#), and references therein). The radius of the BLR approximately is $(10^{11}$ km) and the speeds of clouds in this region are about 5000 km s^{-1} ([Jones and Lambourne, 2004](#)). This is consistent with the small distances at which the clouds orbit the SMBH.

Narrow-Line Region (NLR): is the area which is situated in the outer region of the torus. Narrow (forbidden and permitted) emission lines are generated in this region. NLR is extend from a few hundred parsecs to few kpc depending on the type of the active galaxies as shown

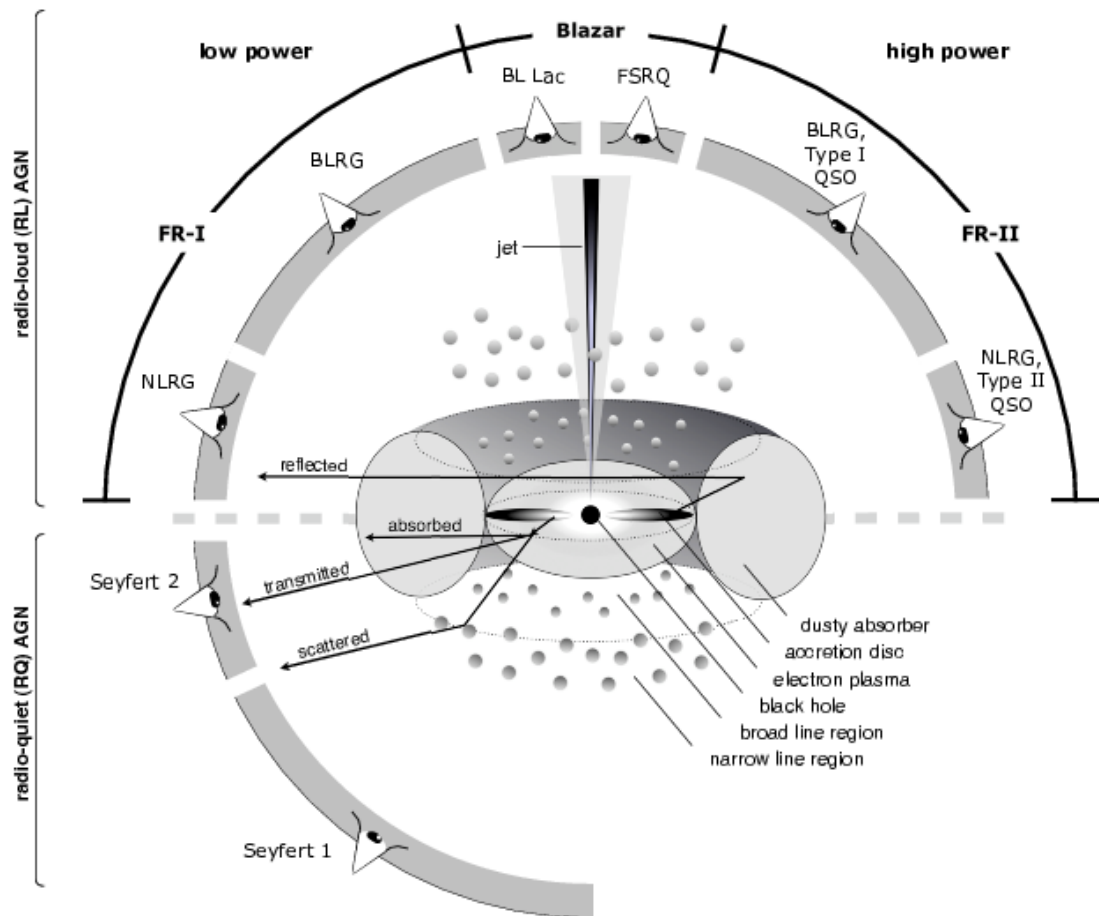


Figure 1.5: Structure of active galaxies Beckmann and Shrader (2012).

1. INTRODUCTION

in these formalis:

$$\text{Seyferts } \textit{Bennert et al. (2002)} : \quad R_{\text{NLR}} \propto L_{[\text{O III}]}^{0.52 \pm 0.06} . \quad (1.1)$$

$$\text{Quasars } \textit{Schmitt et al. (2003)} : \quad R_{\text{NLR}} \propto L_{[\text{O III}]}^{0.33 \pm 0.04} . \quad (1.2)$$

where $L_{[\text{O III}]}$ is the luminosity of $[\text{O III}]$. In general, the forbidden emission lines (e.g. $[\text{O III}]$, $[\text{O II}]$, and $[\text{O I}]$) originate gas much lower in density than the BLR clouds. To explain this difference in the densities in more details: the collision rates of atoms in the forbidden lines are low and the excited states can de-excite via radiation. Also the orbital velocities in this region are much smaller. This leads us to the concept of that there are commonly no broad components in the forbidden and permitted emission lines in the NLR.

The gas temperature in the NLR is $\approx 10^4 K$. The NLR gases are excited by shocks and the nuclear continuum emission. The torus is partly covering the clouds of gas, but the clouds that are directly below or above the level of the torus have a straight line of sight to the nucleus, consequently, the clouds in the NLR are ionized. Finally, for the closest active galaxies the outer parts of NLR are spatially resolvable, unlike the BLR (please check figure 1.5).

Torus: The accretion disc of the active galaxies are surrounded by dust and warm molecular gas in a shape of a “doughnut” as presented in figure 1.5. This region is named torus and it’s wide enough to cover the BLR and obscure it. However, the torus is not wide enough to cover all the NLR, which makes the NLR is resolvable for us in both types of Seyferts. The torus contributes effectively in the AGN activity: First, it’s stores the material for the accretion disc into the SMBH, to be more precise, torus is the active operator feeding the accretion disc towards the BH (*Hopkins et al., 2012*). Second, the central engine of the host is obscured by the torus: when the orientation is face-on, the observer will have a view of the central engine. This type of sources are AGN of Type I. When the orientation is edge-on, the view across the center is obstructed by the torus. In this case the sources are AGN of Type II (*Villarroel and Korn, 2014*).

Jets: Jets are fast highly collimated and energetic outflows from the center of the active galaxies spanning a few kilo-parsecs to a few mega-parsecs. It is connected with the central massive black hole and the accretion disk. The observing angle of the jets are not only important to explain the variability differences between the two kinds of Seyferts. It can explain the appearance of the Blazars. Depending on the unified model, AGN may appear as Blazars if the

jet of the galaxy is very close to the line of sight. This is illustrated in the results of studies of the polarization, the high luminosity, as well as the rapid variability of Blazars.

Accretion disc: An accretion disk is a flattened structure of material rapidly orbiting the SMBH at the center of the host. Signs of relativistic rotation close to the center give us an indication that strong gravity is at work there. This is the direct influence of the supermassive black hole at the center of the host. If the isotropic luminosity increases the isotropic infall of new material to be accreted is blocked. The maximum amount of luminosity that can be produced by isotropic accretion is therefore limited. This limit is named Eddington luminosity and given by this formula (Rybicki and Lightman, 1979):

$$L_{Edd} = \frac{4 \times \pi \times G \times M \times m_H \times c}{\sigma_T}, \quad L_{Edd} \cong 1.26 \times 10^{31} \left(\frac{M}{M_\odot} \right) W \quad (1.3)$$

where G is the gravitational constant, M is the mass of the gravitating object, c is the speed of light, m_H is the mass of the hydrogen atom¹, σ_T is the Thomson cross section². The Eddington limit is linked to the accretion efficiency and connects the observed AGN isotropic radiation output with that generated by maximum spherical accretion.

Super-massive black hole (SMBH): An SMBH is an important part of the central engine of the galaxies. This area exhibits a very strong gravitational attraction, which will not allow any particles or electromagnetic radiation to escape from it. One of the best cases for the existence of a SMBH at the center of a galaxy is Sagittarius A* with a total mass of about 4 million solar masses (A^*) (e.g., Eckart and Genzel, 1996; Eckart *et al.*, 2004, 2013). In general masses of the SMBHs are $\gtrsim 10^5 M_\odot$ (Reis *et al.*, 2012).

1.2.1 Seyfert Galaxies

Seyfert galaxies are one of the main kinds of active galactic nuclei (AGNs) in which the nuclei are dominated by a very powerful SMBH. Seyfert nuclei are 10 to 100 times brighter than their own host galaxies they are residing in. Consequently, these nuclei are responsible for most activities that occur within the central 10-100 pc of these hosts.

Seyferts classified as Type I or II in 1943 by Carl Seyfert, based on the appearance of the emission lines in their spectra (Seyfert, 1943). In 1987 Osterbrock develop the Seyferts classification into subclasses such as Seyfert 1.8 and 1.9, depending on the intensity of the emission

¹ $m_H = 1.6727 \times 10^{-24}$ kg.

² $\sigma_T = 6.65 \times 10^{-25}$ cm².

1. INTRODUCTION

lines of Balmer series in the optical spectrum (e.g., [Osterbrock, 1987](#), and references therein). Depending on the width of the emission lines, one distinguishes between two main categories, Seyfert-1 (S1) and Seyfert-2 (S2): S2 galaxies show only narrow lines ($\lesssim 1000 \text{ km s}^{-1}$), while S1 show additional broad components ($\lesssim 10\,000 \text{ km s}^{-1}$) in the permitted lines as shown in Fig. 1.6¹. As I presented above, there is a large variety in the forbidden and permitted emission lines of active galaxies, which can have widths up $\sim 10\,000 \text{ km s}^{-1}$ that are caused by Doppler broadening. The emission lines are commonly believed to stem from the “broad line region” (BLR) and the “narrow line region” (NLR), that are gas clouds orbiting a central super-massive black hole (SMBH) at very high velocities. The gas clouds are excited by continuum radiation that is produced by an accretion disk of material infalling the central SMBH. According to the unified model (e.g., [Antonucci, 1993](#); [Urry and Padovani, 1995](#)), the existence of S1 galaxies which show broad and narrow lines and S2 galaxies which show only narrow lines can be attributed to inclination effects. One possible scenario to explain the differences between S1 and S2 galaxies is a dusty torus which surrounds the accretion disk and the BLR. It obscures the emission from the BLR if the galaxy is observed with a viewing angle parallel to the torus plane.

Narrow-line Seyfert-1 (NLS1) galaxies are S1 galaxies that show broad components with comparably narrow widths ($\lesssim 2000 \text{ km s}^{-1}$). From an observational point of view it appears that there are two main differences between S2 and narrow line S1 galaxies (NLS1). The first one is that NLS1 objects have Fe II in their spectra (which originate in the BLR) and are absent in the S2 spectra ([Giannuzzo and Stirpe, 1996](#)). The second difference is that some NLS1 sources show strong lines of highly ionized iron in their spectra e.g. [Fe VII] $\lambda 5721 \text{ \AA}$ and [Fe X] $\lambda 6375 \text{ \AA}$ ([Osterbrock, 1985](#); [Osterbrock and Pogge, 1985](#)), these lines are rare and not typical for the S2 spectra.

1.2.2 Quasars

Quasi-stellar (QSO) radio sources (Quasars) belong to the most powerful, energetic, luminous, and remote members of the AGN sources. Due to the large distances towards the QSOs they look similar to stars (point source) in contrast to more extended objects like galaxies. For this reason they are called “quasi-stellar”. Their redshifts of these sources are high and they are

¹Figure credit: <http://www.uni.edu/morgans/astro/course/Notes/section3/new13.html>.

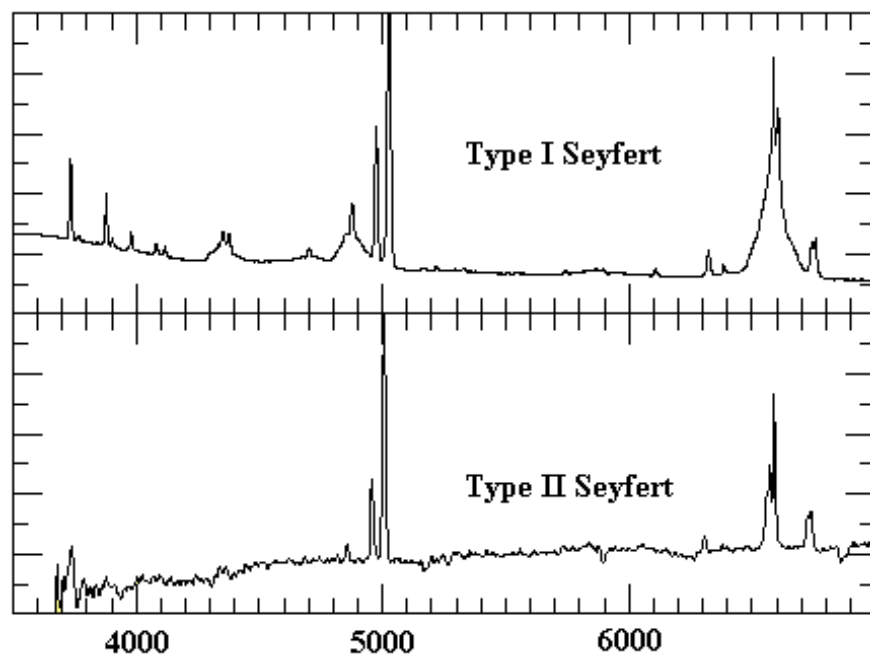


Figure 1.6: Optical spectra for the two types Seyferts: (Top) shows a spectrum for Seyfert 1 with broad and narrow emission lines, (Bottom) shows a spectrum for Seyfert 2 with just narrow emission lines.

1. INTRODUCTION

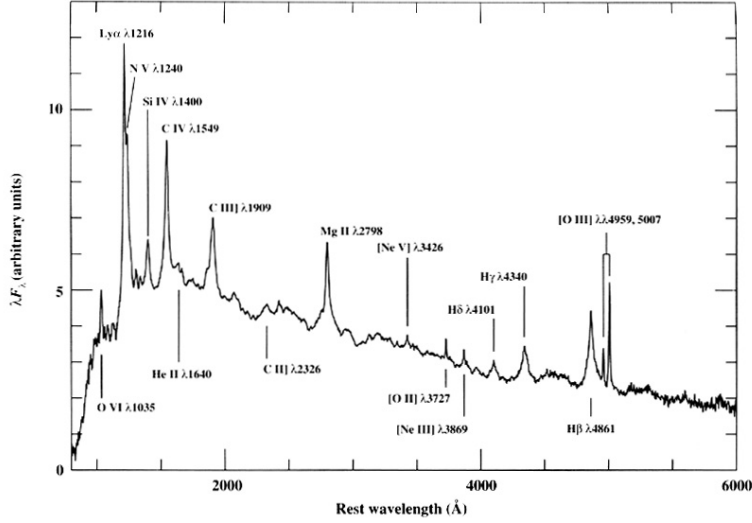


Figure 1.7: A typical QSO spectrum.

mostly distributed at $z \sim 2$ (Hewitt and Burbidge, 1993). Their spectra present very broad emission and absorption lines as shown in Fig. 1.7. This figure shows a typical QSO spectrum. It represents a mean spectrum of 700 QSO taken by the Large Bright Quasars Survey (Francis *et al.*, 1991), presented by Peterson (1997). Generally, quasars split into two class: Type-I quasars, with soft X-ray nuclei and broad lines in their spectra. This type splits again into two subtypes: Radio-loud and Radio-quiet. Type-II quasars, which appear as hard X-ray absorbed nuclei. This type is not yet studied very well. The luminosities of quasars ranges approximately between 10 to $10^5 L_{MW}$ ¹. The quasars luminosity can be calculate using the apparent brightness of the quasar and the distance through this formula (Greenstein, 2013):

$$f = \frac{L}{4 \times \pi \times R^2} \quad (1.4)$$

where L is the luminosity of the quasar, f is the apparent brightness, R is the distance.

1.2.3 Radio galaxies

Radio galaxies are active galaxies that are highly luminous in the radio part of the electromagnetic spectrum: up to $\geq 10^{45}$ erg s^{-1} , while our Milky Way radiates up to 10^{37} erg s^{-1} and the

¹ L_{MW} is the luminosity of the Milky way, where the luminosity of the Milky way is $25 \times 10^{12} L_{\odot}$
http://www.astronomy.ohio-state.edu/~ryden/ast162_8/notes36.html

usual luminosities for starburst galaxies or Seyferts are up to 10^{40} erg s⁻¹ (Burke and Graham-Smith, 1997). The radio radiation from these objects is synchrotron emission. It is a broadband and highly polarized spectra characteristic of these sources. These sources generally are typical elliptical giant galaxies with a jet linked to the supermassive black hole and an accretion disk at the center (e.g., Cao, 1995; Coroniti, 1985; Lovelace *et al.*, 1991). Sometimes, a special back-flow phenomenon can happen along the jet, causing radio galaxies (XRGs) with an X-shaped appearance. These are a special type of radio galaxies with two pairs of lobes, one is active and bright pair and the second is fainter and more diffuse pair (Leahy and Williams, 1984). For a radio galaxy to be classified as an XRG, it needs to have the two pairs of jets strongly misaligned and flowing from the center of the source as shown in figure 1.8; the minor pair must flow in another direction as the major pair, otherwise it would be double-double radio galaxy (DDRG; e.g., Brocksopp *et al.*, 2011, and references therein).

Mainly, the structure of radio galaxies consists of:

- Lobes: the large-scale shapes look like lobes. They are double and mostly symmetrical located away from the core and often contain hot-spots;
- Jets :a beam out-flowing from the center of the galaxy, produced by the accretion disk and the massive black hole at the center;
- Plume: a low luminous structure extended from the jets;
- Core : is the nucleus of the host and is often (frequency dependant) the brightest part of the source coinciding with the location of the SMBH.

Later I will clarify the existence of Lobes and Plumes in radio galaxies, depending on the type of the object. In the 1974 two scientists, Bernie Fanaroff and Julia Riley, divided the radio sources into two types depending on their appearance, structure, and luminosity. These source classes are known now as Fanaroff and Riley Class I (FRI), and Class II (FR II) (Fanaroff and Riley, 1974). The FR-II sources can be split like Seyfert objects into two types depending on the broadening of the emission lines in their spectra. They are called broad line radio galaxies (BLRGs) because of the broad components in their spectra, and they are called narrow line radio galaxies (NLRGs) because of their emission lines in their spectra that are narrow like in Seyfert 2 galaxies (Véron-Cetty and Véron, 2000). Generally, the morphology of BLRGs are N type, with bright nuclei surrounded by diffuse and faint envelopes. Most of these NLRG

1. INTRODUCTION

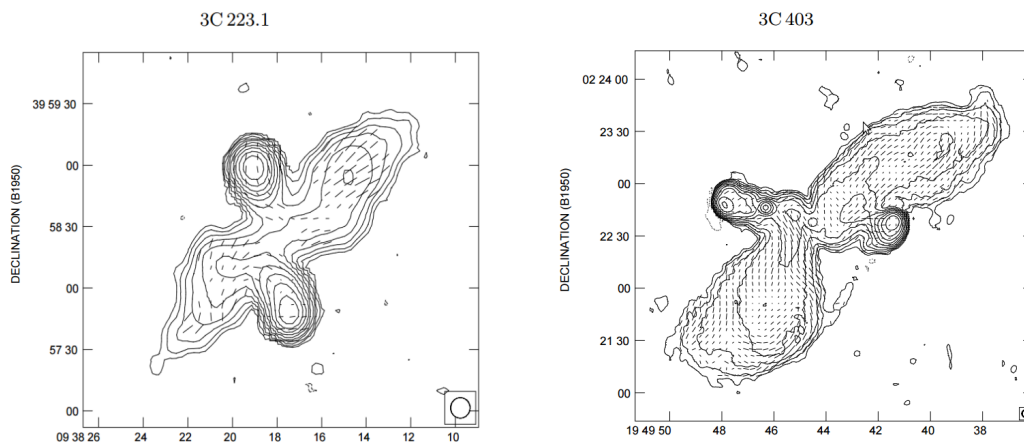


Figure 1.8: X-shape radio galaxies (3C403 and 3C223.1) observed by NRAO VLA, presented by [Dennett-Thorpe *et al.* \(2002\)](#).

sources are giant elliptical galaxies ([Osterbrock and Ferland, 2006](#)), with morphologies of cD, D, or E types.

1.2.3.1 Fanaroff-Riley type I (FR-I)

In this type of radio galaxy the low luminous regions are remote from the brightest region which is the center of the source as shown in figure 1.9. About 80% of the FR-I show jets ([Kembhavi and Narlikar, 1999](#)), and almost the same percentage is present in FR-II sources ([Hardcastle *et al.*, 1998](#)). These jets are expansions towards the two sides of the core. They get very quickly broader towards larger distances from the core forming a plume. As I mention before the brightness in this area is the lowest, but the spectra here are very steep, due the old relativistic particles that radiate in this region ([Kembhavi and Narlikar, 1999](#)). Furthermore, near to core of host, at distances of < 1 kpc - jets can be just one-sided ([Bridle and Perley, 1984](#); [Laing *et al.*, 1999](#); [Parma *et al.*, 1987, 1994](#)), but at larger distances (a few kpc) they have the tendency to become two-sided and extended.

Radio galaxies are associated with different radio luminosities. [Fanaroff and Riley \(1974\)](#) found that FR-I objects are less luminous than FR-II, where the typical luminosity of FR-I at 178 MHz ([Kembhavi and Narlikar, 1999](#)) and 1.4 GHz ([Schneider, 2006](#)) are:

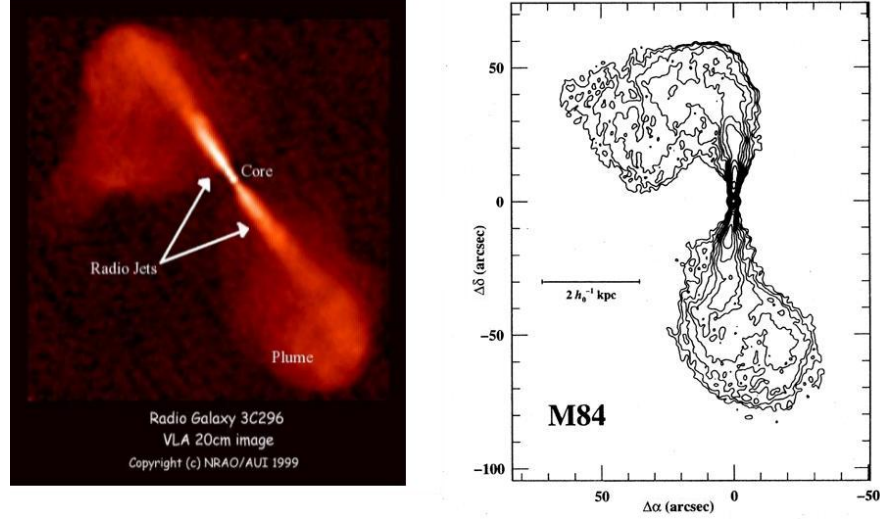


Figure 1.9: FR-I radio galaxies, where the left one is (3C 296) taken by VLA 20cm Leahy and Perley (1991), and the right one is Radio map of FR-I (M84) obtained by VLA at 4.9 GHz Laing and Bridle (1987).

$$L_{178\text{MHz}} \leq 2 \times 10^{25} h_{100}^{-2} \text{ W Hz}^{-1} \text{ Str}^{-1}$$

$$L_{1.4\text{GHz}} \lesssim 10^{32} \text{ erg s}^{-1} \text{ Hz}^{-1} .$$

1.2.3.2 Fanaroff-Riley type II (FR-II)

What distinguishes this type of radio galaxy from the FR-I sources is the existence of the hotspots in their lobes as shown in figure 1.10, as well as the presence of a one-sided jet. This one-sided jet is typical and a noticeable characteristic feature for FR-II sources. In 80% of FR-II galaxies one detects jets close to the core Hardcastle *et al.* (1998). The jets and the cores in FR-II are brighter than those of FR-I sources. These objects are also called edge brightened and the luminosities of these sources are higher than for FR-I sources. The radio luminosity L_ν of FR-II sources at (178 MHz (Kembhavi and Narlikar, 1999) and 1.4 GHz (Schneider, 2006)) are:

$$L_{178\text{MHz}} > 2 \times 10^{25} h_{100}^{-2} \text{ W Hz}^{-1} \text{ Str}^{-1}$$

$$L_{1.4\text{GHz}} \gtrsim 10^{32} \text{ erg s}^{-1} \text{ Hz}^{-1} .$$

1. INTRODUCTION

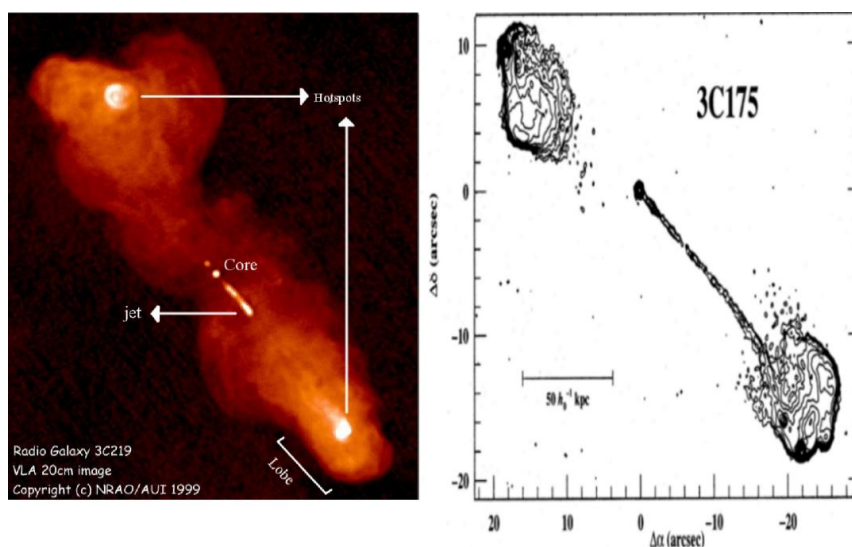


Figure 1.10: FR-II radio galaxies, where the left one (3C 219) taken by VLA at 1.4 GHz [Clarke *et al.* \(1992\)](#), and the right one is Radio map of FR-II (3C 175) obtained by VLA at 4.9 GHz [Bridle *et al.* \(1994\)](#).

Regarding the large variety of environments of FR-I and FR-II objects and their host galaxies, this implies that there are essentially two different kinds of galaxies that are not connected via an evolutionary sequence (e.g., [Gendre *et al.*, 2013](#), and references therein). The FR-II environment does not present an enhanced clustering of galaxies within the environment of these elliptical host galaxies if randomly selected ([Best, 2000](#); [McLure and Dunlop, 2001](#); [Prestage and Peacock, 1988](#)).

1.2.4 Blazars, OVVs, and BL Lac objects

Some active sources show strong and faster variability in their spectra (radio and optical). Because of the synchrotron influences, the radiation of these objects have high degree of linear polarization. These types of sources are named “blazars” and it is thought that they are a very compact, radio-loud subtype of quasars. A rare subclass of Blazars is called optically violent variables quasar (OVVs) OVVs are strongly variable sources up to $\gtrsim 0.5$ mag in few days ([Schramm *et al.*, 1994](#)). BL Lacertae objects (or BL Lac objects) are a class of active galaxies lacking any strong emission or absorption lines in their optical spectra ([Peterson, 1997](#)). There are some mutual properties in BL Lac objects and OVV objects, and that give us an impression that both of these sources are linked to Blazars.

1.3 Broad absorption line quasars (BALQSO)

Many quasars show broad absorption lines (BALs) in their spectra. The percentage of these sources is approximately 15%, with highly ionized ions such as N v λ 1238, C iv λ 1544, Si iv λ 1396, Ly α λ 1213 (Zhang *et al.*, 2010). This is indicative for a strong UV radiation field. These kinds of sources have high velocity outflows that seem to be present in all quasars and could be the main reason of feedback for galaxy evolution (Capellupo *et al.*, 2011). Also these high velocity outflows gases are responsible for creating the broad absorption lines (troughs)(Trump *et al.*, 2006). BALs in the spectra of quasars are thought to be generated by material in a wind, which is mostly created near the central accretion disk and shows radially growth at some position at top of an optically thick torus (e.g., Chiang *et al.*, 1994; Higginbottom *et al.*, 2014; Proga and Kallman, 2004). These lines by definition exhibit velocity widths determined to be $> 2000 \text{ km s}^{-1}$ at absorption depths > 10 per cent from the continuum of spectra (Weymann *et al.*, 1991). These absorptions and exist at shorter wavelengths than the emission lines of the same species. These absorption lines likely exist in 10-15 % of quasars (Gibson *et al.*, 2009; Reichard *et al.*, 2003; Trump *et al.*, 2006). BALQSOs have similar properties comparable to typical BLS1, but the last type have rather high X-ray to optical flux ratios $\left(\frac{S_{1\text{keV}}}{S_{2500\text{\AA}}}\right) \approx 10$ (Elvis *et al.*, 1994), while BALQSOs are typically rather faint in the X-ray domain (Green and Mathur, 1996).

In general, BAL quasars have been classified into two types, high-ionization, low-ionization. But sometimes the low-ionization quasars present a strong character of iron emission-lines features in their spectra. Consequently, these objects are named iron-low-ionization quasars, as I will explain in details in the next three subsection.

1.3.1 HiBAL

The high-ionization BAL (HiBAL) quasars are related to highly ionized species like C iv λ 1548, 1550, N v λ 1238, 1242, and Si iv+O iv λ 1398¹ (Montenegro-Montes *et al.*, 2008). This type is the most common QSO subtype in the universe, where the percentage of HiBAL quasars is 10% (Becker *et al.*, 2000) (see Fig1.11(a)).

¹All wavelengths are in \AA

1. INTRODUCTION

1.3.2 LoBAL

The second type of BALQSOs is named low-ionization BAL (LoBAL) quasars, and is related to low ionized species like $\text{Mg II } \lambda 2799$ and $\text{Al III } \lambda 1856$ (Montenegro-Montes *et al.*, 2008; Voit *et al.*, 1993). They exhibit the above high-ionization absorptions in addition to absorption in Mg II and another low-ionization emission lines (Hall *et al.*, 2002). These types of objects are rarer and less common in the universe. They account for about 1% of the QSOs (Becker *et al.*, 2000) (see Fig1.11(b)).

1.3.3 FeLoBAL

FeLoBAL objects are subclass of LoBAL. This type of QSO has the same lines like LoBALs but it presents (low & high) ionization troughs in their spectra. In addition they show absorption lines of excited states of Fe II , Fe III or both lines (Becker *et al.*, 1997) (see Fig.1.11(c)). Moreover, FeLoBALs are also rare in universein and account for about 1% of the QSOs, and that makes this particular type of objects very interesting for detailed investigations.

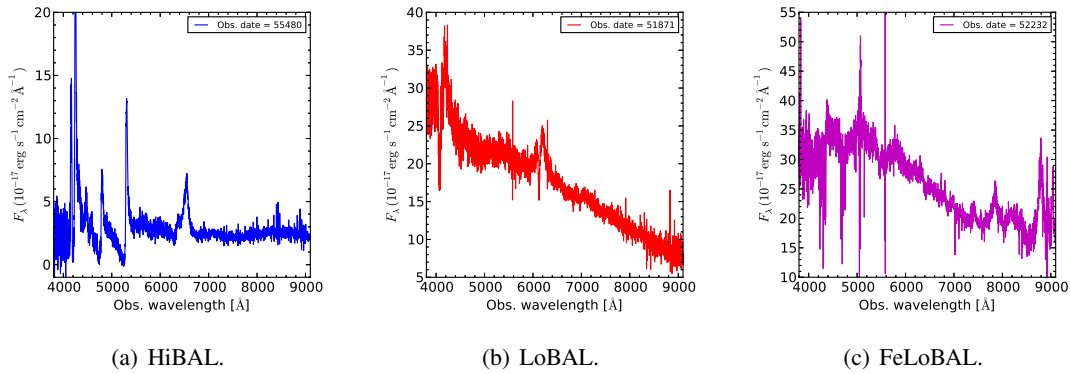


Figure 1.11: BALQSOs spectra for different types.

1.4 LINERS

Low-ionization nuclear emission-line regions (LINER) are galaxies that have spectra similar to those of Seyferts 2 (narrow component), but with bright low ionized lines. This type of sources has been recognized by Heckman (1980). The classification of this type of galaxies it not fully clear so far. The connection between an AGN (cenrral SMBH) and the LINER spectrum is not understood enough to put the LINERs in the section of active galaxy. In figure

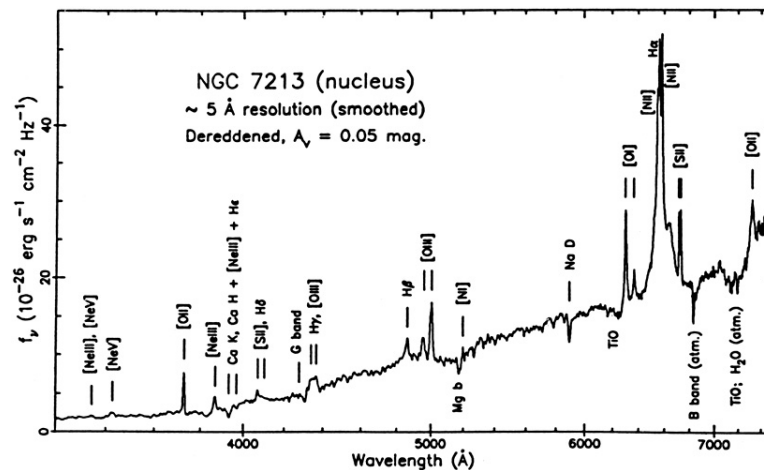


Figure 1.12: An optical spectrum for the LINER galaxy NGC 7213.

1.12 I present an optical spectrum for the LINER NGC 7213 (Filippenko and Halpern, 1984). One of the difference between the LINERs optical spectra and the spectra of Seyferts is: the line ratio of $\left(\frac{O_{III}\lambda 3727 \text{ \AA}}{O_{III}\lambda 5007 \text{ \AA}}\right) \approx 1$, while for Seyferts 1 this ratio is ≤ 0.5 . Furthermore, the emission line $[O I]\lambda 6300 \text{ \AA}$ is very strong, while the emission lines Ne v and Fe VII are not detectable in the LINERs spectra (Blandford *et al.*, 1990). Finally, LINERs hosts are though to be spiral galaxies.

1.5 variability

Active galaxies exhibit a very prominent variability at different wavelengths such as (optical, radio, and X-ray). Investigating this variability will help us to have an initial estimate of the size and structure of the regions that generating this variable radiation. Additionally, studying the variability of active galaxies is a very beneficial approach to understand the evolution of these sources. One of the benefits of the analysis of the spectroscopic variability of active galaxies is to outline the differences between different Seyfert source classes. Furthermore, variability will give us an indication about how the AGN influences the surrounding regions (BLR and NLR) and how these regions vary with time. Many important results have been obtained from AGN samples of different types and sizes. A famous one is anti-correlation between the continuum luminosity and variability, which was first mentioned by Angione and Smith (1972). Additionally, variability has been attracting attention of the astronomers since

1. INTRODUCTION

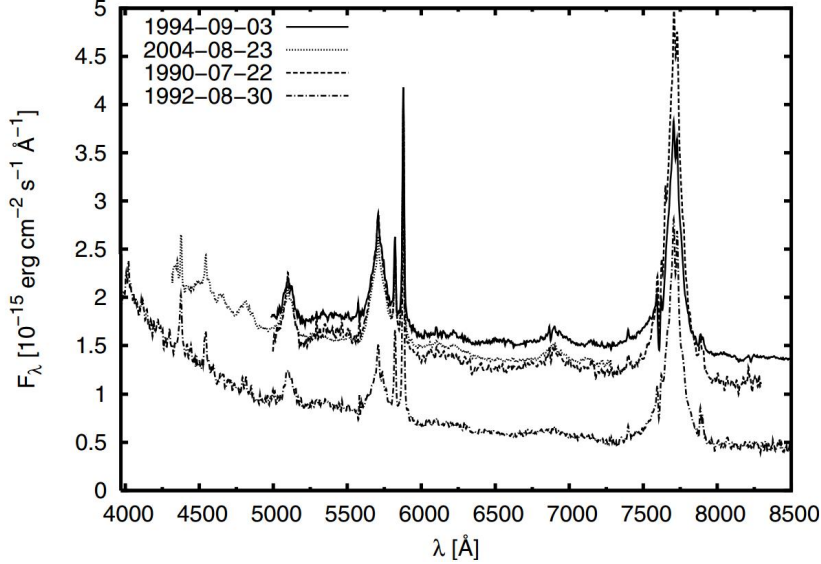


Figure 1.13: Long time scale spectroscopic variability of BLS1 PKS 2349-14. These spectra have been taken between 1990 till 2004. From 1990 – 1994 observed by Calar Alto Observatory, The 2004 spectrum stems from a monitoring program with the Hobby-Eberly Telescope (Kollatschny *et al.*, 2006a).

the sixties of the last century. Such studies are always limited by the capabilities of astronomical instruments. Smith and Hoffleit (1963) found that there is weak variability in the radio galaxy 3C273. Finally, short time scale variability can happen in hours or days in some sources such as OVV, or variability can happen on longer time scales of months or years such as Seyferts or Quasars. In Figure 1.13 I show an example for long time scale spectroscopic variability of BLS1 PKS 2349-14 (Kollatschny *et al.*, 2006a).

1.6 Diagnostic Diagrams

In general diagnostic diagrams play an important role in astrophysics. A three astronomers in 1981 (Baldwin, Phillips, and Terlevich) put forwards the concept of three diagnostic diagrams depending on emission lines ratios, to determine the dominant excitation in emission lines galaxies. Such an analysis helps to distinguish between the emission lines that are produced in star formation regions and other objects like AGN (Baldwin *et al.*, 1981). These diagrams are usually known as Baldwin, Phillips, and Terlevich diagrams (“PBT diagrams”), and depend on optical emission lines ratios of four lines: $(\frac{[\text{O III}] \lambda 5007}{\text{H}\beta}, \frac{[\text{N II}] \lambda 6583}{\text{H}\alpha}, \frac{[\text{O I}] \lambda 6300}{\text{H}\alpha}, \text{ and } \frac{[\text{S II}] \lambda 6716, \lambda 6731}{\text{H}\alpha})$.

1.6 Diagnostic Diagrams

In 2006 Kewley and others developed these diagrams to be more precise about the classification of galaxies, by adding a theoretical "maximum starburst line" on the BPT diagrams by utilizing a collection of stellar population combination samples and detailed self-consistent photo-ionization samples, as presented in figure 1.14 (Kewley *et al.*, 2006).

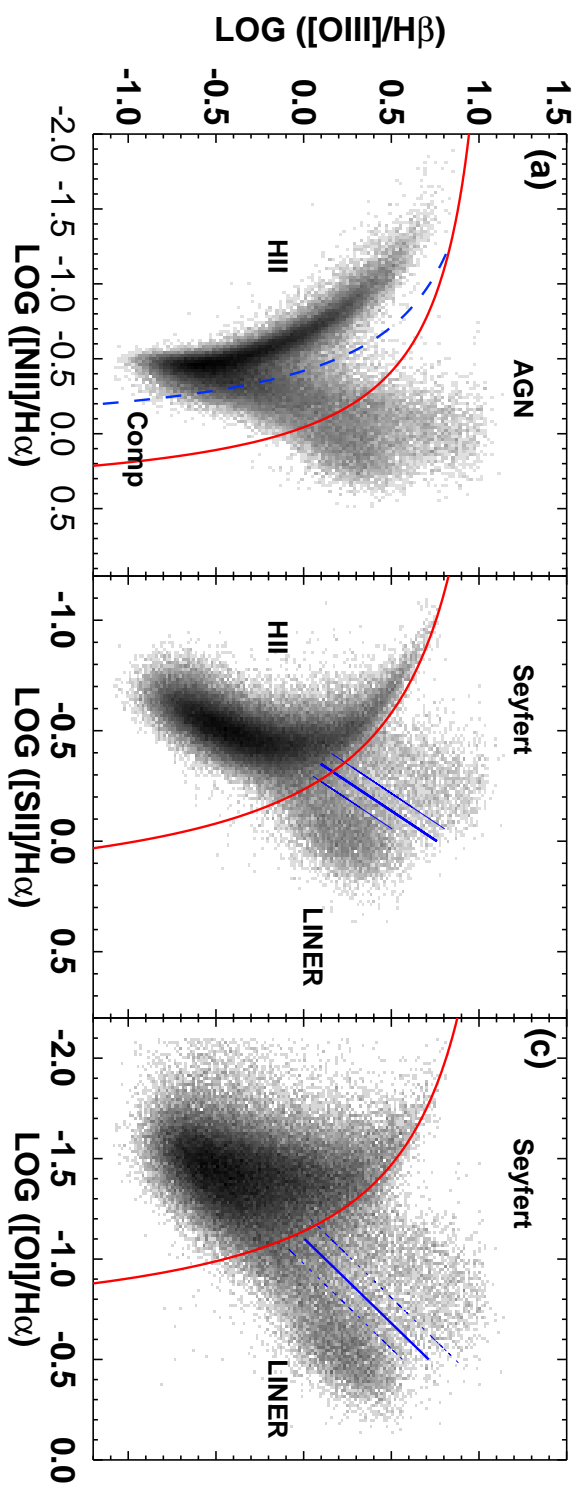


Figure 1.14: PBT diagrams.

2

Instrumentation and Data Reduction

In this chapter, I will talk about three main points:

- Radio and Optical instruments.
- Data reduction and calibration.
- Public astronomical Survey.

2.1 Radio and Optical instruments

In this section I clarify the instruments (radio and optical) that I used to study the astrophysical objects in this thesis.

2.1.1 MERLIN Radio telescopes

Radio interferometry is an essential technique that allows us to obtain high angular resolution images of radio sources. For studies of arcsecond to arcminute scale structures 'local' interferometers are important. Here the stations are linked via cable, microwave-link, or optical fiber. The Multi-Element Radio Linked Interferometer Network (MERLIN) is an interferometric array of seven radio telescopes (Mark II, Lovell Telescope, Defford, Darnhall, Cambridge, Knockin and Pickmere) distributed across England with baselines up to 217 km length as present in Fig. 2.1. MERLIN observes at frequencies between 151 MHz and 24 GHz. The MERLIN observation allow for an angular resolution of less than one arcsecond. MERLIN was upgraded to e-MERLIN by adding new instrumentation and fiber links (replacing the previous radio links) at Jodrell Bank Observatory (JBO). This upgrade is prepared to improve the

2. INSTRUMENTATION AND DATA REDUCTION

sensitivity and data quality of MERLIN by more than an order of magnitude. This is achieved by involving the new instrumentation together with an optical fiber network connecting all telescopes with a bandwidth of 30 Gb/s. The capabilities of the new array are: the resolution will be up to 150 milliarcseconds, the sensitivity will be $\approx 1\mu\text{Jy}$. This array will be used in astrometry, polarimetry, and spectroscopy¹. One of the achievements of the MERLIN array is the co-discovery of the first Einstein ring with the Hubble Space Telescope.

2.1.2 The Large Binocular Telescope and Multi-Object Double Spectrograph

In order to observe faint extragalactic objects it is essential to have as much collecting area as possible. Therefore the 8-10m diameter class optical/infrared telescopes are important for this kind of research. The Large Binocular Telescope (LBT) is an optical observatory placed in Mount Graham, southeastern Arizona, USA, at an altitude of 3200m. LBT is designed to have two identical telescope mirrors placed side-by-side as shown in Fig. 2.2², the diameter of each mirror is 8.4 m. If they are independently used as a binary instrument, the effective aperture will increase to 11.8 m. With these capabilities LBT can be considered to be one of the world's most developed optical telescopes.

Spectroscopy allow us to obtain wavelength dependant information of the sources under investigation. hence we can study emission and absorption line of atoms and molecules and learn about the composition and temperatures etc.. In addition to this - via the Doppler effect - important information on the velocity structure of the sources can be obtained - both the redshift (i.e. the distance to the source) as well as the internal motions within the source can be studied. Each of these two telescope have a spectrograph named the Multi-Object Double Spectrograph (MODS1 and MODS2). In September 2011 MODS1 began the routinely perform service operation for astrophysical observations. While MODS2 started its science service at the end of 2014. In my study I used MOSD1. In the following I give more information about this Spectrograph. It operates between 3200 and 10500Å at a nominal spectral resolution of $\lambda/\delta\lambda \approx 2000$ (i.e., $\sim 150 \text{ km s}^{-1}$). Its field of view is about 6×6 arc-minutes². Furthermore, imaging, long-slit, and multi-object spectroscopy can be used in this instrument, with a slit

¹<http://www.jodrellbank.manchester.ac.uk/e-merlin/>.

²The Figures credit

Left <http://http://www.jpl.nasa.gov/news/news.php?feature=4450;>

Right http://news.bbc.co.uk/2/hi/in_depth/629/629/7068860.stm.

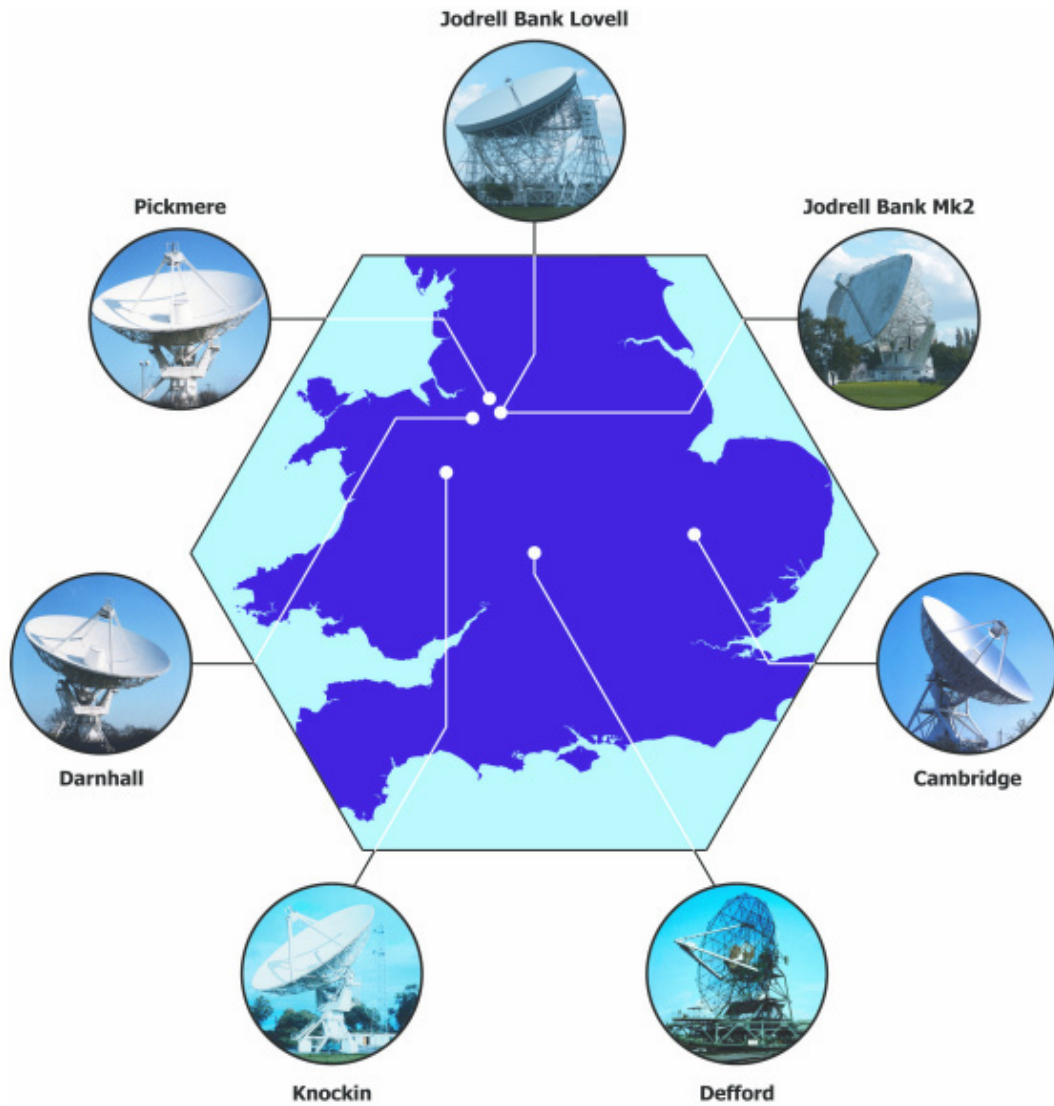


Figure 2.1: Merlin array. Image credit: <http://www.merlin.ac.uk/>.

2. INSTRUMENTATION AND DATA REDUCTION

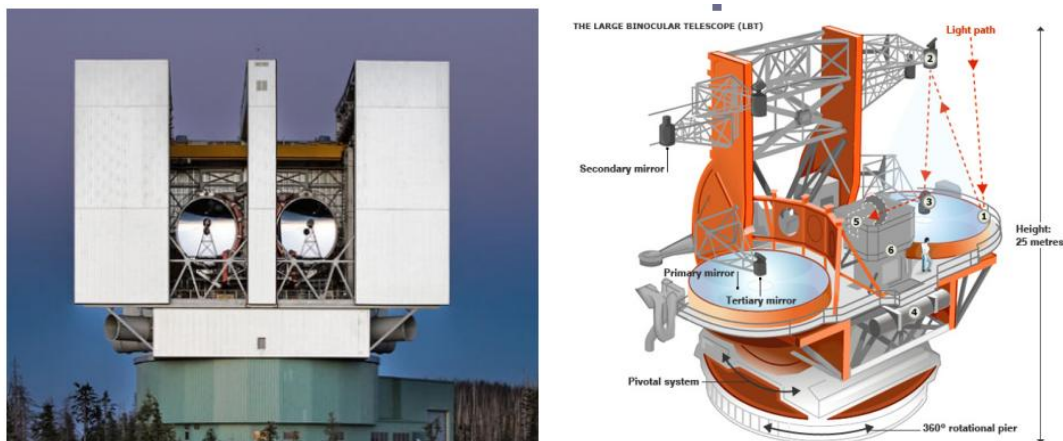


Figure 2.2: LBT telescope.

aperture with of $0''.6$. The MODS charged-coupled device (CCD) detector is an e2vCCD231-68 $8k \times 3k$ with a $15 \mu\text{m}$ pixel pitch. For the grating spectroscopy, the full spectral range was split into a blue and red channel, which cover $3200\text{-}6000 \text{ \AA}$ (blue) and $5000\text{-}10500 \text{ \AA}$ (red) (Pogge *et al.*, 2010, 2012).

2.2 Data reduction and calibration

In the next chapters I describe how I made use of the optical spectroscopic data provided by the LBT telescope. Therefore, in the data reduction section I report on the different data reducing data steps that are specific for LBT spectroscopic observations. This includes the wavelength and flux calibration.

2.2.1 Data Reduction

To reduce the LBT data I used the python software `modsCCDRed`, which is provided by the instrument team. This software package gives us the possibility to create bias correction, flat fielding, normalization, and other standard steps of data reduction. First I create normalized spectral flat field frames for each channel (blue and red) through the following steps¹:

- corrected the bias and trimmed the flat fields images;

¹The user manual can be found at <http://www.astronomy.ohio-state.edu/MODS/Manuals/MODSCCDRed.pdf>.

- median combination of the bias-corrected flats;
- repaired the bad columns using the bad pixel lists for the detector;
- eliminated the color term to produce a normalized “pixel flat”.

After creating the normalized frame (flat field), I will apply this frame to all raw science images using the software “modsCCDRed”. Finally, I will have two-dimensional corrected science images (see Fig. 2.3(a), 2.3(b), and 2.3(c)), but not completely ready to extract the one-dimensional spectrum, because still there are sky emission lines in frame as shown in Fig. 2.3(c). To remove the sky emission lines, I subtracted two corrected frames for the same source and the same channel from each other, and do this step for the rest of my data. Finally, I will have science frame ready to extract the one-dimensional spectrum (see Fig. 2.3(d)), and here I used IRAF to extract the spectrum.

2.2.2 Wavelength calibration

The wavelength calibration is essential to extract accurate spectroscopic information, i.e. spectral lines of the source - and hence information on the physics and the velocity structure and distance of the sources. From the data reduction process I will have two-dimensional (X and Y) science frames. Here I need to convert the X-axis pixel values to the corresponding wavelength values. To do this step, I will create a wavelength-calibration map using a lamp (containing argon, neon, xenon and krypton gas) as provided by the instrument. Here, I used the reduction package IRAF to identify the lamp lines and then transformed the science frames accordingly. Furthermore, I tested the last calibration by applying another method of wavelength-calibration using an OH-skyline atlas (Osterbrock *et al.*, 1996, 1997) and found that both calibration methods (skylines and lamp) are in good agreement with an uncertainty $\leq 3\text{\AA}$. Finally, by using IRAF I will extract the one-dimensional spectra of the objects from the two-dimensional science frames wavelength-calibrated.

2.2.3 Flux calibration

The flux calibration is essential in order to learn about the total energy output of the source, both in continuum as well as in line flux. After the wavelength calibration process, now I will have one-dimensional spectra ready to be flux calibration. Briefly, flux calibration is a

2. INSTRUMENTATION AND DATA REDUCTION

technique to calculate the observed continuum flux F_{λ}^0 , from the measured continuum counts I_{λ}^c , through a e sensitivity function S_{λ} ¹:

$$I_{\lambda}^c = S_{\lambda} \times F_{\lambda}^0 \quad (2.1)$$

These spectra will flux-calibrated using two standard stars: G191B2B and Feige67 for which data was taken under 1''3 seeing conditions. Both standard stars result in a consistent and independent calibration. For the final data product I used both stars for calibration. I used reduction routines on two different software platforms: IDL and IRAF. In the beginning, I extract the one-dimensional spectra from the two-dimensional science frames of the two calibration star using routines in the IRAF package. Calibrating the two stars with each other and comparing the results with published data is an essential step in for test purposes. I also downloaded spectra of these two standard stars from the European Southern Observatory 3 and compared them with my results (check Fig. 2.4).

After following the described calibration procedure and processing the science objects with the two reference stars independently resulted in spectra that agreed very well with each other within an uncertainty of 2% and 3% in the blue and red channel, respectively. I performed that calibration for each source for the red and blue channel and combine these spectra to a single spectrum per source using IRAF. In this process, I found that there are no significant continuum offsets in the overlay area between the red and blue side. While this confirms the consistency of my calibration, the uncertainties in comparing data between different telescopes and instruments is more of the order a few percent, (see e.g., Peterson et al. 2002) i.e. of the same order as reached for the SDSS data releases.

2.3 Public Survey

In this section I will talk about the public survey that I used to complementary my samples, and later on I will analysis this data and test it as described in upcoming chapters. Public Survey are an essential source of information for the astronomical community. depending on the nature of the survey (observing wavelength, provision of imaging and/or spectroscopy, single or multi epoch information, fully calibrated or raw data with calibration information etc.) one can obtain initial or complementary data on specific sources of interest. Work with public survey data was very important for this thesis.

¹<http://ganymede.nmsu.edu/cwc/Teaching/ASTR605/Lectures/fluxcal.pdf>.

2.3.1 The Sloan Digital Sky Survey

The Sloan Digital Sky Survey (SDSS) is one of the more complete and often used optical surveys. It is a sensitive optical imaging and spectroscopic public survey of about 10^4 square degrees of the northern sky (York *et al.*, 2000). It provides a photometric images in 5 different bands (u , g , r , i , and z) at an average seeing of $1''.5$ and down to a limiting magnitude of ~ 22.2 in r band. This survey used optical telescope 2.5 m wide-angle, which is located at Apache Point Observatory in New Mexico, US as present in Fig. 2.5. This telescope can attain a very wide angle 3° distortion-free range using a big secondary mirror and two corrector lenses. In addition to this telescope, the survey used other three secondary instruments: (1) a photometric telescope 0.5 m provided with CCD camera and filter set of the SDSS. The task of this instrument is to calibrate the photometry. (2) a seeing monitor. (3) cloud scanner (Hull *et al.*, 1994). The $R \sim 2000$ spectroscopy covers a wavelength range from 3800-9200 Å. Additionally, in this same wavelength range a high resolution spectroscopy is taken. The SDSS was a great revolution in optical astronomy in plenty aspects. For example, in the topic of active galaxies: a great set of homogeneous data (sensitivity and high quality) helped the astronomers to discovery a large number $> 10^4$ of AGN subclass, such as quasars (Schneider *et al.*, 2010), and Seyferts and LINERs (Kewley *et al.*, 2006).

The (photometric and spectroscopic) data can be download through this website¹, where you need to provide the website with a key information such name or coordinates of the astronomical object, in contrast, the website will give you the possibility to download all the available information about the sources, if the source has been observed in the survey (check Fig. 2.6). Finally, SDSS began its operation in May 2000, and now the survey publish the 12th data release since July 2014. In the next chapter, I used the seventh data release of the SDSS (Abazajian *et al.*, 2009), to obtain the magnitudes for SDSS J080800.99 + 483807.7 (in the following J0808) in the five SDSS bands.

2.3.2 The Wide-field Infrared Survey Explorer

Infrared surveys are important as they provide information in a wavelength band in which nuclear activity as well as general star formation activity can be traced and combined with data obtained at other wavelengths. The Wide-field Infrared Survey Explorer (WISE) was a NASA infrared-wavelength astronomical space telescope as shown in Fig. 2.7², which was

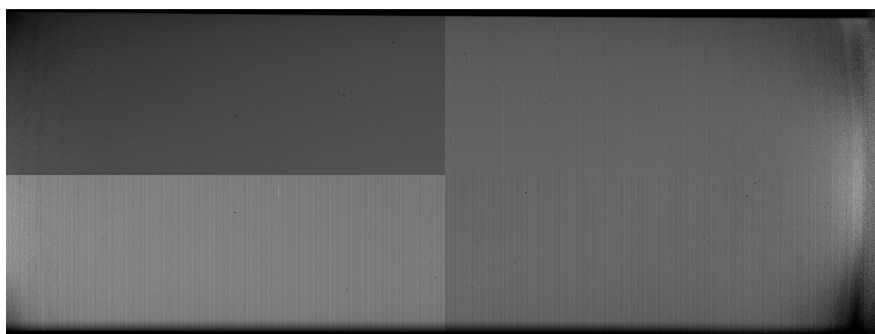
¹<http://skyserver.sdss.org/dr12/en/tools/chart/NavI.aspx>.

²Figure credit:<http://photojournal.jpl.nasa.gov/jpeg/PIA17254.jpg>.

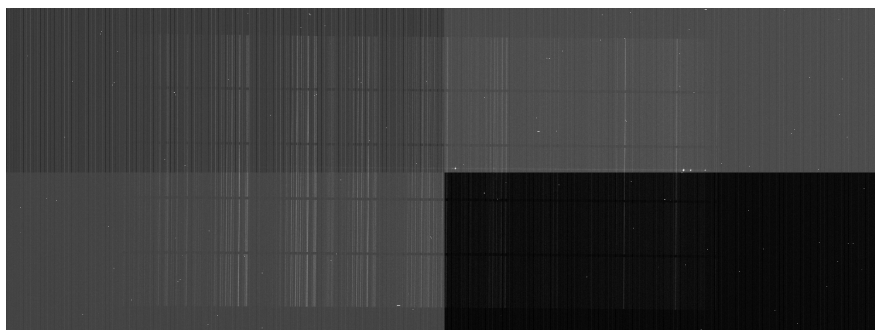
2. INSTRUMENTATION AND DATA REDUCTION

operated between December 2009 to February 2011 (Wright *et al.*, 2010). It performed an all-sky astronomical survey with images in wavelength bands at 3.4 μm , 4.6 μm , 12 μm , and 22 μm , using a 40 cm diameter infrared telescope in Earth orbit. In the next chapter I will use this survey to gain some information about flux densities of J0808 at different wavelength bands. The goal of this survey is to generate an infrared frames of 99% of the sky, with at least 9 frames per location on the sky to improve the accuracy. The spacecraft was in height of 525 km orbiting around the earth, which during the mission 1.5 million frames has been taken, and that mean 1 frame per 11 seconds. Each taken frame cover about 47' field of view. Among the achievements of WISE survey is discovering 33,500 asteroids and comets were unknown before, as well as explored the first Earth Trojan asteroid (2010 TK7)¹. Finally this survey providing us with images to the milky way galaxy, the local solar system, and the remote universe.

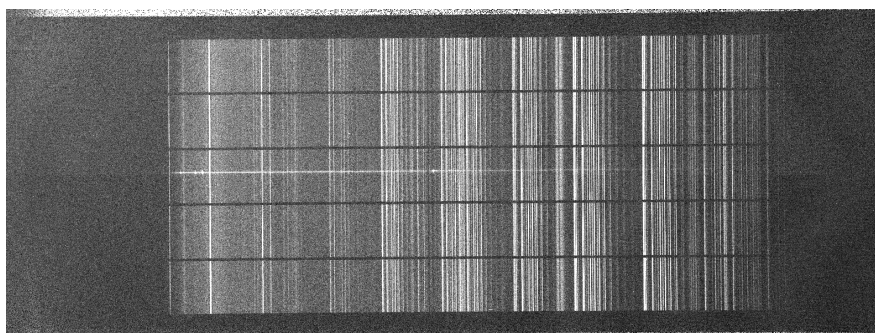
¹<http://www.space.com/12443-earth-asteroid-companion-discovered-2010-tk7.html>.



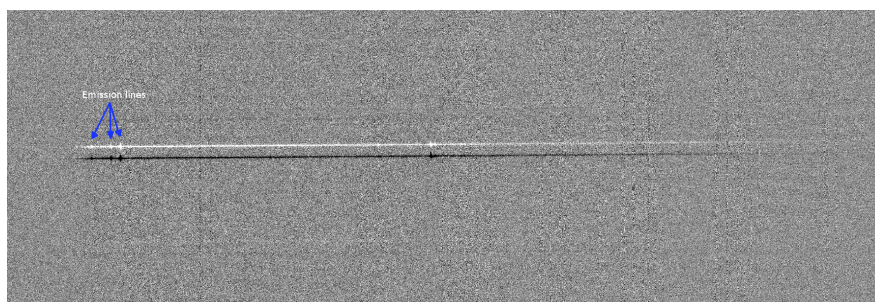
(a) Normalized spectral flat field frame.



(b) Raw science frame.



(c) Flat fielded science frame.



(d) Flat fielded science frame without the sky emission lines.

Figure 2.3: Data reduction steps.

2. INSTRUMENTATION AND DATA REDUCTION

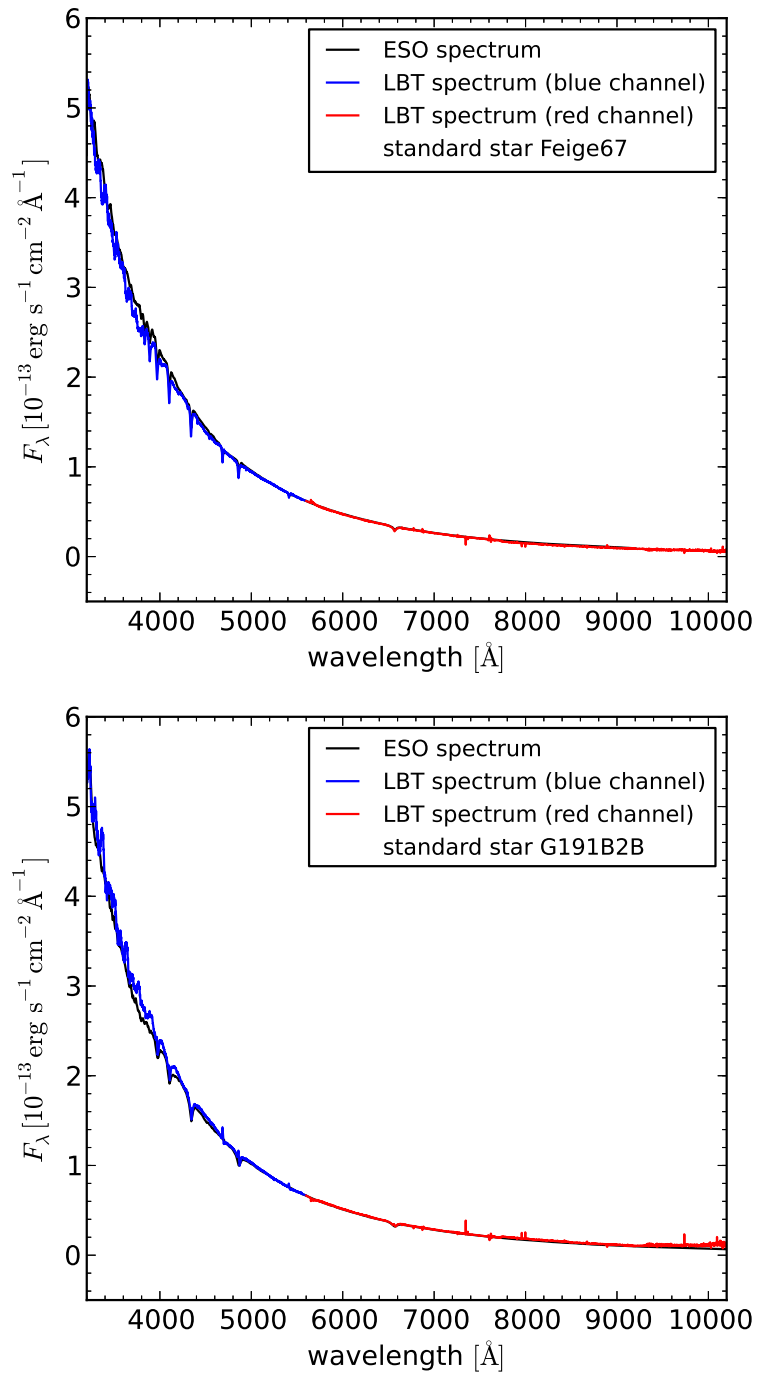


Figure 2.4: The standard stars Feige67 and G191B2B.



Figure 2.5: SDSS telescope.

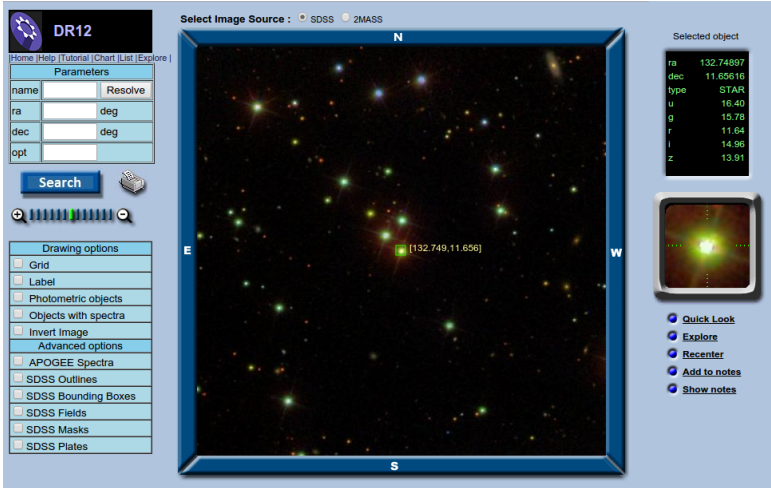


Figure 2.6: The SDSS website.

2. INSTRUMENTATION AND DATA REDUCTION

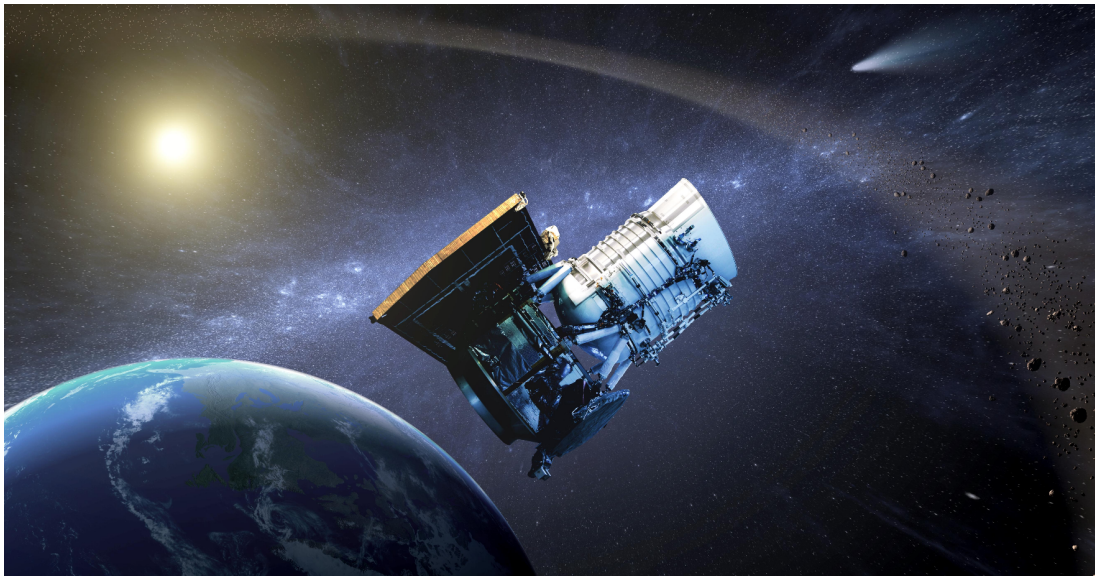


Figure 2.7: WISE space telescope.

3

High-resolution observations of SDSS J080800.99+483807.7 in the optical and radio domains

3.1 Introduction

Based on radio surveys (e.g. the Cambridge surveys in the meter and decimeter wavelength bands) we now know that the typical structure of an extragalactic radio source consists of a core, jets and radio lobes, that are connected to the core via the jets. The first observations of radio galaxies have provided very strong evidence that there are extended jets flowing from the center of some of these sources, spanning a few kilo parsec to a few mega parsecs (e.g., [Bridle and Perley, 1984](#), and references therein). The jets appear to be associated with the central massive black hole and the accretion disk (e.g., [Begelman *et al.*, 1984](#); [Blandford and Payne, 1982](#); [Blandford and Znajek, 1977](#)). It has been widely speculated about the mechanisms for fueling the central massive black hole with matter from the host galaxy and the impact of nuclear activity on the host (i.e., radiation field, outflows, jets, etc.). [Fabian \(2012\)](#) reports on observational evidence for feedback between the radio jet and the interstellar/intergalactic medium, especially in the radio/kinematic mode in which a significant back-flow of material along the periphery of the jet or outflow onto the host occurs ([Silk, 2013](#); [Wagner *et al.*, 2013](#)). [Wagner *et al.* \(2013\)](#) use three-dimensional grid-based hydrodynamical simulations to show that ultrafast outflows from active galactic nuclei (AGN) result in considerable feedback of energy and momentum into the interstellar medium (ISM) of the host galaxy. [Silk \(2013\)](#)

3. HIGH-RESOLUTION OBSERVATIONS OF SDSS J080800.99+483807.7 IN THE OPTICAL AND RADIO DOMAINS

shows that the AGN-induced pressure, which is caused by jets and/or winds that flow back onto a gas-rich host, can lead to pressure-regulated star formation with significantly enhanced star-formation rates. Especially in the case of X-shaped radio galaxies (XRGs), the back-flow phenomenon is essential and has been discussed. The XRGs are a special type of radio galaxies with two pairs of lobes (one active, bright pair and a second fainter, more diffuse pair; [Leahy and Williams, 1984](#)). For a radio galaxy to be classified as an XRG, it needs to have the two pairs of jets strongly misaligned and flowing from the center of the source; the minor pair must flow in another direction as the major pair, otherwise it would be double-double radio galaxy (DDRG; e.g., [Brocksopp et al., 2011](#), and references therein). One finds that 5%-10% of Fanaroff-Riley type II radio galaxies are X-shaped galaxies ([Fanaroff and Riley, 1974](#)). There are several competing interpretations of the physical nature of the radio morphology, e.g., black-hole spin reorientation, plasma back-flows from the lobes, binary black holes, and jet interstellar-medium interaction (cf. [Gopal-Krishna et al., 2012](#), for a review). The nuclei of XRGs, which presumably represent the transition population that lies between FR I and FR II radio sources (e.g., [Landt et al., 2010](#)), are valuable probes of the interaction between the black hole, its jet, and the host (e.g., [Hodges-Kluck and Reynolds, 2011](#); [Wagner and Bicknell, 2011](#)).

3.2 Radio observation of J0808

Interferometric observation of extragalactic often cover a field of view that is larger than the typical extent of the source of interest. In general the entire central half-beam of the single interferometer telescope elements can be mapped. Given the density of radio sources in the sky there are always sources in the field of view that are present in addition to the program source at the center of the observed field. This was the case for the field containing J0808. J0808 was serendipitously identified in our group (data set of 4C 48.21) observation using the interferometer array (MERLIN) at the wavelength 18 cm. Which I classified as a rather compact double-lobed radio galaxy, as I will clarify later. Such objects are particularly interesting since they could be small due to extreme foreshortening or an actual small size. In case of an extreme foreshortening, one would expect the radio jet to be pointed towards the observer under a small angle with respect to the line of sight, such that the central nucleus appears to be bright due to relativistic beaming. In the latter case, one of the lobes is also expected to be brighter and possibly cover the central source due to its extent. However, J0808 appears as a

symmetric double-lobed source with a nuclear component that is very weak with respect to the lobes and somewhat more extended than compact. Hence, I can assume that its small overall apparent size is due to a small physical size. Especially for physically small sources a back-flow may be of special importance. These flows towards the center along the outer regions of the jets is expected. Such a back-flow results in an interaction at the nucleus or with the host galaxy which the nucleus is located in. The possibility of back-flow interactions has also been reported (cf. [Hodges-Kluck and Reynolds, 2011](#)) for X-shaped radio sources. In particular, I complement the radio information with optical spectroscopy of the nuclear region of the galaxy and investigate the possibility of triggered star formation.

In our case the specific 18 cm observations of J0808 were carried out in May 2005. The resulting angular resolution is about $0'.25 \times 0'.15$ with a position angle of 1.5° . The total integration time on J0808 was about 9.2 hours and the noise in the image is about $0.1 \text{ mJy beam}^{-1}$. The central radio component is located within $0'.1$ of the position of the optical source J0808. [Fig. 3.1](#) showing the image of the radio galaxy. Details of the radio observation and data reduction are given in [Zuther et al. \(2012\)](#). An extended structure at the central source component of J0808 gives some evidence for a possible back-flow towards the center that may result in an interaction with the ISM at the nucleus. In fact, J0808 shows extended emission along a position angle that is by at least 50° different from that of the prominent double-lobe structure. In order to search for signatures of the peculiar shape we closely investigated the shape of the contour lines at different levels. Signatures of the peculiar shape are prominent on contour lines as high as at least five times the noise level in the original and the smoothed version of the radio image shown in [Fig. 3.1](#). In general objects that are subject to a significant back-flow along the radio jet onto the host galaxy ([Silk, 2013](#); [Wagner et al., 2013](#)) this is a well known signature for XRG objects.

3.3 Optical and infrared observations of J0808

It may take a long time to complete an ongoing survey, and as such a survey contains a large amount of data which is often complex in terms of calibration. Therefore the survey data is often released in steps, i.e. individual data releases. I used the seventh data release of the SDSS ([Abazajian et al., 2009](#)) to obtain the magnitudes for J0808 in the five SDSS bands, as given in [Tab. 3.1](#). Furthermore, in [Fig. 3.2](#), I show the *i*-band SDSS optical image of the galaxy. Additionally, in the Infrared survey (WISE) the source J0808 is detected at all bands in the

3. HIGH-RESOLUTION OBSERVATIONS OF SDSS J080800.99+483807.7 IN THE OPTICAL AND RADIO DOMAINS

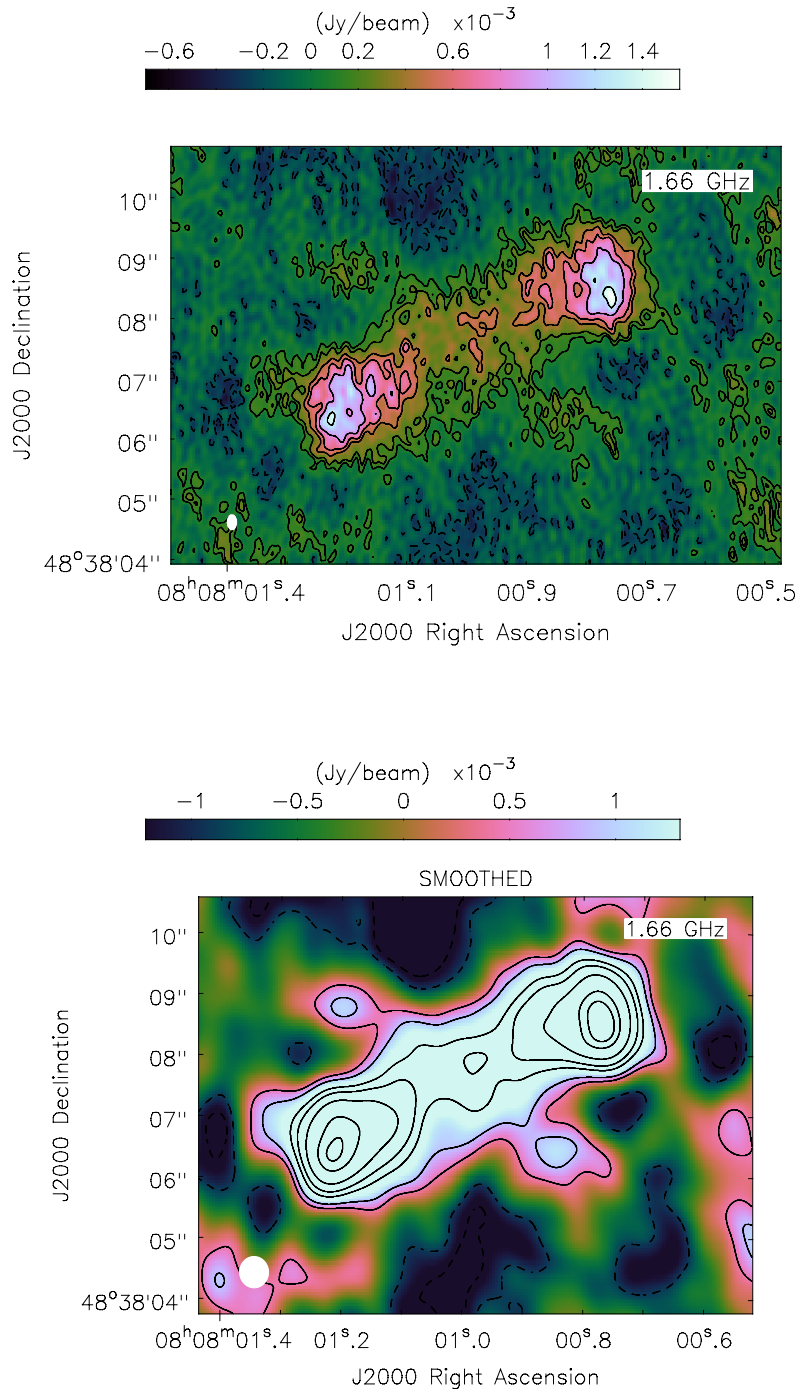


Figure 3.1: 18 cm MERLIN image of SDSS J080800.99+483807.7. The J2000 coordinates of the central source are $\alpha = 08:08:00.99$ and $\delta = +48:38:07.73$. *Top:* original image at a noise level of about 1.1×10^{-4} Jy/beam. *Bottom:* 10 pixel smoothed image at a noise level of about 4.5×10^{-4} Jy/beam. The contour levels are each at -3, -2, 1, 2, 4, 5.5, 8, 12, 14 times the noise level.

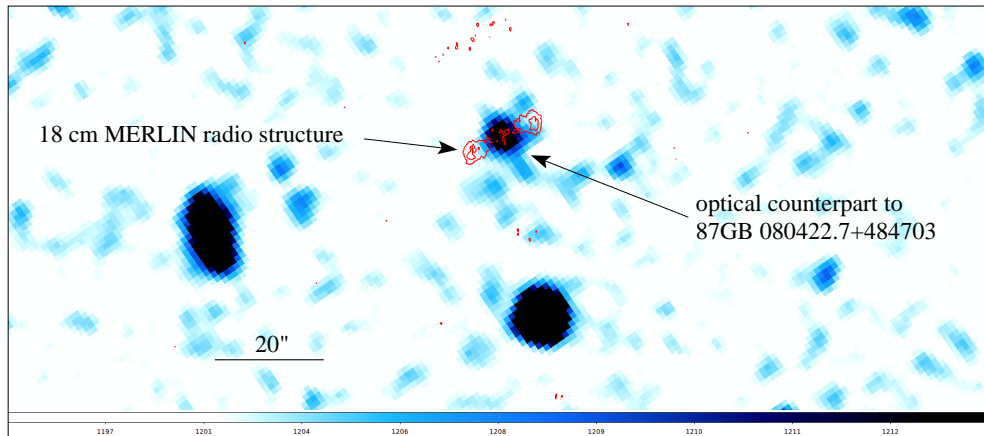


Figure 3.2: SDSS image of J0808, overlaid with MERLIN 18 cm contours in red.

Table 3.1: Photometric measurements of J0808 in the SDSS and WISE photometric systems.

Survey	Band	Magnitude
SDSS	<i>u</i>	23.68 ± 1.35
SDSS	<i>g</i>	24.05 ± 0.91
SDSS	<i>r</i>	21.9 ± 0.20
SDSS	<i>i</i>	20.52 ± 0.10
SDSS	<i>z</i>	19.70 ± 0.15
WISE	$3.4 \mu\text{m}$	15.61 ± 0.06
WISE	$4.6 \mu\text{m}$	15.51 ± 0.15
WISE	$12 \mu\text{m}$	12.30 ± 2.50

all-sky data release from March 14, 2012, except at $22 \mu\text{m}$. The flux densities are listed in Table 3.1. The uncertainty of the $12 \mu\text{m}$ flux density was estimated from the corresponding image provided by the data release.

3.4 Results

3.4.1 Emission-lines measurements

After the final reduction steps the astrophysical data may be extracted from the spectra. The reduced optical spectrum of J0808 is present in Fig. 3.3. Prominent emission lines have been

3. HIGH-RESOLUTION OBSERVATIONS OF SDSS J080800.99+483807.7 IN THE OPTICAL AND RADIO DOMAINS

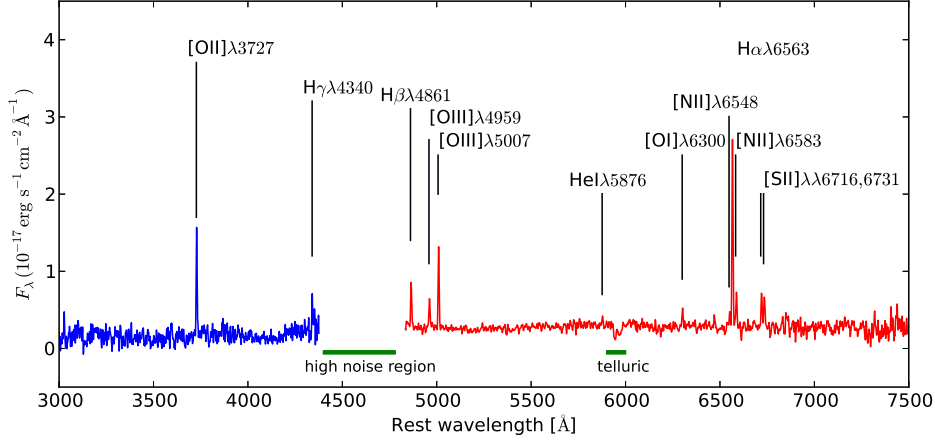


Figure 3.3: Optical spectrum of J0808. The blue and red spectra represent the data from the respective channel. A gap between the two channels that has been excluded because of high noise and a region that shows telluric features are marked.

fitted with the spectral analysis tool Specview assuming Gaussian shape. Positions, resulting redshifts, flux density, and full-width at half maximum (FWHM) of the emission lines are listed in Table 3.2.

A standard and very powerful tool to investigate the physics of nuclear regions is the usage of emission-line diagnostic diagram. In these diagrams ratios of lines close in wavelength to each other are compared. The emission-line diagnostic diagram delivers information about the dominant ionization mechanism of the gas in the studied region. Studies of different samples of narrow emission-line galaxies have also shown some trends in the diagrams that are associated with stellar mass, metallicity and possibly morphology of the host. The evaluation of line ratios is often complicated by the fact the emission is origination from embedded sources. It may happen that the actual information of how extinguished the emitted radiation is, is actually incomplete or even unknown. But there is a solution to this problem: As the extinction is a function of wavelength it is quite similar at neighboring wavelength, such that a correction for extinction may not be needed if the line ratio is calculated. Such ratios are then used in diagnostic diagrams. No reddening corrections has to be applied to calculate line ratios in these diagrams since the emission lines are close to each other in wavelength:

- [NII]/H α vs. [OIII]/H β (Juneau *et al.*, 2011; Kauffmann *et al.*, 2003; Kewley *et al.*, 2001, 2003; Lamareille, 2010; Lamareille *et al.*, 2004; Veilleux and Osterbrock, 1987).

- [S II]/H α vs. [O III]/H β (Juneau *et al.*, 2011; Kewley *et al.*, 2001, 2006; Lamareille, 2010; Lamareille *et al.*, 2004; Veilleux and Osterbrock, 1987).
- [O I]/H α vs. [O III]/H β (Kewley *et al.*, 2001, 2006).

The measured ratios between emission lines are:

- $\log \frac{[\text{O III}] \lambda 5007}{\text{H}\beta} = 0.337 \pm 0.006$
- $\log \frac{[\text{S II}] \lambda 6716, \lambda 6731}{\text{H}\alpha} = -0.448 \pm 0.006$
- $\log \frac{[\text{O I}] \lambda 6300}{\text{H}\alpha} = -1.090 \pm 0.010$
- $\log \frac{[\text{N II}] \lambda 6583}{\text{H}\alpha} = -0.822 \pm 0.005$

To test the actual energy output of the objects one needs to know their distances. On cosmological scales these are given through the Doppler shift i.e. the redshift of the sources. For J0808 the information on the redshift was incomplete. There was only an estimate of a photometric redshift of $z \sim 0.7$ was available from the SDSS. To derive the spectroscopic redshift, I first reduced the data as outlined in the previous section. The optical spectrum is shown in Fig. 3.3. For the emission lines evident in Fig. 3.3 and listed in Table 3.2, I used the equation

$$z = \frac{\lambda_{\text{obs}}}{\lambda_{\text{rest}}} - 1 \quad (3.1)$$

and derived the redshift for each line as present in Ta. 3.2. The mean redshift and its standard deviation are $z = 0.2805 \pm 0.0003$. Combining the redshift with the cosmology constants $H_0 = 70 \text{ km s}^{-1} \text{ Mpc}^{-1}$, $\Omega_m = 0.3$, and $\Omega_\Lambda = 0.7$ (Spergel *et al.*, 2003, which I will use throughout this work), I calculated the luminosity distance D_L (Hogg, 1999) to be 1437.2 Mpc. This corresponds to a linear-size scale conversion factor of 6.98 kpc per arcsecond.

Using ratios of lines that are close in wavelength one does not need to carry out a reddening correction. Such line ratios are the best to be used in diagnostic diagrams. As it shown in the diagnostic diagrams (Fig. 3.4), J0808 is located in the region characteristic for host galaxies with high star-formation rates ([N II]-based diagram) and a tendency to have contributions to line emission from an active nucleus ([O I]-based diagram). J0808 is located closer to the region of star formation and low excitation galaxies, as compared to high excitation galaxies by Kunert-Bajraszewska and Thomasson (2009). In particular, the low [N II]/H α also suggests a low metallicity. The diagnostic diagrams in Fig.12 by Vitale *et al.* (2012) suggest a thermal

3. HIGH-RESOLUTION OBSERVATIONS OF SDSS J080800.99+483807.7 IN THE OPTICAL AND RADIO DOMAINS

rather than a non-thermal origin of the optical emission lines. From the optical images it is difficult to provide a host galaxy classification. For distant galaxies this is a well known problem. The images are mostly dominated by the bright bulges. Fainter disks often need additional integration time to be seen clearly. The host visible in the SDSS images is in agreement either with an elliptical or a bulge of a low-luminosity disk system. The low metallicity then suggests either an early evolutionary stage or an overall low mass of the host galaxy (Kauffmann *et al.*, 2003; Vitale *et al.*, 2013). Interpolating the z -band and $3.4 \mu\text{m}$ flux densities, I get a K-band magnitude of about $K \sim 16.9$ and a flux density of $S_K = 1.09 \times 10^{-4}$ Jy. Where I can estimate the old stellar mass via

$$M_{*,\text{old}}[M_{\odot}] = 2.6 \times 10^8 D^2[\text{Mpc}] S_K[\text{Jy}] \quad (3.2)$$

(Thronson and Greenhouse, 1988). This is equivalent to a population K-band M/L ratio of about 23 and applying the K-band luminosity to flux density relation by Krabbe *et al.* (1994). Using a distance of 1437.2 Mpc, the stellar mass of J0808 was calculated to be about $6 \times 10^{10} M_{\odot}$. This is one to two orders of magnitudes less than the mass of the Milky Way but about an order of magnitude more than the upper limit of $2 \times 10^9 M_{\odot}$ derived for the stellar mass of the starburst galaxy M82 (Greco *et al.*, 2012). M82 is known to have a strong, nuclear starburst driven wind over which a major portion of the newly formed metals can be lost. The comparison presented above clearly shows that J0808 could be a low-mass low-metallicity elliptical.

3.4.2 The linear size of J0808

The linear size of the object is an essential piece of information that may be connected to the object kind and/or evolution. Early studies of the connection between the median linear size of the galaxy D_{med} as a function of redshift z (Eales, 1985) listed in $D_{\text{med}} \propto (1+z)^{-1.1 \pm 0.5}$ for $\Omega_0 = 0$, and $D_{\text{med}} \propto (1+z)^{-1.45 \pm 0.4}$ for $\Omega_0 = 1$. Essentially, there was no signal for a correlation between linear size and luminosity. Nonetheless, Oort *et al.* (1987) show a strong correlation between D_{med} and z of $D_{\text{med}} \propto (1+z)^{-3.3 \pm 0.5}$ at $\Omega_0 = 0$. Follow-up studies by Neeser *et al.* (1995) could not confirm such a strong correlation and listed in an updated correlation between the median size and redshift of $D_{\text{med}} \propto (1+z)^{-1.2 \pm 0.5}$ when $\Omega_0 = 0$ and $D_{\text{med}} \propto (1+z)^{-1.7 \pm 0.4}$ when $\Omega_0 = 1$. Recently, spectroscopic techniques have assisted to understand the physical properties of far sources that appear to be largely unresolved. By using spectroscopic redshifts allows us to calculate the linear size of the radio object host galaxies.

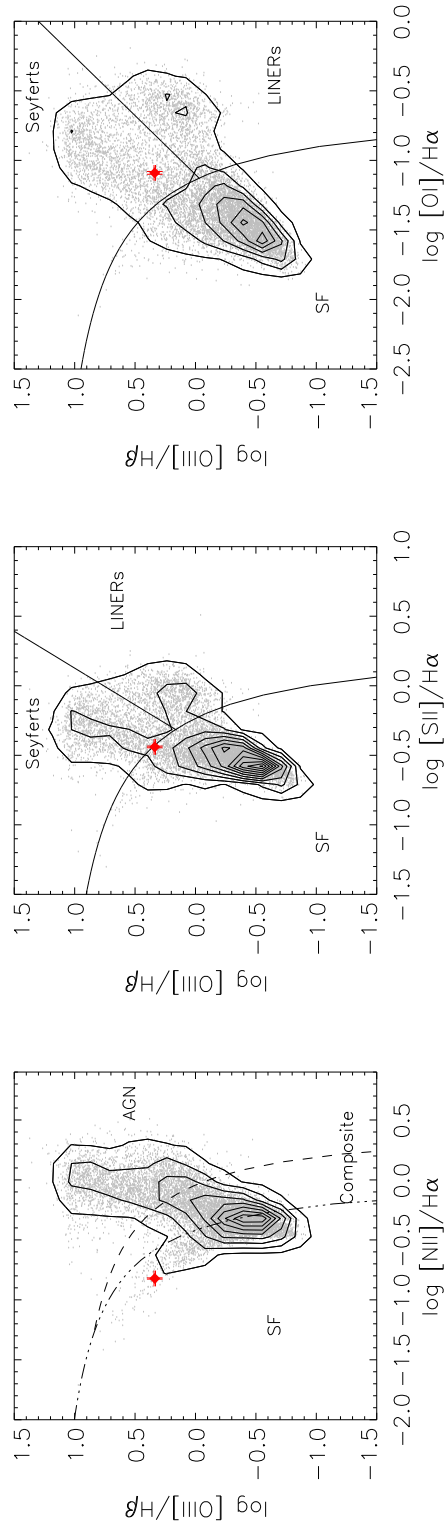


Figure 3.4: Diagnostic diagrams $[N II]/H\alpha$ vs. $[O III]/H\beta$, $[S II]/H\alpha$ vs. $[O III]/H\beta$ and $[O I]/H\alpha$ vs. $[O III]/H\beta$ for the radio emitters taken from Vitale *et al.* (2012). The contours show galaxy densities in steps of 80 galaxies per each additional contour. The position of the source analyzed here is shown as a red dot.

3. HIGH-RESOLUTION OBSERVATIONS OF SDSS J080800.99+483807.7 IN THE OPTICAL AND RADIO DOMAINS

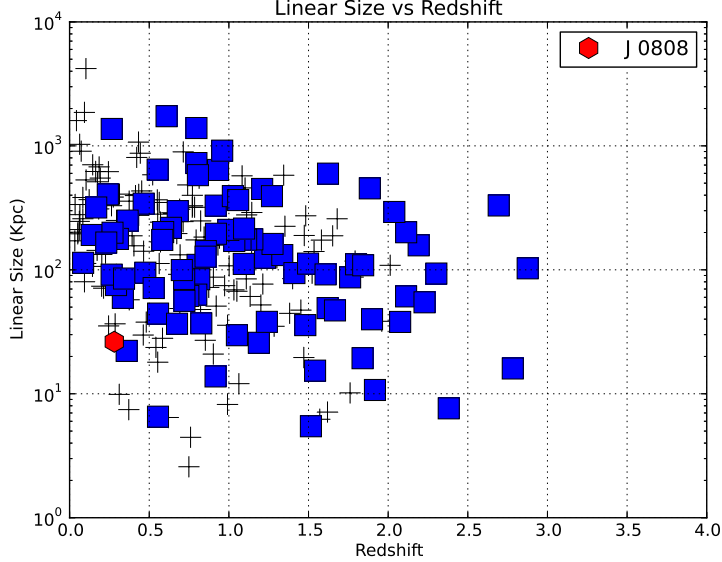


Figure 3.5: Linear size versus redshift. J0808 is shown by the red hexagon, the plus signs represent the position of the 3CRR sources, the square signs represent the 7CRS objects (Wang *et al.*, 2011).

I derive a linear source size via

$$l = \vartheta \times D_A = \frac{\vartheta \times D_L}{(1+z)^2}. \quad (3.3)$$

Here D_A is the angular diameter distance and $\vartheta = 6''.2$ is the angular size of J0808 as calculated from the radio frame as present in Fig. 3.1. This results in a linear size of $l = 26.29$ kpc, which can be compared to the size values found for other objects, as given in, e.g., Wang *et al.* (2011). The comparison is present in Fig. 3.5, and it shows that the J0808 is a relatively compact object compared to other galaxies at the same redshift.

In Fig. 3.6 I compare J0808 to the FR II galaxy 3C438. The reason behind selecting 3C438 for comparison, because it is the same in appearance compared to J0808. The comparison for the two objects shows in overall an increasing intensity distribution from the center towards the edges. Thus the radio structure of J0808 is referred to an edge-brightened FR II galaxy.

3.4.3 The radio loudness of J0808

The indicator for the activity of the galaxy is the radio loudness of it, i.e. for the importance of accretion on the central black hole. J0808 is a prominent radio object. The discrimination

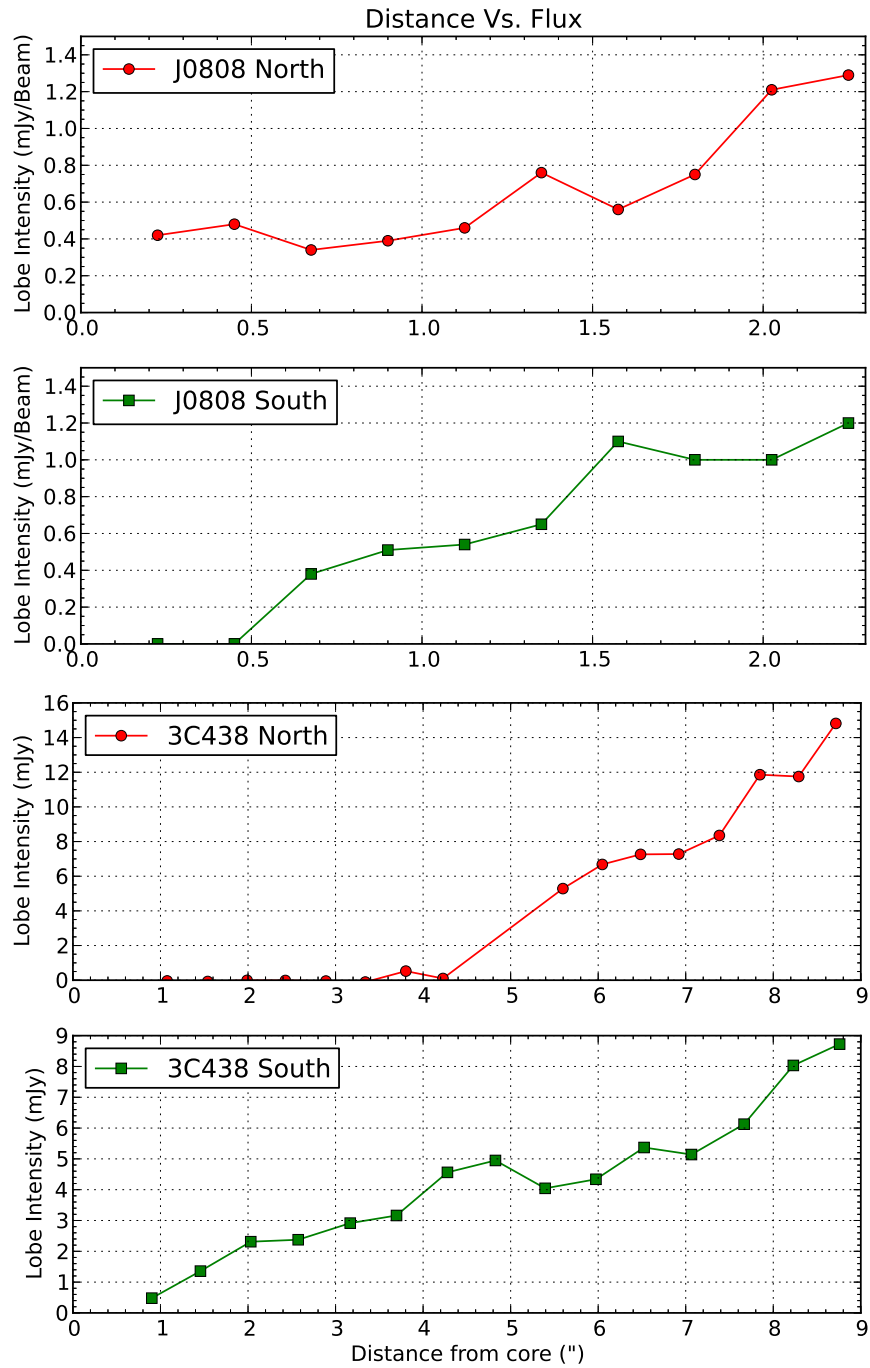


Figure 3.6: Flux density values at different positions for each lobe (Northeast & Southwest) compared with other FR II sources (Treichel *et al.*, 2001).

3. HIGH-RESOLUTION OBSERVATIONS OF SDSS J080800.99+483807.7 IN THE OPTICAL AND RADIO DOMAINS

Table 3.2: Observed emission lines: wavelengths, redshifts, flux densities, and line widths

channel	line	wavelength [Å]	redshift	flux [10^{-17} erg s $^{-1}$ cm $^{-2}$]	FWHM [km s $^{-1}$]
Blue	[O II] λ 3727	4772.1	0.2804	18.80 ± 0.07	445 ± 8
Blue	H γ λ 4340	5555.9	0.2801	4.01 ± 0.13	225 ± 7
Red	H β λ 4861	6226.5	0.2809	6.91 ± 0.04	333 ± 10
Red	[O III] λ 4959	6350.9	0.2806	4.04 ± 0.02	345 ± 10
Red	[O III] λ 5007	6412.5	0.2807	15.03 ± 0.02	355 ± 10
Red	[He I] λ 5876	7523.7	0.2804	1.51 ± 0.04	252 ± 9
Red	[O I] λ 6300	8066.4	0.2803	2.92 ± 0.03	277 ± 8
Red	[N II] λ 6548	8386.1	0.2807	2.65 ± 0.03	302 ± 8
Red	H α λ 6563	8405.0	0.2806	36.02 ± 0.03	290 ± 8
Red	[N II] λ 6583	8431.3	0.2807	5.42 ± 0.03	261 ± 8
Red	[S II] λ 6716	8602.1	0.2808	6.56 ± 0.04	290 ± 8
Red	[S II] λ 6731	8621.2	0.2808	6.25 ± 0.04	324 ± 8

between radio quiet (RQ) and radio loud (RL) objects mostly reflects the various importance of strong emission from lobes and/or radio jets (e.g., [Yuan *et al.*, 2008](#)).

[Kellermann *et al.* \(1981\)](#) introduced a formalism to calculate the radio loudness via comparing the flux density at 5GHz to the flux density at 4400Å:

$$R^* = \frac{S_{5\text{GHz}}}{S_{4400\text{\AA}}} . \quad (3.4)$$

Presently, I don't have flux density measurement at 5 GHz, yet I do have several flux measurements at various frequencies, as present in [Table 3.3](#). Using those, I assessment the spectral index via (cf. [O'Dea *et al.*, 2009](#))

$$\alpha_{\nu_2}^{\nu_1} = \frac{\log \frac{S_{\nu_1}}{S_{\nu_2}}}{\log \frac{\nu_1}{\nu_2}} . \quad (3.5)$$

Here S_{ν_1} and S_{ν_2} are the flux densities at frequencies ν_1 and ν_2 . From the data at 4.85 GHz and 365 MHz in [Tab. 3.3](#), I determine the spectral index to be $\alpha = -0.80$. This indicates a dominant contribution to the radio flux from optically thin synchrotron radiation. Assuming a power law spectrum with $S_\nu = \text{const.} \times \nu^\alpha$, I find a rest-frame 5 GHz flux density of $S_{5\text{GHz}} = 0.076$ Jy. From the optical spectrum of J0808, the flux density at 4400Å calculate to be $S_{4400\text{\AA}} = 6.06 \times 10^{-6}$ Jy. This results in an estimate of the radio loudness of $R^* = 12657$ or $\log R^* = 4.1$. Also,

Table 3.3: Radio flux density at different frequencies.

No.	Observed Passband Frequency (GHz)	Flux Density (Jy)	Luminosity (10^{25} W Hz $^{-1}$)	References
1	4.85	0.077 ± 0.010	1.902	1
2	4.85	0.075 ± 0.011	1.853	2
3	1.66	0.088 ± 0.004	2.175	this study
4	1.4	0.162 ± 0.005	4.003	3
5	0.365	0.563 ± 0.053	13.913	4

I can compare it to other sources following [Blundell \(2003\)](#). To do that, I should calculate the radio luminosities at 5 GHz and 178 MHz. This is done by scaling the distance squared with the flux and a factor of 2π :

$$L_\nu = 4\pi \times D_L^2 \times S_\nu \quad (3.6)$$

and find:

$$\begin{aligned} \log(L_{5\text{GHz}}/\text{erg s}^{-1} \text{ Hz}^{-1}) &= 32.27 \\ \log(L_{5\text{GHz}}/\text{W Hz}^{-1} \text{ sr}^{-1}) &= 25.16 \\ \log(L_{178\text{MHz}}/\text{erg s}^{-1} \text{ Hz}^{-1}) &= 33.83 \\ \log(L_{178\text{MHz}}/\text{W Hz}^{-1} \text{ sr}^{-1}) &= 26.33 . \end{aligned}$$

The comparison of J0808 as RL target with other objects is present in [Figure 3.7](#). This places the J0808 among the RL sources. Generally, this result does not change, although I do the calculation only for the nuclear component, which is an order of magnitude weaker than the total radio luminosity.

The radio spectrum of J0808 is present in [Figure 3.8](#) and can be represented as a straight power law. The fact that the flux density value of J0808 at 18 cm wavelength lies below the power law fit is most likely because of resolution effects. It indicates that not all the flux density of the source was measured on the shortest baselines of the interferometric MERLIN observations for J0808.

3. HIGH-RESOLUTION OBSERVATIONS OF SDSS J080800.99+483807.7 IN THE OPTICAL AND RADIO DOMAINS

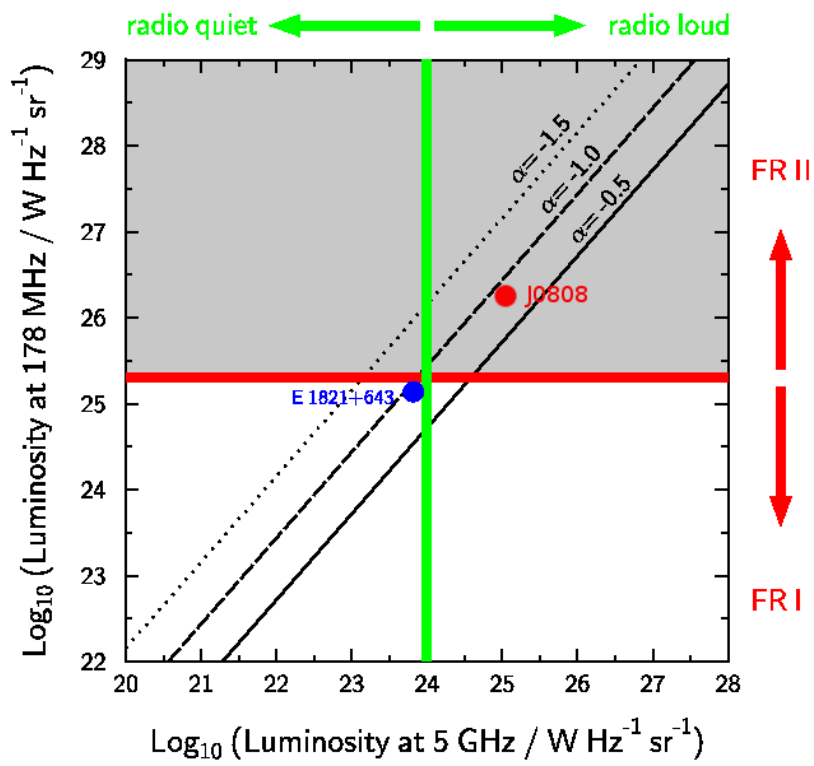


Figure 3.7: Radio loudness scheme (Blundell, 2003).

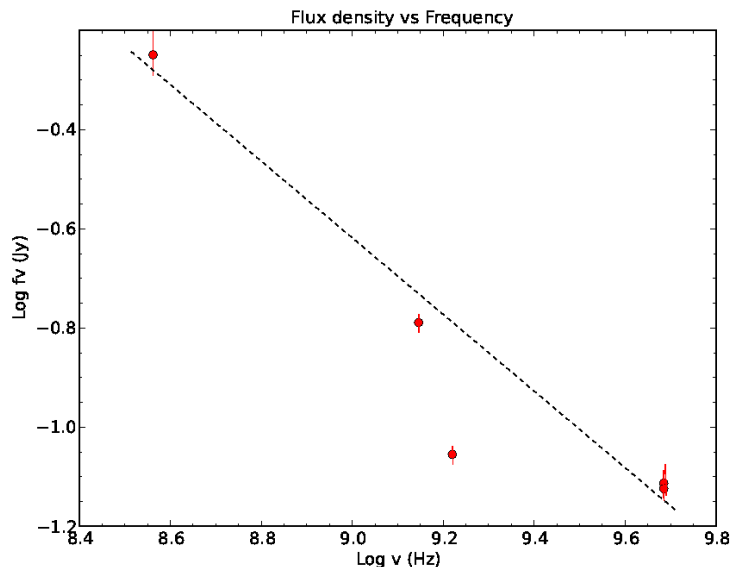


Figure 3.8: Flux density and uncertainty versus frequency of J0808 from different surveys (Becker *et al.*, 1991; Condon *et al.*, 1998; Douglas *et al.*, 1996; Gregory and Condon, 1991).

3.4.4 The central black hole of J0808

There are numerous publications that indicate that most of the galaxies host a super-massive black hole at their centers (e.g., Ferrarese and Ford, 2005; Ferrarese and Merritt, 2000; Gebhardt *et al.*, 2000; Kormendy and Ho, 2013; Magorrian *et al.*, 1998; Melia and Falcke, 2001, and references therein). It is most likely that the super massive black hole coevolved with the central bulge of the hosts. Here, I derived the black hole mass of J0808 through the scaling relation between the black hole mass of the host and stellar velocity dispersion of the host bulge component. Following Ferrarese and Merritt (2000), I used the relation

$$\log \frac{M_{\text{BH}}}{M_{\odot}} = 8.12 + \log \left(\frac{\sigma_{*}}{200 \text{ km s}^{-1}} \right)^{4.24 \pm 0.41}. \quad (3.7)$$

Assuming a Gaussian line shape and an instrumental resolution of 150 km s^{-1} , I obtain a value for σ_{*} via the following expression (Greene and Ho, 2005; Wang and Zhang, 2007):

$$\sigma_{*} = \frac{\sqrt{(\text{FWHM}_{[\text{O III}]})^2 - (150 \text{ km s}^{-1})^2}/2.35}{1.34}. \quad (3.8)$$

3. HIGH-RESOLUTION OBSERVATIONS OF SDSS J080800.99+483807.7 IN THE OPTICAL AND RADIO DOMAINS

From Table 3.2, the FWHM of [O III] is 355 km s^{-1} . Applying this value, I find $\sigma_* = 102.2 \text{ km s}^{-1}$ and a black hole mass of

$$\log\left(\frac{M_{\text{BH}}}{M_{\odot}}\right) = 6.88 \pm 0.12 . \quad (3.9)$$

Since in the active galactic nucleus the [O III] line emission is often connected with outflows from the active nucleus (Boroson, 2003) the [O III] line strength turned out to present large scatter in the scaling relation. A better estimator of the underlying stellar velocity dispersion of the bulge (cf. Komossa and Xu, 2007) appear to be the [S II] emission lines. For comparison, I also determine the black hole mass using the [S II] emission lines with the following equation:

$$\sigma_* = \frac{\sqrt{(\text{FWHM}_{[\text{S II}]})^2 - (150 \text{ km s}^{-1})^2}}{2.35} . \quad (3.10)$$

Furthermore, the two [S II] lines in the spectrum (see Table 3.2), I obtain an average value of FWHM ($[\text{S II}]_{\text{avg}} = 307 \text{ km s}^{-1}$), resulting in a value of $\sigma_* = 114.0 \text{ km s}^{-1}$. Following Komossa and Xu (2007) the black hole mass of J0808 is estimated to be:

$$\log\left(\frac{M_{\text{BH}}}{M_{\odot}}\right) = 6.9 \pm 0.15 . \quad (3.11)$$

Both methods result in a consistent estimate of the black hole mass of about $10^7 M_{\odot}$.

In the discussion of how energy is released in the process of accretion of matter onto very massive and compact objects - the Eddington limit is essential. The Eddington ratio η is a measure of the accretion efficiency because it relates the observed AGN radiation output to that produced by maximum spherical accretion with isotropic radiation. The Eddington ratio compares the two luminosities L_{bol} and L_{edd} via $\eta = L_{\text{bol}}/L_{\text{edd}}$. Here L_{bol} is the bolometric luminosity and L_{edd} is the Eddington luminosity. The bolometric luminosity is usually estimated from single-band measurements. There is considerable uncertainty in the bolometric correction for individual objects, depending on the particular spectral energy distribution, Here, I estimate the bolometric luminosity, following the prescription from Vestergaard (2004), using the rest-frame 5100\AA luminosity density

$$L_{\text{bol}} \approx 9.47 \times \lambda L_{\lambda}(5100\text{\AA}) \text{ erg s}^{-1} . \quad (3.12)$$

I calculated the rest-frame 5100\AA luminosity density by fitting a linear combination of two simple starburst models, the active galactic nucleus power law, and an extinction component

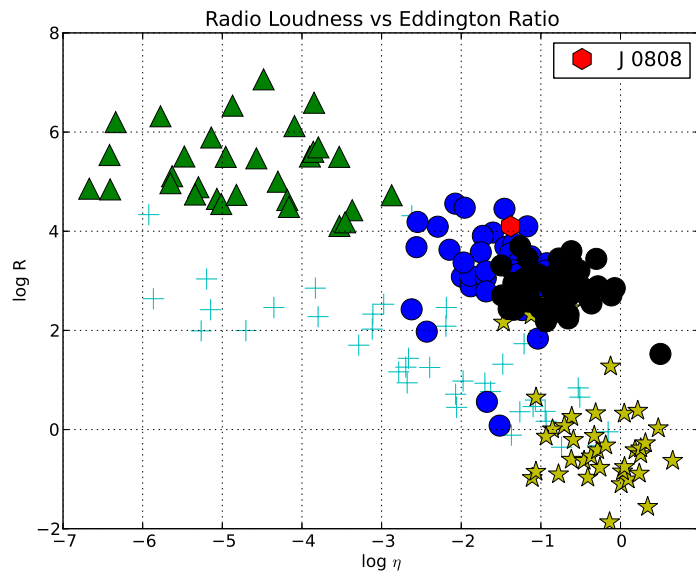


Figure 3.9: Radio loudness (R) versus Eddington ratio η . J0808 is represented by a red hexagon, BLRGs are marked by the blue circles, radio loud quasars by the Black circles, Seyfert galaxies and LINERs by the crosses, FR I radio galaxies by the green triangles, and PG quasars by the yellow stars (Sikora *et al.*, 2007).

to the monitored spectrum (cf. Zuther *et al.*, 2012). I find a 5100\AA continuum luminosity of $\lambda L_{\lambda}(5100\text{\AA}) = 7.4 \times 10^{42} \text{ erg s}^{-1}$. From Eq 3.12, the bolometric luminosity is $L_{\text{bol}} \approx 7.0 \times 10^{43} \text{ erg s}^{-1}$, and with a black hole mass estimate of $\log(M_{\text{BH}}/M_{\odot}) \sim 6.9$, the Eddington luminosity¹ is $L_{\text{Edd}} \approx 1.6 \times 10^{45} \text{ erg s}^{-1}$. This results in a value for the Eddington ratio of $\log \eta = -1.39$. In Figure 3.9 and Figure 3.10 I compare my values with published results. As I show in Fig. 3.9, in $\log \eta - \log R$ space, the source J0808 lies in the region in which we also find the broad emission-line radio-galaxies (BLRG) and RL quasars. The same phenomenon is found in Fig. 3.10 ($\log M_{\text{BH}} - \log R$). However, I find that the mass of the super-massive black hole is apparently lower than that of the bulk of radio galaxies that have been taken into account in the plot.

¹The Eddington luminosity is the luminosity radiated at the Eddington limit and is calculated as $L_{\text{edd}} \approx 1.26 \times 10^{38} \left(\frac{M_{\text{BH}}}{M_{\odot}}\right) \text{ erg s}^{-1}$.

3. HIGH-RESOLUTION OBSERVATIONS OF SDSS J080800.99+483807.7 IN THE OPTICAL AND RADIO DOMAINS

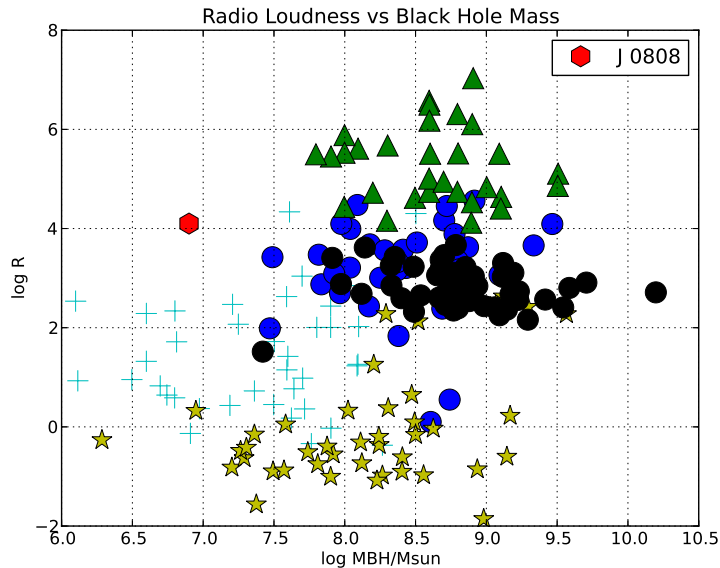


Figure 3.10: Radio loudness versus black hole mass. See caption of Fig. 3.9.

Table 3.4: The rest radio flux densities and luminosities for source components of the J0808 radio counterpart at 18 cm.

Position	Brightest Point		Center		Total Area	
	Flux (10^{-3} Jy per beam)	Luminos. (10^{23} W Hz^{-1} per beam)	Flux (10^{-3} Jy per beam)	Luminos. (10^{23} W Hz^{-1} per beam)	Flux (10^{-2} Jy)	Luminos. (10^{24} W Hz^{-1})
Southeast Lobe	1.28	3.17	0.81	2.01	3.71	9.17
Center Region	0.27	0.67	–	–	0.72	1.79
Northwest Lobe	1.41	3.49	0.45	1.12	4.69	11.59

3.4.5 Star formation in the host galaxy of J0808

The nuclear activity (via accretion onto the central SMBH) and the star formation activity (e.g. the blue luminosity of the bulge or host) are likely to be linked to each other. This results e.g. in the correlation between black hole mass and bulge luminosity or velocity dispersion of the bulge. therefore, in the case of radio galaxies, their hosts may be also characterized by strong star-formation activity. However, this is a matter of intense debate as interactions between the jet and the host ISM may also lead to suppression of star formation, as discussed in, e.g., [Nesvadba et al. \(2010\)](#). Radio galaxies with strong nuclear emission lines have star-formation activity that is a factor of 3-4 higher than in weak-line sources ([Hardcastle et al., 2013](#)). The line emission of J0808 and the fact that it is RL suggests that its star-formation rate is substantial.

To estimate the star-formation rate from optical data, I use the luminosity of the emission line [O II] $\lambda 3728$ ([Ho, 2005](#); [Hopkins et al., 2003](#); [Kennicutt, 1998](#)):

$$\text{SFR}_{[\text{O II}]} [M_{\odot} \text{ yr}^{-1}] = \frac{L_{[\text{O II}]}}{2.97 \times 10^{33} \text{ W}}. \quad (3.13)$$

I correct the reddening of the [O II] using theoretical Balmer decrement $H\alpha/H\beta = 2.86$ and assuming case B recombination for a region with electron density of 10^4 cm^{-3} and temperature $T = 10^4 \text{ K}$ ([Osterbrock, 1989](#)). According to the extinction law of [Calzetti et al. \(1994\)](#), I calculate the luminosity of [O II] $\lambda 3728$ to be $5.82 \times 10^{34} \text{ W}$, resulting in a star-formation rate of $\text{SFR} = 19.59 M_{\odot} \text{ yr}^{-1}$. The WISE infrared survey provides us with additional valuable infrared data on J0808. There the source has been measured at 3.4, 4.6 and $12 \mu\text{m}$. From a sample of dusty galaxies, I randomly picked galaxies from the IRAS point source catalog ([Lonsdale and Helou, 1985](#)) and find that the median flux density ratio between $12 \mu\text{m}$ and $60 \mu\text{m}$ wavelength lies at about 20 with an uncertainty of about 10. From [Helou \(1986\)](#), the ratio between the flux densities S_{60} and S_{100} at $100 \mu\text{m}$ and $60 \mu\text{m}$ wavelength is known to be in order of 2 ± 1 . The fluxes in these two bands are often dominated by continuum emission of warm dust. Hence, I can extrapolate from the WISE detection of J0808 at $12 \mu\text{m}$ to obtain an estimate of the far-infrared (FIR) luminosity of $L_{\text{FIR}} = 23.96 \times 10^5 (2.258 S_{60} + S_{100}) D_L [\text{Mpc}]^2 = (2.2 \pm 1.1) \times 10^{10} L_{\odot}$. This results in a star-formation rate of OBA stars of $\nu_{\text{OBA}} = 2.1 \times 10^{-10} \times L_{\text{FIR}} = 5 \pm 4 M_{\odot} \text{ yr}^{-1}$ ([Thronson and Telesco, 1986](#)). To measure the star-formation rate from radio data, I apply the formalism published by [Bell \(2003\)](#). This formalism is related to the 20 cm luminosity density

$$\left(\frac{\text{SFR}}{M_{\odot} \text{ yr}^{-1}} \right) = 5.52 \times 10^{-22} \left(\frac{L_{20\text{cm}}}{\text{W Hz}^{-1}} \right). \quad (3.14)$$

3. HIGH-RESOLUTION OBSERVATIONS OF SDSS J080800.99+483807.7 IN THE OPTICAL AND RADIO DOMAINS

From the radio spectrum discussed earlier, I obtain the luminosity at 20 cm and find $L_{20\text{ cm}} = 6 \times 10^{23} \text{ W Hz}^{-1}$. Interpreting this radio luminosity in the context of star formation, this implies that only a very small fraction of about 1% of the overall nuclear radio luminosity is required to explain the expected contribution from the above derived star-formation rate. The bulk of the emission may be due to the nuclear jet or the portion of the jet that flows back along the envelope of the jet onto the host.

The radio emission can also have a different source. On global scales the radio emission can also be due to contributions from supernova explosions. The rate of supernova explosions is a measure of the high-mass star formation. Following [Condon and Yin \(1990\)](#), I calculate the supernova rate of J0808 from its central radio flux density via

$$\left(\frac{\text{SNR}}{\text{yr}^{-1}}\right) \approx 7.7 \times 10^{-24} \left(\frac{\nu}{\text{GHz}}\right)^\alpha \left(\frac{L_{\text{NT}}}{\text{WHz}^{-1}}\right). \quad (3.15)$$

Here, SNR is the supernova rate per year, ν is the observing frequency, L_{NT} the non-thermal radio luminosity, and α the radio spectral index.

Using MERLIN observations I was able to calculate the central luminosity at 18 cm to be $L_{18\text{cm}} = 0.67 \times 10^{23} \text{ W Hz}^{-1}$ from table 3.4. For an assumed nuclear spectral index of $\alpha = -0.60$, I calculate the supernova rate at the center as $\text{SNR} \approx 0.4 \text{ yr}^{-1}$. This is consistent with the OBA star-formation rate obtained above from the extrapolation of the WISE $12\mu\text{m}$ measurements. However, the super nova rate may only be considered as an upper limit. Given that the nuclear radio emission may contain a significant amount of non-thermal radiation from the jet and taking into account that the nuclear spectral index could also be steeper than $\alpha = -0.60$, I judge SNR as an upper limit. Following [Hill et al. \(2001\)](#) and [Laine et al. \(2006\)](#), the host is considered to be a Seyfert galaxy if the supernova rate is $\lesssim 1 \text{ yr}^{-1}$. Starburst galaxies have supernova rates of $\text{SNR} \lesssim 10 \text{ yr}^{-1}$.

3.5 Discussion and Conclusions

Imaging and spectroscopic data have given us detailed information on the physics and nature of J0808. These data has made it possible to investigate the physical properties of J0808. Through MERLIN radio observations I have shown that the source J0808 is a compact double lobed radio source at a redshift of $z = 0.2805 \pm 0.0003$; it shows a radio structure reminiscent of those that may present significant back-flow of material along the jet or outflow into the host ([Silk, 2013](#); [Wagner et al., 2013](#)). The host of the radio source has been detected in the optical

and infrared emission in the SDSS and WISE surveys. The optical spectrum as well as the optical and infrared images of the host suggest that it is a compact early-type host galaxy. The LBT MODS1 spectra, an estimate of the FIR luminosity, and the radio flux at the position of the host reveal that the host shows indications of strong star-forming activity. The widths of forbidden lines indicate a black hole mass of $\sim 10^{6.9}M_{\odot}$.

As binary sources need to be resolved the detection of the binarity of sources also clearly depends on the size of the telescope or interferometer used. In order to make sure that the position of J0808 at the lower edge of the distribution shown in Fig.5 is indeed special, I compare the properties of small and large radio double sources that, in fact, form a continuum in separations. O’Dea and Baum (1997) plot power versus projected largest linear size for the complete samples of gigahertz-peaked spectrum (GPS) and compact-steep spectrum (CSS) sources (Fanti *et al.*, 1985, 1995; Fanti, 2009; Stanghellini *et al.*, 1998) and the 3CR (Laing *et al.*, 1983) for the redshift range $0.2 \leq z \leq 1.0$ and find that there is a good overlap between the samples.

The data at hand now allows us to judge on the radio source evolution. The radio source evolution can be constrained by plotting the number of sources as a function of size in the power versus linear size plane. O’Dea and Baum (1997) find that the number of sources is roughly constant per linear size bin for sources less than about 10 kpc. For the larger sources, the number increases with increasing source size. This can be interpreted as an indication for a qualitatively different evolution of the small sources compared to the large ones. In fact, O’Dea (1998) points out that the GPS sources are entirely contained within the extent of the narrow-line region (less than about 1 kpc), while the CSS sources are contained entirely within the host galaxy (less than about 15 kpc). An explanation for this effect may be that the small sources are still embedded in the ISM of the host while the large ones can expand more freely. This shows that the source that I showing here is indeed representative for the smaller (around 10 kpc size) of the large double sources discussed by O’Dea and Baum (1997).

In order to get significant star formation going one needs a large amount of molecular gas. Although the hosts of double radio sources in general do not have significant amounts of molecular gas, they do show signatures of star formation. An exception, on the one hand, are starburst radio galaxies that comprise 15-25 per cent of all powerful extragalactic radio sources (Tadhunter *et al.*, 2011). On the other hand, it appears that the interaction with the radio jet quenches star formation and that hosts of radio galaxies seem to be inefficiently forming stars

3. HIGH-RESOLUTION OBSERVATIONS OF SDSS J080800.99+483807.7 IN THE OPTICAL AND RADIO DOMAINS

(e.g., Nesvadba *et al.*, 2010). O’Dea *et al.* (2005) find no abundant molecular gas reservoirs in GPS radio sources with upper limits of 10^9 to a few times $10^{10} M_{\odot}$.

The excess of ultraviolet (UV) radiation is an important tool to investigate the influence of a non-thermal nucleus or the formation of young massive stars. Fanti *et al.* (2011) and Labiano *et al.* (2008) find that most of the hosts of CSS radio binaries show an excess of ultraviolet (UV) radiation compared to the spectra of local RQ ellipticals. This is despite the apparent lack of large amounts of molecular gas. This UV excess may be due to an active nucleus or to a young stellar population, both of which may be triggered by the same event or influence each other. Similarly, I also find for J0808 diagnostic line ratios that clearly indicate the presence of star formation in the host galaxy. While a merger event may have caused both the ongoing jet activity, I have, however, no indication that the host has been affected by a recent merger event from the available imaging information. Hence the case of J0808 also allows us to follow a different interpretation: This source has an extended nuclear radio structure suggesting an interaction of the host ISM with the back-flowing material. Thus for J0808 the star formation may be triggered by the back-flow along the jet and its interaction with the AGN host.

4

Line and Continuum Variability in Active Galaxies

4.1 Introduction

Active Galactic Nuclei are characterized by their compactness and luminosity that is then intimately linked to the variability of these sources. As variability at almost all wavelengths (Peterson, 2001), As compact accreting objects AGNs are characterized by variability at almost all wavelengths (Peterson, 2001), studying the variability on all time scales is a very useful approach to investigate and understand the physical properties of AGNs. As usual in astrophysics the properties of this class of sources can only be studied for individual cases and - most importantly - in the framework of statistical investigations. There are many systematic studies about the variability of AGN using spectroscopic and photometric observation. Some photometric measurements are used to study the variability, despite the fact that bright line emission is lying within the corresponding passband (Vanden Berk *et al.*, 2004). Studying the spectral variability both in line and in continuum emission has become an important topic that may help to outline differences between different Seyfert source classes. Variability may indicate how the active galactic nuclei (AGN) affect the regions surrounding them (i.e. the BLR and NLR) and how these regions change as a function of time. Many interesting results have been obtained from AGN samples of different type and size. A famous one is the anti-correlation between the continuum luminosity and variability, which was first reported by Angione and Smith (1972). Later additional information on this effect was provided by Hook *et al.* (1994); Zuo *et al.* (2012, 2013). Additionally, other authors (Cid Fernandes and Sodre, 2000; Meusinger

4. LINE AND CONTINUUM VARIABILITY IN ACTIVE GALAXIES

and Weiss, 2013) have clarified that this anti-correlation can qualitatively be described via the standard accretion disk model, by proposing that the variability was caused via the alteration of accretion rate.

Spectroscopic studies can be very time consuming if applied to large statistical samples. There are just a few detailed, spectroscopy-based comparative studies on the variability of AGNs, Spectroscopic studies can be very time consuming, They either concentrated on the reverberation mapping analysis for extensively observed sources (e.g., Kaspi *et al.*, 2007) or depend on just a few epochs of the spectroscopic observations (e.g., Wilhite *et al.*, 2005). Multi epoch spectroscopy observations have advantages compared to photometric observations as they allow us to study the continuum and line emission at the same time. Excepting regions of high emission line density these observations also allow us to extract the underlying continuum spectrum over a broad wavelength range and to study the spectral shape of the lines and the line spectrum in general. The emission line spectra then allow us to study the BLR and NLR regions surrounding the compact variable continuum nuclei.

The continuum variability of QSOs and Seyfert galaxies is essential as it characterizes the accretion physics in these nuclei. Quite a number of extensive investigations about the variability in Seyferts and quasars under the aspect of the continuum and the fluxes of the emission lines can be given, e.g., Guo and Gu (2014); Peterson and Gaskell (1986); Peterson *et al.* (1984, 1998). While the BLR lines are found to reverberate the continuum variability on time scales of days there are also a few reports on long term line variability of the NLR region: Based on a time coverage of 8 years (Clavel and Wamsteker, 1987) find for 3C390.3 that the NLR is photoionized and reverberates the continuum flux. They set an upper limit of 10 light years for the size of the NLR. Based on a time coverage of 5 years (Peterson *et al.*, 2013) find for the S1 galaxy NGC 5548 that the [O III] $\lambda\lambda 4959, 5007$ emission-line flux to vary with time and give a size estimate of 1-3 pc (i.e. 3-9 light years). There is a clear connection between the continuum and line variability. For instance, Peterson *et al.* (1984) found for $\sim 73\%$ of the cases that they studied, that there is variability in the $H\beta$ line flux corresponding to the changes in the continuum. On the other hand, in the same project they found that this correlation is not true for the sources if the continuum changes by more than $\sim 70\%$. They think that for cases in which the $H\beta$ flux is not corresponding to the continuum, light travel time effects may have to be included. Furthermore, there is still no absolute conclusion on the correlation between the

emission lines width and the line luminosity. An anti-correlation was found in a sample of 85 quasars by Brotherton *et al.* (1994), with single-epoch spectroscopic data. On the other hand Wilhite *et al.* (2005) found there is a correlation between the emission lines width and the line luminosity. They conclude this from a spectroscopic sample of 315 quasars.

4.2 How the source samples were selected

In this chapter I investigate the continuum and narrow line variability of a small sample of objects over a good fraction of a decade. In my investigation I made full use of the spectroscopic capabilities of modern instrumentation in the optical wavelength domain. Hence, the spectra I use cover a major fraction of the entire optical wavelength domain from the blue to the red including several prominent lines and having an appreciable signal to noise ratio also on the continuum emission. For such a study it is essential that the spectra are well calibrated such that they can be compared to each other. It is also important to correct for iron emission in order to extract proper values for the line luminosities of species other than iron. As the data has been taken with different instruments and different effective apertures on the sky it is furthermore essential to make sure that aperture effects, as they may occur due to slit losses or from extended and spatially resolved line or continuum emission from the host galaxies, do not contaminate the results of the variability assessment. In the literature one finds rather rarely appropriately calibrated or sufficiently described data sets that are suitable for long term variability studies. Hence, I made the effort to collect and combine a representative spectroscopic data set. This comprises a total of 18 sources (see summary in Sec. 4.6.1). For 8 objects I obtained and/or performed the detailed analysis over the available optical wavelength range using data from the LBT and other observatories (see Sect. 4.3 and Tab. 4.1). For 5 sources (3 NLS1 and only 2 BLS1) I obtained spectroscopic information from the literature. For a further 5 sources (2 NLS1 and 3 BLS1) I found sparser but suitable line and continuum information in the literature. A detailed description of the SDSS data is given in Sect. 4.3, followed by a description of the methods used for my analysis in Sect. 4.4. In Sect. 4.5 I present the results for all galaxies that I used in my study.

As I was aiming at investigation the variability for a limited but representative class of objects I included a range of source identifications. The sample also comprises sources with a range of identifications. For the purpose of this investigation I combined sources that show very prominent broad emission lines, i.e. Broad Line Seyfert 1 and Quasi Stellar Objects (in the

4. LINE AND CONTINUUM VARIABILITY IN ACTIVE GALAXIES

following BLS1 and QSO) in addition to the narrow lines on which my investigation focuses. I also put Seyfert 2 and Narrow Line Seyfert 1 (S2¹ and NLS1) in one group as their spectra are dominated by narrow line emission. An additional justification for this combination is based on the fact that while the unified model of Seyfert galaxies suggests that there are hidden broad-line regions (HBLRs) in all Seyfert 2 galaxies, there is increasing evidence for the presence of a subclass of Seyfert 2 sources lacking these HBLRs (Haas *et al.*, 2007; Zhang and Wang, 2006). In these cases one cannot exclude the possibility of the free sight to the nucleus despite of the fact that the source is classified as a S2 galaxy. I also refer here to the discussion in the review on NLS1 galaxies by Komossa (2008). Hence, if one classifies sources based on the presence of absence of pronounced broad line emission, then S2 and NLS1 may be more comparable to each other than e.g. BLS1 with NLS1 sources. In the discussion in Sect. 5.4 and 4.6.1) the observed degrees of continuum and narrow line variability are analyzed. In retrospect I found that the above described combination of sources is indeed justified by their different variability characteristics.

The investigation I present here can only be a first step. The statistics must be put on a firm and broad footing. Therefore, at some point such an investigation needs to be performed using larger samples. Since an appropriate baseline for variability studies of several years is required such an effort needs time and can only be provided in the near future. However, to study first order effects, the number of sources needs to be only sufficiently large to separate the median or mean properties within the statistical uncertainties. As I outline in this chapter, this can already be done with the current, representative sample that I compiled. In fact, the interpretation I present in Sect. 4.6.2. This chapter may also be taken as a prediction of the effect that the degree of the continuum variability is indeed reverberated by the degree of narrow line variability. This prediction was motivated by the results of the analysis of the small but representative sample that I present in this chapter. A conclusion is given in Sect. 4.7.

4.3 Optical observations LBT and SDSS

Here I use optical data observed by LBT using MODS1 in long-slit mode with a slit width of 0'.8. The spectrograph operates between 3200-10500 Å with a spectral resolution of $R=\lambda/\delta\lambda \approx 2000$ (i.e., $\sim 150 \text{ km s}^{-1}$) where the full spectral range of the grating spectroscopy is split into

¹One of the sample sources is a composite HII/S2 galaxy - but see discussion in Sect. 4.5.1

a blue and red channel, which are 3200-6000 Å (blue) and 5000-10500 Å (red). All objects which I targeted with the LBT observing program are listed in Tab. 4.1.

For SDSS observations, In this research I used the SDSS active galaxies (Seyfert & Quasar) Catalogs based on the seventh data release of the SDSS (Abazajian *et al.*, 2009). All The project targets (except J035409.48+024930.7 and J015328+260939 that are not covered by the SDSS survey) can be found in different SDSS catalogue releases (DR5, DR6, DR7, DR8, and DR9) (Abazajian *et al.*, 2009; Adelman-McCarthy and *et al.*, 2009, 2011; Adelman-McCarthy *et al.*, 2008; Gibson *et al.*, 2009; Inada *et al.*, 2012; Skrutskie *et al.*, 2006; Stoughton *et al.*, 2002; York *et al.*, 2000).

Typical magnitudes of SDSS sources e.g. in the g-band are in the range of $14.47 \leq g \leq 19.21$, the FWHM of the combined bright narrow and broad lines the FWHM typically range from about 300 to 3000 km s⁻¹. In this chapter I analyze the optical spectra of eight galaxies, one is classified as composite HII/S2, 3 sources are classified as S1 (BLS1 & NLS1), and 4 sources are classified as QSOs. Further information about the analyzed objects is presented in Tab. 4.1. In Figs. 4.2 and 4.3, I present images of the sources and a nearby reference star extracted from the same image frame. The flux calibration step is already explained in the second chapter (INSTRUMENTATION AND DATA REDUCTION).

Combining data from different telescopes and from different epochs needs special care. Therefore, in order to insure a sufficient inter-calibration accuracy between telescopes and instruments, a correction has been applied for the slit losses. My target sources was observed (including the two calibrated stars; see above) in typically 1.2 to 1.4 arcsec seeing through a 0.8 arcsec slit. For the two extreme cases a seeing correction based on Fig. 4.1 was applied. For J0153 taken in 1.90'' seeing, the LBT fluxes scaled up by a factor of 1.35. For J1203 taken in 0.82'' seeing, the LBT fluxes scaled down by a factor of 0.70 SDSS.

A particular problem is that the slit loss contribution is time variable. In order to correct for a time variable slit loss contribution I proceeded in the following way: For each target I have 2 to 5 exposures such that I have a good statistical estimate on the flux loss due to the combination of variable seeing and misplacement of the slit. In Fig. 4.1 I present a number histogram of the intensity drop measured in the [OIII] $\lambda 5007$, [OII] $\lambda 3727$, H β or H α line in the corresponding red and blue channel for the fainter exposures with respect to the brightest once. To first order this effect was corrected by adjusting all exposures to the flux level of the brightest exposure per source. Under the assumption that for the brightest exposure the slit was always centered on the source no additional correction for slit losses is necessary (i.e. a factor of unity; case

4. LINE AND CONTINUUM VARIABILITY IN ACTIVE GALAXIES

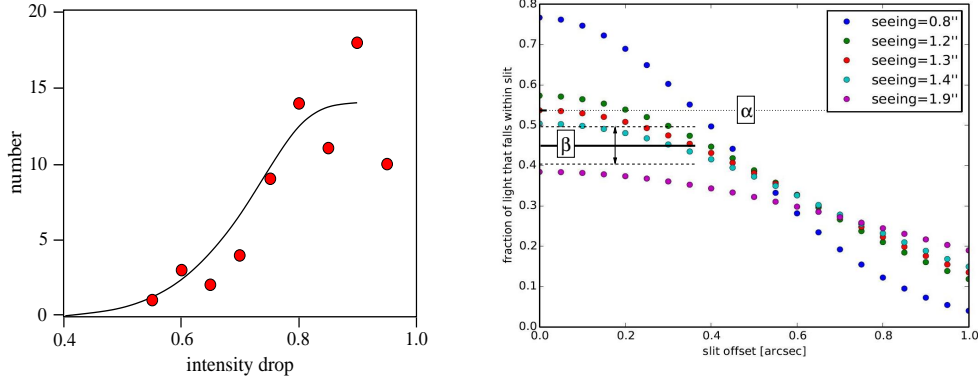


Figure 4.1: Left: For all sources I present the distribution of the intensity drops of the fainter exposures with respect to the brightest once. The data is shown in bin widths of 0.05 (fat dots) and for comparison half the value obtained with a bin width of 0.10 (black line). Right: Intensity drop due to the combination of variable seeing and slit offset. Case α indicates the level (dotted line) to which the spectra can be calibrated if for individual sources the fainter exposures are corrected to the level of the brightest once. For case β I assume that the brightest exposures all are subjected to the mean drop (fat black line) indicated by the statistics of the faintest with respect to the brightest exposures. The arrow and the dashed lines indicate the standard deviation from the mean.

α in Fig. 4.1). The statistical approach must also cover an additional aspect: If I assume that no significant systematical misplacements happened and that the statistics for slit losses for the brightest exposures is similar to the statistics of the fainter exposures then an unfavorable and unlikely case will be that all brightest exposures were taken under conditions of a mean slit loss (case β in Fig. 4.1). To improve the calibration even further, I assumed for a final second order correction for slit losses a case between case α and case β and chose the mean between unity and the factor for mean losses of 1.17 ± 0.10 , i.e. a second order correction factor of 1.08, after having applied the first order correction. Based on Fig. 4.1 the uncertainty on this correction for the time variable slit losses is probably of the order of 5% for the 1.2" to 1.4" seeing cases. For J0153 with 1.9" this correction is probably overestimated by <5% For J1203 with 0.82" seeing the correction may be underestimated by 5-10% especially if one takes into account that for a better seeing slit positioning can also be done more reliably. Given the seeing and aperture combinations for the Beijing and Hiltner telescope measurements (see section 4.5.7 and 4.5.6) as well as the high SDSS calibration quality (see section 4.3) no seeing/slit loss corrections were applied to these data.

As I flux calibrate my observed spectra with the flux calibration stars observed through

the same slits, and as I state that the galaxies are all very compact (see section 4.3 and Fig. 2.4, Fig. 4.1, and section 4.5.1 for the marginally extended source J0938) I assume the inter-calibration uncertainties to be less than 10%.

4.3.1 Measurements of the magnitude

It is essential to take special care in the derivation of magnitudes for our sources. Deriving the magnitude of a source will depend on the method used. For compact objects (as in our case) it is easier than for very extended objects. In the SDSS survey the magnitudes are derived using different methods (Model, Cmodel, Petrosian, and PSF). For this work I used magnitudes derived via the PSF method in which a Gaussian model of the PSF is fitted to the source (dominated by a compact PSF like object). This technique also accounts for the variation of the PSF across the field and was hence considered as most suitable for this study. Such variations are mostly due to optics of the telescope/instrument combination, as wide field operation is often a prime goal in designing these systems.

The data in my study provides both spectroscopic and imaging information. Both kind of data include information on the continuum fluxes of the sources. I compared the flux density value of the photometric observations¹ with those obtained from spectroscopic observation for each source. In this way I can get an estimate on the degree of variability that is present in the nuclei of these objects.

The LBT allows for the usage of a variety of spectrometer slit widths. In my case the observations were carried out using a long slit with aperture of 0'8 was used, while for In the LBT observations a long slit with aperture of 0'8 was used, while for the SDSS observations they using a spectroscopic fiber with radius of 3''. To demonstrate that aperture effects between the fiber and the slit measurements are negligible, I show SDSS z -band images of the galaxies together with images of closeby stars from the same observed frame (Figs. 4.2 and 4.3). The flux for each star was scaled to the level of each galaxy and then subtract the frames from each other. In all eight cases, no emission is left. This shows that the sources are all dominated by emission from an unresolved combination of a stellar bulge and an AGN. Furthermore, I fitted Gaussian functions to the images of the galaxies and the stars. The results are listed in Tab. 4.4,

¹I used the Gemini flux density/magnitude converter (<http://www.gemini.edu/?q=node/11119>) to convert the magnitudes derived from the photometric images in the u, g, r, i , and z -bands into physical units (flux density F_λ in $\text{erg s}^{-1} \text{cm}^{-2} \text{\AA}^{-1}$).

4. LINE AND CONTINUUM VARIABILITY IN ACTIVE GALAXIES

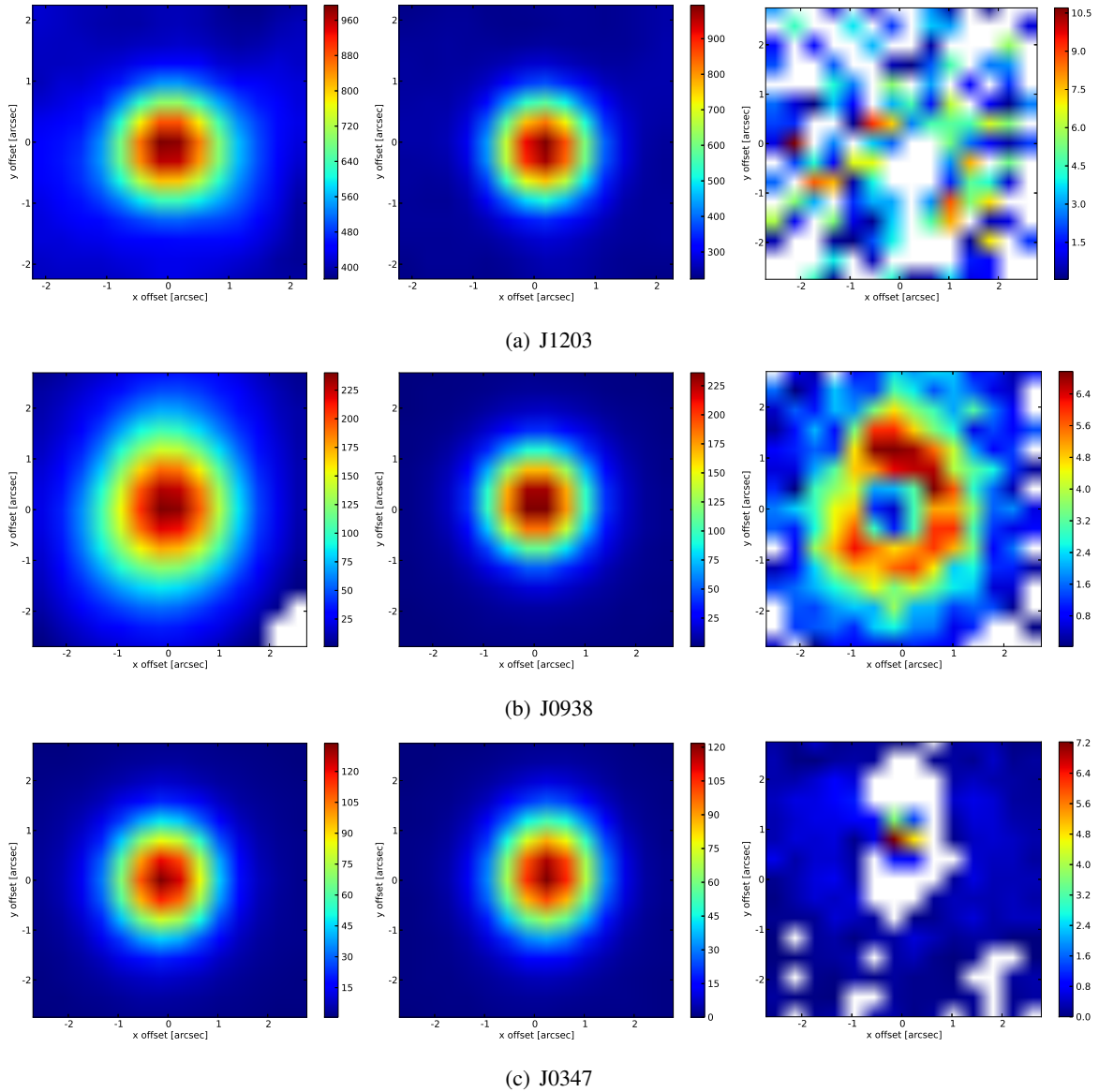


Figure 4.2: The plot shows *from left to right* an SDSS image of the galaxies J1203, J0938, and J0347, a stars/point sources from the same SDSS frame for each object (coordinates are listed in Tab. 4.4) and the residuum that is left after subtracting the scaled star from the galaxy. The same plots for the other galaxies can be found in the next figure (4.3).

4.3 Optical observations LBT and SDSS

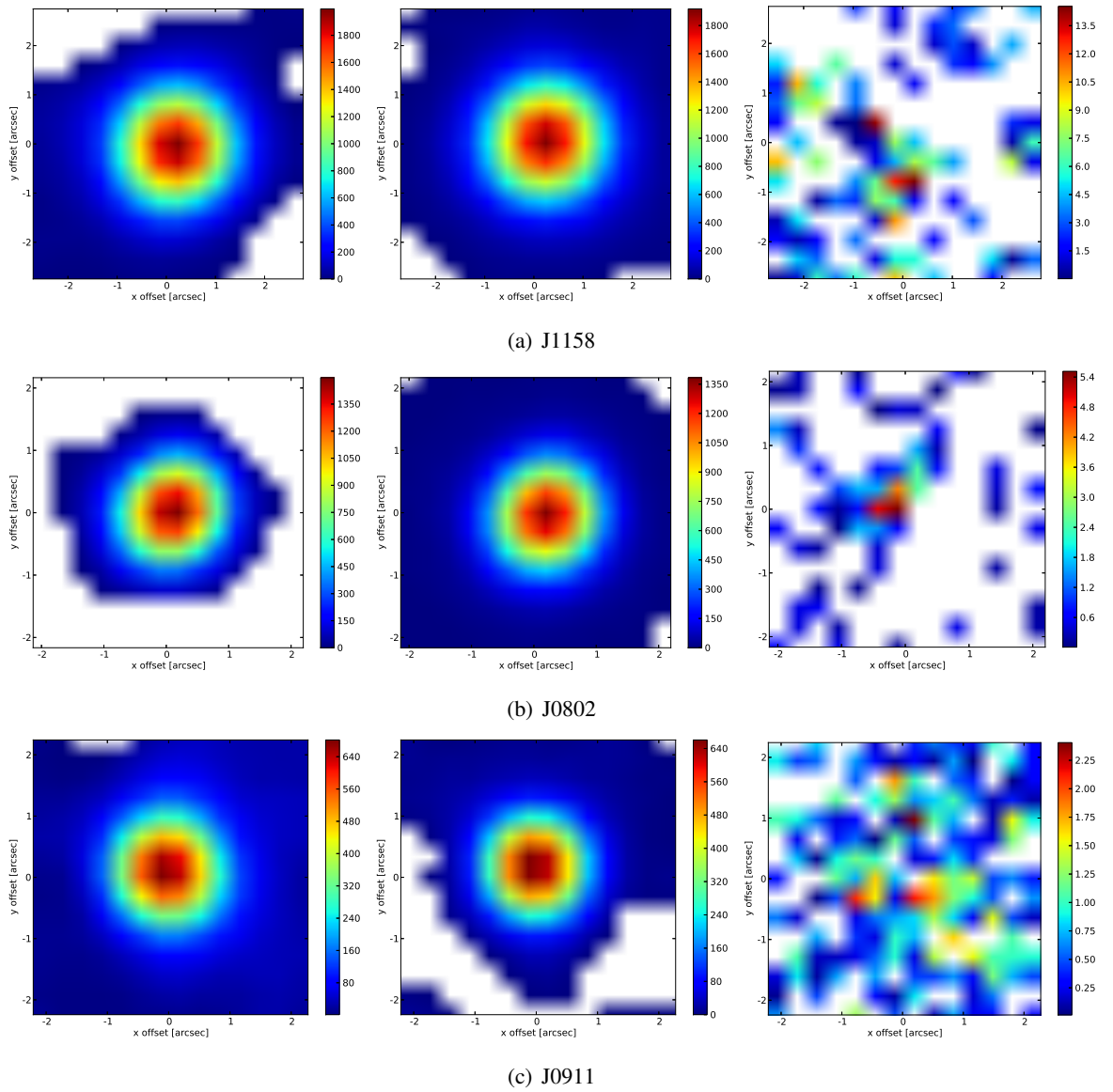


Figure 4.3: The same as Fig. 4.2 but for the other galaxies J1158, J0802, and J0911.

4. LINE AND CONTINUUM VARIABILITY IN ACTIVE GALAXIES

Table 4.1: Coordinates, redshifts, classification and observing parameters for all sources.

name	RA	Dec.	Redshift (z)	Classi.	Obs. date 1	Obs. date 2	Photo. obs. date	D_L	Ref.
	(hh mm ss)	($^{\circ}$ ' ")							
SDSS J120300.19+162443.8	12 03 00.1	16 24 43.8	0.16552 \pm 0.00001	S2	SDSS 04 2007	02 2012	06 2005	794.5	1
SDSS J093801.63+135317.0	09 38 01.6	13 53 17.0	0.10056 \pm 0.00001	HII/S2	SDSS 12 2006	02 2012	01 2006	463.2	2
SDSS J034740.18+010514.0	03 47 40.1	01 05 14.0	0.03149 \pm 0.00003	NLS1	OHP ^(a) 09 2003	02 2012	11 2001	138.1	3,4
SDSS J115816.72+132624.1	11 58 16.7	13 26 24.1	0.43966 \pm 0.00035	QSO	SDSS 05 2004	01 2012	03 2003	2429.5	5,6
SDSS J080248.18+551328.9	08 02 48.1	55 13 28.8	0.66406 \pm 0.00035	QSO	SDSS 01 2005	01 2012	11 2003	3993.9	5,7
SDSS J091146.06+403501.0	09 11 46.0	40 35 01.0	0.44121 \pm 0.00099	QSO	SDSS 01 2003	02 2012	12 2001	2439.7	5,6
2MASX J03540948+0249307 ^(*)	03 54 09.4	02 49 30.7	0.03600 \pm 0.00008	BLS1	Hiltner ^(b) 10 2004	02 2012	—	158.4	3,8
GALEXASC J015328.23+260938.5 ^(*)	01 53 28.2	26 09 39.1	0.32640 \pm 0.00127	QSO	Beijing ^(c) 02 2002	01 2012	—	1711.9	9,10

Notes. References for redshifts and positions: (1) (Adelman-McCarthy *et al.*, 2011); (2) (Sánchez Almeida *et al.*, 2011); (3) (Véron-Cetty and Véron, 2006); (4) (Hewitt and Burbidge, 1991); (5) (Hewitt and Wild, 2010); (6) (Zhang *et al.*, 2010); (7) (Gibson *et al.*, 2009); (8) (Chaman *et al.*, 1981); (9) (Darling and Giovanelli, 2002); (10) (Zhou *et al.*, 2002).

Notes: The 3 QSOs contained in the SDSS catalogue have been classified as low-ionization broad absorption-line (LOBAL) due to a prominent [Mg II] absorption in their spectra. The second spectroscopy observation have always taken by LBT. The photometric observations were always taken by SDSS. For the final two sources in the table no SDSS photometric observations are available.

* Not covered by SDSS survey

^a Telescope of Observatoire de Haute-Provence (OHP)

^b Hiltner Telescope

^c Beijing Observatory

Table 4.2: Comparison of seeing conditions for the sources for which I analyzed the spectra.

Sources	LBT seeing	Comparing Spectro. Inst.	seeing	SDSS photometric Median Seeing (r-band)
	"		"	"
J1203	0.82	SDSS	1.48	1.4
J0938	1.30	SDSS	1.69	1.4
J0347	1.40	OHP	2.5	1.4
J1158	1.40	SDSS	1.22	1.4
J0802	1.20	SDSS	1.49	1.4
J0911	1.20	SDSS	1.23	1.4
J0354	1.20	Hiltner	2.5	–
J0153	1.90	Beijing	2.5	–

supporting the finding that the galaxy emission is dominated by the unresolved point source. In Tab. 4.2 I list the seeing values for the different exposures.

4.4 Analysis

In collaboration with my colleagues I developed a *Python* routine to manually fit the stellar continuum, the power-law contribution from the AGN, as well as the Fe II emission and subtract all of them. In the residual, continuum-subtracted spectrum, I can then fit the emission lines. In following I will clarify each step:

4.4.1 Stellar continuum subtraction

To obtain an accurate measurement of the nuclear emission line fluxes and the equivalent widths, I have to subtract the stellar component of the host or its bulge component. To remove the stellar component a stellar population synthesis model was fitted to the entire spectrum. The templates that have been used in this chapter are given by a sample spectrum built by an often used population synthesis routine in [Bruzual and Charlot \(2003\)](#). Usually two kinds of star burst models are used: A steady star formation contribution and a short time star burst. Both concepts can be combined. The template for the young stellar population spectrum is taken 290 Myr after a star burst with steady star formation rate over 0.1 Gyr and solar metallicity. For

4. LINE AND CONTINUUM VARIABILITY IN ACTIVE GALAXIES

Table 4.3: The observed continuum flux density variability between LBT and SDSS/OHP of J0938, J1203, J1158, J0911, J0802, and J0347 from the photometry and spectroscopy aspect. ^(a)For J0347 first epoch spectroscopy obtained by OHP.

Sources	Filt.	Wa. Å	photometry	spectroscopy	spectroscopy
			SDSS [10^{-16} erg $s^{-1} \text{ cm}^{-2} \text{ Å}^{-1}$]	SDSS ^(a) [10^{-16} erg $s^{-1} \text{ cm}^{-2} \text{ Å}^{-1}$]	LBT [10^{-16} erg $s^{-1} \text{ cm}^{-2} \text{ Å}^{-1}$]
J1203	(u)	3543	1.26 ± 0.03	—	2.04 ± 0.99
	(g)	4770	1.06 ± 0.02	1.20 ± 0.19	1.54 ± 0.38
	(r)	6231	1.53 ± 0.01	1.02 ± 0.31	0.87 ± 0.13
	(i)	7550	1.09 ± 0.01	0.81 ± 0.21	0.61 ± 0.14
	(z)	9134	0.53 ± 0.03	0.65 ± 0.32	0.49 ± 0.13
J0938	(u)	3543	1.60 ± 0.03	—	1.87 ± 0.31
	(g)	4600	2.39 ± 0.02	3.41 ± 0.19	2.66 ± 0.27
	(r)	6231	2.01 ± 0.02	3.30 ± 0.15	2.48 ± 0.31
	(i)	7625	1.67 ± 0.02	3.05 ± 0.17	2.36 ± 0.41
	(z)	9134	1.50 ± 0.02	2.79 ± 0.27	2.12 ± 0.45
J0347 ^(a)	(u)	3543	68.81 ± 0.01	—	52.79 ± 0.09
	(g)	4770	53.90 ± 0.02	44.60 ± 0.21	60.38 ± 0.02
	(r)	6231	44.92 ± 0.01	31.12 ± 0.15	39.23 ± 0.01
	(i)	7625	40.91 ± 0.02	27.71 ± 0.11	33.81 ± 0.02
	(z)	9134	26.93 ± 0.01	—	26.39 ± 0.04
J1158	(u)	3543	5.98 ± 0.04	—	5.12 ± 0.63
	(g)	4770	4.29 ± 0.02	4.62 ± 0.23	3.91 ± 0.33
	(r)	6400	2.87 ± 0.02	2.81 ± 0.14	3.31 ± 0.16
	(i)	7700	2.21 ± 0.02	2.15 ± 0.16	2.65 ± 0.03
	(z)	9134	1.77 ± 0.03	1.48 ± 0.48	1.87 ± 0.07
J0802	(u)	3543	0.41 ± 0.06	—	0.88 ± 0.49
	(g)	4770	0.97 ± 0.01	1.02 ± 0.12	1.37 ± 0.11
	(r)	6231	1.17 ± 0.01	1.14 ± 0.11	1.49 ± 0.06
	(i)	7625	1.24 ± 0.02	1.16 ± 0.20	1.71 ± 0.10
	(z)	9134	1.04 ± 0.02	0.97 ± 0.25	1.23 ± 0.29
J0911	(u)	3543	0.89 ± 0.04	—	0.61 ± 0.27
	(g)	4770	0.86 ± 0.02	0.67 ± 0.04	0.92 ± 0.22
	(r)	6200	0.85 ± 0.01	0.90 ± 0.04	1.10 ± 0.15
	(i)	7700	0.68 ± 0.02	0.72 ± 0.03	0.96 ± 0.07
	(z)	9134	0.54 ± 0.03	0.56 ± 0.10	0.76 ± 0.19

Table 4.4: Comparison of the apparent sizes of the sources and reference stars in the field

source	Star		Star			Galaxy		
	RA (hh mm ss)	Dec. ($^{\circ}$ ' ")	FWHM1 "	FWHM2 "	Angle "	FWHM1 "	FWHM2 "	Angle "
J11203	12 02 59.4	16 24 20.5	0.95 \pm 0.03	1.03 \pm 0.03	1.24 \pm 0.56	1.26 \pm 0.15	1.09 \pm 0.09	10.97 \pm 0.29
J0938	09 38 22.3	13 49 54.4	1.15 \pm 0.01	1.04 \pm 0.01	0.97 \pm 0.13	1.31 \pm 0.07	1.11 \pm 0.08	1.88 \pm 0.48
J0347	03 47 35.8	01 04 08.6	0.99 \pm 0.01	1.31 \pm 0.01	1.81 \pm 0.15	1.09 \pm 0.01	1.35 \pm 0.01	0.87 \pm 0.16
J1158	11 58 14.2	13 25 57.0	1.43 \pm 0.02	3.76 \pm 1.48	0.92 \pm 0.30	1.44 \pm 0.04	1.49 \pm 0.04	0.64 \pm 0.48
J0802	08 01 38.2	55 11 44.2	0.57 \pm 0.01	0.60 \pm 0.01	0.78 \pm 0.17	0.67 \pm 0.04	0.52 \pm 0.03	49.44 \pm 0.46
J0911	09 11 47.7	40 34 38.9	0.75 \pm 0.04	0.81 \pm 0.04	3.22 \pm 0.82	0.87 \pm 0.06	0.91 \pm 0.06	0.79 \pm 0.90

Notes. For each galaxy, the coordinates of each star that I subtracted from each galaxy image are given in this table, as well as the results of a Gaussian fit to galaxy and star. Here I used an elliptically shaped Gaussian function.

4. LINE AND CONTINUUM VARIABILITY IN ACTIVE GALAXIES

Table 4.5: Continuum fits.

name	instrument	A_V (stars)	stars	powerlaw	Fe II
J1203	LBT	0	60%	40%	0%
	SDSS	0	60%	40%	0%
J0938	LBT	1.5	90%	10%	0%
	SDSS	1.5	80%	20%	0%
J0347	LBT	1.2	57%	20%	23%
	OHP	0.8	72%	13%	15%
J1158	LBT	0	0%	85%	15%
	SDSS	0	0%	85%	15%
J0802	LBT	0	50%	30%	20%
	SDSS	0	52%	33%	15%
J0911	LBT	0	50%	40%	10%
	SDSS	0	45%	45%	10%
J0354	LBT	1.8	60%	30%	10%
J0153	LBT	0	62%	23%	15%

Notes. For each observation I give the flux contributions of the stellar component, the AGN/powerlaw component, and the Fe II template, as well as the extinction A_V of the stellar component in the wavelength interval 5100 Å to 5600 Å (rest-frame wavelength).

the intermediate-age population I used template of a 1.4 Gyr old simple stellar population with solar metallicity.

In Tab. 4.5 I present the flux contributions of the stellar component, the AGN/powerlaw component, and the Fe II template, as well as the extinction A_V of the stellar component. The fraction of each component was measured compared to the total flux in the (rest-frame) wavelength interval 5100 Å to 5600 Å. The main purpose of the continuum subtraction was to remove the Fe II emission lines from the spectrum, particularly those who blend other emission lines. Since in most galaxies there are no obvious stellar features, it is difficult to distinguish between different stellar populations. Therefore, I sum up the contributions of the intermediate-age and the young stellar population. Also the fit of the extinction A_V is not reliable but was only chosen to fit the continuum slope as accurate as possible. The data for the line variability as discussed in Sect. 5.4 includes all corrections derived from the fitting described here.

4.4.2 Fe II subtraction

The main goal of the analysis is to be able to make a statement on the variability of certain lines. Reaching this goal is complicated by the fact that there is a contamination line system in the spectra. The optical emission-lines of Fe II represent quite typical features for Seyfert 1 galaxies and quasars. There is huge variety in the strength of these lines, from very clearly shaped and detectable lines in some AGN spectra all the way to very weak and imperceptible lines in other sources. Boroson and Green (1992) (in the following BG92) reported a strong inverse correlation between the strength of Fe II emission-lines and the width of the broad H β line as well as the strength of the [O III] line. This result was confirmed by other groups (e.g., Corbin, 1997; Dong *et al.*, 2011; Kovačević *et al.*, 2010; Zhou *et al.*, 2006). In this work I used the Fe II template from BG92, fitted and scaled the results to my galaxy spectra as shown in Fig. 4.4. However, Tab. 4.5 shows that the contribution of Fe II in the mentioned wavelength range is up to more than 20% and a proper subtraction of Fe II is required. The fitted spectrum was then subtracted from the spectra. Finally, I obtained a spectrum corrected for both, the host continuum (as mentioned in Sect. 4.4.1) and the Fe II.

4.4.3 Fitting the Emission-lines

Measuring the line fluxes requires knowledge on the line shape as we have to integrate over it. To accurately measure the fluxes of emission lines, I used MPFITEXPR (Markwardt, 2009) to fit a several Gaussians or a single Gaussian to the line profile. To fit a narrow or broad components, I depend on the details of their shape or the presence of neighboring features. For example, to fit the H α + [N II] complex, I used four Gaussian components, where the flux ratio of the [N II] λ 6583 Å, 6548 Å doublet is fixed to the theoretical value of 2.96. In addition, their widths are supposed to be identical. Likewise, for the complexes of H β + [O III] λ 5007 Å, I fitted three Gaussian components as shown in Fig. 4.5, and two Gaussian components if the H β line is narrow. Additionally, for some broad lines a Lorentzian profile was fitted, if the width of the lines cannot be represented by Gaussian line profiles. The results of the line fitting are listed in Tab. 4.9.

4.5 Results

A fundamental property of the sources under investigation is their distance from the observer. The distance must be known and taken into account if we want to make statements on the

4. LINE AND CONTINUUM VARIABILITY IN ACTIVE GALAXIES

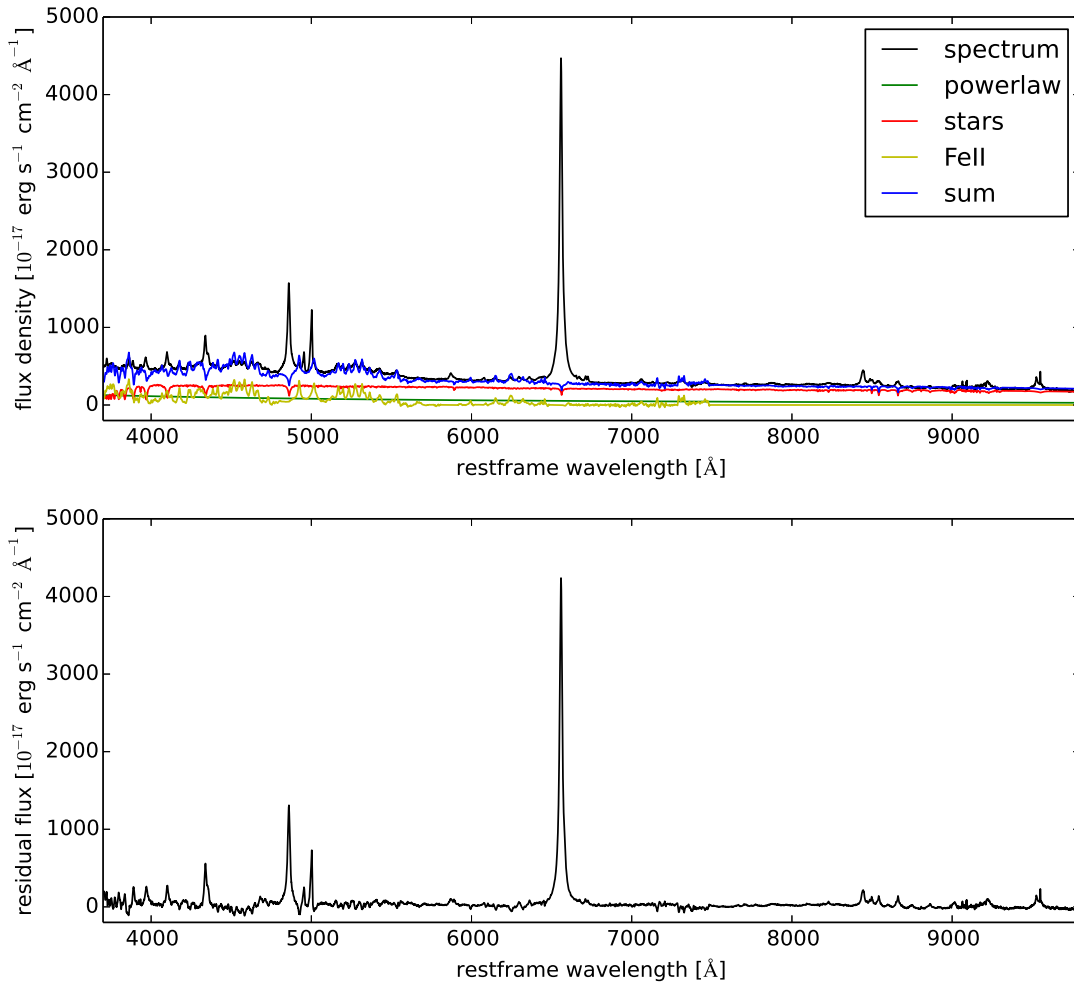


Figure 4.4: Results from the [Fe II] emission-subtraction. In the first plot, I present the spectrum of J034740.18+010514.0 together with a fit of the [Fe II] emission (yellow). In the second plot, shows the spectrum after subtraction of the [Fe II] emission.

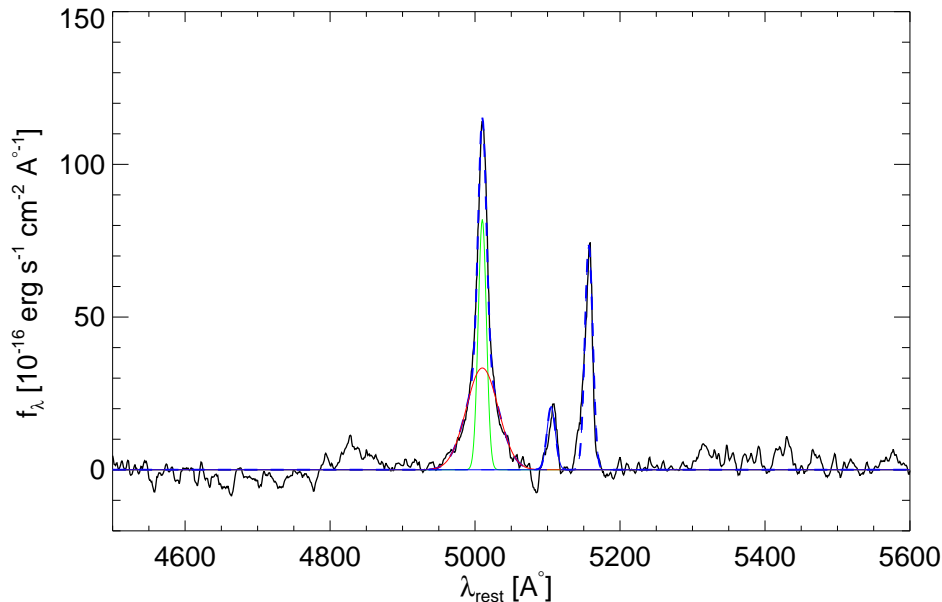


Figure 4.5: The plot shows the fit of the H β and [OIII] emission line complex with multiple Gauss functions for J0347.

luminosity of the sources. Distances to the objects - and hence their observed luminosities - depend on the choice of the cosmology. Redshifts and luminosity distances D_L (Hogg, 1999) are listed in Tab. 4.1. The luminosity distances D_L were calculated using the redshift of the source combined with the cosmology constants assuming a Hubble constant $H_0 = 70 \text{ km s}^{-1} \text{ Mpc}^{-1}$, and a standard cosmology with parameters $\Omega_m = 0.3$, and $\Omega_\Lambda = 0.7$ (Spergel *et al.*, 2003).

The observed continuum flux density variability of the sources derived from LBT and SDSS data is summarized in Tab. 4.3. The line fitting results are listed in Tab. 4.9. All the spectra in this chapter has been plotted in the rest wavelength as shown in Fig. (4.6, 4.7, 4.13, etc.). In addition, I did that by applying $\lambda_{rest} = \lambda_{obs}/1 + z$. Another correction was applied on the flux density (cosmological dilution), to change this value to the rest system via

$$F_{\lambda \text{ rest}} = F_{\lambda \text{ obs.}} \times (1 + z)^3 \quad . \quad (4.1)$$

All continuum flux densities and luminosities listed in the tables are derived as observed quantities (i.e. without corrections). The listed line fluxes and luminosities have been corrected for FeII and stellar continuum as described above.

4. LINE AND CONTINUUM VARIABILITY IN ACTIVE GALAXIES

4.5.1 SDSS J093801.63+135317.0

The source SDSS J093801.63+135317.0 (hereafter J0938) is well known. It has been mentioned in the discovery of a population of the normal extragalactic field galaxies that have luminous and strong FHIL (forbidden high by ionized lines) and HeII λ 4686 emission (Stepanian and Afanas'ev, 2011). The authors used the 'Bolshoi Teleskop Alt-azimutalnyi BTA-6' telescope with 6-m diameter located in Russia and obtained spectra with 0.86Å/px resolution. Stepanian and Afanas'ev (2011) report, in their Table 2, the value of FWHM and flux for each emission lines in the optical spectrum of J0938 taken with two instruments with the same spectral resolution of $R \sim 2000$ at two different epochs. The first one is taken by the SDSS telescope in 18.12.2006 and the other one is taken by BTA-6 in 16.04.2010.

The authors of Yang *et al.* (2013) present results of seven rare extreme coronal line emitting galaxies, and J0938 is among these sources. Coronal line are of interest as they are believed to originate from regions between the BLR and NLR zone. These objects are reported by Wang *et al.* (2012), and four of these galaxies (J0938 and three others) have a large variability in coronal line flux, making them good candidates for tidal disruption events (TDEs). They detected a broad He II λ 4686 emission line in the spectrum of J0938. Yang *et al.* (2013) find broad coronal and high-ionization lines that are superimposed on narrow low-ionization lines. They interpret this finding as indication that J0938 is a composite of a S2 nucleus and a star formation region. In the SIMBAD catalogue the object is listed as an H II galaxy. However, according to the [O I] λ 6300/H α versus [O III] λ 5007/H β diagnostic diagram in Wang *et al.* (2012) and Yang *et al.* (2013) it's appearance to be that the source J0938 is lying in the region between H II and S2 galaxies (here I adopt an HII/S2 composite nucleus classification) and belongs to a sample of sources with spectra that are dominated by the interaction of a super massive black hole with the nuclear environment (Stepanian and Afanas'ev, 2011; Wang *et al.*, 2012; Yang *et al.*, 2013).

The uncertain classification of the source as HII/S2 is reflected in the variability data for this source which support the presence of a highly variable nucleus. In Tab. 4.3 I list the flux density measurements of J0938 for three epoch at different wavelengths as obtained through the LBT observations and via the spectroscopy and photometry results listed by SDSS. I notice that flux values of the continuum of LBT spectroscopy are in good agreement with photometric data of SDSS at the same wavelengths, while both are different to what can be derived from

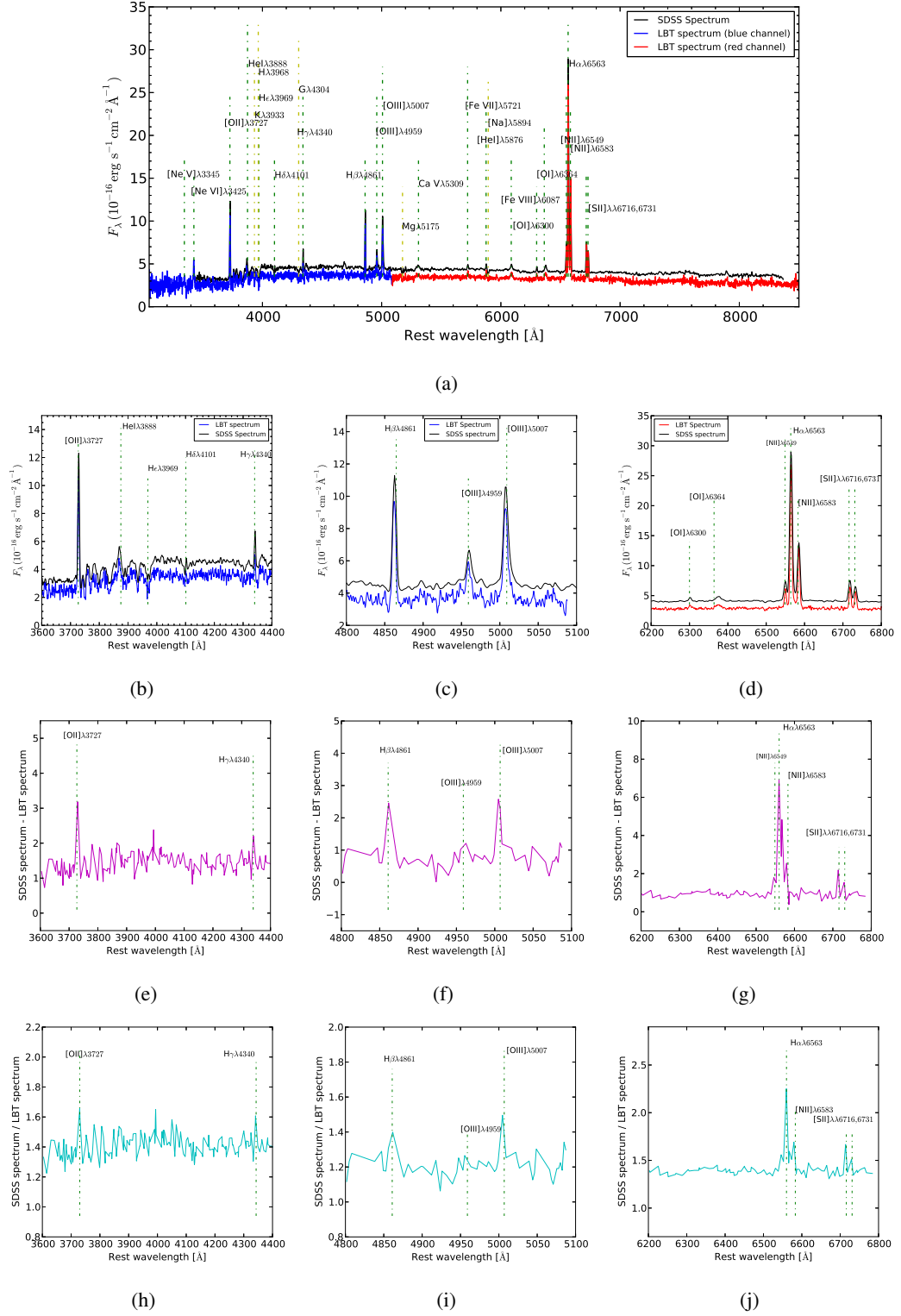


Figure 4.6: The plot shows the optical spectrum of J0938 as observed by SDSS and LBT-MODS. The second row shows zooms into the spectrum in different regions. The third row shows the differences between SDSS and LBT spectrum in these regions, while the fourth row shows the ratios of these spectra.

4. LINE AND CONTINUUM VARIABILITY IN ACTIVE GALAXIES

SDSS spectroscopy. Here, I note that there are of order 30% variations in line and continuum flux between the different epochs that I used for my investigation.

As shown in Fig. 4.3 and as it is evident from the data in Tab. 4.4 the host of the source is extended. Comparison with stars in the field show that just above one half of the continuum flux in the LBT 0.8" slit is due to the unresolved nuclear component. The rest can be attributed to the contribution of the extended host. Thus the continuum variability estimation is probably only an upper limit. However, for completeness I leave the variability estimates in Fig. 4.14 as upper limits. The median deviation and median calculated from this plot is not affected by this. The over-plot of the two optical spectra (LBT and SDSS) of J0938 is shown in Fig. 4.6. In 2012 the LBT spectrum was monitored, while the SDSS spectrum for this source has been taken in 2006. Therefore, here I can discuss the variability on a time scale of 6 years. For this object two types of variability were found: first, there is a difference in the continuum level between the two spectra, where the continuum level of the SDSS spectrum is higher by a factor of ~ 1.3 than the level of the LBT spectrum. This can be seen in Fig. 4.6 (a,b,c, and d) where I plot different sections of the J0938 spectrum. Of course not only the continuum flux level of this source is variable but also the lines. To show this I subtract the two spectra from each other and plot the difference (Fig. 4.6 e, f, and g). Additionally, the variability of these lines is shown by displaying the ratio of the two spectra (see Fig. 4.6 h,i, and j). The most varied emission lines in the spectrum of J0938 are [O II], H β , [O III] λ 5007, and H α . The H α and [O III] lines show a variation of the order 1.25. The measured line fluxes are listed in Tab. 4.9.

4.5.2 SDSS J120300.19+162443.8

The source SDSS J120300.19+162443.8 (henceforth J1203) is contained in several statistical / observational samples. It has been mentioned in Shirazi and Brinchmann (2012) among 2865 galaxies to have a strong nebular He II λ 4686 emission. A strong He II λ 4686 line indicates that the nuclear radiation field of these objects is dominated by highly ionizing radiation. The ionization potential of He⁺ is 54.4 eV corresponding to a UV photon wavelength of $\lambda \approx 228\text{\AA}$.

In Tab. 4.3 I list the flux densities f_λ of J1203 at different wavelengths obtained from the LBT observation and spectroscopy and photometry data as listed by SDSS. I notice that the flux values of the continuum at different wavelengths indicate variability. Moreover, the power law index of the continuum feature of both observations SDSS (photometric & spectroscopy) and LBT (spectroscopy) has also varied as shown in the optical spectrum of J1203 in Fig. 4.7.

The optical emission line spectrum of J1203 is dominated by the NLR (see Fig. 4.7). In Tab. 4.9 I notice that all the emission lines are narrow with FWHM values of $\leq 8.3\text{\AA}$ (where $8.3\text{\AA} \approx 500\text{ km s}^{-1}$). J1203 has very low count rates at the continuum level. The $H\alpha$ complex gives indications of a possible faint broad component. Barth *et al.* (2014) find that all S2 candidates in their sample for which high spectral resolution deep exposures had been taken showed some broad line emission that was not visible in previous spectra. A comparison between the [OIII] $\lambda 5007$ and $H\beta$ line shows to within the uncertainties a very similar line profile. Therefore no significant broad line component can be found and therefore I classify J1203 as a S2 galaxy.

The over-plot of the two optical spectra (SDSS and LBT) for J1203 is shown in Fig. 4.7. The LBT spectrum for J1203 was observed 2012, while The SDSS spectrum for the same object has been monitored 2007. Thus, for this galaxy I can discuss the variability that may happened over 5 years. I find that the variability here is rather fixed to the blue channel region from 3300\AA to 3700\AA where effects of red wing of the "Big Blue Bump BBB" may could be seen (Gaskell, 2008; Starling and Puchnarewicz, 2001), as shown in Fig. 4.7 (d). The observed continuum of the LBT spectrum in this region is higher than the SDSS spectrum. But for the rest of the spectrum both spectra are at the same level till 6000\AA . The line emission varies by about 40% (see Tab. 4.9).

4.5.3 SDSS J115816.72+132624.1

A few detailed studies on the source SDSS J115816.72+132624.1 can be found in the literature. The optical spectrum of the source (hereafter J1158; observing dates see Tab. 4.1) is strongly dominated by Fe II lines (as can be seen in Fig. 4.8 and as reported also in Dong *et al.*, 2011; Kovačević *et al.*, 2010). From Tab. 4.3 one can see that the flux values of the photometric and spectroscopy observations obtained within the SDSS survey are in good agreement. However, both values show a difference with respect to the flux value extracted from the LBT spectrum, indicating variability. In Wang and Rowan-Robinson (2009) the authors refer to J1158 as a faint source and mention it in the Imperial IRAS-FSC Redshift Catalogue (IIFSCz) among 60303 galaxies. Verifying the consistency of source positions they improved the optical, near-infrared, radio identification. According to Zhang *et al.* (2010) J1158 is classified to be a low-ionization broad absorption-line (loBAL) quasar, with [Mg II] absorption-lines with a width of $\Delta v_c \geq 1600\text{ km s}^{-1}$. Additionally, the authors calculate the continuum luminosity at 5100\AA (λL_{5100}) as $7.7 \times 10^{44}\text{ erg s}^{-1}$. From the LBT spectrum I obtain a luminosity at the same wavelength

4. LINE AND CONTINUUM VARIABILITY IN ACTIVE GALAXIES

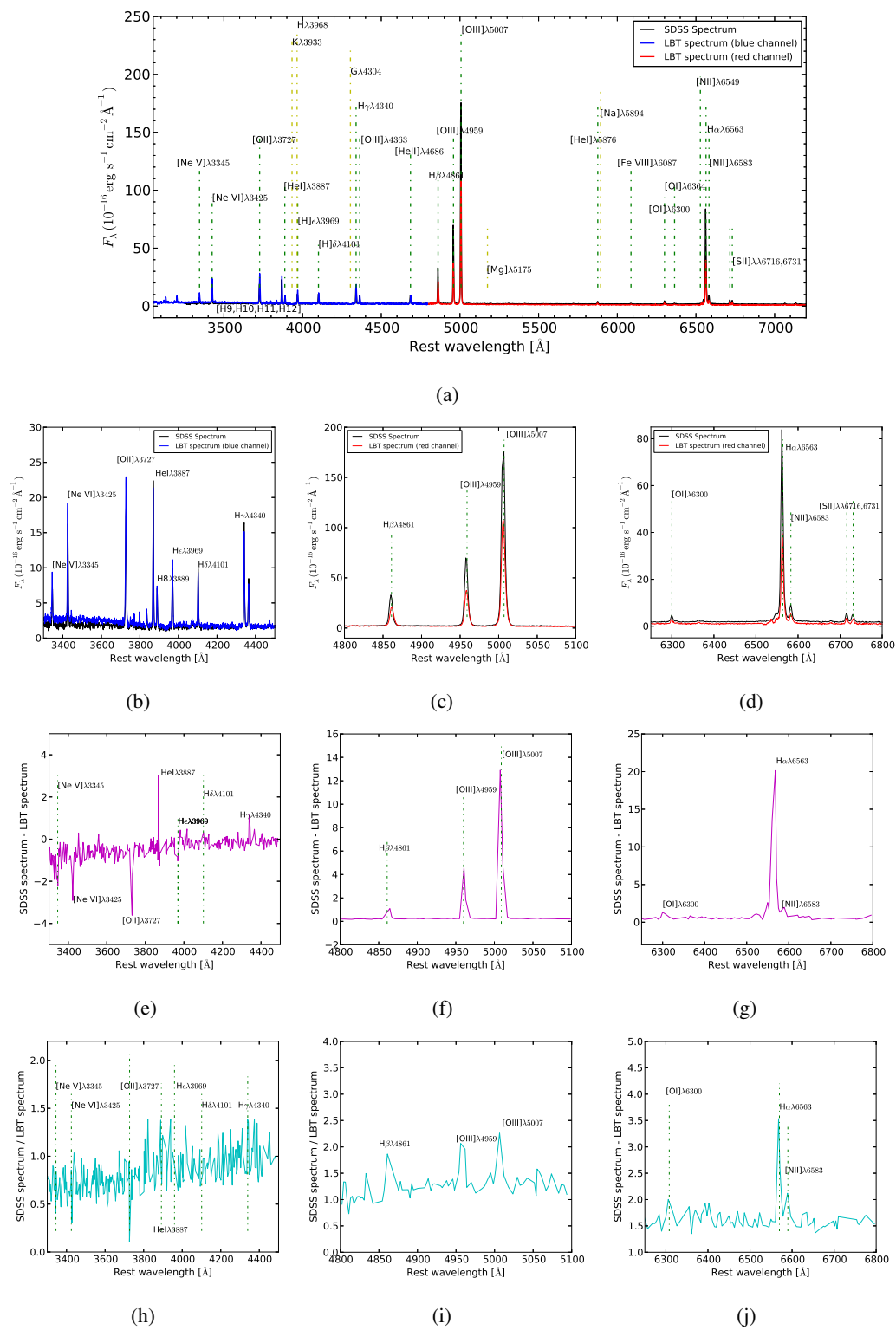


Figure 4.7: The optical spectrum of J1203 and the result of calculating the difference and ratio of spectra from different epochs.

with a flux of $2.81 \times 10^{45} \text{erg s}^{-1}$. The SDSS spectrum results in a value of $2.25 \times 10^{45} \text{erg s}^{-1}$. Consistent with the fluxes listed in Tab. 4.3 I can conclude that the continuum luminosity of this source has varied by a factor of 1.2 over the past 8 years.

For the purpose of comparison I present In Fig. 4.8 the over plot of the LBT and SDSS spectra for J1158. The LBT data have been obtained in January 2012, and the SDSS survey monitored this sources in May 2006. Thus, for this source I will able to discuss and study the spectral variability on a time scale of six years. After overplotting the twwo spectra and calculating the flux densities of the emission lines (Tab. 4.9) for this galaxy, I found that the variability in the continuum spectral index (hereafter PLI) and the continuum level may well be coupled to each other as the red tail of the BBB may be the dominant contributor to the variability behavior. In addition I find strong variability in emission line intensity which confirms that this object harbors an active galactic nucleus.

As shown in Fig. 4.8 (a,b,c, and d) the continuum level of the LBT spectrum is higher than that in the SDSS spectrum. This could be linked to power-law variability over the entire optical spectrum as expected from localized temperature fluctuations of a simple inhomogeneous disk (Ruan *et al.*, 2014). I find the PLI for both spectra to vary from $-0.21 \text{ erg s}^{-1} \text{ cm}^{-2} / \text{\AA}$ for the SDSS spectrum to the PLI of LBT spectrum of $-0.01 \text{ erg s}^{-1} \text{ cm}^{-2} / \text{\AA}$. Among them the $\text{H}\beta\lambda 4861$ and $[\text{O III}]\lambda 5007$ line show the strongest variation by a factor of about 3. In general, the emission lines in this source are more variable than in other objects of my sample. To better illustrate the variability in continuum and the emission lines I subtracted the two spectra from each other. In Fig. 4.8 (a, b, c, d) I plot the SDSS and LBT spectra next to each other and their differences were plotted in Fig. 4.8 (e, f, g, h, i, and j).

4.5.4 SDSS J091146.06+403501.0

The source SDSS J091146.06+403501.0 (hereafter J0911) has been mentioned a few times only in the literature. It has been reported for the first time in McMahon *et al.* (2002) as a radio source. In the third data release of the SDSS survey (Schneider *et al.*, 2005) it is classified as a quasar. Zhang *et al.* (2010) classify J0911 as a low-ionization broad absorption-line (loBAL) quasar, with $[\text{Mg II}]$ absorption-line in its spectrum with a line width of $\Delta v_c \geq 1600 \text{ km s}^{-1}$. J0911 exhibits strong Fe II lines as shown in Fig. 4.9. Based on the SDSS DR5 data Zhang *et al.* (2010) calculate the continuum luminosity of J0911 at 5100\AA (λL_{5100}) to be $2.9 \times 10^{44} \text{erg s}^{-1}$, while at the same wavelength I derive from the LBT spectroscopy data a luminosity value of $3.66 \times 10^{44} \text{erg s}^{-1}$, and for the SDSS spectrum I find $2.84 \times 10^{44} \text{erg s}^{-1}$. These three values,

4. LINE AND CONTINUUM VARIABILITY IN ACTIVE GALAXIES

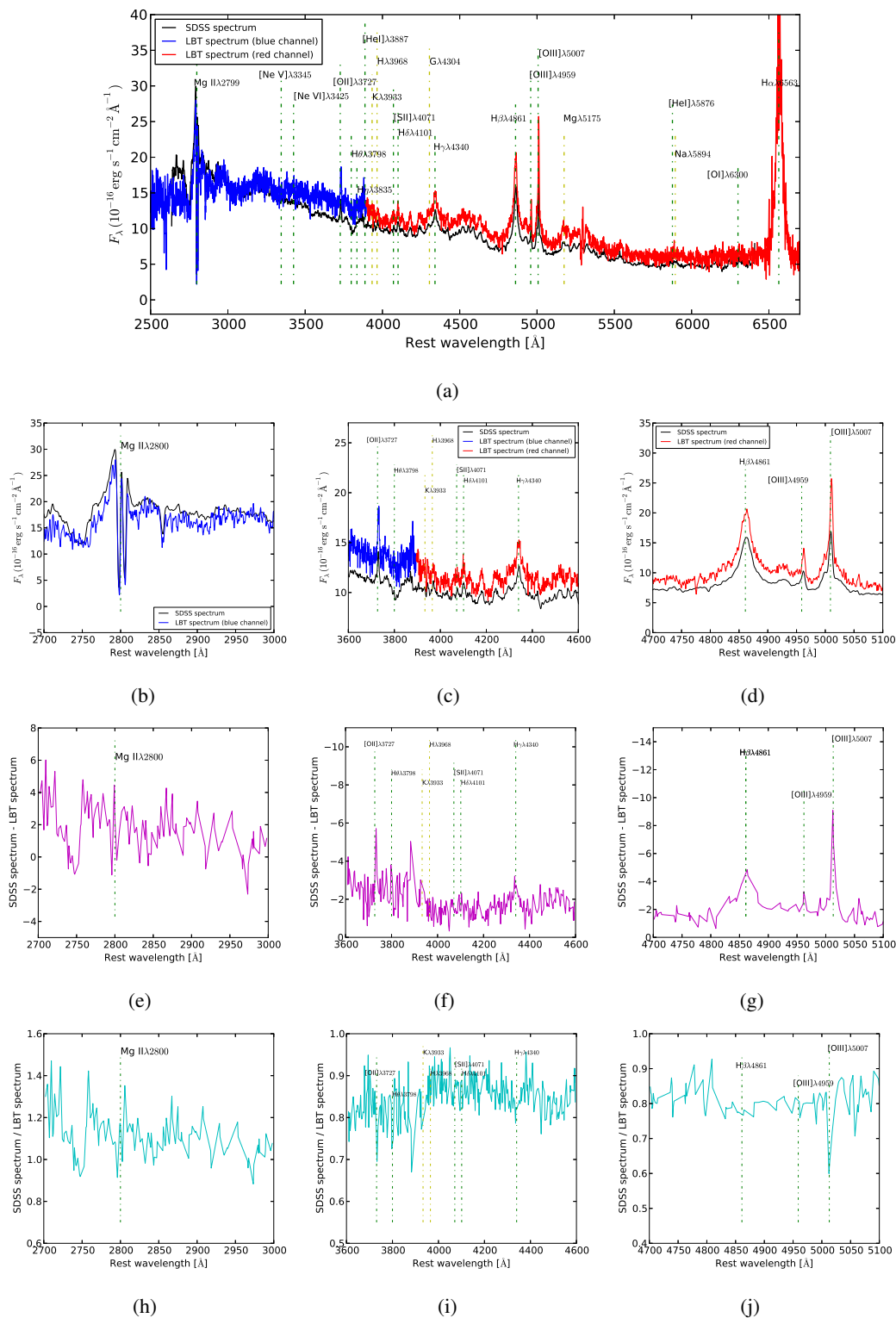


Figure 4.8: The same as Fig. 4.6 but for J1158.

and the measurements in Tab. 4.3, show that there is significant variability in the continuum emission of this source over these three epochs (see Fig. 4.9). This is in contrast to the strong variability that I find for J1158 and supports the consistency of the calibration between the different data sets. As part of the SDSS survey this source has been observed in March 2003, while the LBT spectrum of the source was taken in February 2012. Hence, I look at a time span of 9 years for the variability search. The optical spectra of J0911 can be seen in Fig. 4.9 (a, b, c, and d). As illustrated in this figure, the variability of the source is small compared to other sources in the sample, except for the blue part of the spectrum in Fig. 4.9 (b), where I notice a difference in the continuum slope. This variation in the blue part of the continuum may be caused by an accelerating outflow emanating from the black hole in the center of the galaxy [Shapovalova et al. \(2010\)](#). Additionally, the flux measurements of the emission lines and their FWHM are listed in Tab. 4.9. To show the variability clearly I plot the LBT and SDSS spectra next to each other in Fig. 4.9 (a, b, c, d) and show the difference of the spectra in Fig. 4.9 (e, f, g, h, i and j).

4.5.5 SDSS J080248.18+551328.9

As most of the sources in my investigation - also SDSS J080248.19+551328.9 is mentioned in the SDSS. SDSS J080248.19+551328.9 (in the following J0802) was mentioned first time in the Fifth Data Release DR5 of the SDSS catalogue for quasars ([Schneider et al., 2007](#)). The initial redshift determination $z = 0.66287 \pm 0.00107$ in DR5 ([Schneider et al., 2007](#)), later has been corrected to a value of $z = 0.664065 \pm 0.000355$ ([Hewett and Wild, 2010](#)). [Inada et al. \(2012\)](#); [Schneider et al. \(2010\)](#) J0802 classified this source as a quasar, which is supported by [Allen et al. \(2011\)](#); [Gibson et al. \(2009\)](#); [Lundgren et al. \(2009\)](#) with specific reference to a broad absorption line [Mg II] $\lambda 2800$ in its spectrum. From the optical spectra it is apparent that J0802 is highly dominated by Fe II lines (see Fig. 4.10). I notice that the continuum power law index derived from the LBT and SDSS spectroscopy data as well as the value derived from SDSS photometry are in good agreement (Tab. 4.3). According to these data the continuum spectrum peaks in the i-band. However, comparing the flux densities I find that while values of SDSS photometric and LBT spectroscopy are similar they both are different to what can be derived from SDSS spectroscopy. This indicates that J0802 shows some continuum variability between epochs.

The SDSS spectrum for J0808 has been taken in January 2005, while the LBT spectrum for the same source was taken in January 2012, resulting in a time baseline of 7 years for this

4. LINE AND CONTINUUM VARIABILITY IN ACTIVE GALAXIES

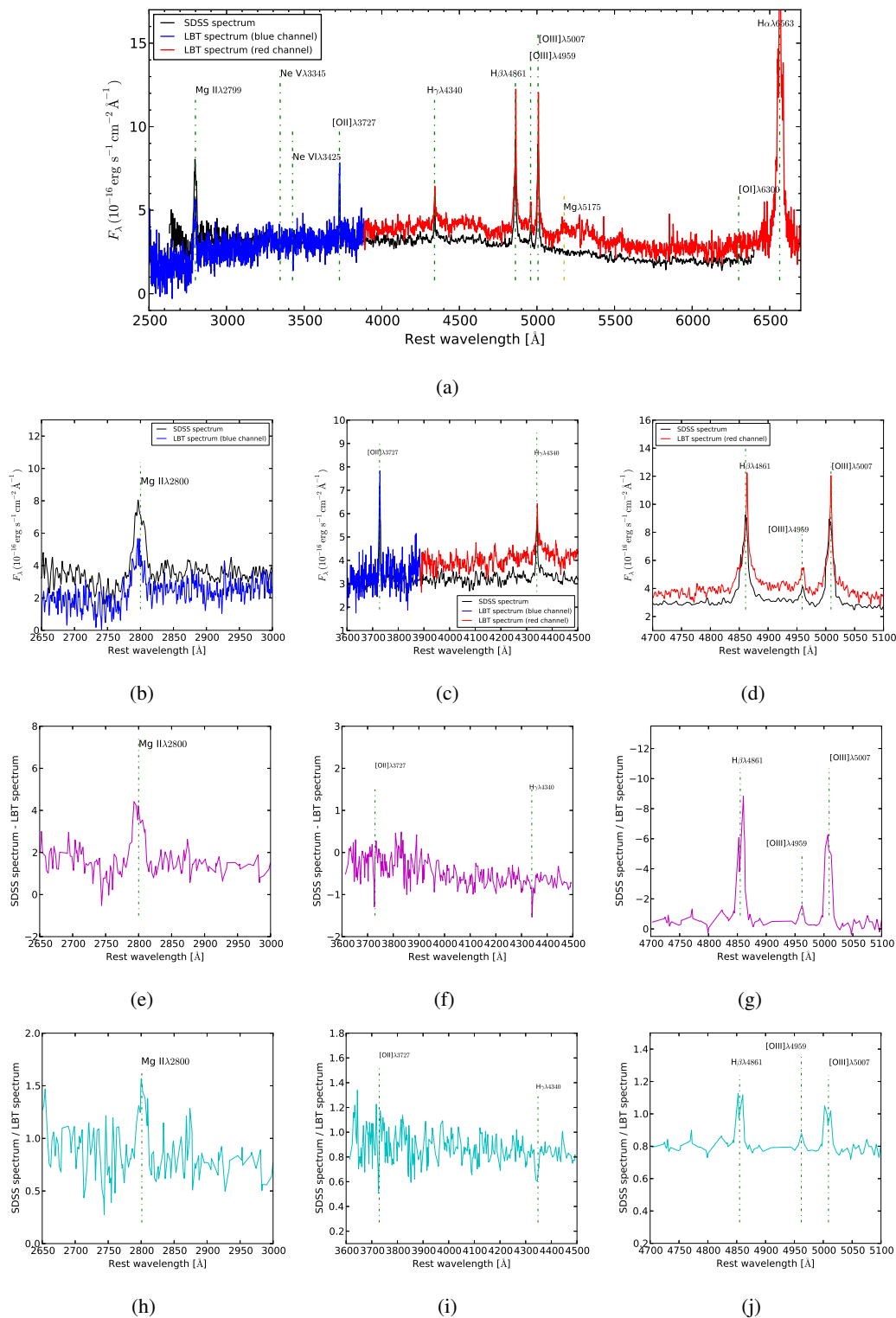


Figure 4.9: The optical spectrum of J0911 and the result of calculating the difference and ratio of spectra from different epochs.

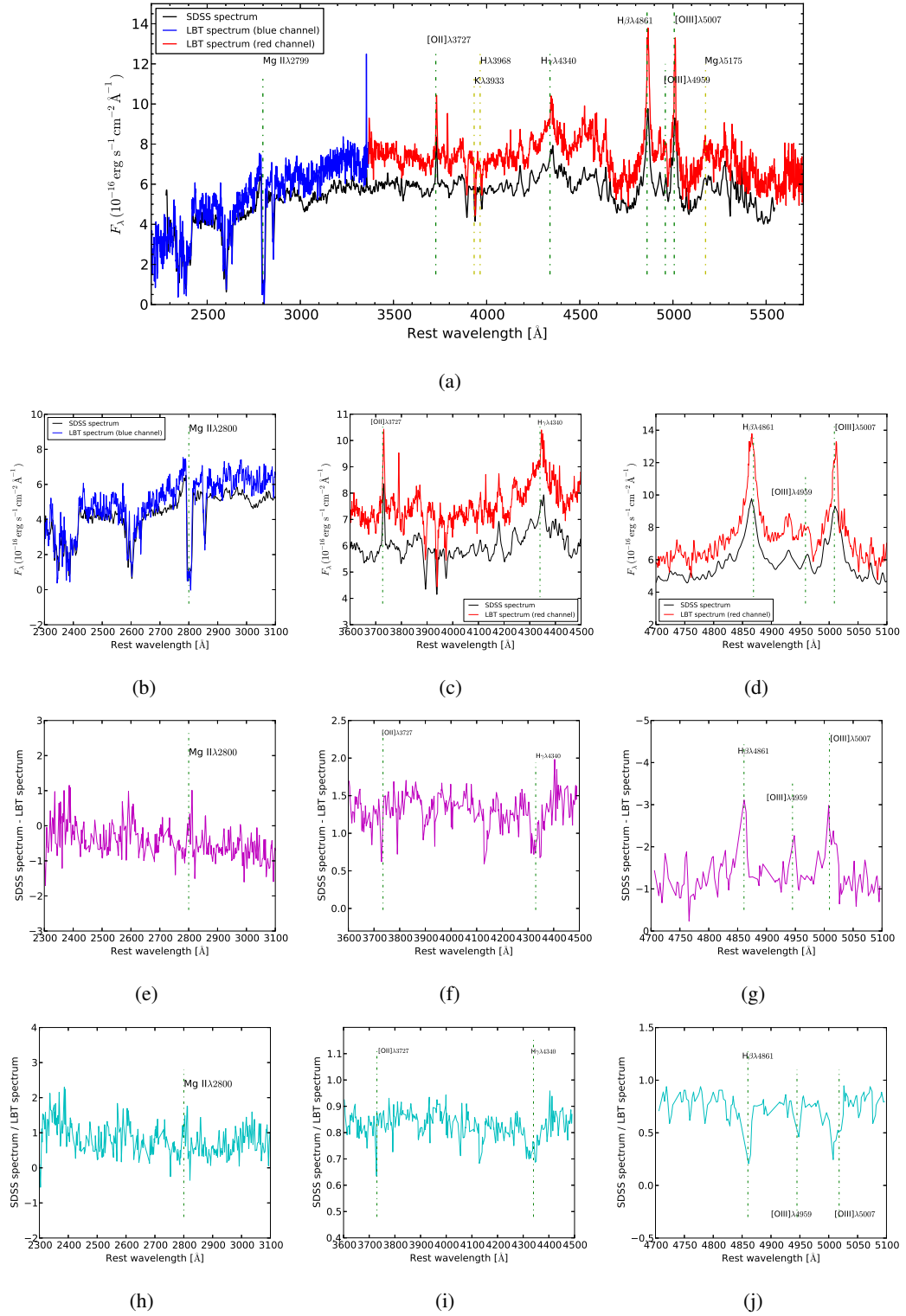


Figure 4.10: The optical spectrum of J0802 and the result of calculating the difference and ratio of spectra from different epochs.

4. LINE AND CONTINUUM VARIABILITY IN ACTIVE GALAXIES

object. Plotting both spectra (SDSS & LBT) for J0802 in Fig. 4.10 (a, b, c, and d) I find that there are spectral similarities to the source J0938. Both spectra have the same continuum slope but the continuum level of the LBT spectrum is higher by a factor of 1.3 compared to the SDSS spectrum. The intensity of the emission lines in LBT spectrum are stronger than those obtained from the SDSS spectrum (see Tab. 4.9). The H γ λ 4340 line present the strongest variation with a factor of 2.06. To demonstrate the variability in the emission lines I present the ratios and the differences between the LBT and SDSS spectra in Fig. 4.10.

4.5.6 2MASX J035409.48+024930.7

Not all source in my investigation have been covered by the SDSS survey. The source 2MASX J035409.48+024930.7 (hereafter J0354) is one of the two sources for which this applies. J0354 has been serendipitously discovered and mentioned together with 18 different objects in [Chanan *et al.* \(1981\)](#) as an AGN X-ray source. In [Bothun *et al.* \(1982\)](#) the authors report that the J0354 spectrum ($M_V \sim 18$) allows for either QSO or Seyfert 1 classification. They outline that compared to other samples (e.g., [Margon *et al.*, 1982](#)) the object is amongst the brightest X-ray sources. They also report that this source has a large ratio of X-ray to optical luminosity $L_x/L_{opt} = 2$ which is above the typical ratio of 0.5 found for quasars. [Haddad and Vanderriest \(1991\)](#) state that J0354 has a gas rich galaxy as a host. They state that it may have originated from as a result of a two-galaxy interaction, where the larger one is either a quasar or S1 and the second one is clearly showing signs of tidal distortion. However, [Hutchings *et al.* \(1982\)](#) suggest that the companion is bluer than the quasar. [Véron-Cetty and Véron \(2006\)](#) classify the object as S1.5.

Here I compare the LBT spectroscopy data for J0354 with a spectroscopy data obtained in Oct 2004 by the 2.4 m Hiltner Telescope at MDM Observatory at Kitt Peak, Arizona, USA published by [Grupe *et al.* \(2005\)](#). The source was observed in 1.5" and 2" slit under moderate seeing conditions. I notice that the continuum level of the LBT spectrum is different than the spectrum of Hiltner Telescope as present in Fig. 4.11, where the continuum level of J0354 taken with the Hiltner telescope is above than the LBT spectrum for the same object, and the emission lines of their observation are more intense than my observation. Furthermore, [Grupe *et al.* \(2005\)](#) mention the line fluxes of [[O III] λ 4959 and λ 5007 as (130 ± 6) and $(413 \pm 15) \times 10^{-16} \text{erg s}^{-1} \text{cm}^{-2}$, respectively. From the LBT data I obtain fluxes of the same lines as $(90) \times 10^{-16} \text{erg s}^{-1} \text{cm}^{-2}$ and $(505) \times 10^{-16} \text{erg s}^{-1} \text{cm}^{-2}$, respectively. The comparison present a variability by a factor of almost 50% in the [O III] λ 5007 line.

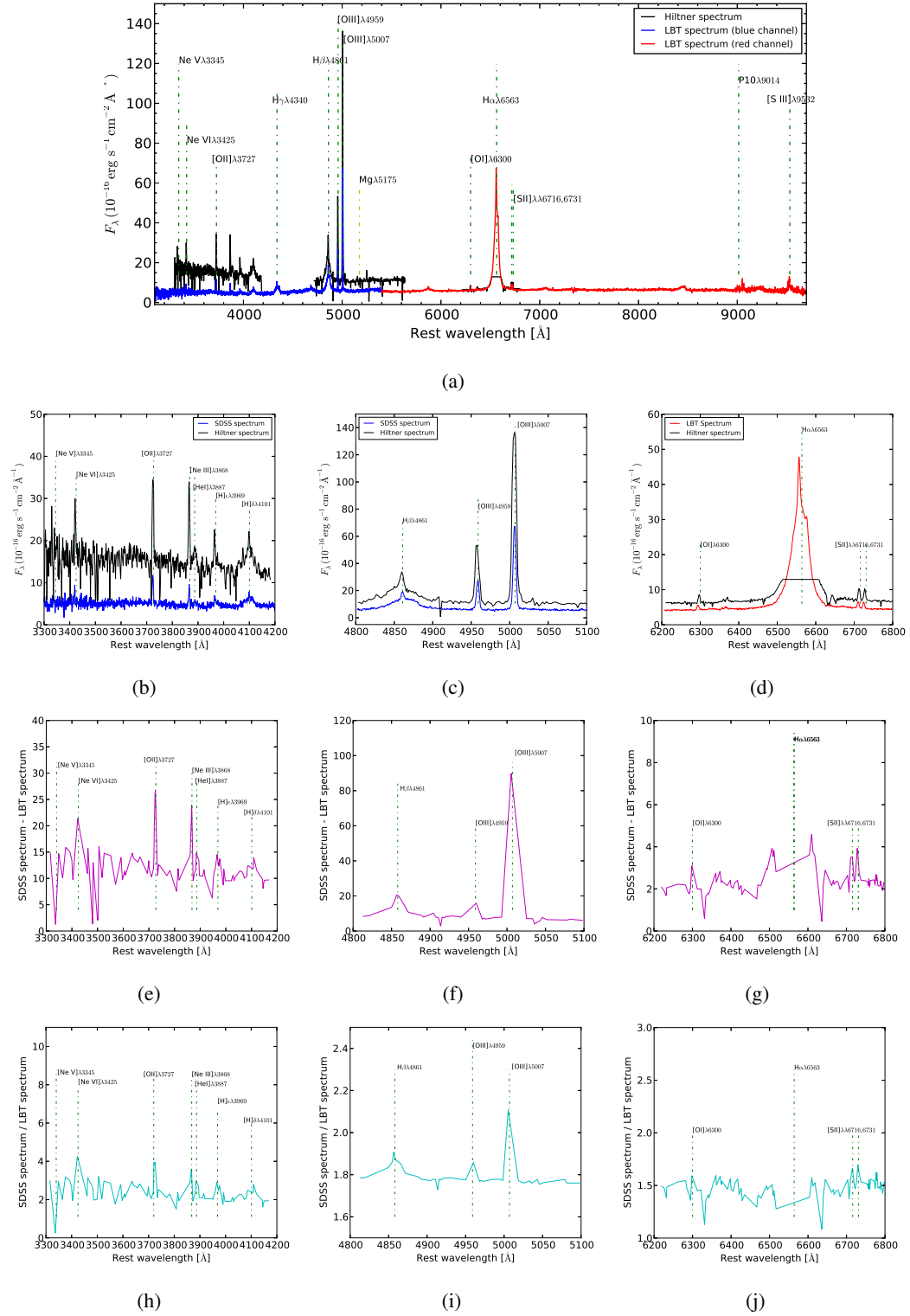


Figure 4.11: The optical spectrum of J0354 and the result of calculating the difference and ratio of spectra from different epochs.

4. LINE AND CONTINUUM VARIABILITY IN ACTIVE GALAXIES

4.5.7 GALEXASC J015328.23+260938.5

The second source that is not exist in the survey of SDSS, for my study in this chapter is GALEXASC J015328.23+260938.5 (henceforward J0153). This object is present in the Infrared Astronomy Satellite (IRAS) Point Source Catalogue (Beichman *et al.*, 1988, using the name IRAS 01506+2554) and in the 2nd XMM-Newton Serendipitous Source Catalog (Memola *et al.*, 2007; Noguchi *et al.*, 2009, , using the name 2XMM J015328.4+26093). From the IRAS survey, I obtained the flux density at two wavelengths, 60 and 100 microns, to be 0.5777 & 1.144 Jy, respectively. In addition to the LBT observations (see Fig. 4.12) a spectrum of J0153 has been taken by Zhou *et al.* (2002) in February 2002 with the Zeiss universal spectrograph located at the Beijing Observatory with 2.16 m telescope, with slit width of 2''.5 and seeing disk of 2''.5. Moreover, the spectral resolution determined on the night sky is 5.2Å FWHM. They found as well that J0153 is a radio-loud quasar with very strong Fe II emission lines, for the far- and near-infrared luminosity, they found $L_{\text{FIR}} \approx 10^{12.7} L_{\odot}$ and $L_{\text{NIR}} \approx 10^{12.5} L_{\odot}$. J0153 is one of 30 galaxies that Combes *et al.* (2011) investigate to follow the galaxy evolution and especially the star formation efficiency (SFE) using CO lines. They find that the SFE of this object is larger than 802 (L_{\odot}/M_{\odot}) which is 4.7 times higher than the local ultra-luminous infrared galaxies (ULIRGs) ($170 L_{\odot}/M_{\odot}$). This clearly indicates that the host of this AGN is actively forming stars with a high efficiency.

4.5.8 SDSS J034740.18+010514.0

My investigation covers a range of sources with different luminosities. Here we deal with the least luminous source in this particular sample that I studied. However, SDSS J034740.18+010514.0 (henceforth J0347) was mentioned first time in a study for high-luminosity sources (Low *et al.*, 1988, using the name IRAS 03450+0055) and classified as quasar with least luminosity among the sample they study. In Hewitt and Burbidge (1991) J0347 was classified as S1 galaxy by Véron-Cetty and Véron (2006) as S1.5. With $L_{\text{FIR}} \approx 10^{10.2}$ Low *et al.* (1988) and Low *et al.* (1989) find J0347 to have the lowest luminosity among other quasars in their sample, additionally they find that this source has an extremely red optical continuum. Since no SDSS spectroscopic observations are available for this object, I used spectroscopic data taken on 21 September 2003 with the CARELEC spectrograph attached to the 1.93m telescope of the Observatoire de Haute-Provence (OHP) with a 2'' slit under 2.5'' seeing.

Giannuzzo and Stirpe (1996) search for variability in a sample of 12 narrow line Seyfert 1

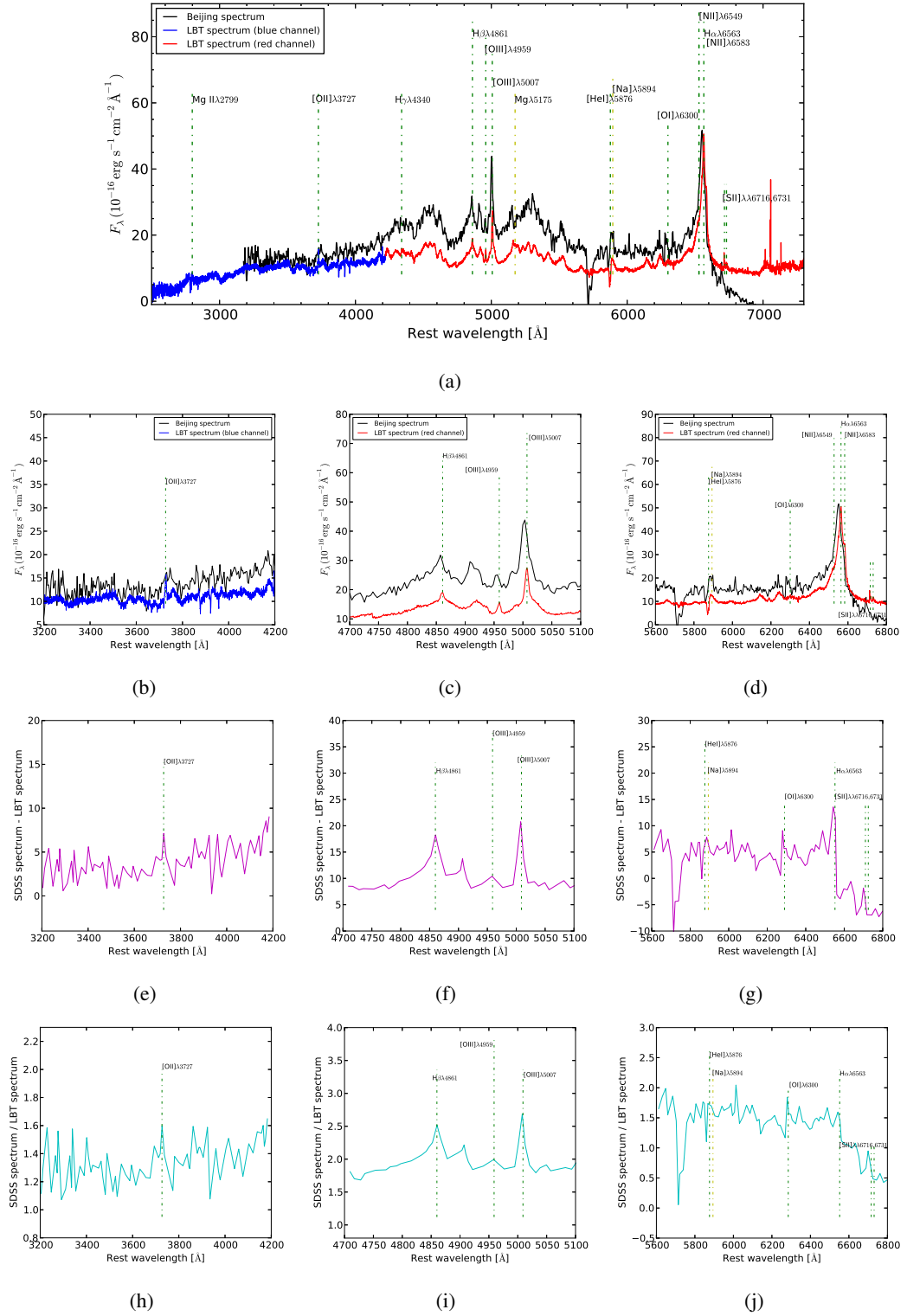


Figure 4.12: The optical spectrum of J0153 and the result of calculating the difference and ratio of spectra from different epochs.

4. LINE AND CONTINUUM VARIABILITY IN ACTIVE GALAXIES

Table 4.6: Median and median deviations for the variability in the continuum & emission lines.

Type	Continuum		Narrow Emission lines	
	μ	$d\mu$	μ	$d\mu$
BLS1& QSO	39.0	17.0	30.0	10.5
S2 & NLS1	27.0	9.0	15.0	6.0

Notes. μ are the median values, $d\mu$ the median deviations as defined in the text.

Table 4.7: The T-test statistic for the variability in the continuum & emission lines.

Type	Continuum					Emission lines				
	n	$\bar{\chi}$	σ	df	T-value	n	$\bar{\chi}$	σ	df	T-value
BLS1& QSO	42	42.25	20.76	75	3.38	18	29.48	10.71	33	4.25
S2 & NLS1	35	29.51	11.72			17	15.51	8.67		

Notes. Here n denotes the number of sample elements, $\bar{\chi}$ are the sample mean values, σ the sample standard deviations, df the degrees of freedom followed by the corresponding T-values.

galaxies, including J0347. They find 10 of these sources to be variable in the flux of the optical permitted lines over a period of one year as well as they found variation in the continuum level. For the variability percentage in the permitted lines $H\beta$ and $H\alpha$ they find 4.58 and 0.599 respectively.

The continuum flux measurements of the SDSS photometry as well as from OHP and LBT spectroscopy are listed in Tab. 4.3. Line flux measurements are presented in Tab. 4.9 (see also plots in Fig. 4.13).

4.6 Discussion

Line emissions and the continuum of AGN help us to study the processes in the immediate vicinity of the Super-massive black hole. The study that I conducted in here allows us to compare the line and continuum variability of two different object samples with different spectroscopic identifications that by themselves imply a different degree of activity. I find that the

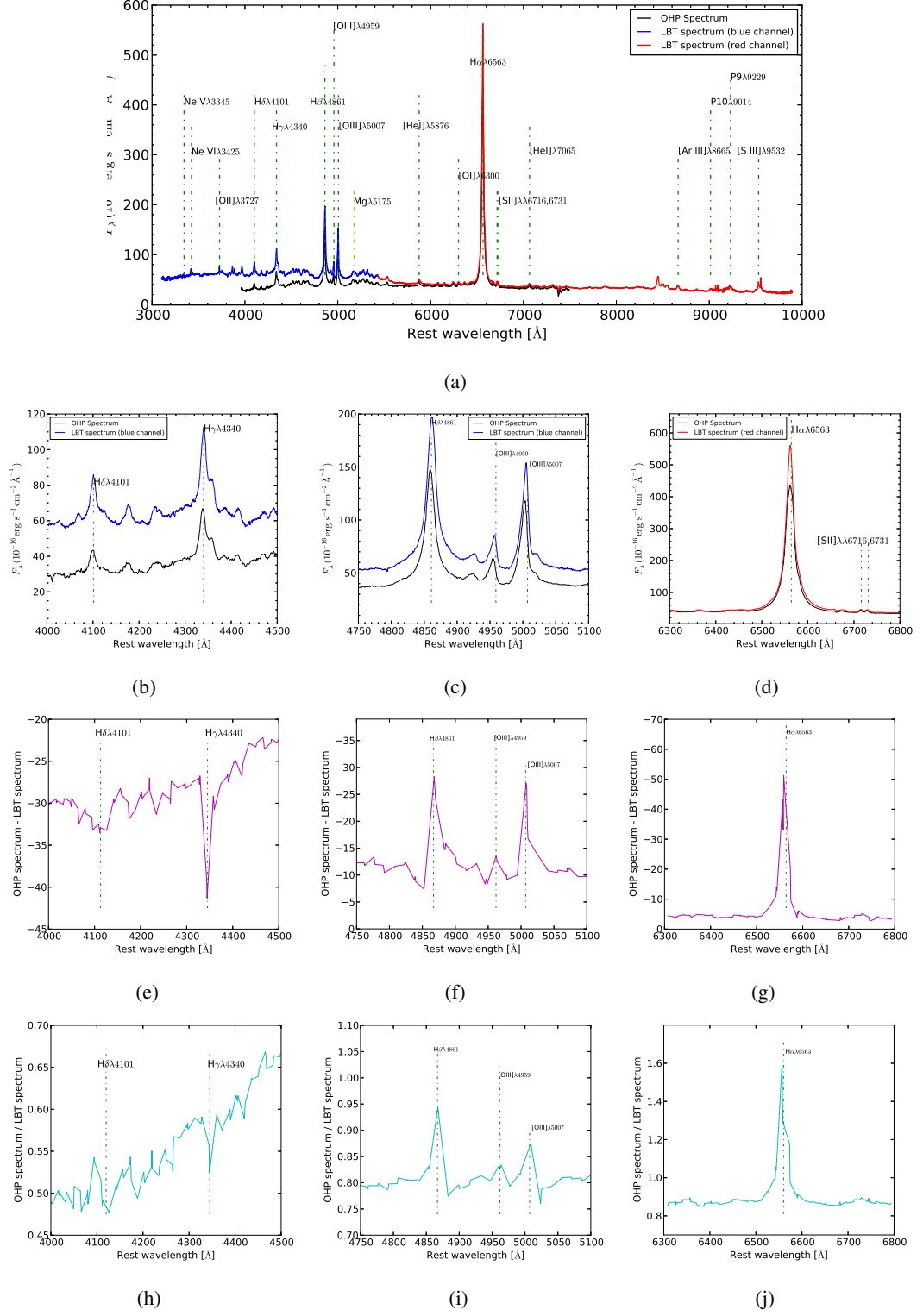


Figure 4.13: The optical spectrum of J0347 and the result of calculating the difference and ratio of spectra from different epochs.

4. LINE AND CONTINUUM VARIABILITY IN ACTIVE GALAXIES

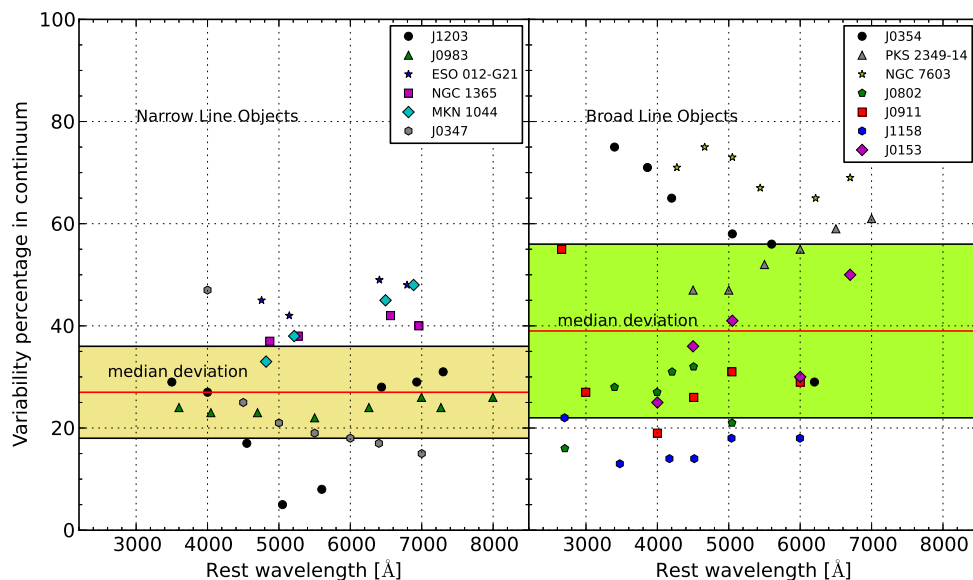


Figure 4.14: The variability percentage in the continuum. The data for the NLS1 sources ESO 012-G21, NGC 1365, and MKN 1044 are taken from [Giannuzzo and Stirpe \(1996\)](#). The data for the BLS1 sources NGC 7603 and PKS 2349-14 are based on spectra from [Kollatschny et al. \(2000\)](#) and [Kollatschny et al. \(2006a\)](#), respectively.

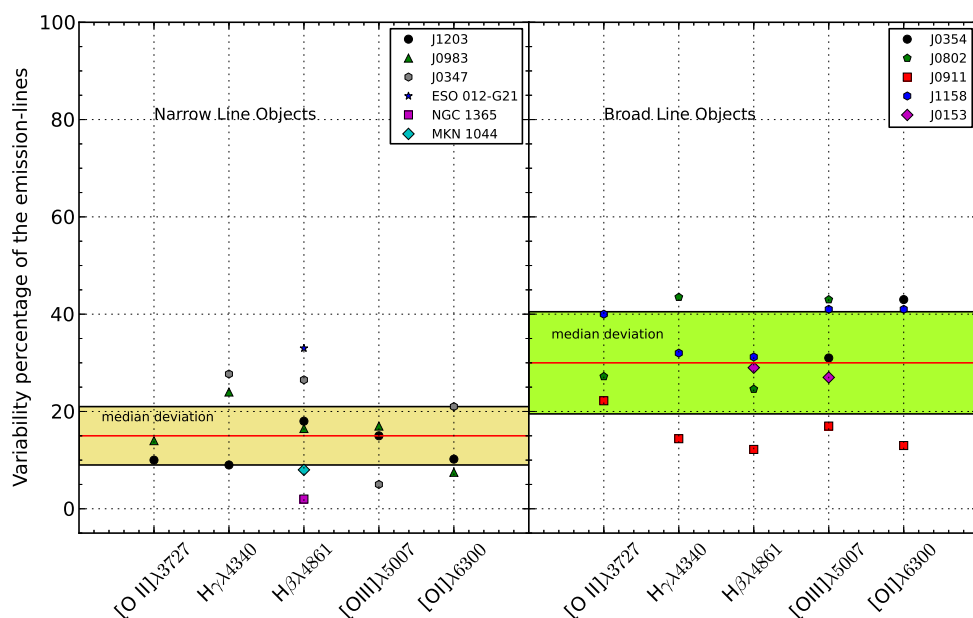


Figure 4.15: The variability percentage in the emission lines. The line measurements of ESO 012-G21, NGC 1365, and MKN 1044 are taken from [Giannuzzo and Stirpe \(1996\)](#).

Seyfert 2/NLS 1 sample shows in general a smaller degree of variability compared to the BLS1 and QSO sample. In the following I probe the significance of this difference and present a possible physical interpretation of the observed phenomenon. The data on the continuum variability are extended by multi epoch information on NGC 1365, ESO 012-G21, and MKN 1044 from [Giannuzzo and Stirpe \(1996\)](#), NGC 7603 from [Kollatschny et al. \(2000\)](#) and PKS 2349-14 from [Kollatschny et al. \(2006a\)](#). The data on multi epoch line variability are extended with ESO 012-G21, NGC 1365 and MKN 1044 from [Giannuzzo and Stirpe \(1996\)](#).

4.6.1 How to probe the degree of variability

Having performed a detailed study of 18 sources (see Tab. 4.1, Tab. 4.8 and captions in Figs. 4.14 and 4.15) I find that there are significant differences in variability between S2&NLS1 (8) sources and BLS1&QSO (10) sources. This applies both for the continuum and the emission lines. In the following I will discuss the relative variability Δ_{max} as the maximum difference δ_{max} with respect to the maximum value S_{max} , i.e. $\Delta_{max} = \delta_{max}/S_{max}$. Correction for relative measurement uncertainties σ of the order of 10% results in

$$\Delta_{max,corr.} = \sqrt{\Delta_{max}^2 - \sigma^2} \quad (4.2)$$

My data indicates that the BLS1&QSO are stronger variable than S2& NLS1. [Ai et al. \(2013a\)](#) came to the same conclusion: NLS1 have systematically a lower degree of variability if compared to BLS1 sources. This is in agreement with the earlier found anti-correlation between AGNs variability and Eddington ratio [Meusinger et al. \(2011\)](#); [Zuo et al. \(2012\)](#). Other authors (e.g., [Webb and Malkan, 2000](#)) concluded from variability studies that the blue part of AGN spectra is relatively stronger variable than the red part. For this study I present this result in Fig. 4.14. I notice that indeed the variability in the blue part of the continuum is, in general, larger than the variability in the red part. For 4 out of 7 objects this trend can be seen individually.

The sources in the two sample show a different behavior in variability. They clearly do not show the same degree of variability. To judge on the difference between the two source samples in their continuum and line variability I calculated the median and median deviation as well as the mean and standard deviation. Also chose the median since I do not know ab-initio if I have normal distributions. Here, the median deviation is defined as the median of the absolute differences between the median and the sample values. The median deviation is usually smaller than the standard deviation as it is less sensitive with respect to outliers. From Tab. 4.6 and

4. LINE AND CONTINUUM VARIABILITY IN ACTIVE GALAXIES

Table 4.8: The variability percentage in continuum at rest wavelength 5100Å and H β , for AGNs taken from reverberation mapping (light curve).

Sources	Cont. 5100Å %	H β %	Type	References
Mrk 335	34	24	NLS1	1,2
Mrk 6	36	25	NLS1	1
3C 120	57	40	BLS1	1
Ark 120	48	47	BLS1	1
Mrk 590	43	50	BLS1	1

Notes. References. (1) (Peterson *et al.*, 1998), (2) (Grier *et al.*, 2012).

Figs. 4.14 and 4.15 I find that the median degree of continuum variability is $27\% \pm 9\%$ for the S2/NLS1 and $39\% \pm 17\%$ for the BLS1/QSO sources. For the median line variability I find $15\% \pm 6\%$ for the S2/NLS1 and $30\% \pm 11\%$ for the BLS1/QSO sources. Furthermore, I find that the median values are separated by about one median deviation.

4.6.1.1 Robustness of the separation

In order to judge the robustness of the separation into subsets that show different variability behavior I used the analysis and argumentation presented below:

Results for narrow and broad line components: In Fig. 4.15 I present the results for the combined narrow and broad line recombination line fluxes in order to compare the data with literature values. However, the difference in the variability behavior between the narrow line and the broad line sources (with $15\% \pm 6\%$ and $30\% \pm 11\%$, respectively) also holds if I investigate the narrow line and broad line components that I obtained from fitting the hydrogen recombination lines (see Tab. 4.10). Here the median value for the variability of the narrow line objects J0347, J1203 and J0938 of 20 ± 4 lies well below the median result for the broad line objects of 41 ± 8 derived from the 4 objects J1158, J0911, J0002 and J0153. Although the separation into the two different source classes has been done using an overall line width criterion, I find that the difference is also present if one can look at the NLR and BLR line components separately (see discussion in section 4.6.3).

Statistical considerations: There are differences in the variability across the observed wave-

length band. For the BLS1/QSO sample one can see the tendency for the variability to be up to 20% stronger in the blue (3000Å) compared to the red (close to 6000Å). However, this tendency is not equally well fulfilled for all sources and rather weak with respect to the overall variability range from about 20% to 70%. However, here I'm more interested in the overall continuum and line variability. Both are estimated for different sources and in different lines or spectral regions of the continuum, which are all subject to different wavelength and line strength dependant calibration uncertainties. Hence, I assume that for the two source samples the variability estimates are sufficiently independent and can be represented by a mean distribution. In this case I can apply a T-test (Senn and Richardson, 1994) to determine the probability that the data sets from both the continuum and line variation originate from different distributions. The relevant test quantities are given in Tab. 4.7.

T-test was applied for two sample experimental statistics for independent groups. The T-value was calculated via

$$T = \frac{\bar{\chi}_1 - \bar{\chi}_2}{\sigma_{diff}} . \quad (4.3)$$

The standard error of the difference I calculated via

$$\sigma_{diff} = \sqrt{\sigma_{\chi_1}^2 + \sigma_{\chi_2}^2} . \quad (4.4)$$

Since the population standard deviation is not know, I used the sample standard deviation to estimate the standard error as the ratio of σ and \sqrt{n} :

$$\sigma_{\bar{\chi}} = \frac{\sigma}{\sqrt{n}} , \quad (4.5)$$

n being the number of sample elements. The number of degrees of freedom df as used for two independent groups obtained as

$$df = (n_1 - 1) + (n_2 - 1) . \quad (4.6)$$

T-tests are carried out very often if one compares different source samples. Therefore, the probabilities that describe the matching of the two samples are tabulated (Senn and Richardson, 1994) as a function of the T-values and the degrees of freedom df . Form these tables I find that the continuum and line variability of the BLS1 and QSO sample originated with a probability of >99.9% from a different distribution compared to the Seyfert 2 and NLS1 sample.

4. LINE AND CONTINUUM VARIABILITY IN ACTIVE GALAXIES

Comparison to other samples: The separation between the narrow line and the broad line sources is best full-fledged for the line variation. As shown in Tab. 4.8 my results are very much consistent with those for a set of NLS1 and BLS1 sources obtained from reverberation measurements carried out by Peterson *et al.* (1998) and Grier *et al.* (2012).

The findings for my small sample are also in full agreement with the results of a comparative study of the optical/ultraviolet variability of NLS1 and BLS1-type sources by Ai *et al.* (2013b) (based on 55 NLS1- and 108 BLS1-type nuclei). This underlines the representative character of my sample. The authors show that the majority of NLS1-type objects exhibit significant variability on timescales from about 10 days up to a few years, but on average their variability amplitudes are much smaller compared to BLS1-type sources (see also, Barth *et al.*, 2014; Yip *et al.*, 2009). Hence, in summary, I assume that the difference in continuum and line variability between the two samples is sufficiently significant to search for a physical explanation for the phenomenon.

4.6.2 Accretion dominated variability

In this section - following first principles - I investigate how the difference in narrow line variability between the objects with spectra dominated by narrow lines and broad lines is linked to the continuum variations of the active nuclei in the different samples.

As we are investigating the variation between samples a special notation helps to clarify the situation: In the following I denote with Δ differentiation with respect to the different samples, i.e. $\Delta = \frac{d}{d \text{ sample}}$. If the variability is due to mass accretion $\frac{d}{dt}M$ onto a super-massive black hole with mass M the continuum luminosity $L_{cont.}$ can be written as

$$L_{cont.} \propto M \times \frac{d}{dt}M . \quad (4.7)$$

The expected difference in continuum variability between the samples can then be expressed as

$$\Delta L_{cont.} \propto \Delta M \times \frac{d}{dt}M + M \times \Delta \frac{d}{dt}M . \quad (4.8)$$

This result can be linked to the detailed physics of the sources. For recombination lines the variation of the nuclear continuum results in a variation of the number of atomic species that reach the next higher state of ionization out of which they can recombine. For collisionally

excited states this next higher state of ionization is the state in which they can be observed at low densities emitting forbidden narrow line radiation. In the following I use the case of the recombination lines to discuss the effect of the reverberation. Since my main interest is in the variation of the narrow line luminosity L_{line} as a reverberation response to the variations in continuum luminosity I can write:

$$L_{line} \propto \frac{h\nu_{line}}{\langle h\nu \rangle} \frac{\alpha_{eff}}{\alpha_B} \frac{d}{dt} M = \xi \frac{d}{dt} M; \quad (4.9)$$

Here ν_{line} is the line frequency, α_{eff} and α_B are the effective and Menzel's case B specific recombination coefficients and $\langle h\nu \rangle$ denotes the mean energy per photon. Through the latter the combined coefficient ξ depends on the ration between the total illuminated cross-section A_C and ionized volume V_C of the reverberating clouds in a single galactic nucleus. This ratio results in a size l of the reverberating volume which has a square root dependency on the continuum luminosity:

$$\xi \propto \frac{V_C}{A_C} \propto l \propto \sqrt{L_{cont.}} . \quad (4.10)$$

Therefore, combining the above equations for the line luminosity I can write:

$$L_{line} \propto \sqrt{M} \left(\frac{d}{dt} M \right)^{\frac{3}{2}} . \quad (4.11)$$

The expected difference in line variability between the samples can then be expressed as

$$\Delta L_{line} \propto \frac{1}{2} M^{-\frac{1}{2}} \Delta M \left(\frac{d}{dt} M \right)^{\frac{3}{2}} + M^{\frac{1}{2}} \frac{3}{2} \left(\frac{d}{dt} M \right)^{\frac{1}{2}} \left(\Delta \frac{d}{dt} M \right) . \quad (4.12)$$

Now I assume that the variation $\Delta \frac{d}{dt} M$ of the accretion stream onto the super-massive black holes from sample to sample is small and a finite difference ΔM in total mean black hole mass per sample needs to be considered. In such a scenario the strength of the accretion stream as such is the dominant quantity for the variations in continuum and line luminosity between different sample members and the two sources sample in general. Hence, the description can be simplified and I can neglect the second terms in equations and and write for the difference in continuum and line luminosity:

$$\Delta L_{cont.} \propto \Delta M \times \frac{d}{dt} M \propto \frac{d}{dt} M \quad (4.13)$$

4. LINE AND CONTINUUM VARIABILITY IN ACTIVE GALAXIES

$$\Delta L_{line} \propto \Delta M \left(\frac{d}{dt}M\right)^{\frac{3}{2}} \propto \left(\frac{d}{dt}M\right)^{\frac{3}{2}} . \quad (4.14)$$

This points at the result, that the increase in activity in continuum and line emission is due to the difference in ΔM between the samples however the but there is an additional modulation for the variability of the line emission that is a function of $\frac{d}{dt}M$. Combining these results I find as a main result:

$$\Delta L_{line} \propto (\Delta L_{cont.})^{\frac{3}{2}} . \quad (4.15)$$

We can investigate if or how well these conditions are actually fulfilled in our case. By looking at the median and mean values for the different samples in Tabs. 4.6 and 4.7 I find that this condition is to first order fullfilled to within about 15% : For the means of the continuum variability I find $(39/30)^{\frac{3}{2}} = 1.5$ whereas the measured ratio of the means of the line variability is $27/15 = 1.8$. For the median values of the continuum variability I find $(42/35)^{\frac{3}{2}} = 1.3$ whereas the measured ratio of the median values of the line variability is $29/16 = 1.8$. This proportionality relation between the continuum and narrow line variability is demonstrated in Fig. 4.17 and discussed in the following section.

4.6.3 NLR response to the nuclear continuum variability

As a new and statistically well based result I find that it the reverberation response to the continuum variability is not only limited to the BLR but can also be detected in the emission from the NLR. The black crosses represent the median values and their uncertainties as shown in Figs. 4.14 & 4.15. In this plot the curved lines represent the relation $\Delta L_{line} = \epsilon(\Delta L_{cont.})^{\frac{3}{2}}$, with $\epsilon=1.0$ for the thick straight line which is followed surprisingly well by the data. However, for my sample of the order of 50% of the continuum flux density is likely to be due to the stellar continuum that is not variable on the time scales discussed here. For more luminous objects this may be of the order of 20% [Kollatschny et al. \(2006b\)](#). This indicates that the pure nuclear continuum variability that is not contaminated by stellar flux may in general be larger by about one third. This results in a value of $\epsilon \sim 1.9$ (dashed line in Fig. 4.17) to match the derived proportionality relation between the continuum and narrow line variability. In this case the data points (black crosses and data points) would have to be shifted up by the same factor on average, to fall close to the corresponding dashed line. The additional strong noise (with

respect to the ideal description of the process) may indicate that some of the simplifications we made to obtain the result are not always fully fulfilled.

I have used the reverberation formalism to interpret the line response to continuum variations. This is usually applied to broad lines only and used to derive the size of the BLR making use of well sampled continuous light curves of the continuum and broad line emission which are then cross-correlated. In Fig. 4.17 I compare my finding with variability data from different broad line QSO samples. The blue filled dots are QSO variability data from the sample listed in Tab.6 by (Kollatschny *et al.*, 2006b) the red filled dots are data from (Peterson *et al.*, 2004) and (Kaspi *et al.*, 2000) as listed in Tab.8 by (Kollatschny *et al.*, 2006b). The comparison shows that the relation also holds for reverberation response of the broad line QSOs. With the mentioned literature data Fig. 4.17 now comprises a total of 61 sources. In this chapter I present, however, the line response that I monitored in my small sample is dominated by forbidden narrow line emission. Only the H β line allows a separation between the broad and narrow line contribution. However, the median and mean derived from the BLR component only is in good agreement with the overall result. My investigation was based on two typically measurements over a baseline in time of the order of 10 years (see Tab. 4.10). Reverberation response of the NLR based on measurements over 5-8 years has also been reported for the radio galaxy 3C390.3 (Clavel and Wamsteker, 1987) and for the S1 galaxy NGC 5548 (Peterson *et al.*, 2013). Within the SDSS survey one can also find example of multi-epoch observations that are consistent with this picture. In Fig. 4.16 I show three epoch SDSS spectra for the NLS1 sources J014412 and J022205. The variability estimates places them well into Fig. 4.17,

Due to the causality principle variability is always coupled to the size of the variable object. Variability can be interpreted as a measure of the size of the variable object as the speed with which information is transported is limited by the speed of light. Variability on time scale of years already sets an upper limit to the size of the responding region. Since the variability is rather significant the line flux contribution of that region is also high. While there is a density and temperature gradient towards the nuclear position (Morse *et al.*, 1995; Ogle *et al.*, 2000; Penston *et al.*, 1990) one also finds that the surface brightness distribution of the NLR flux is very much centrally peaked. The size of the NLR is luminosity dependant (Schmitt *et al.*, 2003), however, the inspection of high angular resolution HST scans across S1 and S2 nuclei shows that the unresolved central peak may contain 50% or more of the more extended nuclear forbidden line flux (Bennert *et al.*, 2006a,b). (Peterson *et al.*, 2013) find for NGC 5548 that 94% of the NLR emission arises from within 18pc (54 ly). (Ogle *et al.*, 2000) derive a density

4. LINE AND CONTINUUM VARIABILITY IN ACTIVE GALAXIES

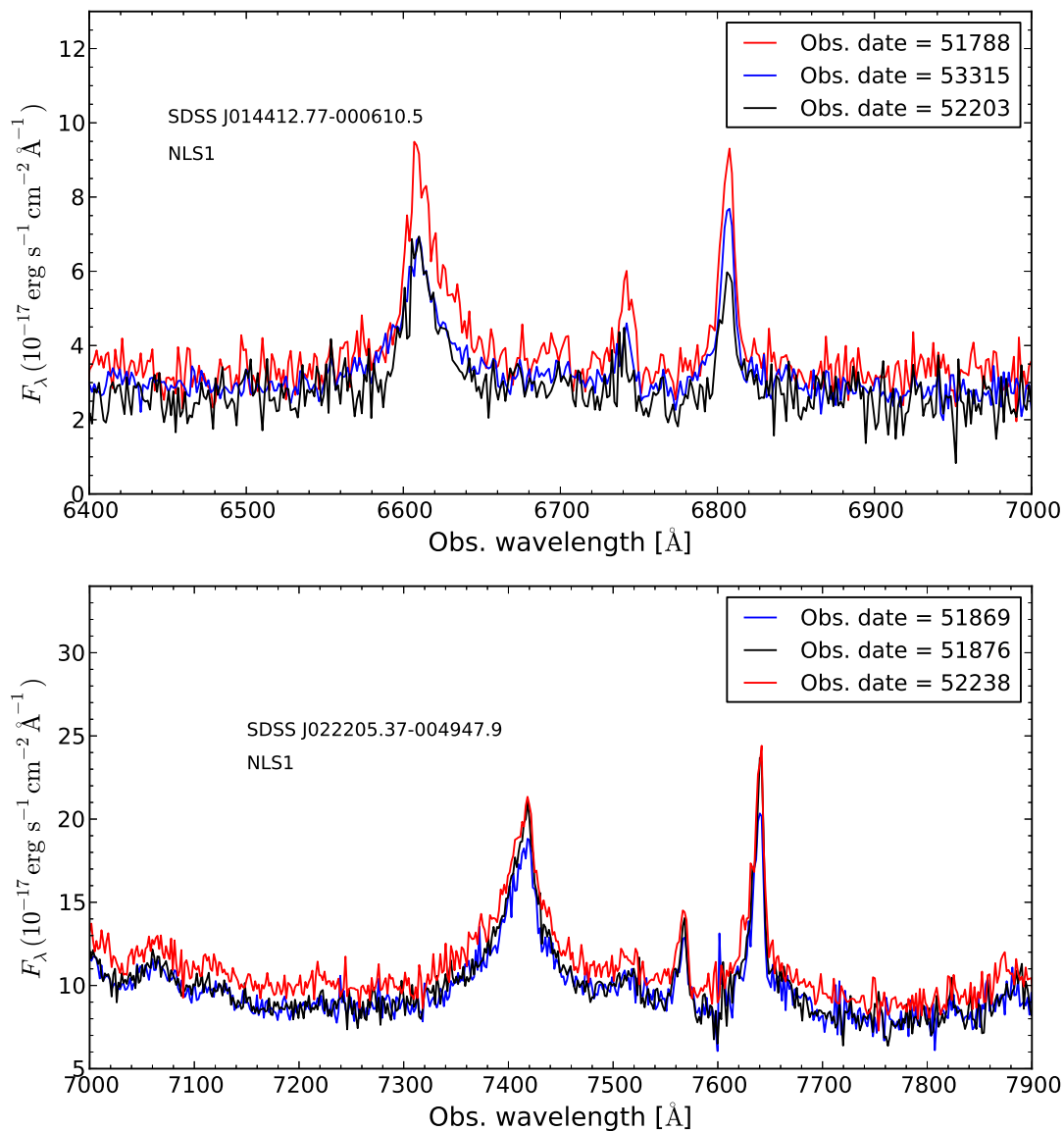


Figure 4.16: Three epoch SDSS spectra for J014412 and J022205. These spectra allow us to derive variability estimates of $\Delta_{cont.}=0.18$ and $\Delta_{line.}=0.45$ for J014412 and $\Delta_{cont.}=0.27$ and $\Delta_{line.}=0.26$ for J022205. These values lie well above the low calibration uncertainties for the SDSS data (section 4.3).

profile of r^{-2} and (Walsh *et al.*, 2008) find that the [S II] line ratio indicates a radial stratification in gas density, with a sharp increase within the inner 10-20 pc, in the majority of the Type 1 (broad-lined) objects.

Based on our data covering a large time interval we find that the main response to the continuum flux density variation must therefore originate in a rather compact region with a diameter of the order of 10 light years. This is in good agreement with the finding for 3C390.3 (Clavel and Wamsteker, 1987) and NGC 5548 (Peterson *et al.*, 2013). Since this formalism fully explains the reverberation of the line emission with respect to the continuum variation (with a surprisingly close proportionality; see Fig. 4.17), this suggests that the region illuminated by the nucleus is almost fully spatially overlapping with the responding line emitting region. Hence, at larger distance the NLRs then show a much weaker response to the continuum variability most likely due to a combination of a lower overall luminosity and a lower volume filling factor. The close correlation to the non-stellar nuclear continuum variability also implies that for the sources that I investigated there are no other significant sources (i.e. star formation, extra nuclear shocks) but the nuclear radiation field that contributes substantially to the line emission of the reverberating region.

4.7 Conclusions

Based on the LBT MODS optical spectroscopy data and on the detailed inter-telescope and inter-epoch calibration that I performed, I obtained the impression that the NLR line variability is lined to the continuum variability. Therefore I combined my observational data with literature data and data from public surveys in order to put this result on a firm footing. I have investigated several source samples of different sizes in order to characterize their line and continuum variability and the relation between those. For 18 sources we carried out a detailed spectroscopic investigation. For 8 objects in Tab. 4.1 I obtained and/or performed the detailed analysis spectroscopy over the available optical wavelength range. For 10 sources I obtained suitable multi-epoch line and continuum data from the literature (see Tab. 4.8 and Figs. 4.14 and 4.15) covering time scales from 5 to 10 years. Fig. 4.17 demonstrates that my findings describe the variability characteristics of a total of 61 sources. This sample size allows me to draw first - statistically well based - conclusions. From the line and continuum variability of these active galactic nuclei I find the following consistent picture that explains the differences between the Seyfert 2/NLS 1 and the BLS1 and QSO sample: The line luminosity L_{line} can be

4. LINE AND CONTINUUM VARIABILITY IN ACTIVE GALAXIES

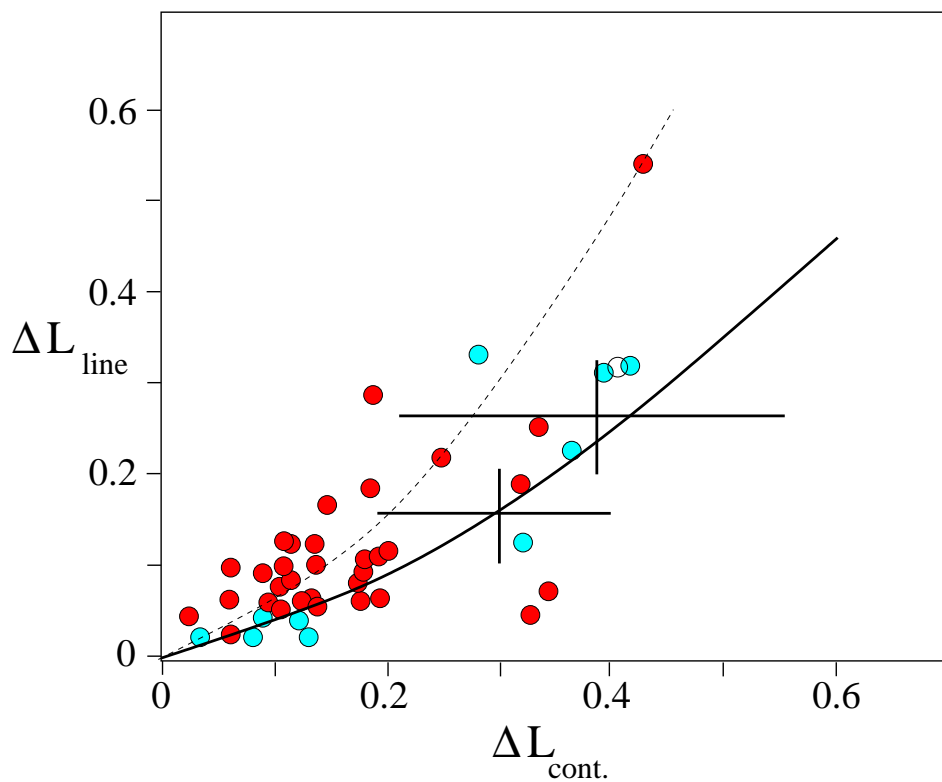


Figure 4.17: The continuum variability plotted against the line variability. The solid and dashed black lines represent the relation $\Delta L_{line} = \epsilon(\Delta L_{cont.})^{3/2}$ (see text). The filled colored dots are QSO variability data ($H\beta$ and continuum) from (Kollatschny *et al.*, 2006b), (Peterson *et al.*, 2004), and (Kaspi *et al.*, 2000). The Black crosses represent the median values and their uncertainties as I derived them for my sample ($H\beta$ and other lines plus continuum) and as they are shown in Figs. 4.14 & 4.15.

described as a reverberation response to the continuum luminosity L_{cont} . This response must mean that the source is reasonably compact. In good agreement with results of previous studies (references in section 4.6.3) I find that the bulk of the NLR emission arises from within 10-20 light years and shows a reverberation response to variability of the nucleus. The differences in variability do not require a variation of the accretion rate $\Delta \frac{d}{dt}M$ between the two samples. It is mainly the difference in black hole mass ΔM that is responsible for the difference between the samples. The increased variability of the line emission can fully be explained by the dependency on the accretion rate $\frac{d}{dt}M$. Other factors may be of importance that give rise to additional noise in the found correlation.

4. LINE AND CONTINUUM VARIABILITY IN ACTIVE GALAXIES

Table 4.9: The line fitting results for J0938, J1203, 1158, J0911, J0802, J0354, J0153, and J0347.

Sources	Em. lines	Ob. Wa. Å	Inst.1		Inst.2	
			Flux [10^{-16} erg s^{-1} cm^{-2}]	FWHM Å	Flux [10^{-16} erg s^{-1} cm^{-2}]	FWHM Å
			SDSS ^(a)		LBT	
J0938	[O II] λ 3727	4102 \pm 1	50.12 \pm 2.39	5.66 \pm 0.49	43.08 \pm 2.38	6.05 \pm 0.47
	[Ne III] λ 3868	4258 \pm 1	11.28 \pm 0.91	10.67 \pm 0.93	7.97 \pm 1.14	8.38 \pm 0.79
	H γ λ 4340	4777 \pm 1	25.18 \pm 1.58	6.31 \pm 0.88	18.95 \pm 1.10	6.91 \pm 0.71
	He II λ 4686	5157 \pm 2	8.50 \pm 0.73	16.81 \pm 1.12	4.04 \pm 0.36	10.66 \pm 0.87
	H β * λ 4861	5350 \pm 1	50.28 \pm 2.54	5.61 \pm 0.49	41.95 \pm 2.83	5.91 \pm 0.73
	[O III] λ 5007	5510 \pm 1	45.06 \pm 1.57	7.34 \pm 0.57	37.43 \pm 2.01	7.27 \pm 0.66
	[Fe VII] λ 5721	6298 \pm 1	4.60 \pm 0.39	10.56 \pm 0.35	6.55 \pm 1.11	11.74 \pm 0.64
	[Fe VII] λ 6087	6699 \pm 1	11.55 \pm 0.75	18.63 \pm 0.51	11.19 \pm 1.48	19.65 \pm 0.72
	[O I] λ 6300	6935 \pm 1	4.94 \pm 0.40	6.75 \pm 0.41	5.30 \pm 1.14	9.14 \pm 0.83
	H α λ 6563	7224 \pm 1	208.83 \pm 5.89	7.75 \pm 0.57	164.56 \pm 5.03	6.43 \pm 0.61
	[N II] λ 6583	7246 \pm 1	80.04 \pm 2.57	7.77 \pm 0.52	57.33 \pm 2.70	6.17 \pm 0.65
	[S II] λ 6716	7393 \pm 1	28.90 \pm 1.25	7.46 \pm 0.54	23.08 \pm 1.45	5.92 \pm 0.52
	[S II] λ 6731	7409 \pm 1	19.28 \pm 0.96	7.15 \pm 0.56	16.48 \pm 1.32	6.02 \pm 0.51
			SDSS		LBT	
J1203	[Ne V] λ 3345	3898 \pm 1	20.42 \pm 1.41	5.75 \pm 0.22	27.82 \pm 1.02	5.18 \pm 0.31
	[Ne VI] λ 3425	3993 \pm 1	55.54 \pm 2.84	4.67 \pm 0.25	67.57 \pm 1.93	5.08 \pm 0.24
	[O II] λ 3727	4344 \pm 1	83.03 \pm 1.53	6.14 \pm 0.14	93.17 \pm 2.87	6.19 \pm 0.22
	H ϵ λ 3969	4625 \pm 2	38.36 \pm 1.21	4.92 \pm 0.36	48.01 \pm 1.75	4.98 \pm 0.76
	H γ λ 4340	5059 \pm 1	89.24 \pm 1.49	5.64 \pm 0.41	81.84 \pm 2.04	5.41 \pm 0.75
	H β * λ 4861	5665 \pm 2	154.54 \pm 1.78	5.88 \pm 0.75	126.39 \pm 1.11	5.64 \pm 0.97
	[O III] λ 5007	5835 \pm 2	803.60 \pm 6.39	5.67 \pm 0.88	681.90 \pm 7.66	5.29 \pm 0.85
	[O I] λ 6300	7343 \pm 3	12.53 \pm 0.75	7.33 \pm 0.13	11.25 \pm 0.54	7.94 \pm 0.12
	H α λ 6543	7648 \pm 2	364.01 \pm 3.60	7.64 \pm 0.55	168.34 \pm 3.95	7.12 \pm 0.71
	[N II] λ 6583	7671 \pm 1	25.11 \pm 1.63	6.59 \pm 0.18	13.17 \pm 0.94	6.31 \pm 0.34
	[S II] λ 6716	7827 \pm 3	17.09 \pm 1.71	7.00 \pm 0.11	10.37 \pm 0.91	7.40 \pm 0.14
	[S II] λ 6731	7844 \pm 3	16.92 \pm 1.28	7.81 \pm 0.12	8.98 \pm 0.88	6.61 \pm 0.11
				SDSS		LBT
J0911	[Mg II] λ 2799	4030 \pm 1	60.43 \pm 1.53	29.01 \pm 0.95	35.40 \pm 3.01	29.01 \pm 1.32
	[O II] λ 3727	5372 \pm 2	11.80 \pm 0.84	7.35 \pm 0.48	15.26 \pm 0.55	7.77 \pm 0.32
	H γ λ 4340 (broad)	6258 \pm 2	15.71 \pm 1.14	54.14 \pm 1.87	18.42 \pm 0.77	51.78 \pm 2.01
	H γ λ 4340 (narrow)	6258 \pm 2	6.92 \pm 0.75	10.35 \pm 0.69	8.03 \pm 0.41	11.06 \pm 0.73
	H β λ 4861 (broad)	7007 \pm 2	46.05 \pm 2.94	54.14 \pm 1.87	52.55 \pm 2.49	51.78 \pm 2.01

Continued on next page

4.7 Conclusions

Table 4.9: Continued.

	H β λ 4861 (narrow)	7007 \pm 2	17.09 \pm 1.06	9.65 \pm 0.62	19.24 \pm 0.82	10.59 \pm 0.99
	[O III] λ 5007	7218 \pm 1	28.76 \pm 1.53	9.88 \pm 0.84	34.49 \pm 1.55	10.12 \pm 1.02
	[O I] λ 6300	9082 \pm 2	4.75 \pm 0.35	20.22 \pm 1.22	5.43 \pm 0.87	16.14 \pm 1.76
			SDSS		LBT	
J1158	[O II] λ 3727	5366 \pm 1	10.61 \pm 0.67	8.35 \pm 0.51	7.12 \pm 0.71	9.85 \pm 0.88
	H γ λ 4340 (broad)	6245 \pm 3	58.82 \pm 2.83	75.32 \pm 2.92	29.63 \pm 2.16	94.16 \pm 2.56
	H γ λ 4340 (narrow)	6245 \pm 3	12.61 \pm 0.56	14.83 \pm 0.81	7.40 \pm 0.61	14.35 \pm 1.47
	H β λ 4861 (broad)	6994 \pm 3	201.01 \pm 3.31	75.32 \pm 2.92	105.69 \pm 4.46	94.16 \pm 2.56
	H β λ 4861(narrow)	6994 \pm 3	28.21 \pm 0.96	12.91 \pm 0.88	17.05 \pm 1.14	13.98 \pm 0.94
	[O III] λ 5007	7208 \pm 3	59.41 \pm 1.24	12.01 \pm 0.91	41.92 \pm 1.88	13.65 \pm 1.18
	[O I] λ 6300	9071 \pm 3	5.81 \pm 0.90	6.55 \pm 0.75	3.98 \pm 0.60	8.49 \pm 0.98
			SDSS		LBT	
J0802	[O II] λ 3727	6203 \pm 1	18.43 \pm 1.23	15.48 \pm 1.31	25.33 \pm 0.99	12.91 \pm 0.89
	H γ λ 4340 (broad)	7227 \pm 2	33.82 \pm 2.43	80.11 \pm 2.02	60.36 \pm 0.95	82.39 \pm 2.89
	H γ λ 4340 (narrow)	7229 \pm 2	8.62 \pm 1.29	12.00 \pm 0.79	15.41 \pm 0.55	11.29 \pm 0.47
	H β λ 4861 (broad)	8092 \pm 1	84.23 \pm 2.18	80.11 \pm 2.02	95.07 \pm 2.76	82.39 \pm 2.89
	H β λ 4861 (narrow)	8092 \pm 1	20.97 \pm 1.63	11.98 \pm 0.85	43.22 \pm 1.54	13.65 \pm 1.98
	[O III] λ 5007	8331 \pm 1	16.40 \pm 1.42	11.51 \pm 0.81	28.41 \pm 1.62	13.41 \pm 1.12
			Beijing ^(b) (1)		LBT	
J0153	H β λ 4861 (broad)	6453 \pm 3	420.80 \pm ---	77.01 \pm ---	299.92 \pm 10.98	51.36 \pm 3.98
	H β λ 4861 (narrow)	6453 \pm 3	99.60 \pm ---	18.34 \pm ---	68.20 \pm 3.01	14.96 \pm 1.34
	[O III] λ 5007	6654 \pm 1	155.90 \pm ---	13.37 \pm ---	113.36 \pm 4.51	14.12 \pm 2.45
			Hiltner ^(c) (2)		LBT	
J0354	[Ne V] λ 3346	3544 \pm 2	26.00 \pm 10.00	4.51 \pm 1.75	11.91 \pm 0.97	3.09 \pm 0.68
	[O III] λ 5007	5183 \pm 1	413.00 \pm 15.00	5.51 \pm 0.94	284.84 \pm 4.42	4.53 \pm 0.26
	[O I] λ 6300	6522 \pm 1	15.15 \pm 1.34	5.93 \pm 0.92	8.70 \pm 2.00	6.60 \pm 0.67
	[S II] λ 6716	6952 \pm 1	14.45 \pm 1.16	5.82 \pm 0.34	10.90 \pm 1.00	5.79 \pm 0.49
	[S II] λ 6731	6967 \pm 1	12.52 \pm 0.96	5.85 \pm 0.36	8.40 \pm 1.00	5.09 \pm 0.42
J0347			OHP ^(d)		LBT	
	H γ λ 4340 (broad)	4475 \pm 2	752.63 \pm 18.28	51.78 \pm 2.68	1094.56 \pm 9.19	51.78 \pm 2.95
	H γ λ 4340 (narrow)	4475 \pm 2	273.21 \pm 5.23	10.96 \pm 1.23	324.91 \pm 9.19	10.01 \pm 0.55
	H β λ 4861 (broad)	5010 \pm 1	1644.70 \pm 16.46	51.78 \pm 3.54	2280.33 \pm 21.87	51.78 \pm 0.92
	H β λ 4861(narrow)	5010 \pm 1	1058.20 \pm 11.89	13.18 \pm 1.02	1398.38 \pm 20.46	11.77 \pm 0.92
	[O III] λ 5007	5156 \pm 1	951.10 \pm 10.87	12.71 \pm 2.33	996.74 \pm 20.80	11.53 \pm 0.64
	[O I] λ 6300	6495 \pm 2	124.29 \pm 2.67	16.19 \pm 1.11	157.30 \pm 5.79	18.78 \pm 1.78

References. (1) (Zhou et al., 2002), (2) (Grupe et al., 2005).

Notes: (*) Means H β are narrow. (a) The Sloan Digital Sky Survey. (b) Beijing Observatory. (c) Hiltner Telescope. (d) Telescope of Observatoire de Haute-Provence (OHP).

4. LINE AND CONTINUUM VARIABILITY IN ACTIVE GALAXIES

Table 4.10: Broad and narrow emission lines variability.

Type	Sources	Narrow line components		Broad line components		
		line type	Varib. %	line type	Varib. %	
Narrow lines objects	J0347	H γ λ 4340	15.9	H γ λ 4340	31.2	
		H β λ 4861	24.3	H β λ 4861	27.8	
	J1203	H γ λ 4340	12.4	H γ λ 4340	–	
		H β λ 4861	18.2	H β λ 4861	–	
	J0938	H γ λ 4340	24.7	H γ λ 4340	–	
		H β λ 4861	16.5	H β λ 4861	–	
	Broad lines objects	J1158	H γ λ 4340	31.8	H γ λ 4340	32.2
			H β λ 4861	33.6	H β λ 4861	31.4
		J0911	H γ λ 4340	19.8	H γ λ 4340	14.7
H β λ 4861			11.1	H β λ 4861	12.3	
J0802		H γ λ 4340	43.9	H γ λ 4340	60.5	
		H β λ 4861	51.4	H β λ 4861	11.4	
J0153	H β λ 4861	31.5	H β λ 4861	28.7		

5

Variability in a Broad Absorption Lines Quasars (BAL QSO)

5.1 Introduction

Many quasars are characterized by broad absorption lines (troughs) in their spectra. These wide troughs may originate in material close to the nucleus. Hence, they appear to be good candidates to study the variability, These troughs represent are ideal probes along the line of sight, sensitive to small and large variations directly or indirectly caused by the AGN. The broadening of these troughs is cause by the high velocity outflows of the gas. These outflows have a significantly affect on the quasars properties through. This is most evident through the absorption in the ultraviolet lines as well as the presence of emission-lines from highly ionized species (Gibson *et al.*, 2009, e.g.). Furthermore, high velocity outflows might have a positive feedback on the accretion efficiency onto the SMBH as they may help to remove angular momentum from the accretion disk (e.g., Arav *et al.*, 2013, and references therein). It is thought that these outflows are generated from the accretion disk at distance of 10 to 100 light days away from the SMBH (Filiz Ak *et al.*, 2013). This implies that the outflow material needs typically timescales of 1-9 years to cross this region and cause changes in the spectra of BAL quasars. I will present evidence for this in section 5.3.

For these objects one can in general distinguish two main types: HiBAL and LoBAL sources. In addition there is a sub-type of LoBAL sources that exhibits a strong iron line - in particular populations of Fe II and/or Fe III emission-lines in their spectra. This phenomenon give rise to the sub-type name FeLoBAL (see Sec. 1.3).

5. VARIABILITY IN A BROAD ABSORPTION LINES QUASARS (BAL QSO)

Detailed studies of the variability of BALQSO sources have been carried out since the eighties of the last century. [Smith and Penston \(1988\)](#) found that over a timescale of 2-7 years the spectra of two BALQSOs (Q1246-057 and Q1309-056) show a significant amount of variability in the spectra. These variations occurred specifically in the troughs of Si iv $\lambda 1398\text{\AA}$ and C iv $\lambda 1544\text{\AA}$ lines. Furthermore, they suggested that the troughs variations are associated with changes in the spectral continuum. In the nineties [Barlow \(1993\)](#) expanded the variability study of BALQSOs by increasing the number of objects to 54 BALQSOs. Among them a total of 23 BALQSO showed significant variability in their spectra. In addition, they supported the conclusions that were reached earlier by [Smith and Penston \(1988\)](#). Recent research allowed to draw new conclusions on the variability properties of BAL sources. [Capellupo et al. \(2012\)](#) suggested that the Si iv troughs are more variable than the C iv troughs.

In this chapter, I am studying the variability in BAL quasars from a different aspect. First, I study the individual variability that occurs in the two types of BAL active galaxies HiBAL and LoBAL. Second, I will do a comparison between the variability behavior of these two types.

5.2 The LBT, SDSS, and MMT observations

In this chapter, I summarize the observational results for three QSOBALs sources as listed in Tab. 5.1. Two of them have been classified as HiBAL: SDSS J012412.45-010049.9¹ and SDSS J093403.96+315331.3²). One source was classified as a LoBAL object: FBQS J072831.64+402616.0³. For the optical spectroscopy data I can resort to two observing dates for each object. Except for J0728, the first epoch has not been taken with the SDSS telescope. In order to compensate this deficiency in spectroscopy data for J0728 I used spectroscopy data taken with the MMT⁴ telescope as listed in Tab. 5.1. While all the second epoch observations were carried out with the LBT telescope using the MODS1 spectrograph. Furthermore, I have photometric data at different wavelengths band (u, g, r, I, and z) for all sources monitored by the SDSS telescope. I will use this data later to briefly summarize the continuum variability that (see Tab. 5.2). I will also use these photometric observations to support that the differences between the slit and fiber apertures is negligible, as I did in the last chapter of section 4.3.1. In Tab. 5.3 I listed the coordinates and FWHM of each stars that used in last process.

¹In the following J0124

²In the following J0934

³In the following J0728

⁴ Multiple Mirror Telescope (MMT)

Moreover, in the LBT observations I utilized a long slit with aperture of $0''.8$, whereas for the SDSS spectroscopy observations a fiber with radius $3''$ as used. I can show that for the results obtained, the difference in the apertures (slit versus fiber) are insignificant. I present SDSS z -band images of our objects simultaneously with images of stars close to their positions in the sky located on the same data frames (Figs. 5.1). I first scaled the peak flux level of the target galaxies and then subtracted the frames from each other. I notice that - within the measurements uncertainties - in all three cases, no significant residuals are left. This supports my suggestion that to a very good approximation these these objects are point sources and differences due to possible aperture effects are negligible.

Finally, the magnitudes of these objects were taken from the SDSS survey. In their case the PSF fitting technique was used. This was done by fitting a Gaussian function as the PSF to the point like object. For more information about this technique and the conversion from magnitudes to physical units please refer to section 4.3.1. The reduction of the LBT data has been done in the same way as for the objects described in chapters 3 and 4. Moreover, this process is explained in details in chapter 2.

5.3 Results

5.3.1 SDSS J012412-010049

In almost all SDSS catalog releases (Data Release: DR1, DR2, DR3, DR5, and DR7) J0124 was mentioned as a quasars (Schneider *et al.*, 2002, 2003, 2005, 2007, 2010). In Trump *et al.* (2006) the source J0124 is classified as a HiBAL as shown in Tab. 5.1, in which the MgII emission line is not within the spectral range or has a low S/N ratio. In Fig. 5.2 I present the overplot of the LBT and SDSS spectra for J0124. The SDSS spectrum has been obtained in September 2000, while the LBT spectrum for this source has been taken in February 2012. Therefore, for this object I can discuss the variability over a time span of 11.5 years. Strong variability in the spectral continuum is evident after overplotting both spectra and measuring the flux densities of the continuum in different wavelengths band Tab. 5.2. The continuum level of the LBT spectrum is higher than that in the SDSS spectrum as seen in Fig. 5.2 (a,b,c, and d), especially, the red part of the LBT spectrum is higher by a a factor of 1.8 on average. In the blue part of the spectrum, this number decreases to a value of 1.6 at a wavelength of 1300 \AA . Finally, at a wavelength of 1000 \AA , both spectra do match each other within the uncertainties. This phenomenon (the optical continuum variability) was reported by Rengstorf *et al.* (2006);

5. VARIABILITY IN A BROAD ABSORPTION LINES QUASARS (BAL QSO)

Table 5.1: Coordinates, redshifts, classification and observing parameters for all sources.

name	RA (hh mm ss)	Dec. ($^{\circ}$ ' ")	Redshift (z)	Classi.	Inst.	First epoch Da.(M Y)	seeing	Inst.	Second epoch Da.(M Y)	seeing	D_L Mpc	Ref.
SDSS J012412.45-010049.9	01 24 12.45	-01 00 49.9	2.830 \pm 0.0541	HBAL	SDSS	09 2000	1.21	LBT	02 2012	1.40	24239.8	1,2,3,4
SDSS J093403.96+315331.3	09 34 03.96	31 53 31.3	2.419 \pm 0.0010	HBAL	SDSS	01 2005	1.35	LBT	02 2012	1.20	19679.1	5,6,7,8
FBQS J072831.64+402616.0	07 28 31.64	40 26 16.0	0.656 \pm 0.0004	LoBAL	MMT ^(a)	11 1997	–	LBT	01 2012	1.10	3934.8	5,6,7,8

References for redshifts and positions: (1) (Hewett and Wild, 2010); (2) (Trump *et al.*, 2006); (3) (Adelman-McCarthy *et al.*, 2009); (4) (Allen *et al.*, 2011); (5) (White *et al.*, 2000); (6) (Becker *et al.*, 2000); (7) (DIPompeo *et al.*, 2013); (8) (DIPompeo *et al.*, 2010).

Notes: ^a Multiple Mirror Telescope.

Table 5.2: The continuum flux density variability between LBT and SDSS of J0124, J0934, and J0728 from the photometry and spectroscopy aspect.

Sources	Filt.	Wa. Å	photometry		Spectroscopy (1)		Spectroscopy (2)	
			Flux [10^{-16} erg $s^{-1} \text{ cm}^{-2} \text{ Å}$]	Inst.	Flux [10^{-16} erg $s^{-1} \text{ cm}^{-2} \text{ Å}$]	Inst.	Flux [10^{-16} erg $s^{-1} \text{ cm}^{-2} \text{ Å}$]	Inst.
J0124	(u)	3543	0.44 ± 0.08		—		6.34 ± 5.08	
	(g)	4770	1.62 ± 0.01		2.27 ± 0.16		3.23 ± 0.31	
	(r)	6231	2.48 ± 0.01	SDSS	2.44 ± 0.11	SDSS	3.83 ± 0.23	LBT
	(i)	7625	3.10 ± 0.01		3.53 ± 0.21		5.80 ± 0.23	
	(z)	9134	3.24 ± 0.01		3.70 ± 0.29		5.82 ± 0.51	
J0934	(u)	3543	3.00 ± 0.02		—		3.75 ± 0.89	
	(g)	4770	3.37 ± 0.01		3.68 ± 0.18		3.25 ± 0.33	
	(r)	6231	3.10 ± 0.01	SDSS	3.01 ± 0.21	SDSS	2.75 ± 0.18	LBT
	(i)	7625	2.68 ± 0.01		2.51 ± 0.23		2.62 ± 0.27	
	(z)	9134	2.33 ± 0.01		2.13 ± 0.32		2.23 ± 0.21	
J0728	(u)	3543	62.23 ± 0.00		43.73 ± 3.42		27.17 ± 1.42	
	(g)	4770	49.63 ± 0.00		54.84 ± 1.73		31.86 ± 1.35	
	(r)	6231	25.33 ± 0.01	SDSS	26.76 ± 1.14	MMT	16.94 ± 0.62	LBT
	(i)	7625	20.90 ± 0.00		21.34 ± 2.36		15.97 ± 0.61	
	(z)	9134	14.84 ± 0.00		—		11.06 ± 0.93	

5. VARIABILITY IN A BROAD ABSORPTION LINES QUASARS (BAL QSO)

Table 5.3: Comparison of apparent sizes of target galaxies and stars.

source	Obs. date	Star		Star		Galaxy			
		RA Da.(M Y) (hh mm ss)	Dec. ($^{\circ}$ ' $'$ $''$)	FWHM1 "	FWHM2 "	Angle "	FWHM1 "	FWHM2 "	Angle "
J0124	11 2000	01 24 15.1	-01 02 05.5	1.01 ± 0.02	1.39 ± 0.03	4.38 ± 0.35	1.12 ± 0.02	1.27 ± 0.02	8.94 ± 0.35
J0934	04 2003	09 34 05.8	31 55 08.4	1.16 ± 0.02	1.14 ± 0.02	4.61 ± 0.26	1.11 ± 0.02	1.14 ± 0.02	0.93 ± 0.36
J0728	10 2003	07 28 23.5	40 24 10.3	0.50 ± 0.01	0.45 ± 0.01	5.69 ± 0.25	0.50 ± 0.01	0.45 ± 0.01	5.69 ± 0.26

Notes. For each galaxy, I give the coordinates of the star that I subtracted from the galaxy image as well as results of a Gaussian fit to galaxy and star. I used an elliptically shaped Gaussian function.

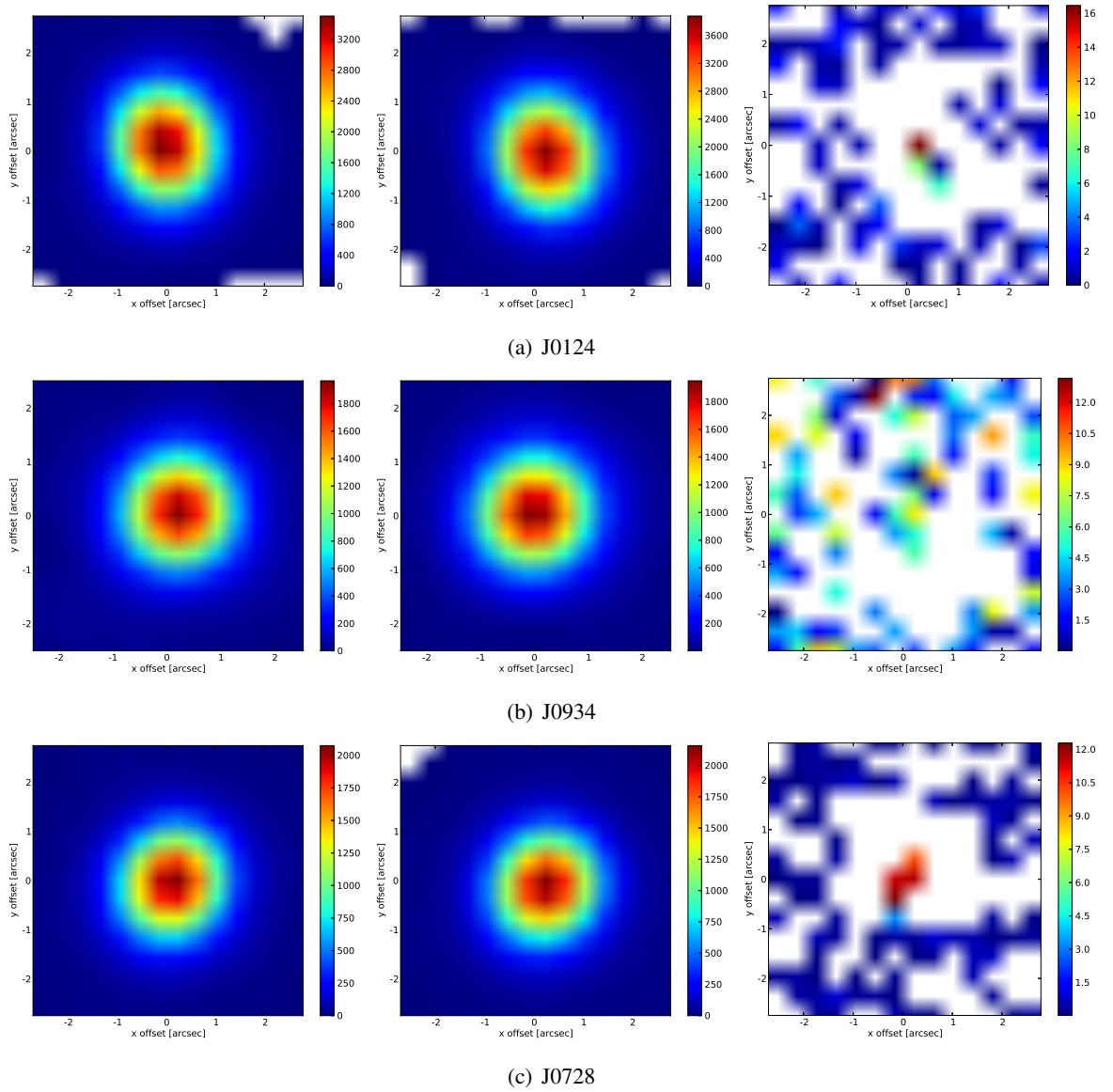


Figure 5.1: The plot shows *from left to right* an SDSS image of the galaxies J0124, J0934, and J0728, a star as a point sources reference from the same SDSS frame for each object (coordinates are listed in Tab. 5.3) and the residuum that is left after subtracting the scaled star from the galaxy.

5. VARIABILITY IN A BROAD ABSORPTION LINES QUASARS (BAL QSO)

Welling *et al.* (2014), where Welling *et al.* (2014) they found that the continuum variability tends to higher in BAL radio QSOs over long time scales of years. To better visualize the variability in the continuum I subtracted the two spectra from each other and plot their difference in Fig. 5.2 (e,f,g, h, i, and j).

5.3.2 SDSS J093403+315331

The source J0934 has been classified as BALQSO, where close to wavelengths of $\sim 4400\text{\AA}$ and $\sim 4887\text{\AA}$ the broad absorption BAL troughs can be found (Richards, 2001). Additionally, the authors describe that the continuum variations of J0934 is not clearly following the variability in the absorption troughs. The source J0934 has been examined as one among 30 radio BALQSOs in DiPompeo *et al.* (2010). Goal was to study the spectro-polarimetric properties of these sources. In this work J0934 was classified as a HiBAL, as shown in Tab. 5.1.

In Fig. 5.3 I present an overplot of the two optical spectra (LBT & SDSS) of J0934. The LBT spectrum was taken in February 2012, while the SDSS spectrum for this source has been observed in April 2003. Therefore, for this galaxy I can study the variability on a time scale of 7 years. The continuum flux density measurements of J0934 for three different epochs at various wavelengths is listed in Tab. 5.2. These measurements have been obtained through the LBT observations I describe in this thesis and via the spectroscopy and photometry results cataloged by SDSS. According to these measurements and as shown in the overplot of the both spectra Fig. 5.3 (a,b,c, and d), I notice that the continuum level of three different epochs (LBT spectrum, SDSS spectrum, and the SDSS photometric observations) are in good agreement. Hence, the source is behaving in a different way as the source J0124. Although, there is this match in continuum, I notice there is a difference in Ly α $\lambda 1213\text{\AA}$ as shown in Fig. 5.3 (d). This kind of variability in Ly α is quite typical in QSOs (e.g., Bregman *et al.*, 1986; Gondhalekar, 1990), since the bulk of this line emission originates close to the central ionizing nucleus. To illustrate the continuum and the emission-lines variability in an efficient way, I subtracted the two spectra from each other and plot their difference in Fig. 5.3 (e,f,g, h, i, and j).

5.3.3 FBQS J072831.64+402616.0

For the source J0728 it has been stated that it belongs to the group of BAL QSOs, that match quite well with the distribution of CSS¹/GPS² sources (Montenegro-Montes *et al.*, 2008), as

¹Compact Steep spectrum (CSS).

²Gigahertz Peaked Spectrum (GPS).

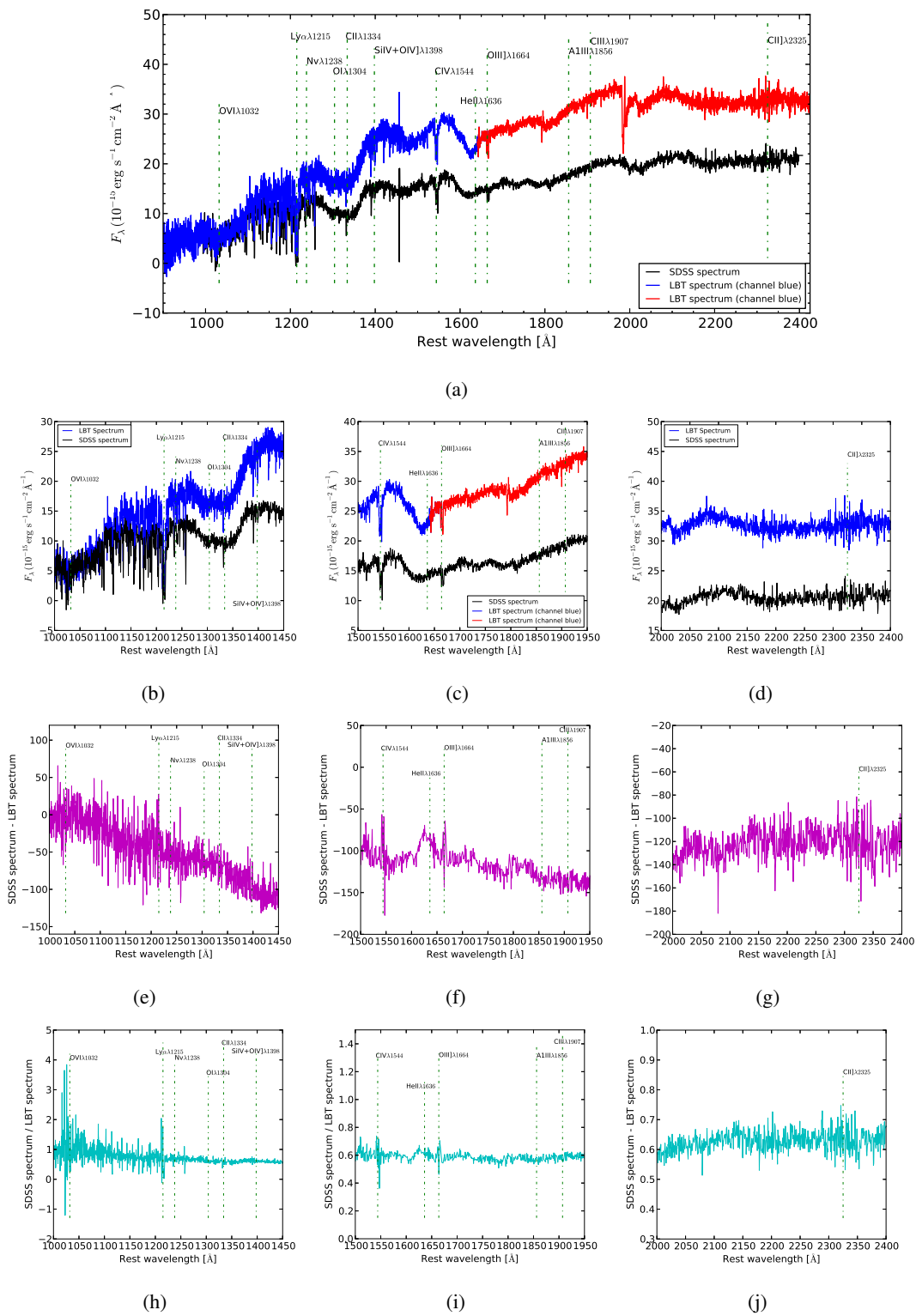


Figure 5.2: The optical spectrum of J0124 and the result of calculating the difference and ratio of spectra from different epochs.

5. VARIABILITY IN A BROAD ABSORPTION LINES QUASARS (BAL QSO)

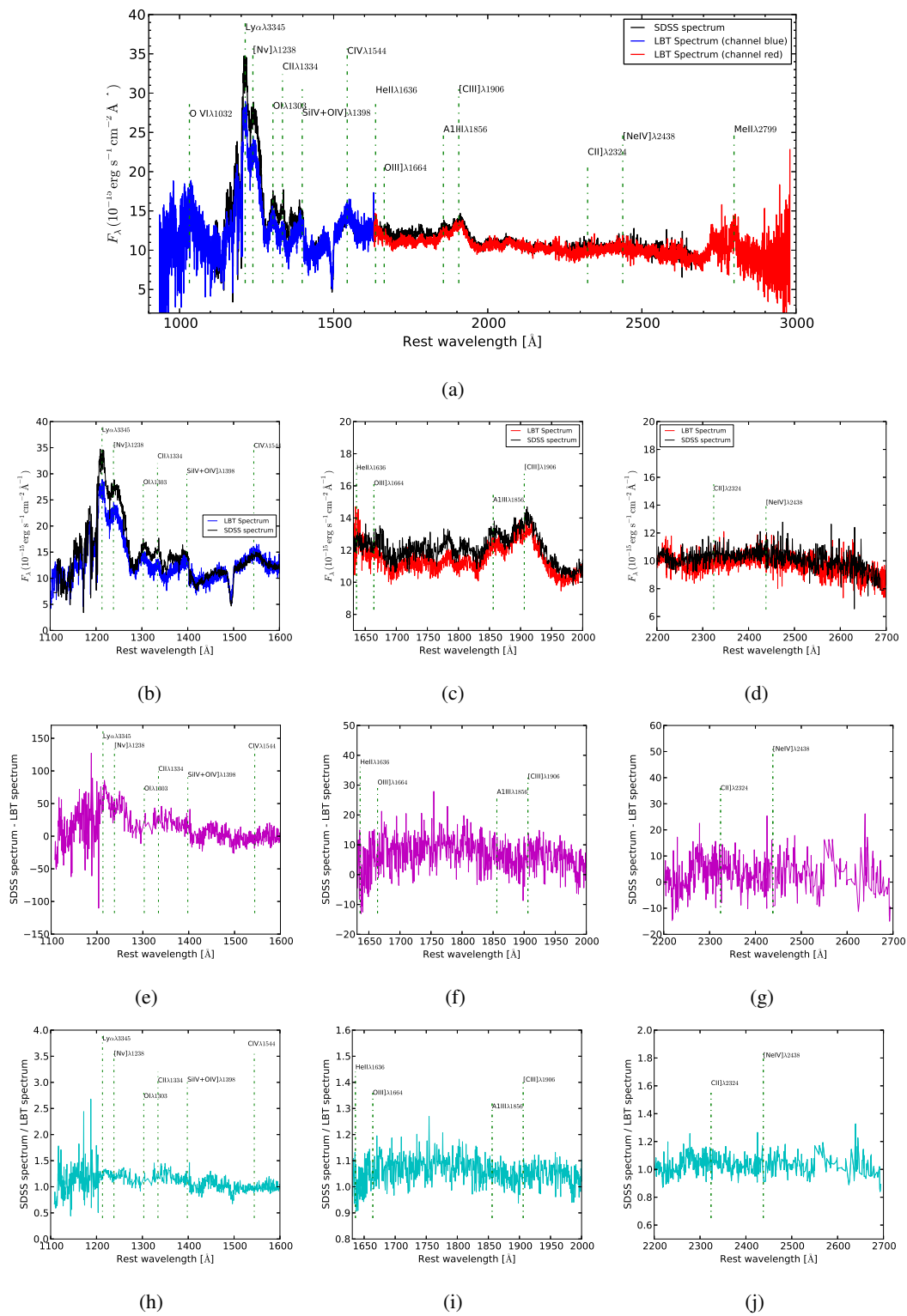


Figure 5.3: The optical spectrum of J0934 and the result of calculating the difference and ratio of spectra from different epochs.

it shows a simple convex spectrum. Additionally, the authors outline that J0728 is radio loud object. In Liu *et al.* (2008) J0728 was found to be a point source and the authors of this article confirmed the classification of this object as LoBAL. Furthermore, they measure the flux density of J0728 to be 18 mJy at a wavelength of 18 cm using the VLA radio telescope.

For this sources I do not have spectroscopy data from SDSS survey, because the source was just observed photometrically. Therefore in this case I substituted the SDSS spectroscopy data with spectroscopy observation taken by Multiple Mirror Telescope (MMT) located on Mount Hopkins, Arizona, USA. The observations were carried out in November 1997, with a slit width of 1.0'' (White *et al.*, 2000). Consequently, for this object I will be able to study the variability that occurred over a time scale of 15 years. The overplot of the both spectra (LBT& MMT) is presented in Fig. 5.4 (a, b, c, and d), where, specially in blue region of the spectrum, a strong variability in the continuum level can be seen. This phenomena is support by the comparison that I made between the photometric observations of SDSS and the spectroscopic data by (LBT& MMT) as shown Tab. 5.2. In this object I noticed that the variability was particularly strong in the blue part, where the factor between the fluxes of SDSS and MMT was 1.4 in the u-band. In the same band the factor is even higher 2.2 comparing the data taken at the SDSS and LBT. In the red part of the spectrum in the z-band this factor is less 1.2. This behave in the continuum variability was the opposite to the continuum variability that happened in J0124. To demonstrate the variability in continuum and the emission-line, I plot the difference and the ratios between the MMT and LBT spectra in Fig. 5.4 (e,f,g, h, i, and j).

5.4 Discussion and Conclusions

I describe my investigation of the variability of Broad Absorption Lines Quasars (BAL QSO). The research presented was based on two epoch spectrophotometric data in the optical covering a 5-10 year baseline in time. Inspection of the spectra of the three sources SDSS J012412.45-010049.9, SDSS J093403.96+315331.3, and J072831.64+402616.0 shows that they exhibit different spectral slopes. In order to investigate this phenomenon more closely I extend the samples using the SDSS data. For this I randomly selected 50 objects for each of the following subgroups: HiBal, LoBal, and intermediate class objects. The result obtained for the three sources for which I reduced newly taken LBT is consistent with the results found for SDSS extended source samples.

5. VARIABILITY IN A BROAD ABSORPTION LINES QUASARS (BAL QSO)

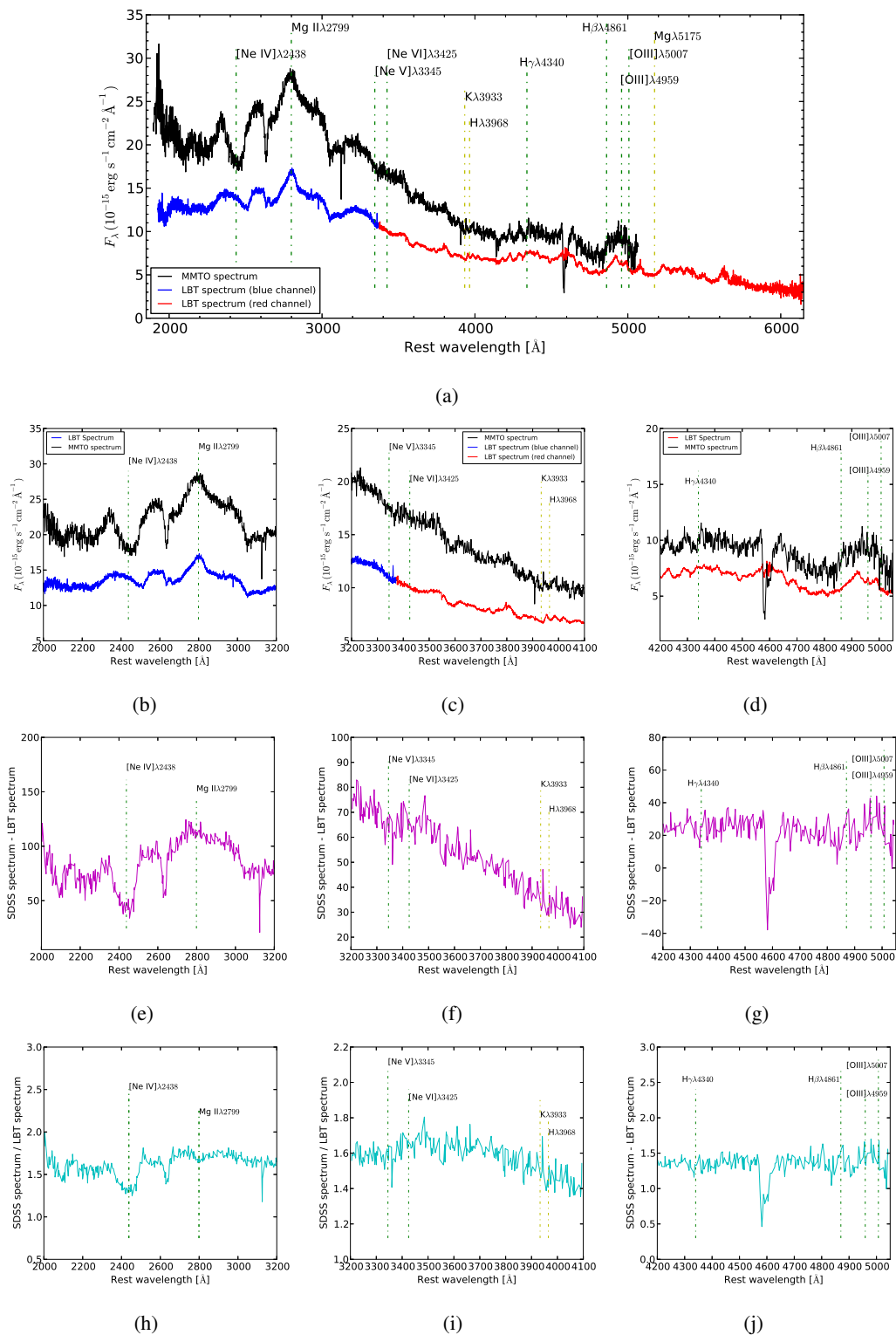


Figure 5.4: The optical spectrum of J0728 and the result of calculating the difference and ratio of spectra from different epochs.

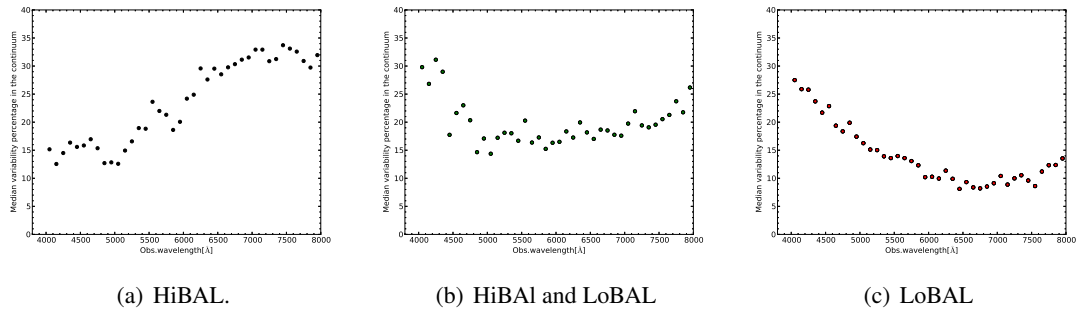


Figure 5.5: Median variability percentage for continuum of the BAL quasars.

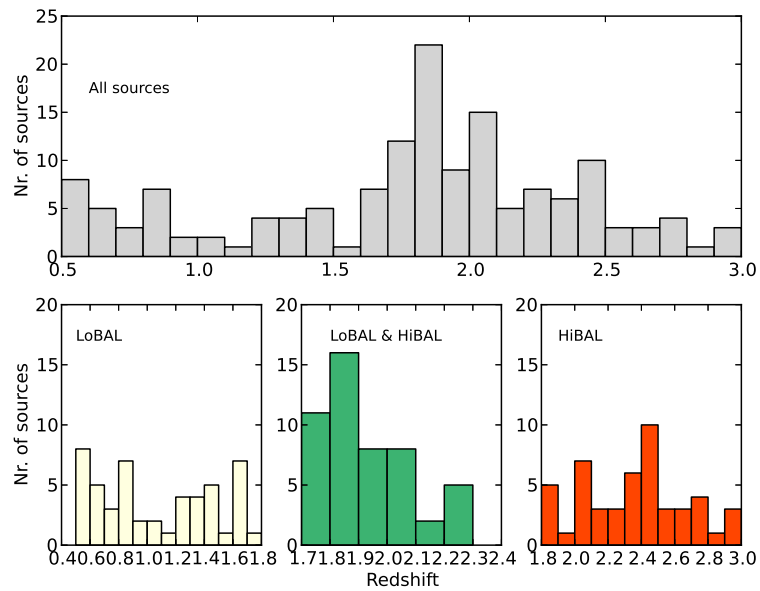


Figure 5.6: histogram for the redshift distribution of BALQSs of my samples..

5. VARIABILITY IN A BROAD ABSORPTION LINES QUASARS (BAL QSO)

In Fig. 5.5 (a, b, and c) show that the wavelength averaged variability properties of these sources classes. They show clear differences with an apparent transition between the source classes. The figures show that the LoBALs show increased variability towards the red part of the spectrum. I find that the HiBALs show systematically increased variability towards the blue part of the spectrum. The intermediate source lie in between with no clear tendency towards an increase in variability towards either of the two sides. There are two possible reasons for this behavior:

1) It may be due to the different average redshifts of these source classes (see Fig. 5.6). The LoBALs have a typical average redshift of about $z=1.0$. The HiBals lie on average at $z=2.4$. Including the properties of the intermediate source class and the cosmological spectral wavelength shifts that are proportional to $1+z$ all sources may belong to the same class of objects showing a minimum of variability in the intrinsic spectrum around 350 nm to 450 nm. Below and above this wavelength the variability then rises.

2) A second reason for a different behavior could be due to the different average luminosities. The sources at higher redshifts are clearly more luminous than the close once by at least about half an order of magnitude. Implying different physical conditions in the very center.

It is very likely that these differences in variability properties will also be reflected in the line variability. It is a goal to investigate this aspect more clearly in the near future. This may show if there are reverberation responses and if the reverberation time scales are different (luminosity dependant) and if the influence on the BLR/NLR regions close to the SMBH is different for these different source classes.

6

Summary and Outlook

In three projects involving multi-frequency data on AGN I could show that the activity of the immediate surroundings of the nuclear SMBH has far-reaching influences on structures of the entire host galaxy. In the double-lobe radio galaxy SDSS J080800.99+483807.7 I used interferometric radio data obtained with MERLIN and optical spectroscopy data obtained with MODS at the LBT to study the possible interaction between a back-flow along the jet and the host galaxy. I could show that indeed through an action over several kiloparsecs star formation in the host is triggered on a global scale by an activity that originates at the very nucleus of the galaxy.

An interaction of the SMBH with the immediate nuclear environment can be monitored via the reverberation of the line emission as a consequence of the nuclear continuum variations. I could show that this reverberation is not only limited to the BLR but is also detectable in the NLR line emission. This implies that the bright part of the NLR region in these objects is rather compact - of the order of 10-20 light years.

For the broad line region I could show that there is at least an observational difference between the low and high luminosity BALs. If this goes along with a physical difference will be shown in a future investigation.

As an outlook it is evident that a larger sample of double-lobe X-shaped sources should be investigated in more detail - in particular the star formation activity in their host galaxies. If all of them show indications for a higher star formation activity on a global scale, this would show that in these objects the back-flow effects are essential for the overall evolution of the host. Using large aperture telescopes in the optical such investigations will be possible for larger samples in the near future. Similarly the reverberation of the narrow line region is very

6. SUMMARY AND OUTLOOK

interesting. New public survey data will now allow to determine how frequent this effect is and how compact the bright part of the NLR is in general. Essential for this work will be a high quality inter-epoch and inter-telescope calibration.

Acknowledgements

Kindly, I would like to thank the entire staff of the Iraqi ministry of higher education and scientific research as well as the DAAD¹ for excellent support. I'm fully supported by them. Thanks as well to BCGS² for the support in the last phase of my Ph.D study. The work is also supported in part by the Deutsche Forschungsgemeinschaft (DFG) via grant SFB 956.

This work has benefited from research funding from the European Community's sixth Framework Programme under RadioNet R113CT 2003 5058187. Radio observations were made with MERLIN, a National Facility operated by the University of Manchester at Jodrell Bank Observatory on behalf of STFC.

The spectroscopic observations reported here were obtained at the LBT Observatory, a joint facility of the Smithsonian Institution and the University of Arizona. LBT observations were obtained as part of the Rat Deutscher Sternwarten guaranteed time on Steward Observatory facilities through the LBTB cooperation. This work uses data taken with the MODS spectrographs built with funding from NSF grant AST-9987045 and the NSF Telescope System Instrumentation Program (TSIP), with additional funds from the Ohio Board of Regents and the Ohio State University Office of Research. The Sloan Digital Sky Survey is a joint project of the University of Chicago, Fermilab, the Institute for Advanced Study, the Japan Participation Group, Johns Hopkins University, the Max-Planck-Institute for Astronomy, the Max-Planck-Institute for Astrophysics, New Mexico State University, Princeton University, the United States Naval Observatory, and the University of Washington. Apache Point Observatory, site of the SDSS, is operated by the Astrophysical Research Consortium. Funding for the project has been provided by

¹Deutscher Akademischer Austauschdienst

²Bonn-Cologne Graduate School

the Alfred P. Sloan Foundation, the SDSS member institutions, NASA, the NSF, the Department of Energy, the Japanese Monbukagakusho, and the Max-Planck Society. The SDSS Web site is <http://www.sdss.org>.

Of course, I am very grateful to all group members at I. Institute of Physics, specially Jens Zuther, Monica Valencia-S., Maca García-Marín, Gerold Busch, Mariangela Vitale, Marcus Bremer, Anas Al-Moatahni, Abhijeet Borkar, Banafsheh Shahzamanian, Senol Yazici, Nadeen Sabha, Konstantinos Markakis, Petra Neubauer-Guenther, Peter A. Schuller, and all the others for fruitful discussions and help.

Deeply, I would like to thank my family, relatives, and my friends in Baghdad, as well as my beloved wife because they always hear me and support me.

Father, I would like to thank you deep from my heart, you are always my idol. I hope I made you proud.

Finally, very special thank to my supervisor Prof. Dr. Andreas Eckart for his kindness and support, without his help this work would never be done.

References

- Abazajian, K. N., Adelman-McCarthy, J. K., Agüeros, M. A., Allam, S. S., Allende Prieto, C., An, D., Anderson, K. S. J., Anderson, S. F., Annis, J., Bahcall, N. A., and et al. (2009). The Seventh Data Release of the Sloan Digital Sky Survey. *ApJS*, **182**, 543–558. [29](#), [37](#), [61](#)
- Adelman-McCarthy, J. K. and et al. (2009). The SDSS Photometric Catalog, Release 7 (Adelman-McCarthy+, 2009). *VizieR Online Data Catalog*, **2294**, 0. [61](#), [108](#)
- Adelman-McCarthy, J. K. and et al. (2011). The SDSS Photometric Catalog, Release 8 (Adelman-McCarthy+, 2011). *VizieR Online Data Catalog*, **2306**, 0. [61](#), [66](#)
- Adelman-McCarthy, J. K., Agüeros, M. A., Allam, S. S., Allende Prieto, C., Anderson, K. S. J., Anderson, S. F., Annis, J., Bahcall, N. A., Bailer-Jones, C. A. L., Baldry, I. K., Barentine, J. C., Bassett, B. A., Becker, A. C., Beers, T. C., Bell, E. F., Berlind, A. A., Bernardi, M., Blanton, M. R., Bochanski, J. J., Boroski, W. N., Brinchmann, J., Brinkmann, J., Brunner, R. J., Budavári, T., Carliles, S., Carr, M. A., Castander, F. J., Cinabro, D., Cool, R. J., Covey, K. R., Csabai, I., Cunha, C. E., Davenport, J. R. A., Dilday, B., Doi, M., Eisenstein, D. J., Evans, M. L., Fan, X., Finkbeiner, D. P., Friedman, S. D., Frieman, J. A., Fukugita, M., Gänsicke, B. T., Gates, E., Gillespie, B., Glazebrook, K., Gray, J., Grebel, E. K., Gunn, J. E., Gurbani, V. K., Hall, P. B., Harding, P., Harvanek, M., Hawley, S. L., Hayes, J., Heckman, T. M., Hendry, J. S., Hindsley, R. B., Hirata, C. M., Hogan, C. J., Hogg, D. W., Hyde, J. B., Ichikawa, S.-i., Ivezić, Ž., Jester, S., Johnson, J. A., Jorgensen, A. M., Jurić, M., Kent, S. M., Kessler, R., Kleinman, S. J., Knapp, G. R., Kron, R. G., Krzesinski, J., Kuropatkin, N., Lamb, D. Q., Lampeitl, H., Lebedeva, S., Lee, Y. S., Leger, R. F., Lépine, S., Lima, M., Lin, H., Long, D. C., Loomis, C. P., Loveday, J., Lupton, R. H., Malanushenko, O., Malanushenko, V., Mandelbaum, R., Margon, B., Marriner, J. P., Martínez-Delgado, D., Matsumura, T., McGehee, P. M., McKay, T. A., Meiksin, A., Morrison, H. L., Munn, J. A., Nakajima, R., Neilsen, Jr., E. H., Newberg, H. J., Nichol, R. C., Nicinski, T., Nieto-Santesteban, M., Nitta, A., Okamura, S., Owen, R., Oyazui, H., Padmanabhan, N., Pan, K., Park, C., Peoples, Jr., J., Pier, J. R., Pope, A. C., Purger, N., Raddick, M. J., Re Fiorentin, P., Richards, G. T., Richmond, M. W., Riess, A. G., Rix, H.-W., Rockosi, C. M., Sako, M., Schlegel, D. J., Schneider, D. P., Schreiber, M. R., Schwobe, A. D., Seljak, U., Sesar, B., Sheldon, E., Shimasaku, K., Sivarani, T., Smith, J. A., Snedden, S. A., Steinmetz, M., Strauss, M. A., SubbaRao, M., Suto, Y., Szalay, A. S., Szapudi, I., Szkody, P., Tegmark, M., Thakar, A. R., Tremonti, C. A., Tucker, D. L., Uomoto, A., Vanden Berk, D. E., Vandenberg, J., Vidrih, S., Vogeley, M. S., Voges, W., Vogt, N. P., Wadadekar, Y., Weinberg, D. H., West, A. A., White, S. D. M., Wilhite, B. C., Yanny, B., Yocum, D. R., York, D. G., Zehavi, I., and Zucker, D. B. (2008). The Sixth Data Release of the Sloan Digital Sky Survey. *ApJS*, **175**, 297–313. [61](#)
- Ai, Y. L., Yuan, W., Zhou, H., Wang, T. G., Dong, X.-B., Wang, J. G., and Lu, H. L. (2013a). A Comparative Study of Optical/Ultraviolet Variability of Narrow-line Seyfert 1 and Broad-line Seyfert 1 Active Galactic Nuclei. *AJ*, **145**, 90. [91](#)
- Ai, Y. L., Yuan, W., Zhou, H., Wang, T. G., Dong, X.-B., Wang, J. G., and Lu, H. L. (2013b). A Comparative Study of Optical/Ultraviolet Variability of Narrow-line Seyfert 1 and Broad-line Seyfert 1 Active Galactic Nuclei. *AJ*, **145**, 90. [94](#)
- Allen, J. T., Hewett, P. C., Maddox, N., Richards, G. T., and Belokurov, V. (2011). A strong redshift dependence of the broad absorption line quasar fraction. *MNRAS*, **410**, 860–884. [81](#), [108](#)
- Angione, R. J. and Smith, H. J. (1972). Optical Variability of Twenty-Two Quasi-Stellar Objects. In D. S. Evans, D. Wills, and B. J. Wills, editors, *External Galaxies and Quasi-Stellar Objects*, volume 44 of *IAU Symposium*, page 171. [19](#), [57](#)
- Antonucci, R. (1993). Unified models for active galactic nuclei and quasars. *ARA&A*, **31**, 473–521. [10](#)
- Arav, N., Borguet, B., Chamberlain, C., Edmonds, D., and Danforth, C. (2013). Quasar outflows and AGN feedback in the extreme UV: HST/COS observations of HE 0238-1904. *MNRAS*, **436**, 3286–3305. [105](#)
- Baldry, I. K. (2008). Hubble's galaxy nomenclature. *Astronomy and Geophysics*, **49**(5), 25–5. [3](#)
- Baldwin, J. A., Phillips, M. M., and Terlevich, R. (1981). Classification parameters for the emission-line spectra of extragalactic objects. *PASP*, **93**, 5–19. [20](#)
- Barlow, T. A. (1993). *Time variability of broad absorption-line QSO's*. Ph.D. thesis, California University. [106](#)
- Barth, A. J., Voevodkin, A., Carson, D. J., and Woźniak, P. (2014). A Search for Optical Variability of Type 2 Quasars in SDSS Stripe 82. *AJ*, **147**, 12. [77](#), [94](#)
- Becker, R. H., White, R. L., and Edwards, A. L. (1991). A new catalog of 53,522 4.85 GHz sources. *ApJS*, **75**, 1–229. [xiii](#), [49](#)
- Becker, R. H., Gregg, M. D., Hook, I. M., McMahon, R. G., White, R. L., and Helfand, D. J. (1997). The FIRST Radio-loud Broad Absorption Line QSO and Evidence for a Hidden Population of Quasars. *ApJ*, **479**, L93–L96. [18](#)
- Becker, R. H., White, R. L., Gregg, M. D., Brotherton, M. S., Laurent-Muehleisen, S. A., and Arav, N. (2000). Properties of Radio-selected Broad Absorption Line Quasars from the First Bright Quasar Survey. *ApJ*, **538**, 72–82. [17](#), [18](#), [108](#)
- Beckmann, V. and Shrader, C. (2012). The AGN phenomenon: open issues. In *Proceedings of "An INTEGRAL view of the high-energy sky (the first 10 years)" - 9th INTEGRAL Workshop and celebration of the 10th anniversary of the launch (INTEGRAL 2012). 15-19 October 2012. Bibliothèque Nationale de France, Paris, France. Published online at <http://pos.sissa.it/cgi-bin/reader/conf.cgi?confid=176>"* <http://pos.sissa.it/cgi-bin/reader/conf.cgi?confid=176>, id.69, page 69. [xi](#), [7](#)
- Begelman, M. C., Blandford, R. D., and Rees, M. J. (1984). Theory of extragalactic radio sources. *Reviews of Modern Physics*, **56**, 255–351. [35](#)
- Beichman, C. A., Neugebauer, G., Habing, H. J., Clegg, P. E., and Chester, T. J., editors (1988). *Infrared astronomical satellite (IRAS) catalogs and atlases. Volume 1: Explanatory supplement*, volume 1. [86](#)
- Bell, E. F. (2003). Estimating Star Formation Rates from Infrared and Radio Luminosities: The Origin of the Radio-Infrared Correlation. *ApJ*, **586**, 794–813. [53](#)
- Bennett, N., Falcke, H., Schulz, H., Wilson, A. S., and Wills, B. J. (2002). Size and Structure of the Narrow-Line Region of Quasars. *ApJ*, **574**, L105–L109. [8](#)
- Bennett, N., Jungwiert, B., Komossa, S., Haas, M., and Chini, R. (2006a). Size and properties of the narrow-line region in Seyfert-1 galaxies from spatially-resolved optical spectroscopy. *A&A*, **459**, 55–69. [97](#)

REFERENCES

- Bennert, N., Jungwiert, B., Komossa, S., Haas, M., and Chini, R. (2006b). Size and properties of the narrow-line region in Seyfert-2 galaxies from spatially-resolved optical spectroscopy. *A&A*, **456**, 953–966. [97](#)
- Best, P. N. (2000). The cluster environments of the $z \sim 1$ 3CR radio galaxies. *MNRAS*, **317**, 720–736. [16](#)
- Blandford, R. D. and Payne, D. G. (1982). Hydromagnetic flows from accretion discs and the production of radio jets. *MNRAS*, **199**, 883–903. [35](#)
- Blandford, R. D. and Znajek, R. L. (1977). Electromagnetic extraction of energy from Kerr black holes. *MNRAS*, **179**, 433–456. [35](#)
- Blandford, R. D., Netzer, H., Woltjer, L., Courvoisier, T. J.-L., and Mayor, M., editors (1990). *Active Galactic Nuclei*. [19](#)
- Blundell, K. M. (2003). The under-explored radio-loudness of quasars and the possibility of radio-source-environment interactions. *New A Rev.*, **47**, 593–597. [xii](#), [47](#), [48](#)
- Boroson, T. A. (2003). Does the Narrow [O III] $\lambda 5007$ Line Reflect the Stellar Velocity Dispersion in Active Galactic Nuclei? *ApJ*, **585**, 647–652. [50](#)
- Boroson, T. A. and Green, R. F. (1992). The emission-line properties of low-redshift quasi-stellar objects. *ApJS*, **80**, 109–135. [71](#)
- Bothun, G. D., Chanan, G. A., Romanishin, W., Margon, B., and Schommer, R. A. (1982). Detection of neutral hydrogen emission and optical nebulosity in the low redshift QSO 0351+026. *ApJ*, **257**, 40–46. [84](#)
- Bregman, J. N., Glassgold, A. E., Huggins, P. J., and Kinney, A. L. (1986). Variability of Lyman-alpha and the ultraviolet continuum of 3C 446. *ApJ*, **301**, 698–702. [112](#)
- Bridle, A. H. and Perley, R. A. (1984). Extragalactic Radio Jets. *ARA&A*, **22**, 319–358. [14](#), [35](#)
- Bridle, A. H., Hough, D. H., Lonsdale, C. J., Burns, J. O., and Laing, R. A. (1994). Deep VLA imaging of twelve extended 3CR quasars. *AJ*, **108**, 766–820. [xi](#), [16](#)
- Brocksopp, C., Kaiser, C. R., Schoenmakers, A. P., and de Bruyn, A. G. (2011). Double-double radio galaxies: further insights into the formation of the radio structures. *MNRAS*, **410**, 484–498. [13](#), [36](#)
- Brotherton, M. S., Wills, B. J., Steidel, C. C., and Sargent, W. L. W. (1994). Statistics of QSO broad emission-line profiles. 2: The C IV wavelength 1549, C III wavelength 1909, and MG II wavelength 2798 lines. *ApJ*, **423**, 131–142. [59](#)
- Bruzual, G. and Charlot, S. (2003). Stellar population synthesis at the resolution of 2003. *MNRAS*, **344**, 1000–1028. [67](#)
- Burke, B. F. and Graham-Smith, F. (1997). *An introduction to radio astronomy*. Cambridge University Press 1997. [13](#)
- Calzetti, D., Kinney, A. L., and Storchi-Bergmann, T. (1994). Dust extinction of the stellar continua in starburst galaxies: The ultraviolet and optical extinction law. *ApJ*, **429**, 582–601. [53](#)
- Cao, X. (1995). Dynamical Properties of a Centrifugally Driven Outflow From a Disc Near a Black Hole. *Ap&SS*, **226**, 165–168. [13](#)
- Capellupo, D. M., Hamann, F., Shields, J. C., Rodríguez Hidalgo, P., and Barlow, T. A. (2011). Variability in quasar broad absorption line outflows - I. Trends in the short-term versus long-term data. *MNRAS*, **413**, 908–920. [17](#)
- Capellupo, D. M., Hamann, F., Shields, J. C., Rodríguez Hidalgo, P., and Barlow, T. A. (2012). Variability in quasar broad absorption line outflows - II. Multi-epoch monitoring of Si IV and C IV broad absorption line variability. *MNRAS*, **422**, 3249–3267. [106](#)
- Chanan, G. A., Downes, R. A., and Margon, B. (1981). Optical identification of serendipitous Einstein sources - 19 X-ray-selected active galactic nuclei. *ApJ*, **243**, L5–L8. [66](#), [84](#)
- Chiang, J., Murray, N., Grossman, S. A., and Voit, G. M. (1994). Accretion Disk Winds from Active Galactic Nuclei: A Model for the Dynamics of Broad Absorption Line Regions. In *American Astronomical Society Meeting Abstracts*, volume 26 of *Bulletin of the American Astronomical Society*, page 1363. [17](#)
- Choudhuri, A. R. (2010). *Astrophysics for Physicists*. Cambridge University Press, 2010. [5](#)
- Cid Fernandes, R. and Sodre, L. (2000). Poissonian analysis of quasar variability: Theory & Application. In *American Astronomical Society Meeting Abstracts #196*, volume 32 of *Bulletin of the American Astronomical Society*, page 751. [57](#)
- Clarke, D. A., Bridle, A. H., Burns, J. O., Perley, R. A., and Norman, M. L. (1992). Origin of the structures and polarization in the classical double 3C 219. *ApJ*, **385**, 173–187. [xi](#), [16](#)
- Clavel, J. and Wamsteker, W. (1987). The fading of the narrow-line region in 3C 390.3. *ApJ*, **320**, L9–L14. [58](#), [97](#), [99](#)
- Combes, F., García-Burillo, S., Braine, J., Schinnerer, E., Walter, F., and Colina, L. (2011). Galaxy evolution and star formation efficiency at $0.2 < z < 0.6$. *A&A*, **528**, A124. [86](#)
- Condon, J. J. and Yin, Q. F. (1990). A new starburst model applied to the clumpy irregular galaxy Markarian 325. *ApJ*, **357**, 97–104. [54](#)
- Condon, J. J., Cotton, W. D., Greisen, E. W., Yin, Q. F., Perley, R. A., Taylor, G. B., and Broderick, J. J. (1998). The NRAO VLA Sky Survey. *AJ*, **115**, 1693–1716. [xiii](#), [49](#)
- Corbin, M. R. (1997). The Emission-Line Properties of Low-Redshift Quasars. II. The Relation to Radio Type. *ApJS*, **113**, 245–267. [71](#)
- Coroniti, F. V. (1985). Accretion disk electrodynamics. In M. R. Kundu and G. D. Holman, editors, *Unstable Current Systems and Plasma Instabilities in Astrophysics*, volume 107 of *IAU Symposium*, pages 453–467. [13](#)
- Darling, J. and Giovanelli, R. (2002). A Search for OH Megamasers at $z > 0.1$. III. The Complete Survey. *AJ*, **124**, 100–126. [66](#)
- Dennett-Thorpe, J., Scheuer, P. A. G., Laing, R. A., Bridle, A. H., Pooley, G. G., and Reich, W. (2002). Jet reorientation in active galactic nuclei: two winged radio galaxies. *MNRAS*, **330**, 609–620. [xi](#), [14](#)
- DiPompeo, M. A., Brotherton, M. S., Becker, R. H., Tran, H. D., Gregg, M. D., White, R. L., and Laurent-Muehleisen, S. A. (2010). Spectropolarimetry of Radio-selected Broad Absorption Line Quasars. *ApJS*, **189**, 83–103. [108](#), [112](#)
- DiPompeo, M. A., Brotherton, M. S., and De Breuck, C. (2013). The orientation and polarization of broad absorption line quasars. *MNRAS*, **428**, 1565–1578. [108](#)
- Dong, X.-B., Wang, J.-G., Ho, L. C., Wang, T.-G., Fan, X., Wang, H., Zhou, H., and Yuan, W. (2011). What Controls the Fe II Strength in Active Galactic Nuclei? *ApJ*, **736**, 86. [71](#), [77](#)
- Douglas, J. N., Bash, F. N., Bozyan, F. A., Torrence, G. W., and Wolfe, C. (1996). The Texas Survey of Radio Sources Covering -35.5 degrees $<$ declination $<$ 71.5 degrees at 365 MHz. *AJ*, **111**, 1945. [xiii](#), [49](#)
- Dressler, A. (1980). A catalog of morphological types in 55 rich clusters of galaxies. *ApJS*, **42**, 565–609. [2](#)

REFERENCES

- Eales, S. A. (1985). A Sample of 6c Sources Selected at the Peak of the Source Counts - Part Three - an Investigation of the Variation of the Sizes of Radio Sources with Cosmic Epoch. *MNRAS*, **217**, 179. [42](#)
- Eckart, A. and Genzel, R. (1996). Observations of stellar proper motions near the Galactic Centre. *Nature*, **383**, 415–417. [9](#)
- Eckart, A., Baganoff, F. K., Morris, M., Bautz, M. W., Brandt, W. N., Garmire, G. P., Genzel, R., Ott, T., Ricker, G. R., Straubmeier, C., Viehmann, T., Schödel, R., Bower, G. C., and Goldston, J. E. (2004). First simultaneous NIR/X-ray detection of a flare from Sgr A*. *A&A*, **427**, 1–11. [9](#)
- Eckart, A., Mužić, K., Yazıcı, S., Sabha, N., Shahzamanian, B., Witzel, G., Moser, L., Garcia-Marin, M., Valencia-S., M., Jalali, B., Bremer, M., Straubmeier, C., Rauch, C., Buchholz, R., Kunneriath, D., and Moultaqa, J. (2013). Near-infrared proper motions and spectroscopy of infrared excess sources at the Galactic center. *A&A*, **551**, A18. [9](#)
- Elvis, M., Wilkes, B. J., McDowell, J. C., Green, R. F., Bechtold, J., Willner, S. P., Oey, M. S., Polomski, E., and Cutri, R. (1994). Atlas of quasar energy distributions. *ApJS*, **95**, 1–68. [17](#)
- Fabian, A. C. (2012). Observational Evidence of Active Galactic Nuclei Feedback. *ARA&A*, **50**, 455–489. [35](#)
- Fanaroff, B. L. and Riley, J. M. (1974). The morphology of extragalactic radio sources of high and low luminosity. *MNRAS*, **167**, 31P–36P. [13](#), [14](#), [36](#)
- Fanti, C., Fanti, R., Parma, P., Schilizzi, R. T., and van Breugel, W. J. M. (1985). Compact Steep Spectrum 3CR radio sources - VLBI observations at 18 CM. *A&A*, **143**, 292–306. [55](#)
- Fanti, C., Fanti, R., Dallacasa, D., Schilizzi, R. T., Spencer, R. E., and Stanghellini, C. (1995). Are compact steep-spectrum sources young? *A&A*, **302**, 317. [55](#)
- Fanti, C., Fanti, R., Zanichelli, A., Dallacasa, D., and Stanghellini, C. (2011). The B3-VLA CSS sample. VIII. New optical identifications from the Sloan Digital Sky Survey The ultraviolet-optical spectral energy distribution of the young radio sources. *A&A*, **528**, A110. [56](#)
- Fanti, R. (2009). CSS and GPS research: A status report. *Astronomische Nachrichten*, **330**, 303. [55](#)
- Ferrarese, L. and Ford, H. (2005). Supermassive Black Holes in Galactic Nuclei: Past, Present and Future Research. *Space Sci. Rev.*, **116**, 523–624. [49](#)
- Ferrarese, L. and Merritt, D. (2000). A Fundamental Relation between Supermassive Black Holes and Their Host Galaxies. *ApJ*, **539**, L9–L12. [49](#)
- Filippenko, A. V. and Halpern, J. P. (1984). NGC 7213 - A key to the nature of liners? *ApJ*, **285**, 458–474. [19](#)
- Filiz Ak, N., Brandt, W. N., Hall, P. B., Schneider, D. P., Anderson, S. F., Hamann, F., Lundgren, B. F., Myers, A. D., Pâris, I., Petitjean, P., Ross, N. P., Shen, Y., and York, D. (2013). Broad Absorption Line Variability on Multi-year Timescales in a Large Quasar Sample. *ApJ*, **777**, 168. [105](#)
- Francis, P. J., Hewett, P. C., Foltz, C. B., Chaffee, F. H., Weymann, R. J., and Morris, S. L. (1991). A high signal-to-noise ratio composite quasar spectrum. *ApJ*, **373**, 465–470. [12](#)
- Gaskell, C. M. (2008). Accretion Disks and the Nature and Origin of AGN Continuum Variability. In *Revista Mexicana de Astronomía y Astrofísica Conferencia Series*, volume 32 of *Revista Mexicana de Astronomía y Astrofísica Conferencia Series*, pages 1–11. [77](#)
- Gebhardt, K., Bender, R., Bower, G., Dressler, A., Faber, S. M., Filippenko, A. V., Green, R., Grillmair, C., Ho, L. C., Kormendy, J., Lauer, T. R., Magorrian, J., Pinkney, J., Richstone, D., and Tremaine, S. (2000). A Relationship between Nuclear Black Hole Mass and Galaxy Velocity Dispersion. *ApJ*, **539**, L13–L16. [49](#)
- Gendre, M. A., Best, P. N., Wall, J. V., and Ker, L. M. (2013). The relation between morphology, accretion modes and environmental factors in local radio AGN. *MNRAS*, **430**, 3086–3101. [16](#)
- Giannuzzo, E. M. and Stirpe, G. M. (1996). A search for variability in Narrow Line Seyfert 1 Galaxies. *A&A*, **314**, 419–429. [xiv](#), [10](#), [86](#), [90](#), [91](#)
- Gibson, R. R., Jiang, L., Brandt, W. N., Hall, P. B., Shen, Y., Wu, J., Anderson, S. F., Schneider, D. P., Vanden Berk, D., Gallagher, S. C., Fan, X., and York, D. G. (2009). A Catalog of Broad Absorption Line Quasars in Sloan Digital Sky Survey Data Release 5. *ApJ*, **692**, 758–777. [17](#), [61](#), [66](#), [81](#), [105](#)
- Gondhalekar, P. M. (1990). Ultraviolet spectra of a large sample of quasars. II - Variability of Ly-alpha and C IV emission lines. *MNRAS*, **243**, 443–458. [112](#)
- Gopal-Krishna, Biermann, P. L., Gergely, L. Á., and Wiita, P. J. (2012). On the origin of X-shaped radio galaxies. *Research in Astronomy and Astrophysics*, **12**, 127–146. [36](#)
- Gott, III, J. R., Jurić, M., Schlegel, D., Hoyle, F., Vogeley, M., Tegmark, M., Bahcall, N., and Brinkmann, J. (2005). A Map of the Universe. *ApJ*, **624**, 463–484. [1](#)
- Greco, J. P., Martini, P., and Thompson, T. A. (2012). Measurement of the Mass and Stellar Population Distribution in M82 with the LBT. *ApJ*, **757**, 24. [42](#)
- Green, P. J. and Mathur, S. (1996). Broad Absorption Line Quasars Observed by the ROSAT PSPC. *ApJ*, **462**, 637. [17](#)
- Greene, J. E. and Ho, L. C. (2005). A Comparison of Stellar and Gaseous Kinematics in the Nuclei of Active Galaxies. *ApJ*, **627**, 721–732. [49](#)
- Greenstein, G. (2013). *Understanding the Universe*. Cambridge University Press, 2013. [12](#)
- Gregory, P. C. and Condon, J. J. (1991). The 87GB catalog of radio sources covering delta between O and + 75 deg at 4.85 GHz. *ApJS*, **75**, 1011–1291. [xiii](#), [49](#)
- Grier, C. J., Peterson, B. M., Pogge, R. W., Denney, K. D., Bentz, M. C., Martini, P., Sergeev, S. G., Kaspi, S., Minezaki, T., Zu, Y., Kochanek, C. S., Siverd, R., Shappee, B., Stanek, K. Z., Araya Salvo, C., Beatty, T. G., Bird, J. C., Bord, D. J., Borman, G. A., Che, X., Chen, C., Cohen, S. A., Dietrich, M., Doroshenko, V. T., Drake, T., Efimov, Y. S., Free, N., Ginsburg, I., Henderson, C. B., King, A. L., Koshida, S., Mogren, K., Molina, M., Mosquera, A. M., Nazarov, S. V., Okhmat, D. N., Pejcha, O., Raftar, S., Shields, J. C., Skowron, J., Szczygiel, D. M., Valluri, M., and van Saders, J. L. (2012). Reverberation Mapping Results for Five Seyfert 1 Galaxies. *ApJ*, **755**, 60. [92](#), [94](#)
- Grupe, D., Pradhan, A. K., and Frank, S. (2005). Studying the Variation of the Fine-Structure Constant Using Emission-Line Multiplets. *AJ*, **130**, 355–366. [84](#), [103](#)
- Guo, H. and Gu, M. (2014). The Optical Variability of SDSS Quasars from Multi-epoch Spectroscopy. I. Results from 60 Quasars with \geq Six-epoch Spectra. *ApJ*, **792**, 33. [58](#)
- Haas, M., Siebenmorgen, R., Pantin, E., Horst, H., Smette, A., Käuff, H.-U., Lagage, P.-O., and Chini, R. (2007). VISIR/VLT mid-infrared imaging of Seyfert nuclei: nuclear dust emission and the Seyfert-2 dichotomy. *A&A*, **473**, 369–376. [60](#)
- Haddad, B. and Vanderriest, C. (1991). Bidimensional spectrography of 5 interacting quasar-galaxy systems. *A&A*, **245**, 423–435. [84](#)

REFERENCES

- Hall, P. B., Anderson, S. F., Strauss, M. A., York, D. G., Richards, G. T., Fan, X., Knapp, G. R., Schneider, D. P., Vanden Berk, D. E., Geballe, T. R., Bauer, A. E., Becker, R. H., Davis, M., Rix, H.-W., Nichol, R. C., Bahcall, N. A., Brinkmann, J., Brunner, R., Connolly, A. J., Csabai, I., Doi, M., Fukugita, M., Gunn, J. E., Haiman, Z., Harvanek, M., Heckman, T. M., Hennessy, G. S., Inada, N., Ivezić, Ž., Johnston, D., Kleinman, S., Krolik, J. H., Krzesinski, J., Kunszt, P. Z., Lamb, D. Q., Long, D. C., Lupton, R. H., Miknaitis, G., Munn, J. A., Narayanan, V. K., Neilsen, E., Newman, P. R., Nitta, A., Okamura, S., Pentericci, L., Pier, J. R., Schlegel, D. J., Snedden, S., Szalay, A. S., Thakar, A. R., Tsvetanov, Z., White, R. L., and Zheng, W. (2002). Unusual Broad Absorption Line Quasars from the Sloan Digital Sky Survey. *ApJS*, **141**, 267–309. [18](#)
- Hardcastle, M. J., Alexander, P., Pooley, G. G., and Riley, J. M. (1998). FR II radio galaxies with $z < 0.3$ - I. Properties of jets, cores and hotspots. *MNRAS*, **296**, 445–462. [14](#), [15](#)
- Hardcastle, M. J., Ching, J. H. Y., Virdee, J. S., Jarvis, M. J., Croom, S. M., Sadler, E. M., Mauch, T., Smith, D. J. B., Stevens, J. A., Baes, M., Baldry, I. K., Brough, S., Cooray, A., Dariush, A., De Zotti, G., Driver, S., Dunne, L., Dye, S., Eales, S., Hopwood, R., Liske, J., Maddox, S., Michalowski, M. J., Rigby, E. E., Robotham, A. S. G., Steele, O., Thomas, D., and Valiante, E. (2013). Herschel-ATLAS/GAMA: a difference between star formation rates in strong-line and weak-line radio galaxies. *MNRAS*, **429**, 2407–2424. [53](#)
- Heckman, T. M. (1980). An optical and radio survey of the nuclei of bright galaxies - Activity in normal galactic nuclei. *A&A*, **87**, 152–164. [18](#)
- Helou, G. (1986). The IRAS colors of normal galaxies. *ApJ*, **311**, L33–L36. [53](#)
- Hewett, P. C. and Wild, V. (2010). Improved redshifts for SDSS quasar spectra. *MNRAS*, **405**, 2302–2316. [66](#), [81](#), [108](#)
- Hewitt, A. and Burbidge, G. (1991). An optical catalog of extragalactic emission-line objects similar to quasi-stellar objects. *ApJS*, **75**, 297–356. [66](#), [86](#)
- Hewitt, A. and Burbidge, G. (1993). A revised and updated catalog of quasi-stellar objects. *ApJS*, **87**, 451–947. [12](#)
- Higginbottom, N., Proga, D., Knigge, C., Long, K. S., Matthews, J. H., and Sim, S. A. (2014). Line-driven Disk Winds in Active Galactic Nuclei: The Critical Importance of Ionization and Radiative Transfer. *ApJ*, **789**, 19. [17](#)
- Hill, T. L., Heisler, C. A., Norris, R. P., Reynolds, J. E., and Hunstead, R. W. (2001). Starburst or Seyfert? Adding a Radio and Far-Infrared Perspective to the Investigation of Activity in Composite Galaxies. *AJ*, **121**, 128–139. [54](#)
- Ho, L. C. (2005). [O II] Emission in Quasar Host Galaxies: Evidence for a Suppressed Star Formation Efficiency. *ApJ*, **629**, 680–685. [53](#)
- Hodges-Kluck, E. J. and Reynolds, C. S. (2011). Hydrodynamic Models of Radio Galaxy Morphology: Winged and X-shaped Sources. *ApJ*, **733**, 58. [36](#), [37](#)
- Hogg, D. W. (1999). Distance measures in cosmology. *arXiv Astrophysics e-prints*, **41**, 73
- Hook, I. M., McMahon, R. G., Boyle, B. J., and Irwin, M. J. (1994). The Variability of Optically Selected Quasars. *MNRAS*, **268**, 305. [57](#)
- Hopkins, A. M., Miller, C. J., Nichol, R. C., Connolly, A. J., Bernardi, M., Gómez, P. L., Goto, T., Tremonti, C. A., Brinkmann, J., Ivezić, Ž., and Lamb, D. Q. (2003). Star Formation Rate Indicators in the Sloan Digital Sky Survey. *ApJ*, **599**, 971–991. [53](#)
- Hopkins, P. F., Hayward, C. C., Narayanan, D., and Hernquist, L. (2012). The origins of active galactic nuclei obscuration: the ‘torus’ as a dynamical, unstable driver of accretion. *MNRAS*, **420**, 320–339. [8](#)
- Hubble, E. (1926a). No. 324. Extra-galactic nebulae. *Contributions from the Mount Wilson Observatory / Carnegie Institution of Washington*, **324**, 1–49. [3](#)
- Hubble, E. and Humason, M. L. (1931). The Velocity-Distance Relation among Extra-Galactic Nebulae. *ApJ*, **74**, 43. [2](#)
- Hubble, E. P. (1926b). Extragalactic nebulae. *ApJ*, **64**, 321–369. [3](#)
- Hubble, E. P. (1927). The classification of spiral nebulae. *The Observatory*, **50**, 276–281. [3](#)
- Hubble, E. P. (1936). *Realm of the Nebulae*. Yale University Press, 1936. ISBN 9780300025002. [3](#)
- Hull, C. L., Limmongkol, S., and Siegmund, W. A. (1994). Sloan Digital Sky Survey cloud scanner. In L. M. Stepp, editor, *Advanced Technology Optical Telescopes V*, volume 2199 of *Society of Photo-Optical Instrumentation Engineers (SPIE) Conference Series*, pages 852–857. [29](#)
- Hutchings, J. B., Campbell, B., and Crampton, D. (1982). Color imaging QSO-galaxy interactions. *ApJ*, **261**, L23–L29. [84](#)
- Inada, N., Oguri, M., Shin, M.-S., Kayo, I., Strauss, M. A., Morokuma, T., Rusu, C. E., Fukugita, M., Kochanek, C. S., Richards, G. T., Schneider, D. P., York, D. G., Bahcall, N. A., Frieman, J. A., Hall, P. B., and White, R. L. (2012). The Sloan Digital Sky Survey Quasar Lens Search. V. Final Catalog from the Seventh Data Release. *AJ*, **143**, 119. [61](#), [81](#)
- Jones, M. H. and Lambourne, R. J. A. (2004). *An Introduction to Galaxies and Cosmology*. Co-published with The Open University, Milton Keynes. Cambridge, UK: Cambridge University Press, 2004. [6](#)
- Juneau, S., Dickinson, M., Alexander, D. M., and Salim, S. (2011). A New Diagnostic of Active Galactic Nuclei: Revealing Highly Absorbed Systems at Redshift > 0.3 . *ApJ*, **736**, 104. [40](#), [41](#)
- Karachentseva, V. E. (1973). The Catalogue of Isolated Galaxies.. *Astrofizičeskie Issledovaniia Izvestiya Spetsial'noj Astrofizičeskoj Observatorii*, **8**, 3–49. [xi](#), [2](#)
- Kaspi, S., Smith, P. S., Netzer, H., Maoz, D., Jannuzi, B. T., and Giveon, U. (2000). Reverberation Measurements for 17 Quasars and the Size-Mass-Luminosity Relations in Active Galactic Nuclei. *ApJ*, **533**, 631–649. [xv](#), [97](#), [100](#)
- Kaspi, S., Brandt, W. N., Maoz, D., Netzer, H., Schneider, D. P., and Shemmer, O. (2007). Reverberation Mapping of High-Luminosity Quasars: First Results. *ApJ*, **659**, 997–1007. [58](#)
- Kauffmann, G., Heckman, T. M., Tremonti, C., Brinchmann, J., Charlot, S., White, S. D. M., Ridgway, S. E., Brinkmann, J., Fukugita, M., Hall, P. B., Ivezić, Ž., Richards, G. T., and Schneider, D. P. (2003). The host galaxies of active galactic nuclei. *MNRAS*, **346**, 1055–1077. [40](#), [42](#)
- Kellermann, K. I., Downes, A. J. B., Pauliny-Toth, I. I. K., Preuss, E., Witzel, A., and Shaffer, D. B. (1981). VLBI observations of the nucleus of the radio galaxy Cygnus A. *A&A*, **97**, L1–L4. [46](#)
- Kembhavi, A. K. and Narlikar, J. V. (1999). *Quasars and active galactic nuclei : an introduction*. Cambridge University Press, 1999. [14](#), [15](#)
- Kennicutt, Jr., R. C. (1998). Star Formation in Galaxies Along the Hubble Sequence. *ARA&A*, **36**, 189–232. [53](#)
- Kewley, L. J., Dopita, M. A., Sutherland, R. S., Heisler, C. A., and Trevena, J. (2001). Theoretical Modeling of Starburst Galaxies. *ApJ*, **556**, 121–140. [40](#), [41](#)
- Kewley, L. J., Geller, M. J., and Jansen, R. A. (2003). [OII] as a SFR indicator and the Cosmic Star Formation History. In *American Astronomical Society Meeting Abstracts*, volume 35 of *Bulletin of the American Astronomical Society*, page #119.01. [40](#)

REFERENCES

- Kewley, L. J., Groves, B., Kauffmann, G., and Heckman, T. (2006). The host galaxies and classification of active galactic nuclei. *MNRAS*, **372**, 961–976. [21](#), [29](#), [41](#)
- Kollatschny, W., Bischoff, K., and Dietrich, M. (2000). Strong spectral variability in NGC 7603 over 20 years. *A&A*, **361**, 901–912. [xiv](#), [90](#), [91](#)
- Kollatschny, W., Zetzl, M., and Dietrich, M. (2006a). Spectral line variability amplitudes in active galactic nuclei. *A&A*, **454**, 459–472. [xii](#), [xiv](#), [20](#), [90](#), [91](#)
- Kollatschny, W., Zetzl, M., and Dietrich, M. (2006b). Spectral line variability amplitudes in active galactic nuclei. *A&A*, **454**, 459–472. [xv](#), [96](#), [97](#), [100](#)
- Komossa, S. (2008). Narrow-line Seyfert 1 Galaxies. In *Revista Mexicana de Astronomía y Astrofísica Conference Series*, volume 32 of *Revista Mexicana de Astronomía y Astrofísica Conference Series*, pages 86–92. [60](#)
- Komossa, S. and Xu, D. (2007). Narrow-Line Seyfert 1 Galaxies and the $M_{BH}-\sigma$ Relation. *ApJ*, **667**, L33–L36. [50](#)
- Kormendy, J. and Ho, L. C. (2013). Coevolution (Or Not) of Supermassive Black Holes and Host Galaxies. *ARA&A*, **51**, 511–653. [49](#)
- Kovačević, J., Popović, L. Č., and Dimitrijević, M. S. (2010). Analysis of Optical Fe II Emission in a Sample of Active Galactic Nucleus Spectra. *ApJS*, **189**, 15–36. [71](#), [77](#)
- Krabbe, A., Sternberg, A., and Genzel, R. (1994). Near-infrared spectral imaging of NGC 1808: Probing the starburst. *ApJ*, **425**, 72–90. [42](#)
- Kunert-Bajraszewska, M. and Thomasson, P. (2009). A survey of Low Luminosity Compact sources. *Astronomische Nachrichten*, **330**, 210. [41](#)
- Labiano, A., O’Dea, C. P., Barthel, P. D., de Vries, W. H., and Baum, S. A. (2008). Star formation in the hosts of GHz peaked spectrum and compact steep spectrum radio galaxies. *A&A*, **477**, 491–501. [56](#)
- Laine, S., Kotilainen, J. K., Reunanen, J., Ryder, S. D., and Beck, R. (2006). Examining the Seyfert-Starburst Connection with Arcsecond-Resolution Radio Continuum Observations. *AJ*, **131**, 701–715. [54](#)
- Laing, R. A. and Bridle, A. H. (1987). Rotation measure variation across M84. *MNRAS*, **228**, 557–571. [xi](#), [15](#)
- Laing, R. A., Riley, J. M., and Longair, M. S. (1983). Bright radio sources at 178 MHz - Flux densities, optical identifications and the cosmological evolution of powerful radio galaxies. *MNRAS*, **204**, 151–187. [55](#)
- Laing, R. A., Parma, P., de Ruiter, H. R., and Fanti, R. (1999). Asymmetries in the jets of weak radio galaxies. *MNRAS*, **306**, 513–530. [14](#)
- Lamareille, F. (2010). Spectral classification of emission-line galaxies from the Sloan Digital Sky Survey. I. An improved classification for high-redshift galaxies. *A&A*, **509**, A53. [40](#), [41](#)
- Lamareille, F., Mouhcine, M., Contini, T., Lewis, I., and Maddox, S. (2004). The luminosity-metallicity relation in the local Universe from the 2dF Galaxy Redshift Survey. *MNRAS*, **350**, 396–406. [40](#), [41](#)
- Landt, H., Cheung, C. C., and Healey, S. E. (2010). The optical spectra of X-shaped radio galaxies. *MNRAS*, **408**, 1103–1112. [36](#)
- Leahy, J. P. and Perley, R. A. (1991). VLA images of 23 extragalactic radio sources. *AJ*, **102**, 537–561. [xi](#), [15](#)
- Leahy, J. P. and Williams, A. G. (1984). The bridges of classical double radio sources. *MNRAS*, **210**, 929–951. [13](#), [36](#)
- Liu, Y., Jiang, D. R., Wang, T. G., and Xie, F. G. (2008). The compact structure of radio-loud broad absorption line quasars. *MNRAS*, **391**, 246–253. [115](#)
- Lonsdale, C. J. and Helou, G. (1985). *Cataloged galaxies and quasars observed in the IRAS survey*. Jet Propulsion Laboratory (JPL). [53](#)
- Lovelace, R. V. E., Berk, H. L., and Contopoulos, J. (1991). Magnetically driven jets and winds. *ApJ*, **379**, 696–705. [13](#)
- Low, F. J., Cutri, R. M., Huchra, J. P., and Kleinmann, S. G. (1988). Infrared color-selected quasars and Seyfert 1 galaxies. *ApJ*, **327**, L41–L45. [86](#)
- Low, F. J., Cutri, R. M., Kleinmann, S. G., and Huchra, J. P. (1989). The properties of infrared color-selected quasars. *ApJ*, **340**, L1–L4. [86](#)
- Lundgren, B. F., Brunner, R. J., York, D. G., Ross, A. J., Quashnock, J. M., Myers, A. D., Schneider, D. P., Al Sayyad, Y., and Bahcall, N. (2009). A Cross-Correlation Analysis of Mg II Absorption Line Systems and Luminous Red Galaxies from the SDSS DR5. *ApJ*, **698**, 819–839. [81](#)
- Magorrian, J., Tremaine, S., Richstone, D., Bender, R., Bower, G., Dressler, A., Faber, S. M., Gebhardt, K., Green, R., Grillmair, C., Kormendy, J., and Lauer, T. (1998). The Demography of Massive Dark Objects in Galaxy Centers. *AJ*, **115**, 2285–2305. [49](#)
- Margon, B., Chanan, G. A., and Downes, R. A. (1982). The luminosity of serendipitous X-ray QSOs. *ApJ*, **253**, L7–L11. [84](#)
- Markwardt, C. B. (2009). Non-linear Least-squares Fitting in IDL with MPFIT. In D. A. Bohlender, D. Durand, and P. Dowler, editors, *Astronomical Data Analysis Software and Systems XVIII*, volume 411 of *Astronomical Society of the Pacific Conference Series*, page 251. [71](#)
- McLure, R. J. and Dunlop, J. S. (2001). The cluster environments of powerful radio-loud and radio-quiet active galactic nuclei. *MNRAS*, **321**, 515–524. [16](#)
- McMahon, R. G., White, R. L., Helfand, D. J., and Becker, R. H. (2002). Optical Counterparts for 70,000 Radio Sources: APM Identifications for the FIRST Radio Survey. *ApJS*, **143**, 1–23. [79](#)
- Melia, F. and Falcke, H. (2001). The Supermassive Black Hole at the Galactic Center. *ARA&A*, **39**, 309–352. [49](#)
- Memola, E., Caccianiga, A., Cocchia, F., Della Ceca, R., Maccacaro, T., Severgnini, P., Fyfe, D. J., Mateos, S., Watson, M. G., and Lamer, G. (2007). Searching for absorbed AGN in the 2XMM-Newton pre-release EPIC Serendipitous Source Catalogue. *A&A*, **465**, 759–764. [86](#)
- Meusinger, H. and Weiss, V. (2013). Ultraviolet variability of quasars: dependence on the accretion rate. *A&A*, **560**, A104. [57](#)
- Meusinger, H., Hinze, A., and de Hoon, A. (2011). Spectral variability of quasars from multi-epoch photometric data in the Sloan Digital Sky Survey Stripe 82. *A&A*, **525**, A37. [91](#)
- Montenegro-Montes, F. M., Mack, K.-H., Vigotti, M., Benn, C. R., Carballo, R., González-Serrano, J. I., Holt, J., and Jiménez-Luján, F. (2008). Radio spectra and polarization properties of radio-loud broad absorption-line quasars. *MNRAS*, **388**, 1853–1868. [17](#), [18](#), [112](#)
- Morse, J. A., Wilson, A. S., Elvis, M., and Weaver, K. A. (1995). Extended soft X-ray emission in Seyfert galaxies: ROSAT HRI observations of NGC 3516, NGC 4151, and Markarian 3. *ApJ*, **439**, 121–131. [97](#)
- Neeser, M. J., Eales, S. A., Law-Green, J. D., Leahy, J. P., and Rawlings, S. (1995). The Linear-Size Evolution of Classical Double Radio Sources. *ApJ*, **451**, 76. [42](#)
- Nesvadba, N. P. H., Boulanger, F., Salomé, P., Guillard, P., Lehnert, M. D., Ogle, P., Appleton, P., Falgarone, E., and Pineau Des Forets, G. (2010). Energetics of the molecular gas in the H₂ luminous radio galaxy 3C 326: Evidence for negative AGN feedback. *A&A*, **521**, A65. [53](#), [56](#)

REFERENCES

- Noguchi, K., Terashima, Y., and Awaki, H. (2009). A New Sample of Buried Active Galactic Nuclei Selected from the Second XMM-Newton Serendipitous Source Catalogue. *ApJ*, **705**, 454–467. [86](#)
- O’Dea, C. P. (1998). The Compact Steep-Spectrum and Gigahertz Peaked-Spectrum Radio Sources. *PASP*, **110**, 493–532. [55](#)
- O’Dea, C. P. and Baum, S. A. (1997). Constraints on Radio Source Evolution from the Compact Steep Spectrum and GHz Peaked Spectrum Radio Sources. *AJ*, **113**, 148–161. [55](#)
- O’Dea, C. P., Gallimore, J., Stanghellini, C., Baum, S. A., and Jackson, J. M. (2005). A Search for Molecular Gas in GHz-peaked Spectrum Radio Sources. *AJ*, **129**, 610–614. [56](#)
- O’Dea, C. P., Daly, R. A., Kharb, P., Freeman, K. A., and Baum, S. A. (2009). Physical properties of very powerful FR II radio galaxies. *A&A*, **494**, 471–488. [46](#)
- Ogle, P. M., Marshall, H. L., Lee, J. C., and Canizares, C. R. (2000). Chandra Observations of the X-Ray Narrow-Line Region in NGC 4151. *ApJ*, **545**, L81–L84. [97](#)
- Oort, M. J. A., Katgert, P., and Windhorst, R. A. (1987). A direct determination of linear-size evolution of elliptical radio galaxies. *Nature*, **328**, 500. [42](#)
- Osterbrock, D. E. (1985). Henry Crew and an Early Astronomical Concave Grating Spectrograph. *PASP*, **97**, 906. [10](#)
- Osterbrock, D. E. (1987). Seyfert Galaxies: Classification, Morphology, Observations at Optical Wavelengths, Environmental Factors Seyferts. In E. E. Khachikian, K. J. Fricke, and J. Melnick, editors, *Observational Evidence of Activity in Galaxies*, volume 121 of *IAU Symposium*, page 109. [10](#)
- Osterbrock, D. E. (1989). *Astrophysics of gaseous nebulae and active galactic nuclei*. University Science Books. [53](#)
- Osterbrock, D. E. (1991). Active galactic nuclei. *Reports on Progress in Physics*, **54**, 579–633. [6](#)
- Osterbrock, D. E. and Ferland, G. J. (2006). Book Review: Astrophysics of Gaseous Nebulae and Active Galactic Nuclei (2ND Edition) / University Science Books, 2005. *Mercury*, **35**(1), 40. [14](#)
- Osterbrock, D. E. and Pogge, R. W. (1985). The spectra of narrow-line Seyfert 1 galaxies. *ApJ*, **297**, 166–176. [10](#)
- Osterbrock, D. E., Fulbright, J. P., Martel, A. R., Keane, M. J., Trager, S. C., and Basri, G. (1996). Night-Sky High-Resolution Spectral Atlas of OH and O2 Emission Lines for Echelle Spectrograph Wavelength Calibration. *PASP*, **108**, 277. [27](#)
- Osterbrock, D. E., Fulbright, J. P., and Bida, T. A. (1997). Night-Sky High-Resolution Spectral Atlas of OH Emission Lines for Echelle Spectrograph Wavelength Calibration. II. *PASP*, **109**, 614–623. [27](#)
- Parma, P., Fanti, C., Fanti, R., Morganti, R., and de Ruiter, H. R. (1987). VLA observations of low-luminosity radio galaxies. VI - Discussion of radio jets. *A&A*, **181**, 244–264. [14](#)
- Parma, P., de Ruiter, H. R., Fanti, R., and Laing, R. (1994). Brightness Asymmetries and Velocities of Jets in Low Luminosity Radio Galaxies. In G. V. Bicknell, M. A. Dopita, and P. J. Quinn, editors, *The Physics of Active Galaxies*, volume 54 of *Astronomical Society of the Pacific Conference Series*, page 241. [14](#)
- Penston, M. V., Robinson, A., Alloin, D., Appenzeller, I., Aretxaga, I., Axon, D. J., Baribaud, T., Barthel, P., Baum, S. A., Boisson, C., de Bruyn, A. G., Clavel, J., Colina, L., Dennefeld, M., Diaz, A., Dietrich, M., Durret, F., Dyson, J. E., Gondhalekar, P., van Groningen, E., Jablonka, P., Jackson, N., Kollatschny, W., Laurikainen, E., Lawrence, A., Masegosa, J., McHardy, I., Meurs, E. J. A., Miley, G., Moles, M., O’Brien, P., O’Dea, C., del Olmo, A., Pedlar, A., Perea, J., Perez, E., Perez-Fournon, I., Perry, J., Pilbratt, G., Rees, M., Robson, I., Rodriguez-Pascual, P., Rodriguez Espinosa, J. M., Santos-Lleo, M., Schilizzi, R., Stasińska, G., Stirpe, G. M., Tadhunter, C., Terlevich, E., Terlevich, R., Unger, S., Vila-Vilaro, V., Vilchez, J., Wagner, S. J., Ward, M. J., and Yates, G. J. (1990). The extended narrow line region of NGC 4151. I - Emission line ratios and their implications. *A&A*, **236**, 53–62. [97](#)
- Peterson, B. M. (1997). *An Introduction to Active Galactic Nuclei*. Cambridge, New York Cambridge University Press. [12](#), [16](#)
- Peterson, B. M. (2001). Variability of Active Galactic Nuclei. In I. Aretxaga, D. Kunth, and R. Mújica, editors, *Advanced Lectures on the Starburst-AGN*, page 3. [57](#)
- Peterson, B. M. and Gaskell, C. M. (1986). Emission-line variability of three Seyfert galaxies. *AJ*, **92**, 552–556. [58](#)
- Peterson, B. M., Crenshaw, D. M., Meyers, K. A., Byard, P. L., and Foltz, C. B. (1984). Variability of the emission-line spectra and optical continua of Seyfert galaxies. II. *ApJ*, **279**, 529–540. [6](#), [58](#)
- Peterson, B. M., Wanders, I., Bertram, R., Hunley, J. F., Pogge, R. W., and Wagner, R. M. (1998). Optical Continuum and Emission-Line Variability of Seyfert 1 Galaxies. *ApJ*, **501**, 82–93. [58](#), [92](#), [94](#)
- Peterson, B. M., Ferrarese, L., Gilbert, K. M., Kaspi, S., Malkan, M. A., Maoz, D., Merritt, D., Netzer, H., Onken, C. A., Pogge, R. W., Vestergaard, M., and Wandel, A. (2004). Central Masses and Broad-Line Region Sizes of Active Galactic Nuclei. II. A Homogeneous Analysis of a Large Reverberation-Mapping Database. *ApJ*, **613**, 682–699. [xv](#), [97](#), [100](#)
- Peterson, B. M., Denney, K. D., De Rosa, G., Grier, C. J., Pogge, R. W., Bentz, M. C., Kochanek, C. S., Vestergaard, M., Kilerci-Eser, E., Dalla Bontà, E., and Ciofi, S. (2013). The Size of the Narrow-line-emitting Region in the Seyfert 1 Galaxy NGC 5548 from Emission-line Variability. *ApJ*, **779**, 109. [58](#), [97](#), [99](#)
- Pogge, R. W., Atwood, B., Brewer, D. F., Byard, P. L., Derwent, M. A., Gonzalez, R., Martini, P., Mason, J. A., O’Brien, T. P., Osmer, P. S., Pappalardo, D. P., Steinbrecher, D. P., Teiga, E. J., and Zhelem, R. (2010). The multi-object double spectrographs for the Large Binocular Telescope. In *Society of Photo-Optical Instrumentation Engineers (SPIE) Conference Series*, volume 7735 of *Society of Photo-Optical Instrumentation Engineers (SPIE) Conference Series*. [26](#)
- Pogge, R. W., Atwood, B., O’Brien, T. P., Byard, P. L., Derwent, M. A., Gonzalez, R., Martini, P., Mason, J. A., Osmer, P. S., Pappalardo, D. P., Zhelem, R., Stoll, R. A., Steinbrecher, D. P., Brewer, D. F., Colarosa, C., and Teiga, E. J. (2012). On-sky performance of the Multi-Object Double Spectrograph for the Large Binocular Telescope. In *Society of Photo-Optical Instrumentation Engineers (SPIE) Conference Series*, volume 8446 of *Society of Photo-Optical Instrumentation Engineers (SPIE) Conference Series*. [26](#)
- Prestage, R. M. and Peacock, J. A. (1988). The cluster environments of powerful radio galaxies. *MNRAS*, **230**, 131–160. [16](#)
- Proga, D. and Kallman, T. R. (2004). Dynamics of Line-driven Disk Winds in Active Galactic Nuclei. II. Effects of Disk Radiation. *ApJ*, **616**, 688–695. [17](#)
- Reichard, T. A., Richards, G. T., Schneider, D. P., Hall, P. B., Tolea, A., Krolik, J. H., Tsvetanov, Z., Vanden Berk, D. E., York, D. G., Knapp, G. R., Gunn, J. E., and Brinkmann, J. (2003). A Catalog of Broad Absorption Line Quasars from the Sloan Digital Sky Survey Early Data Release. *AJ*, **125**, 1711–1728. [17](#)

REFERENCES

- Reis, R. C., Miller, J. M., Reynolds, M. T., Gültekin, K., Maitra, D., King, A. L., and Strohmayer, T. E. (2012). A 200-Second Quasi-Periodicity After the Tidal Disruption of a Star by a Dormant Black Hole. *Science*, **337**, 949–9
- Rengstorf, A. W., Brunner, R. J., and Wilhite, B. C. (2006). A Synoptic Multi-wavelength Analysis of a Large Quasar Sample. *AJ*, **131**, 1923–1933. 107
- Richards, G. T. (2001). Intrinsic Absorption in Radio-Selected Quasars. *ApJS*, **133**, 53–75. 112
- Rodriguez-Pascual, P. M., Mas-Hesse, J. M., Sanz Fernandez de Cordoba, L., Mirabel, I. F., Makino, F., and Otani, C. (1993). X-ray, UV and FIR emission of Seyfert galaxies. *Ap&SS*, **205**, 113–121. 5
- Rosenblatt, E. I., Malkan, M. A., Sargent, W. L. W., and Readhead, A. C. S. (1992). The broad emission line and continuum variations of Seyfert galaxies. I - Time scales and amplitudes. *ApJS*, **81**, 59–81. 6
- Ruan, J. J., Anderson, S. F., Dexter, J., and Agol, E. (2014). Evidence for Large Temperature Fluctuations in Quasar Accretion Disks from Spectral Variability. *ApJ*, **783**, 105. 79
- Rybicki, G. B. and Lightman, A. P. (1979). *Radiative processes in astrophysics*. John Wiley & Sons, Inc., in 1979. 9
- Sánchez Almeida, J., Aguerri, J. A. L., Muñoz-Tuñón, C., and Huertas-Company, M. (2011). Relationship between Hubble Type and Spectroscopic Class in Local Galaxies. *ApJ*, **735**, 125. 66
- Schmitt, H. R., Donley, J. L., Antonucci, R. R. J., Hutchings, J. B., Kinney, A. L., and Pringle, J. E. (2003). A Hubble Space Telescope Survey of Extended [O III] λ 5007 \AA Emission in a Far-Infrared-Selected Sample of Seyfert Galaxies: Results. *ApJ*, **597**, 768–779. 8, 97
- Schneider, D. P., Richards, G. T., Fan, X., Hall, P. B., Strauss, M. A., Vanden Berk, D. E., Gunn, J. E., Newberg, H. J., Reichard, T. A., Stoughton, C., Voges, W., Yanny, B., Anderson, S. F., Annis, J., Bahcall, N. A., Bauer, A., Bernardi, M., Blanton, M. R., Boroski, W. N., Brinkmann, J., Briggs, J. W., Brunner, R., Burles, S., Carey, L., Castander, F. J., Connolly, A. J., Csabai, I., Doi, M., Friedman, S., Frieman, J. A., Fukugita, M., Heckman, T. M., Hennessy, G. S., Hindsley, R. B., Hogg, D. W., Ivezić, Ž., Kent, S., Knapp, G. R., Kunzst, P. Z., Lamb, D. Q., Leger, R. F., Long, D. C., Loveday, J., Lupton, R. H., Margon, B., Meiksin, A., Merelli, A., Munn, J. A., Newcomb, M., Nichol, R. C., Owen, R., Pier, J. R., Pope, A., Rockosi, C. M., Saxé, D. H., Schlegel, D., Siegmund, W. A., Smee, S., Snir, Y., SubbaRao, M., Szalay, A. S., Thakar, A. R., Uomoto, A., Waddell, P., and York, D. G. (2002). The Sloan Digital Sky Survey Quasar Catalog. I. Early Data Release. *AJ*, **123**, 567–577. 107
- Schneider, D. P., Fan, X., Hall, P. B., Jester, S., Richards, G. T., Stoughton, C., Strauss, M. A., SubbaRao, M., Vanden Berk, D. E., Anderson, S. F., Brandt, W. N., Gunn, J. E., Gray, J., Trump, J. R., Voges, W., Yanny, B., Bahcall, N. A., Blanton, M. R., Boroski, W. N., Brinkmann, J., Brunner, R., Burles, S., Castander, F. J., Doi, M., Eisenstein, D., Frieman, J. A., Fukugita, M., Heckman, T. M., Hennessy, G. S., Ivezić, Ž., Kent, S., Knapp, G. R., Lamb, D. Q., Lee, B. C., Loveday, J., Lupton, R. H., Margon, B., Meiksin, A., Munn, J. A., Newberg, H. J., Nichol, R. C., Niederste-Ostholt, M., Pier, J. R., Richmond, M. W., Rockosi, C. M., Saxé, D. H., Schlegel, D. J., Szalay, A. S., Thakar, A. R., Uomoto, A., and York, D. G. (2003). The Sloan Digital Sky Survey Quasar Catalog. II. First Data Release. *AJ*, **126**, 2579–2593. 107
- Schneider, D. P., Hall, P. B., Richards, G. T., Vanden Berk, D. E., Anderson, S. F., Fan, X., Jester, S., Stoughton, C., Strauss, M. A., SubbaRao, M., Brandt, W. N., Gunn, J. E., Gray, J., Trump, J. R., Voges, W., Yanny, B., Bahcall, N. A., Blanton, M. R., Boroski, W. N., Brinkmann, J., Brunner, R., Csabai, I., Doi, M., Eisenstein, D. J., Frieman, J. A., Fukugita, M., Gray, J., Harvanek, M., Heckman, T. M., Ivezić, Ž., Kent, S., Kleinman, S. J., Knapp, G. R., Kron, R. G., Krzesinski, J., Long, D. C., Loveday, J., Lupton, R. H., Margon, B., Munn, J. A., Neilsen, E. H., Newberg, H. J., Newman, P. R., Nichol, R. C., Nitta, A., Pier, J. R., Rockosi, C. M., Saxé, D. H., Schlegel, D. J., Snedden, S. A., Szalay, A. S., Thakar, A. R., Uomoto, A., Voges, W., and York, D. G. (2005). The Sloan Digital Sky Survey Quasar Catalog. III. Third Data Release. *AJ*, **130**, 367–380. 79, 107
- Schneider, D. P., Hall, P. B., Richards, G. T., Strauss, M. A., Vanden Berk, D. E., Anderson, S. F., Brandt, W. N., Fan, X., Jester, S., Gray, J., Gunn, J. E., SubbaRao, M. U., Thakar, A. R., Stoughton, C., Szalay, A. S., Yanny, B., York, D. G., Bahcall, N. A., Barentine, J., Blanton, M. R., Brewington, H., Brinkmann, J., Brunner, R. J., Castander, F. J., Csabai, I., Frieman, J. A., Fukugita, M., Harvanek, M., Hogg, D. W., Ivezić, Ž., Kent, S. M., Kleinman, S. J., Knapp, G. R., Kron, R. G., Krzesiński, J., Long, D. C., Lupton, R. H., Nitta, A., Pier, J. R., Saxé, D. H., Shen, Y., Snedden, S. A., Weinberg, D. H., and Wu, J. (2007). The Sloan Digital Sky Survey Quasar Catalog. IV. Fifth Data Release. *AJ*, **134**, 102–117. 81, 107
- Schneider, D. P., Richards, G. T., Hall, P. B., Strauss, M. A., Anderson, S. F., Boroski, T. A., Ross, N. P., Shen, Y., Brandt, W. N., Fan, X., Inada, N., Jester, S., Knapp, G. R., Krawczyk, C. M., Thakar, A. R., Vanden Berk, D. E., Voges, W., Yanny, B., York, D. G., Bahcall, N. A., Bizyaev, D., Blanton, M. R., Brewington, H., Brinkmann, J., Eisenstein, D., Frieman, J. A., Fukugita, M., Gray, J., Gunn, J. E., Hiben, P., Ivezić, Ž., Kent, S. M., Kron, R. G., Lee, M. G., Lupton, R. H., Malanushenko, E., Malanushenko, V., Oravetz, D., Pan, K., Pier, J. R., Price, III, T. N., Saxé, D. H., Schlegel, D. J., Simmons, A., Snedden, S. A., SubbaRao, M. U., Szalay, A. S., and Weinberg, D. H. (2010). The Sloan Digital Sky Survey Quasar Catalog. V. Seventh Data Release. *AJ*, **139**, 2360. 29, 81, 107
- Schneider, P. (2006). *Extragalactic Astronomy and Cosmology*. Berlin: Springer, 2006. 14, 15
- Schramm, K.-J., Borgeest, U., Kuehl, D., von Linde, J., Linnert, M. D., and Schramm, T. (1994). The Hamburg quasar monitoring program (HQM) at Calar Alto. III. Lightcurves of optically violent variable sources. *A&AS*, **106**, 349–359. 16
- Senn, S. and Richardson, W. (1994). The first t-test. *Statistics in Medicine* **13** (8), 785, 803. 93
- Seyfert, C. K. (1943). Nuclear Emission in Spiral Nebulae. *ApJ*, **97**, 28. 9
- Shapovalova, A. I., Popović, L. Č., Burenkov, A. N., Chavushyan, V. H., Ilić, D., Kovačević, A., Bochkarev, N. G., and León-Tavares, J. (2010). Long-term variability of the optical spectra of NGC 4151. II. Evolution of the broad H α and H β emission-line profiles. *A&A*, **509**, A106. 81
- Shirazi, M. and Brinchmann, J. (2012). Strongly star forming galaxies in the local Universe with nebular He II λ 6866 emission. *MNRAS*, **421**, 1043–1063. 76
- Sikora, M., Stawarz, Ł., and Lasota, J.-P. (2007). Radio Loudness of Active Galactic Nuclei: Observational Facts and Theoretical Implications. *ApJ*, **658**, 815–828. xiii, 51
- Silk, J. (2013). Unleashing Positive Feedback: Linking the Rates of Star Formation, Supermassive Black Hole Accretion, and Outflows in Distant Galaxies. *ApJ*, **772**, 112. 35, 37, 54
- Skrutskie, M. F., Cutri, R. M., Stiening, R., Weinberg, M. D., Schneider, S., Carpenter, J. M., Beichman, C., Capps, R., Chester, T., Elias, J., Huchra, J., Liebert, J., Lonsdale, C., Monet, D. G., Price, S., Seitzer, P., Jarrett, T., Kirkpatrick, J. D., Gizis, J. E., Howard, E., Evans, T., Fowler, J., Fullmer, L., Hurt, R., Light, R., Kopan, E. L., Marsh, K. A., McCallon, H. L., Tam, R., Van Dyk, S., and Wheelock, S. (2006). The Two Micron All Sky Survey (2MASS). *AJ*, **131**, 1163–1183. 61
- Smith, H. J. and Hoeffleit, D. (1963). Light Variations in the Superluminous Radio Galaxy 3C273. *Nature*, **198**, 650–651. 20
- Smith, L. J. and Penston, M. V. (1988). On variability in the broad absorption line troughs of the QSO 1246-057. *MNRAS*, **235**, 551–564. 106
- Sparke, L. S. and Gallagher, III, J. S. (2007). *Galaxies in the Universe: An Introduction*. Cambridge University Press. 1

REFERENCES

- Spergel, D. N., Verde, L., Peiris, H. V., Komatsu, E., Nolta, M. R., Bennett, C. L., Halpern, M., Hinshaw, G., Jarosik, N., Kogut, A., Limon, M., Meyer, S. S., Page, L., Tucker, G. S., Weiland, J. L., Wollack, E., and Wright, E. L. (2003). First-Year Wilkinson Microwave Anisotropy Probe (WMAP) Observations: Determination of Cosmological Parameters. *ApJS*, **148**, 175–194. [41](#), [73](#)
- Stanghellini, C., O’Dea, C. P., Dallacasa, D., Baum, S. A., Fanti, R., and Fanti, C. (1998). A complete sample of GHz-peaked-spectrum radio sources and its radio properties. *A&AS*, **131**, 303–315. [55](#)
- Starling, R. L. C. and Puchnarewicz, E. M. (2001). XMM-Newton observations of the variable ultrasoft AGN REJ2248-511. In *Two Years of Science with Chandra*. [77](#)
- Stepanian, J. A. and Afanas’ev, V. L. (2011). New type of extragalactic objects? *Astrophysics*, **54**, 340–354. [74](#)
- Stoughton, C., Lupton, R. H., Bernardi, M., Blanton, M. R., Bures, S., Castander, F. J., Connolly, A. J., Eisenstein, D. J., Frieman, J. A., Hennesy, G. S., Hindsley, R. B., Ivezić, Ž., Kent, S., Kunszt, P. Z., Lee, B. C., Meiksin, A., Munn, J. A., Newberg, H. J., Nichol, R. C., Nicinski, T., Pier, J. R., Richards, G. T., Richmond, M. W., Schlegel, D. J., Smith, J. A., Strauss, M. A., SubbaRao, M., Szalay, A. S., Thakar, A. R., Tucker, D. L., Vanden Berk, D. E., Yanny, B., Adelman, J. K., Anderson, Jr., J. E., Anderson, S. F., Annis, J., Bahcall, N. A., Bakken, J. A., Bartelmann, M., Bastian, S., Bauer, A., Berman, E., Böhringer, H., Boroski, W. N., Bracker, S., Briegel, C., Briggs, J. W., Brinkmann, J., Brunner, R., Carey, L., Carr, M. A., Chen, B., Christian, D., Colestock, P. L., Crocker, J. H., Csabai, I., Czarapata, P. C., Dalcanton, J., Davidsen, A. F., Davis, J. E., Dehnen, W., Dodelson, S., Doi, M., Dombek, T., Donahue, M., Ellman, N., Elms, B. R., Evans, M. L., Eyer, L., Fan, X., Federwitz, G. R., Friedman, S., Fukugita, M., Gal, R., Gillespie, B., Glazebrook, K., Gray, J., Grebel, E. K., Greenawalt, B., Greene, G., Gunn, J. E., de Haas, E., Haiman, Z., Haldeman, M., Hall, P. B., Hamabe, M., Hansen, B., Harris, F. H., Harris, H., Harvanek, M., Hawley, S. L., Hayes, J. J. E., Heckman, T. M., Helmi, A., Henden, A., Hogan, C. J., Hogg, D. W., Holmgren, D. J., Holtzman, J., Huang, C.-H., Hull, C., Ichikawa, S.-I., Ichikawa, T., Johnston, D. E., Kauffmann, G., Kim, R. S. J., Kimball, T., Kinney, E., Klaene, M., Kleinman, S. J., Klypin, A., Knapp, G. R., Korienek, J., Krolik, J., Kron, R. G., Krziesiński, J., Lamb, D. Q., Leger, R. F., Limmongkol, S., Lindemeyer, C., Long, D. C., Loomis, C., Loveday, J., MacKinnon, B., Mannery, E. J., Mantsch, P. M., Margon, B., McGehee, P., McKay, T. A., McLean, B., Menou, K., Merelli, A., Mo, H. J., Monet, D. G., Nakamura, O., Narayanan, V. K., Nash, T., Neilsen, Jr., E. H., Newman, P. R., Nitta, A., Odenkirchen, M., Okada, N., Okamura, S., Ostrik, J. P., Owen, R., Pauls, A. G., Peoples, J., Peterson, R. S., Petravick, D., Pope, A., Pordes, R., Postman, M., Protopop, A., Quinn, T. R., Rechenmacher, R., Rivetta, C. H., Rix, H.-W., Rockosi, C. M., Rosner, R., Ruthmansdorfer, K., Sandford, D., Schneider, D. P., Scranton, R., Sekiguchi, M., Sergey, G., Sheth, R., Shimasaku, K., Smee, S., Snedden, S. A., Stebbins, A., Stubbs, C., Szapudi, I., Szkody, P., Szokoly, G. P., Tabachnik, S., Tsvetanov, Z., Uomoto, A., Vogeley, M. S., Voges, W., Waddell, P., Walterbos, R., Wang, S.-i., Watanabe, M., Weinberg, D. H., White, R. L., White, S. D. M., Wilhite, B., Wolfe, D., Yasuda, N., York, D. G., Zehavi, I., and Zheng, W. (2002). Sloan Digital Sky Survey: Early Data Release. *AJ*, **123**, 485–548. [61](#)
- Tadhunter, C., Holt, J., González Delgado, R., Rodríguez Zaurín, J., Villar-Martín, M., Morganti, R., Emons, B., Ramos Almeida, C., and Inskip, K. (2011). Starburst radio galaxies: general properties, evolutionary histories and triggering. *MNRAS*, **412**, 960–978. [55](#)
- Thronson, Jr., H. A. and Greenhouse, M. A. (1988). Near-infrared mass-to-light ratios in galaxies - Stellar mass and star formation in the heart of the Whirlpool. *ApJ*, **327**, 671–679. [42](#)
- Thronson, Jr., H. A. and Telesco, C. M. (1986). Star formation in active dwarf galaxies. *ApJ*, **311**, 98–112. [53](#)
- Treichel, K., Rudnick, L., Hardcastle, M. J., and Leahy, J. P. (2001). Spectral Structure in FR II Radio Galaxies and Jets. *ApJ*, **561**, 691–702. [xii](#), [45](#)
- Trump, J. R., Hall, P. B., Reichard, T. A., Richards, G. T., Schneider, D. P., Vanden Berk, D. E., Knapp, G. R., Anderson, S. F., Fan, X., Brinkman, J., Kleinman, S. J., and Nitta, A. (2006). A Catalog of Broad Absorption Line Quasars from the Sloan Digital Sky Survey Third Data Release. *ApJS*, **165**, 1–18. [17](#), [107](#), [108](#)
- Urry, C. M. and Padovani, P. (1995). Unified Schemes for Radio-Loud Active Galactic Nuclei. *PASP*, **107**, 803. [10](#)
- Vanden Berk, D. E., Wilhite, B. C., Kron, R. G., Anderson, S. F., Brunner, R. J., Hall, P. B., Ivezić, Ž., Richards, G. T., Schneider, D. P., York, D. G., Brinkmann, J. V., Lamb, D. Q., Nichol, R. C., and Schlegel, D. J. (2004). The Ensemble Photometric Variability of ~25,000 Quasars in the Sloan Digital Sky Survey. *ApJ*, **601**, 692–714. [57](#)
- Veilleux, S. and Osterbrock, D. E. (1987). Spectral classification of emission-line galaxies. *ApJS*, **63**, 295–310. [40](#), [41](#)
- Véron-Cetty, M. P. and Véron, P. (2000). The emission line spectrum of active galactic nuclei and the unifying scheme. *A&A Rev.*, **10**, 81–133. [13](#)
- Véron-Cetty, M.-P. and Véron, P. (2006). A catalogue of quasars and active nuclei: 12th edition. *A&A*, **455**, 773–777. [66](#), [84](#), [86](#)
- Vestergaard, M. (2004). Early Growth and Efficient Accretion of Massive Black Holes at High Redshift. *ApJ*, **601**, 676–691. [50](#)
- Villarroel, B. and Korn, A. J. (2014). The different neighbours around Type-1 and Type-2 active galactic nuclei. *Nature Physics*, **10**, 417–420. [8](#)
- Vitale, M., Zuther, J., García-Marín, M., Eckart, A., Bremer, M., Valencia-S., M., and Zensus, A. (2012). Classifying radio emitters from the Sloan Digital Sky Survey. Spectroscopy and diagnostics. *A&A*, **546**, A17. [xii](#), [41](#), [43](#)
- Vitale, M., Mignoli, M., Cimatti, A., Lilly, S. J., Carollo, C. M., Contini, T., Kneib, J.-P., Le Fevre, O., Mainieri, V., Renzini, A., Scodreggio, M., Zamorani, G., Bardelli, S., Barnes, L., Bolzonella, M., Bongiorno, A., Bordoloi, R., Bschorr, T. J., Cappi, A., Caputi, K., Coppa, G., Cucchiati, O., de la Torre, S., de Ravel, L., Franzetti, P., Garilli, B., Iovino, A., Kampeczyk, P., Knobel, C., Koekemoer, A. M., Kovač, K., Lamareille, F., Le Borgne, J.-F., Le Brun, V., López-Sanjuan, C., Maier, C., McCracken, H. J., Moresco, M., Nair, P., Oesch, P. A., Pello, R., Peng, Y., Pérez Montero, E., Pozzetti, L., Presotto, V., Silverman, J., Tanaka, M., Tasca, L., Tresse, L., Vergani, D., Welikala, N., and Zucca, E. (2013). Investigating the relationship between AGN activity and stellar mass in zCOSMOS galaxies at $0 < z < 1$ using emission-line diagnostic diagrams. *A&A*, **556**, A11. [42](#)
- Voit, G. M., Weymann, R. J., and Korista, K. T. (1993). Low-ionization broad absorption lines in quasars. *ApJ*, **413**, 95–109. [18](#)
- Wagner, A. Y. and Bicknell, G. V. (2011). Relativistic Jet Feedback in Evolving Galaxies. *ApJ*, **728**, 29. [36](#)
- Wagner, A. Y., Umemura, M., and Bicknell, G. V. (2013). Ultrafast Outflows: Galaxy-scale Active Galactic Nucleus Feedback. *ApJ*, **763**, L18. [35](#), [37](#), [54](#)
- Walsh, J. L., Barth, A. J., Ho, L. C., Filippenko, A. V., Rix, H.-W., Shields, J. C., Sarzi, M., and Sargent, W. L. W. (2008). Hubble Space Telescope Spectroscopic Observations of the Narrow-Line Region in Nearby Low-Luminosity Active Galactic Nuclei. *AJ*, **136**, 1677–1702. [99](#)
- Wanders, I. and Peterson, B. M. (1996). A Long-Term Study of Broad Emission Line Profile Variability in NGC 5548. *ApJ*, **466**, 174. [6](#)
- Wang, J.-M. and Zhang, E.-P. (2007). The Unified Model of Active Galactic Nuclei. II. Evolutionary Connection. *ApJ*, **660**, 1072–1092. [49](#)
- Wang, L. and Rowan-Robinson, M. (2009). The Imperial IRAS-FSC Redshift Catalogue. *MNRAS*, **398**, 109–118. [77](#)
- Wang, T.-G., Zhou, H.-Y., Komossa, S., Wang, H.-Y., Yuan, W., and Yang, C. (2012). Extreme Coronal Line Emitters: Tidal Disruption of Stars by Massive Black Holes in Galactic Nuclei? *ApJ*, **749**, 115. [74](#)

REFERENCES

- Wang, Y., Knigge, C., Croston, J. H., and Pavlovski, G. (2011). The entrainment-limited evolution of FR II sources: maximum sizes and a possible connection to FR Is. *MNRAS*, **418**, 1138–1145. [xii, 44](#)
- Webb, W. and Malkan, M. (2000). Rapid Optical Variability in Active Galactic Nuclei and Quasars. *ApJ*, **540**, 652–677. [91](#)
- Welling, C. A., Miller, B. P., Brandt, W. N., Capellupo, D. M., and Gibson, R. R. (2014). Broad absorption line variability in radio-loud quasars. *MNRAS*, **440**, 2474–2497. [112](#)
- Weymann, R. J., Morris, S. L., Foltz, C. B., and Hewett, P. C. (1991). Comparisons of the emission-line and continuum properties of broad absorption line and normal quasi-stellar objects. *ApJ*, **373**, 23–53. [17](#)
- White, R. L., Becker, R. H., Gregg, M. D., Laurent-Muehleisen, S. A., Brotherton, M. S., Impey, C. D., Petry, C. E., Foltz, C. B., Chaffee, F. H., Richards, G. T., Oegerle, W. R., Helfand, D. J., McMahon, R. G., and Cabanela, J. E. (2000). The FIRST Bright Quasar Survey. II. 60 Nights and 1200 Spectra Later. *ApJS*, **126**, 133–207. [108, 115](#)
- Whitmore, B. C., Gilmore, D. M., and Jones, C. (1993). What determines the morphological fractions in clusters of galaxies? *ApJ*, **407**, 489–509. [2](#)
- White, B. C., Vanden Berk, D. E., Kron, R. G., Schneider, D. P., Perea, N., Brunner, R. J., Richards, G. T., and Brinkmann, J. V. (2005). Spectral Variability of Quasars in the Sloan Digital Sky Survey. I. Wavelength Dependence. *ApJ*, **633**, 638–648. [58, 59](#)
- Wright, E. L., Eisenhardt, P. R. M., Mainzer, A. K., Ressler, M. E., Cutri, R. M., Jarrett, T., Kirkpatrick, J. D., Padgett, D., McMillan, R. S., Skrutskie, M., Stanford, S. A., Cohen, M., Walker, R. G., Mather, J. C., Leisawitz, D., Gautier, III, T. N., McLean, I., Benford, D., Lonsdale, C. J., Blain, A., Mendez, B., Irace, W. R., Duval, V., Liu, F., Royer, D., Heinrichsen, I., Howard, J., Shannon, M., Kendall, M., Walsh, A. L., Larsen, M., Cardon, J. G., Schick, S., Schwalm, M., Abid, M., Fabinisky, B., Naes, L., and Tsai, C.-W. (2010). The Wide-field Infrared Survey Explorer (WISE): Mission Description and Initial On-orbit Performance. *AJ*, **140**, 1868–1881. [30](#)
- Yang, C.-W., Wang, T.-G., Ferland, G., Yuan, W., Zhou, H.-Y., and Jiang, P. (2013). Long-term Spectral Evolution of Tidal Disruption Candidates Selected by Strong Coronal Lines. *ApJ*, **774**, 46. [74](#)
- Yip, C. W., Connolly, A. J., Vanden Berk, D. E., Scranton, R., Krughoff, S., Szalay, A. S., Dobos, L., Tremonti, C., Taghizadeh-Popp, M., Budavári, T., Csabai, I., Wyse, R. F. G., and Ivezić, Ž. (2009). Probing Spectroscopic Variability of Galaxies and Narrow-Line Active Galactic Nuclei in the Sloan Digital Sky Survey. *AJ*, **137**, 5120–5133. [94](#)
- York, D. G., Adelman, J., Anderson, Jr., J. E., Anderson, S. F., Annis, J., Bahcall, N. A., Bakken, J. A., Barkhouser, R., Bastian, S., Berman, E., Boroski, W. N., Bracker, S., Briegel, C., Briggs, J. W., Brinkmann, J., Brunner, R., Burles, S., Carey, L., Carr, M. A., Castander, F. J., Chen, B., Colestock, P. L., Connolly, A. J., Crocker, J. H., Csabai, I., Czarapata, P. C., Davis, J. E., Doi, M., Dombeck, T., Eisenstein, D., Ellman, N., Elms, B. R., Evans, M. L., Fan, X., Federwitz, G. R., Fiscelli, L., Friedman, S., Frieman, J. A., Fukugita, M., Gillespie, B., Gunn, J. E., Gurbani, V. K., de Haas, E., Haldeman, M., Harris, F. H., Hayes, J., Heckman, T. M., Hennessy, G. S., Hindsley, R. B., Holm, S., Holmgren, D. J., Huang, C.-h., Hull, C., Husby, D., Ichikawa, S.-I., Ichikawa, T., Ivezić, Ž., Kent, S., Kim, R. S. J., Kinney, E., Klaene, M., Kleinman, A. N., Kleinman, S., Knapp, G. R., Korienek, J., Kron, R. G., Kunszt, P. Z., Lamb, D. Q., Lee, B., Leger, R. F., Limmongkol, S., Lindenmeyer, C., Long, D. C., Loomis, C., Loveday, J., Lucinio, R., Lupton, R. H., MacKinnon, B., Mannery, E. J., Mantsch, P. M., Margon, B., McGehee, P., McKay, T. A., Meiksin, A., Merelli, A., Monet, D. G., Munn, J. A., Narayanan, V. K., Nash, T., Neilsen, E., Neswold, R., Newberg, H. J., Nichol, R. C., Nicinski, T., Nonino, M., Okada, N., Okamura, S., Ostriker, J. P., Owen, R., Pauls, A. G., Peoples, J., Peterson, R. L., Petravick, D., Pier, J. R., Pope, A., Pordes, R., Protopio, A., Rechenmacher, R., Quinn, T. R., Richards, G. T., Richmond, M. W., Rivetta, C. H., Rockosi, C. M., Ruthmansdorfer, K., Sandford, D., Schlegel, D. J., Schneider, D. P., Sekiguchi, M., Sergey, G., Shimasaku, K., Siegmund, W. A., Smee, S., Smith, J. A., Snedden, S., Stone, R., Stoughton, C., Strauss, M. A., Stubbs, C., SubbaRao, M., Szalay, A. S., Szapudi, I., Szokoly, G. P., Thakar, A. R., Tremonti, C., Tucker, D. L., Uomoto, A., Vanden Berk, D., Vogeley, M. S., Waddell, P., Wang, S.-i., Watanabe, M., Weinberg, D. H., Yanny, B., Yasuda, N., and SDSS Collaboration (2000). The Sloan Digital Sky Survey: Technical Summary. *AJ*, **120**, 1579–1587. [29, 61](#)
- Yuan, W., Zhou, H. Y., Komossa, S., Dong, X. B., Wang, T. G., Lu, H. L., and Bai, J. M. (2008). A Population of Radio-Loud Narrow-Line Seyfert 1 Galaxies with Blazar-Like Properties? *ApJ*, **685**, 801–827. [46](#)
- Zhang, E.-P. and Wang, J.-M. (2006). The Unified Model of Active Galactic Nuclei. I. Non-Hidden Broad-Line Region Seyfert 2 and Narrow-Line Seyfert 1 Galaxies. *ApJ*, **653**, 137–151. [60](#)
- Zhang, S., Wang, T.-G., Wang, H., Zhou, H., Dong, X.-B., and Wang, J.-G. (2010). Low-z Mg II Broad Absorption-line Quasars from the Sloan Digital Sky Survey. *ApJ*, **714**, 367–383. [17, 66, 77, 79](#)
- Zhou, H., Wang, T., Yuan, W., Lu, H., Dong, X., Wang, J., and Lu, Y. (2006). A Comprehensive Study of 2000 Narrow Line Seyfert 1 Galaxies from the Sloan Digital Sky Survey. I. The Sample. *ApJS*, **166**, 128–153. [71](#)
- Zhou, H.-Y., Wang, T.-G., Zhou, Y.-Y., Cheng-Li, and Dong, X.-B. (2002). Discovery of a Radio-loud Superstrong Fe II-emitting Quasar. *ApJ*, **581**, 96–102. [66, 86, 103](#)
- Zuo, W., Wu, X.-B., Liu, Y.-Q., and Jiao, C.-L. (2012). The Correlations between Optical Variability and Physical Parameters of Quasars in SDSS Stripe 82. *ApJ*, **758**, 104. [57, 91](#)
- Zuo, W., Wu, X.-B., Liu, Y.-Q., and Jiao, C.-L. (2013). The correlations between optical variability and physical parameters of quasars in SDSS Stripe 82. In C. M. Zhang, T. Belloni, M. Méndez, and S. N. Zhang, editors, *IAU Symposium*, volume 290 of *IAU Symposium*, pages 373–374. [57](#)
- Zuther, J., Fischer, S., and Eckart, A. (2012). Compact radio emission from $z \sim 0.2$ X-ray bright AGN. *A&A*, **543**, A57. [37, 51](#)

Erklärung zur Dissertation

Ich versichere, dass die von mir vorgelegte Dissertation selbstständig angefertigt, die benutzten Quellen und Hilfsmittel vollständig angegeben und Stellen der Arbeit-einschließlich Tabellen, Karten und Abbildungen -, die anderen Werken im Wortlaut oder dem Sinn nach entnommen sind, in jedem Einzelfall als Entlehnung kenntlich gemacht habe; dass diese Dissertation noch keiner anderen Fakultät oder Universität zur Prüfung vorgelegen hat; dass sie - abgesehen von unten angegebenen Teilpublikationen - noch nicht veröffentlicht worden ist sowie, dass ich eine solche Veröffentlichung vor Abschluss des Promotionsverfahrens nicht vornehmen werde.

Die Bestimmungen dieser Promotionsordnung sind mir bekannt. Die von mir vorgelegte Dissertation ist von **Prof. Dr. Andreas Eckart** betreut worden.

Yasir Ezzuldeen Rashed
I. Physikalisches Institut
Universität zu Köln
Zülpicher Straße 77
50937 Köln
+49-017683209455
yasir@ph1.uni-koeln.de

Teilpublikationen

- Erstautor von: High-resolution observations of SDSS J080800.99+483807.7 in the optical and radio domains. A possible example of jet-triggered star formation, *Astronomy and Astrophysics*, July 2013
- Erstautor von: Line and Continuum Variability in Active Galaxies, *Monthly Notices of the Royal Astronomical Society*, September 2015
- Ko-autor von: The Galactic Center as a paradigm for low-luminosity nuclei? What can be learned from SgrA* for the central engine and conditions of star formation in nuclei of Seyfert galaxies and low luminosity nearby QSOs; The K-band identification of the DSO/G2 source from VLT and Keck data , 2012
- Ko-autor von: Are Narrow Line Seyfert 1 galaxies a special class of Active Galactic Nuclei?, 2013
- Ko-autor von: The infrared K-band identification of the DSO/G2 source from VLT and Keck data, 2013

Lebenslauf

Ausbildung

Name, Vorname: Rashed, Yasir Ezzuldeen
Anschrift: Freiburger-Str. 12
51375, Leverkusen. Germany
Telefon: +49-017683209455
Email: yasir@ph1.uni-koeln.de
Geburtsort: Irakische
Geburtsdatum: 23 Januar 1981

Ausbildung

Seit Oct 2011 Promotionstudent
I Physikalisches Institut der Universitaet zu Koeln
Koeln, Deutschland

2003-2006 Magisters Abschluss in Astronomie (Galaxien Dynamik) mit 80,67%
Universität Bagdad, Akademie für Naturwissenschaften,
Abteilung für Astronomie
Bagdad, Irak

1999-2002 Abschluss in Astronomie mit 71,83%; Platz 1 von 22 Studenten
Universität Bagdad, Akademie für Naturwissenschaften,
Abteilung für Astronomie
Bagdad, Irak

Berufliche Laufbahn

2005 2011 Dozententätigkeit in der Universität Bagdad, Akademie für Naturwissenschaften, Abteilung für Astronomie, Bagdad, Irak

Köln, 2015